Electrochemical Detection of Thiol Containing Molecules

A thesis submitted for the degree of Doctor of Philosophy
in Physical and Theoretical Chemistry

Patricia T. Lee

St. Cross College

July 2015

Abstract

This thesis presents the experimental work with the main aim of developing new electrochemical based methods for detecting thiol-containing molecules, specifically homocysteine, glutathione, and cysteine, with little to no sample treatment in an aqueous system. The first chapter introduces the principles and techniques of electrochemistry. The second chapter gives a brief introduction to the importance of thiol containing molecules in biological systems; thus, the need for its analytical determination and quantification.

This thesis reports a suitable electrochemical methodology to selectively detect thiols using a combination of different *ortho*-quinone derived mediators and carbon electrode materials. The methodology exploits two *ortho*-quinone reaction pathways with a thiol molecule, electrocatalytic and 1,4-Michael addition reaction. Proof-of-concept was carried out in buffered systems then realized in synthetic and real biological sample; where ultimately, quantitative performance in 'real world' sample was shown to be analogous to a commercially available enzyme test.

Finally, screen-printed electrodes are employed in the presented study to show the prospect for a point-of-care system. The compact design, such as having a three-electrode system printed onto a single strip, allows versatility and easy utilization. These electrochemical chips are ideal and advantageous for high throughput applications.

Overall, the development of a quick, easy, and cheap methodology for thiol determination discussed in this thesis makes a significant contribution to the clinical and biomedical community as an alternative and simpler diagnostic pathway.

Acknowledgements

I would like to first and foremost thank my supervisor, Professor Richard G. Compton, for all his help, guidance, and advice over the last three years. Thank you for taking me on as a D.Phil student and providing me with such amazing opportunities and experiences during my time here in Oxford-I will never forget! I also must thank Professor Greg Wildgoose who introduced me to electrochemistry beyond fuel cells and encouraged me to pursue my D.Phil degree-I would have not found my way to the Compton group without you!

Thank you to all the past and present members of the Compton group for making the lab and office such an enjoyable place to work. In particular, thank you to Dr. Qian Li for her warm welcome on my first day here in the lab-I'll never forget the memorable soup at the PTCL. To Professor Denise Lowinsohn, Dr. Emma Stuart, Mr. Tom Bartlett, Dr. Eduardo Laborda, Dr. Kristina Tschulik, Mr. Chris Neumann, Ms. Dia Ngamchuea, Dr. Eddy Barnes, and Ms. Ivana Lin, thank you for the memorable lunches, dinners, trips, May day experience, laughter and never ending support. A special thanks to Ms. Her Shuang Toh, my look-a-like sister from another country and partner-in-crime! Thank you for the positivity, sanity checks, immeasurable support, and encouragement over the last three years-we finally made it! I will miss our mini celebrations in the lab when we get results and late night discussions on experimental troubleshooting and other science 'stuff'.

I am also grateful to my brother, who has been so supportive and my confidant throughout my life. Finally to my fiancé, Giovanni, who has been my number one supporter since day one, 10 years ago! Thank you for your endless love, support, encouragement, corny jokes, and ability to believe in me when I doubt myself. Your ability to be right and 'jedi powers' still amazes me today-thank you!

Contents

Glossary

Roman Symbols

Symbol	Definition	Units
a_i	Activity of species i	
A	Area of electrode	m^2
C	Concentration of bulk solution	mol m^{-3}
C_i	Concentration of species i	mol m^{-3}
C_i^*	Concentration of species i at the electrode surface	mol m^{-3}
D	Diffusion coefficient of species i	m^2 s^{-1}
E	Potential applied to the working electrode	V
E_f'	Formal potential	V
E^0	Standard potential	V
F	Faraday constant ≈ 96485	C mol^{-1}
f	Frequency	Hz
I	Current	A
J	Flux	mol m^{-2} s^{-1}
$k_{red/ox}$	Rate constants of the reduction/oxidation reactions	m s^{-1}
m	Number of moles	mol
n	Number of electrons	
n'	Number of electrons transferred before the rate determining step	
Q	Charge	C
R	Molar gas constant ≈ 8.314	J K^{-1} mol^{-1}
t	Time	s
T	Temperature	K
x	x coordinate in Cartesian space	m

Greek Symbols

Symbol	Definition	Units
γ	Activity coefficient	
α	Butler-Volmer transfer coefficient for reduction	
β	Butler-Volmer transfer coefficient for oxidation	
Γ	Surface coverage	mol cm^{-2}
υ	Scan rate	V s^{-1}

Abbreviations

Abbreviation	Definition
AA	Ascorbic acid
ACE	Angiotensin-converting enzyme
CA	Chronoamperometry
CAF	Caffeic Acid
CAP	Captopril
CAT	Catechol
CE	Counter electrode
CNT	Carbon nanotubes
CPE	Carbon paste electrode
CTC	Cyclotricatechylene
CTV	Cyclotriveratrylene
CV	Cyclic voltammetry
Cys	Cysteine

DMEM	Dulbecco's Modified Eagle Media
DPV	Differential pulse voltammetry
GCE	Glassy carbon electrode
GSH	Glutathione (reduced)
GSSG	Glutathione (oxidized)
HCys	Homocysteine
HPLC	High performance liquid chromatography
IHP	Inner Helmholtz plane
LOD	Limit of detection
LSV	Linear sweep voltammetry
MSE	Mercury/mercurous sulphate electrode
NC	Nanocarbon
OHP	Outer Helmholtz plane
RE	Reference electrode
SCE	Saturated calomel electrode
SHE	Standard hydrogen electrode
SPE	Screen-printed electrode
SWV	Square wave voltammetry
WE	Working electrode

Chapter 1

Introduction to electrochemistry

This thesis develops the methodology of using electrochemical techniques to detect thiol-containing molecules. However, an understanding of fundamental electrochemistry and the techniques used to carry out those studies is required beforehand. This chapter presents an elementary introduction to and overview of those principles necessary to understand the practice and interpretation of electrochemical experiments and the results presented in this thesis.

1.1 Chemical equilibrium

Electrochemistry is the study of charge transfer across the interface of an electronic conductor (an electrode) and an ionic conductor (an electrolyte). [1, 2] Consider the following simple electrochemical equilibrium at an electrode-solution interface,

$$A + e^- \leftrightarrows B \tag{1.1}$$

where A is the oxidized species in solution, which gains an electron from the electrode to form B, the reduced species. In order to determine the equilibrium potential of the electroactive species, the Nernst equation (Equation 1.2) can be used to predict the relationship between potential and activities of species A and B [3],

$$E = E^0 + \frac{RT}{F}\ln\frac{a_A}{a_B} \tag{1.2}$$

where a_A and a_B represent the activities of the oxidized and reduced species respectively, E is the potential, E^0 is the standard electrode potential, R is the universal gas constant (8.314 J K^{-1} mol^{-1}), T is the absolute temperature (unit in Kelvin), and F is the Faraday constant (96485 C mol^{-1}). The activities for species A and B can be expressed in respect to their corresponding concentration, C_A and C_B, by

$$a_A = \gamma\, C_A \tag{1.3a}$$

$$a_B = \gamma\, C_B \tag{1.3b}$$

where γ is the activity coefficient (unitless). The standard electrode potential, E^0, is the potential value measured with respect to the standard hydrogen electrode at standard conditions (1atm, 298K, 1 unit activity). However, the activities of species are not quite measurable experimentally because activity coefficients are often unknown. So Equation 1.2 can alternatively be written in terms of concentrations to their respective species,

$$E = E_f' + \frac{RT}{F}\ln\frac{C_A}{C_B} \tag{1.4}$$

where the E_f' is the formal potential, which potential reflects the composition of the solution under study (i.e. temperature, pressure, and other electrolytes present). Finally, the formal potential in respect to standard potential and activity coefficient can be expressed as,

$$E_f' = E^0 + \frac{RT}{nF}\ln\frac{\gamma_A}{\gamma_B} \tag{1.5}$$

1.2 Electrode kinetics

In this section, we discuss the basis of electrode kinetics. Apart from thermodynamics, the rate of electron transfer needs to be taken under consideration at the electrode-solution interface. Consider, for example, a typical one electron reaction:

$$A + e^- \underset{k_{ox}}{\overset{k_{red}}{\leftrightarrows}} B \tag{1.6}$$

where k_{red} and k_{ox} represent the rate constants for reduction and oxidation respectively for a heterogeneous electron transfer.

The basis of electrode kinetic interpretation can be found in the Butler-Volmer model. [3] This model, in particular, describes the rate constants dependence on the potential applied, *E*,

$$k_{red} = k^0 \, exp \left[\frac{-\alpha F}{RT} (E - E_f^0) \right] \tag{1.7}$$

$$k_{ox} = k^0 \, exp \left[\frac{+\beta F}{RT} (E - E_f^0) \right] \tag{1.8}$$

where k_0 is the standard electrochemical rate constant, α and β are the transfer coefficients ($\alpha + \beta = 1$) [4, 5], and E_f^0 is the formal potential. These equations show that in a one electron process, the rate constant are exponentially dependent on the overpotential, ($E - E_f^0$) [6, 7], where the overpotential is the "driving force" required for the oxidation or reduction reaction to occur. [8] Thus, the net current, *I*, can be expressed by the Butler-Volmer equation [3, 9, 10]:

$$I = - FAk_0 \left[\exp \left[\frac{-\alpha F(E - E_f^0)}{RT} \right] C_A^* - \exp \left[\frac{+\beta F(E - E_f^0)}{RT} \right] C_B^* \right] \tag{1.9}$$

where C_A^* and C_B^* are the surface concentration of the corresponding species discussed in Equation 1.4. This equation describes how the observed current varies as a function of the transfer coefficient and overpotential. When there is a large k_0, little to no overpotential is required to drive the electrochemical reaction; this is known as reversible process. However, when the k_0 is small, a larger overpotential is required; otherwise known as an irreversible process. These processes will be further discussed in Section 1.7.1.

In contrast to the Butler-Volmer model, the Marcus-Hush model rationalizes the electron transfer kinetics in terms of the system's properties, such as electrode material, electroactive species, and/or solution. [2, 11-15] Marcus-Hush theory is non-empirical and extracts information about the rearrangement of chemical and solvents bonds. On the contrary to Butler-Volmer where the rate constants increases exponentially with increasing overpotential, the rate constant reaches a limiting value in the Marcus-Hush theory. [11] However, this in true for metallic electrodes with different Fermi levels, as this thesis mainly uses carbon electrodes, this model does not necessarily hold true for non-metallic electrodes. Nonetheless, this highlights the importance of mass transport, which is to be discussed in the next section.

1.3 Mass transport

Mass transport is the movement of species from one location to another in the solution. [1] Especially when electrode kinetics can become relatively fast, reaction rates can be controlled by the transport of electroactive materials. Mass transport is a fundamental process in electrochemistry and controls much of the observed behaviour

alongside electron transfer theory. [1, 2] There are three main forms of mass transport, diffusion, migration, and convection. [1, 2, 16]

1.3.1 Diffusion

Diffusion is an important factor in any electrode process, as it is the spontaneous movement of species as a result of a change in concentration gradient. [1, 2] When a potential is applied to an electrode placed in a solution containing electroactive species, a depletion of this species occurs resulting in a change in concentration gradient at the electrode surface. Therefore, diffusion allows new species from the bulk solution to be renewed at the electrode surface. For the general case of linear diffusion to a planar surface, Fick's first law applies [17],

$$J = -D\,\frac{dC}{dx} \tag{1.10}$$

where J is the flux, $\frac{dC}{dx}$ is the concentration gradient at the point x and D is the diffusion coefficient. The law states that at a given point, the flux (moles cm^{-2} s^{-1}) is proportional to the diffusion coefficient and concentration gradient of the product. Then, to express the flux in terms measured current, I, in respect to the number of moles passing through a unit area in a unit time, the flux is quantified by

$$J = \frac{I}{nFA} \tag{1.11}$$

where n is the number of electrons, F is the Faraday constant (96485 C mol^{-1}), and A is the area of the electrode.

In the case of 'diffusion only' conditions, Fick's second law (Equation 1.10) describes the rate of concentration change in solution over time.

$$\frac{\partial c}{\partial t} = D\frac{\partial^2 C}{\partial x^2} \tag{1.12}$$

1.3.2 Migration

Migration is the movement of charged species under the influence of an external electric field and it is the second form of mass transport to be discussed. [1] This type of transport at the electrode-solution interface is due to the potential difference between the electrode and the solution. [8] Often this becomes a problem in experimental reality as the movement of charged species is not easily predictable. To overcome this, a chemically and electrochemically inert background electrolyte is added to the solution at high concentrations. [2, 8] The large quantity of electrolyte increases the conductivity of the solution and thus decreases the resistivity for the passing current. [8] In addition, adding supporting electrolyte decreases the potential difference at the electrode-solution interface and maintains a constant ionic strength in the solution during electrolysis, in comparison to the species already present in the solution. The latter is important to species which are easily influenced by ionic strength. Other benefits of adding supporting electrolyte includes fixing the activity coefficients in order to facilitate in the use of formal potentials and it compresses the diffusion layer to a distance that is compatible with electron tunnelling. For electrochemical experiments described in this thesis, 0.1 M potassium chloride was typically added to each solution.

1.3.3 Convection

Convection is the movement of material in solution resulting from external mechanical forces. [1] There are two forms of convection; natural and forced convection. In the case of natural convention, it can occur either from random vibrations in the laboratory or from density/thermal gradients due to a chemical change at the electrode surface when a potential is applied. Nonetheless, natural convection is usually undesirable and can cause experimental irreproducibility. In the case of forced convection, it usually consists of stirring or sparging the solution with an inert gas in order to deliver fresh electroactive species to the electrode surface at a known rate. This is often used in hydrodynamic studies (i.e. sonoelectrochemistry, rotating disc electrodes, or flow cells) where these studies intentionally incorporate mechanical convection to avoid natural convection. [2, 18, 19]

1.4 Faradaic and non-Faradaic processes

There are two types of processes that could occur at the electrode: Faradaic and non-Faradaic. [1, 2] When the electroactive species is able to oxidize or reduce due to the transfer of electrons at the solution-electrode interface, this process is Faradaic. This process in is dictated by Faraday's law,

$$m = \frac{Q}{nF} \tag{1.13}$$

where m is moles of product formed or consumed reactant, Q is charge, and n is the number of electrons. The Faraday constant is the value of the charge passed per mole of electrons. However, in experimental reality not all observed current passed at the

electrode-solution interface is purely Faradaic. The currents described in this thesis *may* have contribution of non-Faradaic processes.

A non-Faradaic process is defined as any reaction where the electrons do not cross at the electrode-solution interface. [1, 2] Contributions towards a non-Faradaic process may come from a change in solution compositions at the electrode-solution interface. This interface is otherwise known as the electrical double layer.

1.5 Electrical double layer

The electrical double layer is essentially where an array of different ions and solution dipoles adjacent to the charged electrode surface can reorganize when a potential is applied. [1, 2] First postulated by Helmholtz, it is the simplest model describing the double layer structure. [20, 21] In his model, the counter-charge resides at the surface of the electrode once it is placed in solution; this results in a charge separation at the electrode-solution interface.

Figure 1.1 depicts a schematic representation of the electric double layer. In the first region closest to the electrode, there are ions and solvent molecules that are specifically adsorbed onto the electrode surface; the distance, x_1, from the electrical centers of these molecules to the electrode surface is referred to as the inner Helmholtz plane (IHP). The next layer is referred to as the outer Helmholtz plane (OHP); this is the closest distance, x_2, to which solvated ions can approach the electrode surface. [1, 2] The extent of the double layer from the electrode surface varies with potential and electrolyte concentration. The potential decreases linearly with distance from the electrode surface to the OHP then decreases exponentially from the OHP to the bulk

solution. For experimental electrochemistry, the double layer compresses with increasing supporting electrolyte concentrations.

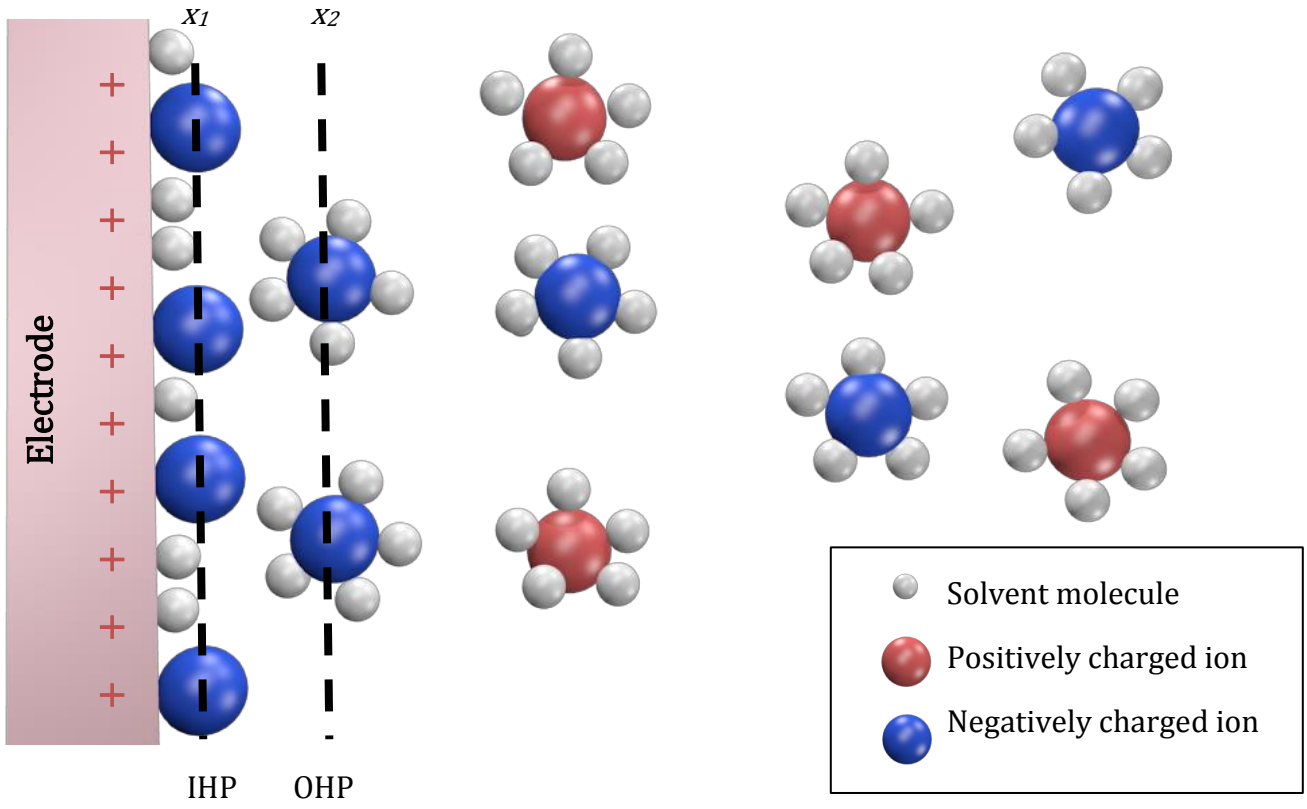

Figure 1.1 Schematic representation of the electrical double layer.

1.6 Electrochemical cell

In order to measure the current at the electrode-solution interface, an electrochemical cell containing electrodes must be set-up, such that a closed circuit is established. For large sized electrodes, a three-electrode system is commonly used and is comprised of a working electrode (WE), a reference electrode (RE), and a counter electrode (CE) (see Figure 1.2). Typically, a potential is applied to the working electrode

and measured accurately alongside to the reference electrode, whilst a current is passed between the working and counter electrodes. The working electrode is where the reaction of interest and under study takes place (specifics pertaining to this thesis are discussed in Section 3.3). The function of the counter electrode is to pass the same current seen flowing through the working electrode, therefore, the choice of counter electrode material is important as it should be inert and sufficiently large enough to hold the passing current (i.e. carbon rod or platinum wire/mesh).

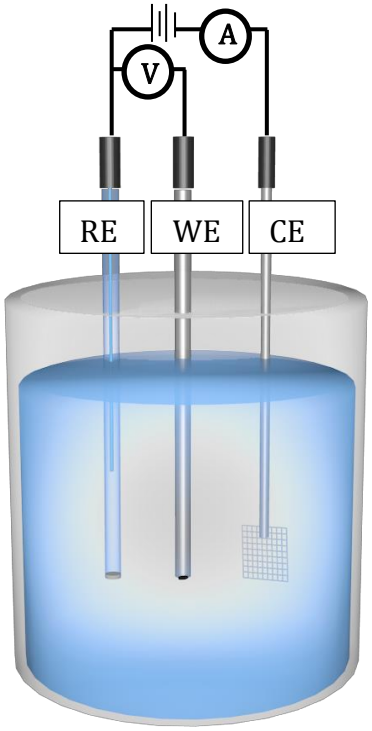

Figure 1.2: Schematic diagram of a three electrode electrochemical cell.

The reference electrode is important in an electrochemical system as its purpose is to provide a stable and accurate reference potential value against the measurement of

the working electrode. Typically, the standard hydrogen electrode (SHE) is the primary reference and by convention, its potential is zero. The equilibrium for SHE is as follows:

$$\mathrm{Pt} \mid \mathrm{H_2}\ (g, 1\mathrm{atm}) \mid \mathrm{H^+}\ (aq, a = 1) \qquad (1.14)$$

Although, this standard of reference is not ideal for regular experimental practice, a range of suitable reference electrodes are available to the users based on the experimental conditions (most notably, the solvent). [22] This thesis will describe experiments undertaken in aqueous conditions with a saturated calomel reference electrode (SCE) whereas in some experiments involving screen-printed electrodes, a quasi-silver reference electrode built into the chip is utilized.

A saturated calomel reference electrode is comprised of a seal tube containing saturated potassium chloride solution with potassium chloride solids. The solution is in contact with mercurous chloride (Hg_2Cl_2) mixed with liquid mercury. This tube is usually sealed with a porous frit at the end allowing the chloride activity to be constant between the electrode and the bulk solution. The potential determining equilibrium for the saturated calomel electrode is as follows:

$$\mathrm{Hg} \mid \mathrm{Hg_2Cl_2} \mid \mathrm{KCl\ (saturated\ in\ water)} \qquad (0.242\ \mathrm{V}\ \textit{vs.}\ \mathrm{SHE}) \qquad (1.15)$$

For the silver quasi-reference electrode built into the screen-printed electrode, its potential equilibrium is not well-defined, in respect to the SHE., due to its sensitive dependency of the electrolyte environment. The term ‘quasi’ suggests that it is ‘essentially’ or ‘almost’ a reference electrode. [1, 22] It is often employed as a reference electrode in sensors or when undesirable for the test solution to be contaminated with species from the reference junction, examples include chloride or sulfate ions. As a result of this, the quasi-reference is prone to large variation with up to *ca.* estimated 40

mV shifts in reference potential. [1, 22, 23] For the interest of the studies described in this thesis, a saturated calomel reference electrode was initially used first to obtain a more accurate potential measurement then a quasi-silver reference electrode was subsequently employed.

1.7 Electrochemical methods

As this thesis will utilize electrochemical techniques in order to determine a methodology for detection of thiol-containing molecules, a basic understanding of those techniques is necessary. The following section will describe the background on cyclic voltammetry and square wave voltammetry.

1.7.1 Cyclic voltammetry

1.7.1.1 Diffusional system

In cyclic voltammetry (CV), a potential is applied to the working electrode and is varied linearly with time from the initial potential, E_1, to the second, E_2, at a sweep rate, υ, and then back to E_1. The potentials E_1 and E_2 are chosen to embrace the process of interest. Figure 1.2 shows how the triangular potential sweep relates to the voltage scan rate, υ, and the resulting cyclic voltammetry profile for a reversible system. The resulting current-potential voltammogram depicts the current flow measurement at the working electrode as a function of the applied potential. Depending on the scan direction selected, an oxidation or reduction reaction will occur.

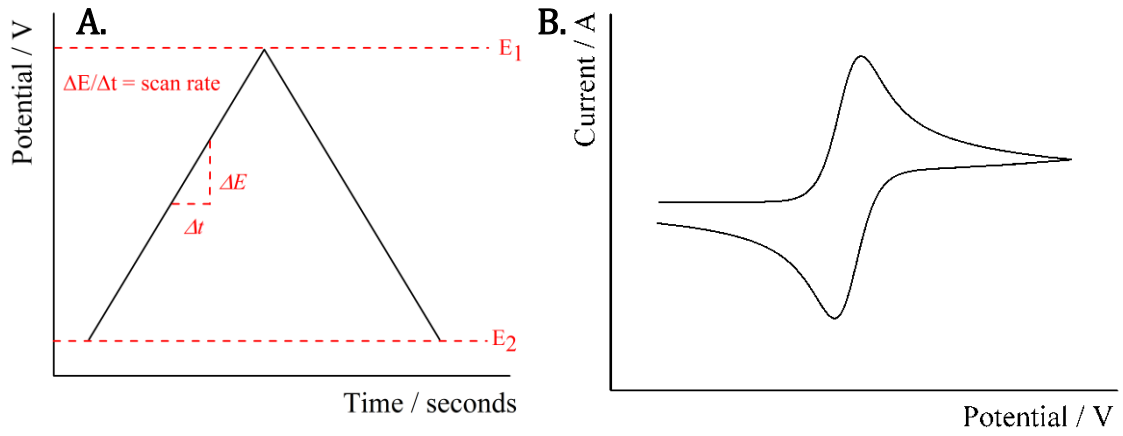

Figure 1.3: A. triangular potential sweep used in cyclic voltammetry and B. cyclic voltammetric profiles at a macroelectrode for a reversible reaction.

For a general reversible diffusional system, a typical cyclic voltammogram is shown in Figure 1.3. At the beginning, no faradaic current is measured due to insufficient potential being applied to drive the electrode process. As the potential increases, the current increases approximately exponentially until the mass transport of electroactive species to the electrode becomes limited at the higher potentials for which then the current decreases thus giving rise to the observed peak in the voltammogram. Subsequently on the reverse scan, an analogous peak is observed in the voltammogram, due to the product undergoing the reverse processes, electrolyte reconversion and then depletion.

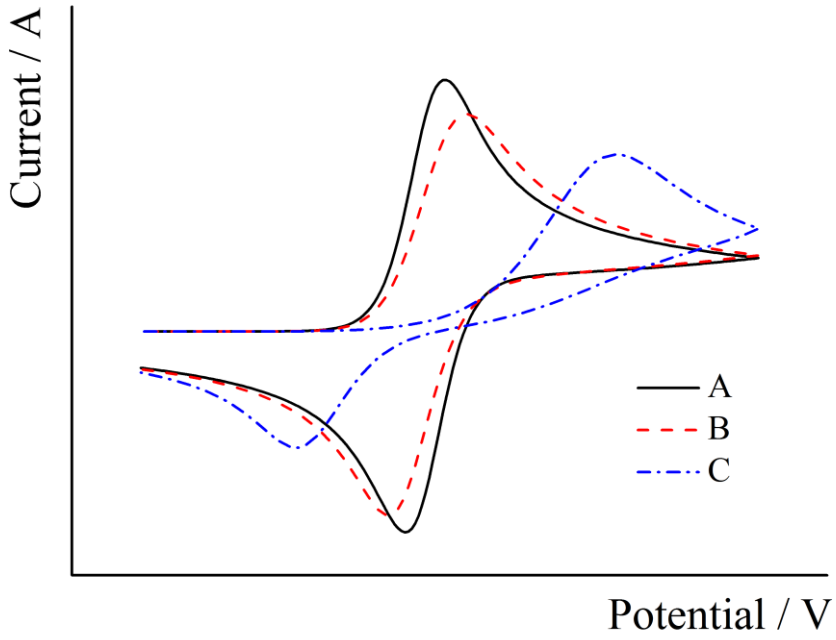

Figure 1.4: Cyclic voltammetry profiles of A. reversible, B. quasi-reversible, and C. irreversible electrode process.

There are three general voltammetric profiles for a simple schematic voltammogram for the reaction in Equation 1.1, one can observe on a macroelectrode using cyclic voltammetry; reversible, quasi-reversible, and irreversible (illustrated in Figure 1.4). The interpretation of these classifications on the voltammogram can generally be based on two criteria; the peak current as a function of scan rate and the peak-to-peak separation of the forward and backward scans. In this thesis, the interpretation of the mass transport mechanism of the reaction of interest is strongly based on these criteria. In the reversible scenario, the electrode kinetics is fast relative to the mass transport on the time scale that the A/B redox equilibrium is achieved at the electrode surface such that the Nernst equation described the surface conditions of A and B,

$$A + ne^- \leftrightarrows B \tag{1.16}$$

The peak current, I_p, can be described by the Randles-Ševčík equation [1, 2, 24-26]:

$$I_p = (2.69\ x\ 10^5)n^{1.5}AD^{0.5}Cv^{0.5} \quad (1.17)$$

where n is the number of electrons transferred, C is the concentration of the electroactive species at the electrode surface, A is the area of the electrode surface, D is the diffusional coefficient and υ is the scan rate. Note that the peak current is proportional to the square root of scan rate. The other criterion to help identify a voltammetric response of the reversible reaction is the peak-to-peak separation of the forward and backward peaks. This separation of the forward and backward peaks potential is given by $2.3RT/nF$, where when taking the difference of those potentials results in $57/n$ mV at 298K.

For the case of an irreversible process, the forward peak (oxidation or reduction) observed on the initial sweep has a large peak potential separation to its corresponding reverse peak. This is due to a large overpotential required to drive the electrode reaction. The peak current in this scenario is given by the Randles-Ševčík equation for an irreversible process [1, 2]:

$$I_p = 2.99\ x\ 10^5\ n(n' + \alpha_{n'})^{1/2}ACD^{1/2}v^{1/2} \quad (1.18)$$

where α is the transfer coefficient, n' is the number of electrons transferred before the rate determining step and all other coefficients are mentioned are similar to the reverse case. Note again, that the peak current is proportional to the square root of scan rate in this scenario. For the case of a quasi-reversible system, it is an intermediate between these two extreme cases.

1.7.1.2 Surface bound and thin layer voltammetry

Up until now the discussion in this chapter has been focused on diffusional systems, where the electroactive species can diffuse towards the electrode surface from the bulk. In some cases which will be covered in this thesis, species can adsorb onto the electrode surface thus eliminating diffusion effects in the experiments or a very thin layer of solution containing the electroactive species may be contained in the space above the electrode surface. [27-29] These may result in an observable difference in the cyclic voltammograms when compared to the semi-infinite diffusional system (see Figure 1.5). The characteristics are slightly different to the diffusional scenario but the same principles can be applied.

In the reversible case, the current is now only controlled by the potential and the amount of electroactive species on the surface. Once the species at the surface is oxidized or reduced on the forward scan, it may remain adsorbed to the surface until it is to be reduced or oxidized respectively on the reverse scan. In the electrochemically irreversible case, the same principle applies but the only difference is the peak-to-peak separation. The forward and backward peaks become more separated as compared to the electrochemically reversible case due to slower kinetics and thus requiring a larger overpotential to drive the reaction. Overall for such a case of surface bound species / thin layer system, the peak current, I_p, is proportional to scan rate, υ.

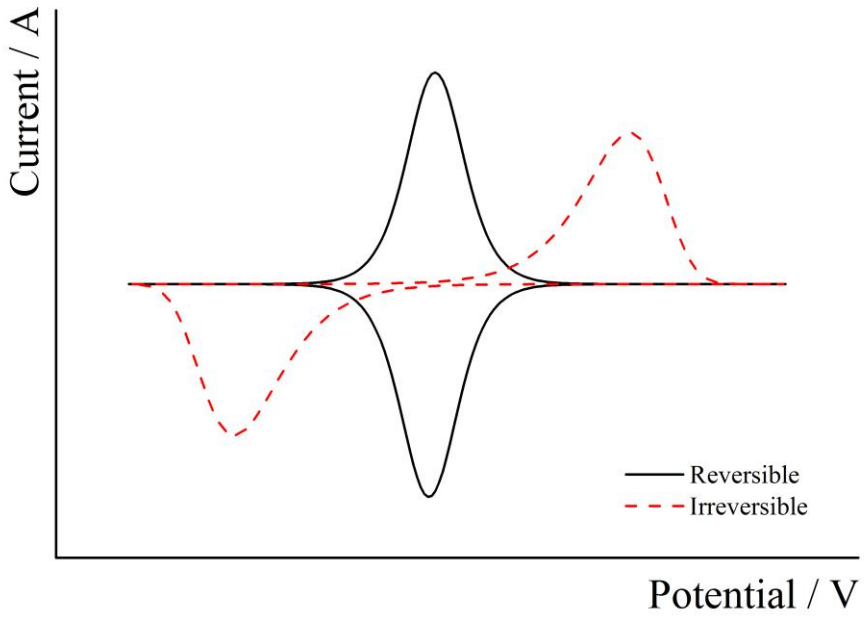

Figure 1.5: Reversible (solid) and irreversible (dotted) cyclic voltammetry profiles of surface bound species.

1.7.2 Square wave voltammetry

Square wave voltammetry (SWV) is a pulse technique based on a series of potential steps and heights on a linear time scale. [1, 2] The square wave parameters are characterized by pulse height, ΔE_p, staircase height, ΔE_s, pulse time, t_p, and cycle period, t_s. The pulse time term can often be expressed in terms of frequency, f,

$$f = \frac{1}{2t_p} \tag{1.19}$$

and since the staircase changes with ΔE_s at the start of each cycle, the scan rate can be expressed with

$$\frac{\Delta E_s}{2t_p} = f\Delta E_s \tag{1.20}$$

The basis for a square waveform and measurement can be seen in Figure 1.6. The figure shows that the measurement is made at two points of each cycle (point 1 and 2 in

Figure 1.6). These points represent the end of the forward and backward peaks respectively, where the difference can be seen expressed as $\Delta I = I_1 - I_2$ in Figure 1.7. This produces an advantage to using square wave voltammetry as the subtraction of I_1 from I_2 and the potential steps between the forward and backward interval is small; this results in high measurement sensitivity and the cancellation of the capacitative contribution.

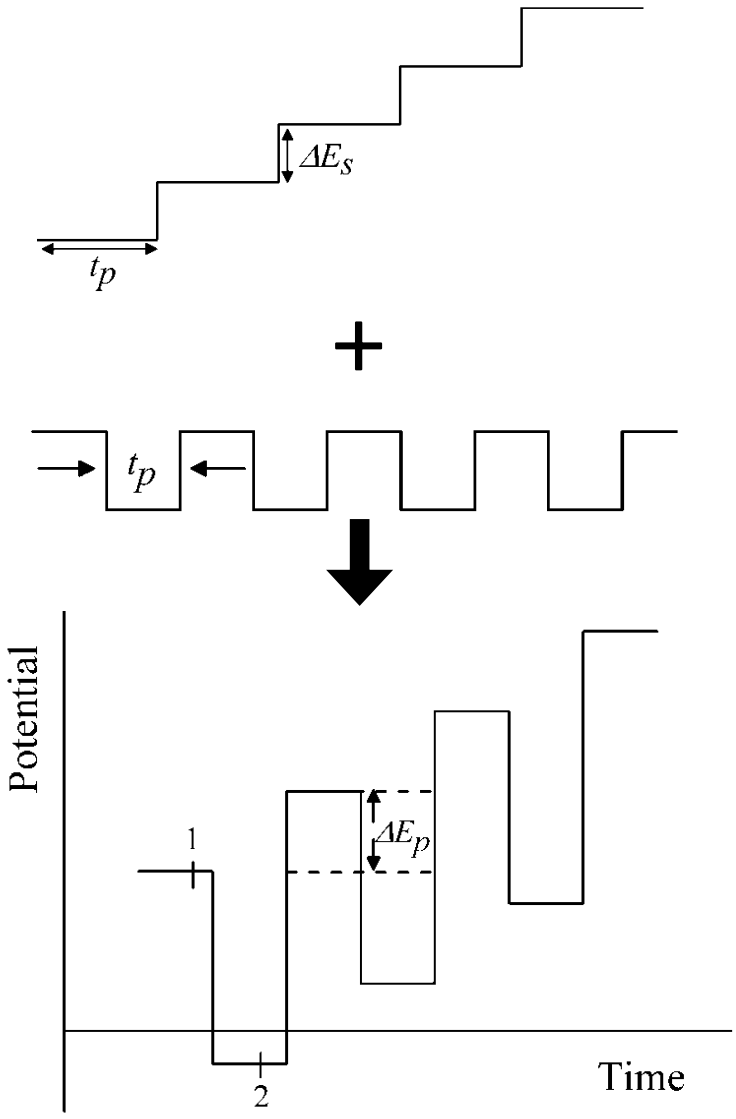

Figure 1.6: Square waveform and measurement schematic

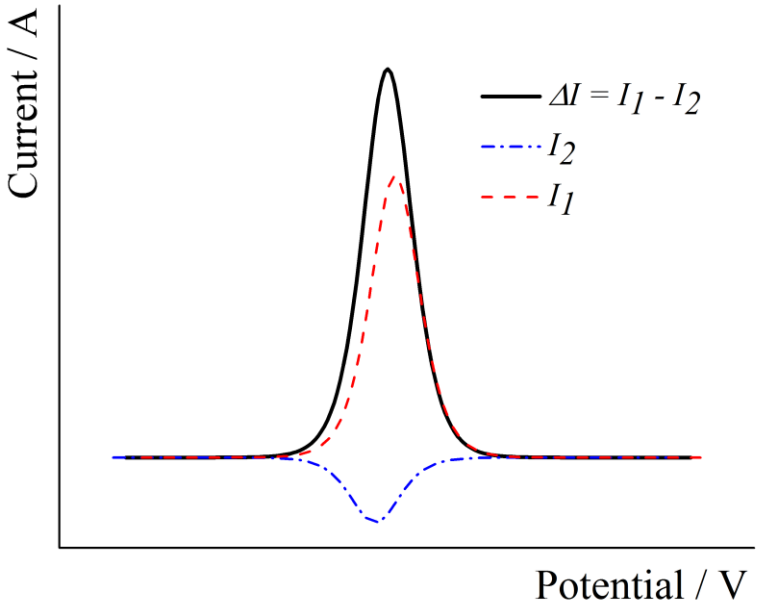

Figure 1.7: General depiction of a square wave voltammogram.

1.8 Conclusions

This chapter has described a brief overview on the fundamental electrochemistry and techniques necessary to support the discussions in this thesis. The following chapter provides an introduction to thiol containing molecules; particularly, their importance in biological systems and the state-of-the-art methods used to analytically detect them.

Chapter 2

Introduction to thiols

This chapter will discuss the importance of thiol-containing molecules in biological systems and their quantification using various analytical methods/techniques currently available for researchers and clinicians. These can be either non-electrochemically or electrochemically based. Depending on the application, the user typically chooses which option is best suited. Herein, the different methods to quantify thiol-based molecules will be compared and contrasted to and opportunities and needs identified.

2.1 Biological role

Thiol-containing molecules such as cysteine (Cys), homocysteine (HCys), and glutathione (GSH) are ubiquitous molecules prevalent in many biological systems (see Figure 2.1 for chemical structures). [30-34] They each have an important role in maintaining cellular metabolism and antioxidation protection. [32, 35-38] Their concentration levels are especially important as they are a reflection of the condition of the metabolic functions and homeostasis. [35, 39, 40] Thus, these thiol-containing molecules can be valuable biomarkers for clinical and/or biomedical related studies. Fortunately, thiol related compounds can often be found in various physiological fluids, such as blood plasma and saliva. [41-43] Therefore, clinicians and researchers can study

a variety of physiological fluids in order to better understand the biological processes at the cellular level. [30-33, 41, 42, 44-58] Table 2.1 shows the typical concentration range of each thiol found in their respective physiological fluid.

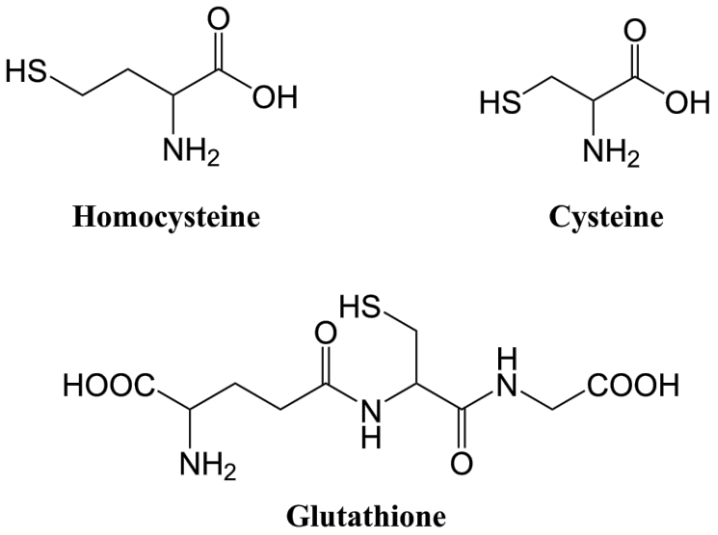

Figure 2.1: Chemical structures of some thiol-containing molecules.

Thiol name	Normal Range in plasma / µM	Normal Range in saliva / µM	References for plasma	References for saliva
Cysteine	10 - 30	5 – 100	[31, 42, 43, 59]	[46, 60]
Homocysteine	5 -15	2 – 5	[43, 61-64]	[46, 60]
Glutathione	2 - 12	5 - 30	[34, 41, 43, 52, 54, 58, 59, 65]	[46, 60]

Table 2.1: Literature values of thiol-containing molecules found in "apparently healthy" human subjects.

Apart from studies showing regular thiol management at the cellular level, case studies linking thiol concentrations to various subject-types are becoming more important and popular. Reports show that elevated levels of thiols may reflect deleterious conditions such as cancer [52, 65, 66], atherosclerosis [55, 65, 67, 68],

cardiovascular disease [42, 55, 61, 65, 69], Parkinson's disease [41, 42, 55], Alzheimer's disease [41, 42, 55, 70, 71], AIDs-related dementia [37, 55, 65], leukemia [36, 65, 66, 72], cystinosis [42, 64], hyperhomocystienemia [42], atherothrombotic vascular disease [68, 73], arterial disease [67, 73], diabetes [74], cardiovascular diseases [75, 76], xerostomia (dry mouth) [44], halitosis (breath malodour) [77, 78], and periodontitis. [77, 79-81] As such, selective detection and quantification is important for the biomedical community as it may provide a versatile diagnostic pathway to monitor various conditions.

2.2 Methods of analytical detection

This section will discuss the different types of analytical techniques, non-electrochemical and electrochemical, that are typically used in biomedical research and/or clinical applications to selectively detect thiols.

2.2.1 Non-electrochemical methods

There are a variety of non-electrochemical based methods and/or techniques available. [30, 38, 50, 55, 65, 79, 82-85] They often include chromatography coupled with mass spectroscopy [69-71, 86, 87], fluorescence [69, 70, 76], spectrophotometry [46, 62, 83, 88], and/or immunoassays. [69-71, 73] In particular, the use of high performance liquid chromatography (HPLC) is popular when compared to the number of other methods mentioned due to its high sensitivity and selectivity. [43, 58, 85, 89-92] Nonetheless, there are many options for the investigators to choose from to aid them in their scientific inquiries.

However, these methodologies and techniques often require complex instrumentations, laborious technical handling and chemical derivatization. [58, 69-71, 86, 91, 93-95] They also lack qualities that may be desired in a fast paced health-care environment such as rapid response, little to no sample preparation, cost effectiveness and ease of use. In addition, the monetary expenditures to procure, maintain, and handle the equipment can be quite expensive. Therefore, advances in applying a direct electrochemical measurement, in the form of electrochemical sensors [37, 38, 49, 96-109], would be preferred over these analytical techniques for their simplicity and practical use in real-world applications.

2.2.2 Electrochemical methods

The use of electroanalytical methods offer many potential advantages, especially in the form of a point-of-care sensor system, as it can be fast, cheap, and easy to use. [110, 111] Electrochemical sensor offers the option for the end user to have access to a simple portable unit promoting a point-of-use application with little to no sample preparation. [57, 87, 97] One common type of point-to-care sensor is based on screen-printed electrodes. [20-23] These compact, versatile, robust, and disposable electrochemical chip allows access to the users to perform tests wherever and whenever it is necessary. Screen-printed electrodes are becoming more attractive to the ever growing technology as they are ideal for applications that require high throughput. [112, 113]

However, reports have shown that electrochemical detection of thiols becomes a challenging task as the direct oxidation at a bare solid electrode gives a poor voltammetric response. [114] Redox mediators are often used to overcome this issue

but difficulties may lie in differentiating between similarly structured thiols. [36, 87] There have been tremendous efforts put forth towards developing a method for selective thiol detection with the use of electrochemistry but unfortunately not many offer selectivity without the use of extensive sample pre-treatments. [48, 49, 57, 85, 87, 89, 92, 93, 101, 103, 106, 115-117] When pre-treatments are required, they often include a separation technique (mentioned earlier) [48, 64] or use a scavenger reagent to prevent other analogous thiols from interfering in the electrochemical measurement in a partially non-aqueous system. [87, 118, 119] Therefore, a *selective* detection of thiol-containing molecule in aqueous solutions using electrochemical methods would be advantageous.

2.3 Aim and scope of thesis

The aim of this thesis will be to determine a suitable methodology for *selective* electrochemical detection of thiols, including cysteine, homocysteine, and/or glutathione. This is done by a combination of differing *ortho*-quinone derived mediators and carbon electrodes materials. Once the methodology is established, screen-printed electrodes are implemented to demonstrate the viability of a point-of-care type sensor; initially in buffer solutions then realized in synthetic and real physiological fluids.

Chapter 3

Experimental methods

This chapter outlines all chemical reagents, experimental methods, and electrode preparation procedures used for the experiments presented in this thesis; specific descriptions of each experiment and/or reagents can be found in the relevant experimental sections of Chapters 5-7.

3.1 Chemical reagents

All reagents described in this thesis can be found in Table 3.1 along with their purity and supplier.

Chemical name	Formula	Purity	Supplier
5,5'-dithiobis(2-nitrobenzoic acid)	$C_{14}H_8N_2O_8S_2$	≥98 %	Sigma-Aldrich
5-sulfosalicyclic acid dihydrate	$C_7H_6O_6S$	≥99 %	Sigma-Aldrich
Acetic acid	$C_2H_4O_2$	99.50%	Sigma-Aldrich
Ammonia nitrate	NH_4NO_3	≥98%	Sigma-Aldrich
Ascorbic acid	$C_6H_8O_6$	99%	Sigma-Aldrich
Boric acid	H_3BO_3	99.50%	Sigma-Aldrich
Caffeic acid	$C_9H_8O_4$	>98 %	Sigma-Aldrich
Captopril	$C_9H_{15}NO_3S$	≥98 %	Cambridge Biosciences Ltd.
Catechol	$C_6H_6O_2$	99%	Sigma-Aldrich

Citric acid	$C_6H_8O_7$	98%	Sigma-Aldrich
Cysteine	$C_3H_7NO_2S$	97%	Lancaster Synthesis
Deionized water	H_2O	18.2 MΩ cm	Millipore
Dimethyl sulfoxide	C_2H_6OS	≥99.9 %,	Sigma-Aldrich
Dulbecco's Modified Eagles's Media	–	–	Sigma-Aldrich
Ethylenediaminetetraacetic acid	$C_{10}H_{16}N_2O_8$	≥98 %	Sigma-Aldrich
Glutathione (oxidized)	$C_{20}H_{32}N_6O_{12}S_2$	≥98 %	Sigma-Aldrich
Glutathione (reduced)	$C_{10}H_{17}N_3O_6S$	98%	Sigma-Aldrich
Glutathione reductase	–	–	Sigma-Aldrich
Graphite powder	–	≥99.99 %	Sigma-Aldrich
Homocysteine	$C_4H_9NO_2S$	≥95 %	Sigma-Aldrich
Human plasma	–	–	Sigma-Aldrich
Hydrochloric acid	HCl	37%	Fisher Scientific
Mineral oil	–	–	Sigma-Aldrich
Multi-walled carbon nanotube	–	>95 %	Nanolab Inc.
Nanocarbon	–	99%	Cabot Corporation
β-Nicotinamide adenine dinucleotide (NADH)	$C_{21}H_{27}N_7Na_2O_{14}P_2$	≥97%	Sigma-Aldrich
β-Nicotinamide adenine dinucleotide 2′-phosphate (NADPH)	$C_{21}H_{29}N_7O_{17}P_3$	≥97%	Sigma-Aldrich
Phosphoric acid	H_3PO_4	85%	Sigma-Aldrich
Potassium chloride	KCl	99%	Sigma-Aldrich
Potassium dihydrogen phosphate	KH_2PO_4	>98 %	Sigma-Aldrich
Potassium monohydrogen phosphate	K_2HPO_4	99%	Sigma-Aldrich
Potassium nitrate	KNO_3	99%	Sigma-Aldrich
Sodium bicarbonate	$NaHCO_3$	99.70%	Sigma-Aldrich
Sodium borohydride	$NaBH_4$	Technical grade	Fisher Scientific

Sodium carbonate	Na_2CO_3	ACS grade	BDH
Sodium citrate monobasic	$NaC_6H_5O_7$	98%	Sigma-Aldrich
Sodium nitrate	$NaNO_3$	≥99.5%	Fisons Analytical
Synthetic saliva	–	–	Synthetic Urine e.K
Tetrabutyl ammonia nitrate	$(CH_3CH_2CH_2CH_2)_4N(NO_3)$	≥99%	Fluka
Tetraethyl ammonia nitrate	$(C_2H_5)_4N(NO_3)$	≥99%	Fluka

Table 3.1: List of chemical reagents used in this thesis.

3.1.1 Buffer solutions

All buffer solutions were prepared with deionized water at a resistivity of no less than 18.2 MΩ cm^{-1} at 25 °C. Using the chemical listed in Table 3.1, the buffers were made according to the pH range required: Britton-Robinson buffer solution for pH range 1 – 2, citric acid/sodium citrate for pH range 3 – 6, potassium monohydrogen phosphate/potassium dihydrogen phosphate for pH range 7 - 8, and sodium carbonate/sodium bicarbonate for pH range 9 – 10. Britton-Robinson buffer is consisted of mixing boric acid, phosphoric acid, and acetic acid. All buffer solutions were made up with supporting electrolyte of 0.10 M potassium chloride (KCl). All pH measurements were conducted using a pH213 Microprocessor pH meter (Hanna instruments, UK). The pH meter was calibrated at 25 °C using Duracal buffers of pH 4.01 $\pm$ 0.01, pH 7.00 $\pm$ 0.01, and pH 10.01 $\pm$ 0.01 (Hamiliton, CH).

3.1.2 Synthetic saliva

Synthetic saliva was used as received in electrochemical experiments described in Section 7.2. The proprietary formulation of the synthetic saliva reflects the standardized production process of DIN 53160-1 [120], which contains no added thiol compound.

3.1.3 Commercial glutathione assay kit

The chemicals listed in the Sigma-Aldrich Glutathione Enzyme Assay Kit were purchased individually from Sigma-Aldrich. [121] The procedure was carried out accordingly and results are discussed in Section 7.3. They are comprised of ethylenediaminetetraacetic acid (EDTA, ≥ 98 %), glutathione reductase, reduced glutathione (98%), 5,5'-dithiobis(2-nitrobenzoic acid) (≥ 98 %, DTNB), 5-sulfosalicyclic acid dihydrate (≥ 99 %), β-nicotinamide adenine dinucleotide 2′-phosphate reduced tetrasodium salt hydrate (≥ 95 %, NADPH), and dimethyl sulfoxide (≥ 99.9 %, DMSO).

3.2 Electrochemical cell set-up

All electrochemical experiments were carried out in a Faraday cage containing a three electrode system. The three-electrode system consists of a saturated calomel electrode (SCE, Hach Lange, UK) as the reference electrode, a platinum mesh (99.99 %, Goodfellow, UK) as the counter electrode, and a glassy carbon electrode (GCE, CH Instruments, USA) as the working electrode (details are discussed Section 3.3).

For experiments involving screen-printed electrodes, the three electrodes employed in those studies are printed on a disposable chip (details are described in

Section 3.3.3). However, the quasi-silver reference electrode printed on the chip was occasionally substituted by a saturated calomel electrode, for a more reliable potential measurement. This will be discussed further in the corresponding sections presented in this thesis.

The three-electrode system is connected to a computer-controlled potentiostat, PGSTAT 101 (ECO-chemie, The Netherlands) and a temperature-controlled bath was used to ensure that all solutions are carried out at the desire temperature, (20 ± 0.1)°C.

3.3 Working electrode preparations

This section describes the preparation of the working electrode, glassy carbon electrode (GCE), carbon paste electrode (CPE), and multi-walled carbon nanotube screen-printed electrode (CNT-SPE), which are used in Chapter 5 - Chapter 7. In each experiment described and explained in this thesis, at least three electrodes (n=3) were performed three times.

3.3.1 Glassy carbon electrodes

Prior to all electrochemical experiments, a glassy carbon electrode (GCE, CH Instrument, USA) was polished with either alumina (Buehler, Germany) or diamond spray (Kemet, UK) on a polishing pad. Specifics will be noted throughout this thesis. For alumina, polishing was done sequentially in 1.0, 0.3, and 0.05 μm while polishing with diamond spray was done sequentially in 3.0, 1.0, and 0.1 μM. Afterwards, the polished electrode was rinsed twice with deionized water and dried carefully. The following two sections will describe the modification procedure performed on the glassy carbon

electrode modified that was used in accordingly in Chapter 5 and Chapter 6. The modifications were done with different carbon nanomaterials, nanocarbon and multi-walled carbon nanotubes.

3.3.1.1 Modification with nanocarbon

To prepare the nanocarbon modified glassy carbon electrode (NC-GCE) described in Sections 5.2 and 6.1, the immobilization of the nanocarbon (diameter = 14 ± 10 nm) onto the surface of the GCE was done via drop cast method. The drop cast method requiring taking a 3.0 μL aliquot of a nanocarbon-ethanol suspension (1:1 wt:wt) and dropping onto the surface of the polished GCE. A layer of carbon material remains at the surface of the carbon electrode after allowing the volatile solvent to evaporate at room temperature. A total of 50 μg nanocarbon was used to modify the NC-GCE. A sonication bath (Fisher Scientific, 230 V, 50 Hz) was used to ensure a full suspension of the nanocarbon-ethanol solution prior to drop casting. The modification to make the nanocarbon modified glassy carbon electrode (NC-GCE) was done prior to each experiment.

3.3.1.2 Modification with multi-walled carbon nanotubes

The modification of the glassy carbon electrode with bamboo-like multi-walled carbon nanotubes (30 ± 10 nm in diameter, 5 - 20 μM in length) was made at the start of each electrochemical experiment described in Sections 5.2 and 6.2. The carbon nanotubes (CNT) were immobilized onto the surface of a freshly polished glassy carbon electrode through drop casting method as described in the previous section (Section

3.3.1.1). The drop cast suspension consisted of CNT in ethanol at a ratio of 0.1 mg/mL, where a total of 6 µg carbon nanotube was used to modify the GCE by drop casting 3.0 µL aliquot of the suspension. It was briefly sonicated using a sonication bath prior to drop casting to ensure a full suspension of the CNT-ethanol solution.

3.3.2 Carbon paste electrodes

Carbon paste electrodes (CPE) were utilized in some experiments discussed in this thesis (Section 5.4). Generally, these electrodes are comprised of a mixture of carbon powder, and a nonelectrolytic binder. [122, 123] Then the mixture is packed into a cavity of the working electrode. The working electrode is consisted of a Teflon tube with a copper rod (Figure 3.1) thus they can be facile, relatively cheap to fabricate, and easy to use. [122, 123] One of the advantages of carbon paste is the diverse applicability of the carbon material. [122-124] For results discussed in this thesis, the carbon powder was impregnated with a mediator precursor prior to preparing the paste. The paste consisted of mixing 70 µL of mineral oil with 200 mg of modified graphite powder, then packed into the cavity of the working electrode for it to be 'electrochemically activated' *in situ* prior to experiments.

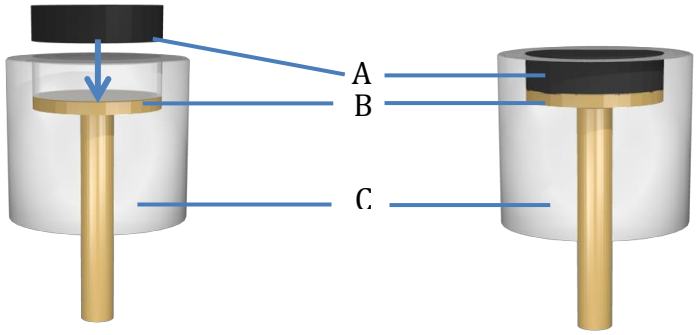

Figure 3.1: Diagram of carbon paste electrode. A. carbon-binder mixture, B. electrical contact, and C. Teflon tube housing.

3.3.3 Screen-printed electrodes

Some results discussed in this thesis are based on experiments performed at a multi-walled carbon nanotube screen printed electrode (CNT-SPE). This is done to demonstrate a quick and simple point-of-care technology for thiol detection. The disposable screen printed electrodes were acquired from DropSens (Asturias, Spain). They have a ceramic substrate and consist of a multi-walled carbon nanotube working electrode, a carbon counter electrode and a silver quasi-reference electrode. The surface area of the CNT-SPE was determined in-house with a variable scan rate study of the one electron reduction of 1.0 x 10^{-4} M hexaammineruthenium(III) chloride and 0.1 M potassium chloride solution; the average surface area was (0.11 $\pm$ 0.07) cm^2. Other characterization, for example scanning electron microscopy (SEM), can be found on the DropSens website. [125] For electrochemical experiments involving all three electrodes supplied on the screen-printed electrodes, an aliquot of approximately 50 µL of sample solution was deposited onto the ceramic chip taking care to ensure that all the electrodes were covered.

Prior to electrochemical experiments, the CNT-SPE underwent a pre-treatment to get rid of any *possible* silver residue on the working electrode as supplied. The pre-treatment essentially comprises of applying a potential cycling from -0.5 V to $+0.2$ V for an optimum time of 20 minutes (*ca.* 86 scans) in a solution of 0.1 M sodium nitrate with a mercury/mercurous sulphate reference electrode (MSE). After pre-treatment, the screen printed electrode was carefully rinsed with deionized water and dried. Figure 3.2 shows a cyclic voltammogram (50 mV s^{-1}) comparison of the screen-printed electrode before (solid line) and after (dashed line) the pre-treatment in 0.15 M phosphate buffer solution (PBS, pH 7.0). The figure shows that before pre-treatment, the peaks at potentials *ca.* $+0.1$ V and -0.05 V (*vs.* SCE) are associated with the oxidation of silver to form silver chloride and its reverse reaction. After the pre-treatment is applied, the cyclic voltammogram shows no appearance of the peaks associated with possible silver. For electrochemical experiments involving the screen-printed electrodes, a new electrode was used to prevent cross contamination.

Note that the silver quasi-reference electrodes built into the screen-printed electrodes are prone to large variation with up to, *ca.* estimated 40 mV shifts in reference potential. [1] As mentioned in Section 3.2, this thesis will discuss some results based on potential measurement at a saturated calomel electrode at the screen-printed electrode. This is to provide a more consistent reference value before employing the quasi-silver reference electrode printed on the chip.

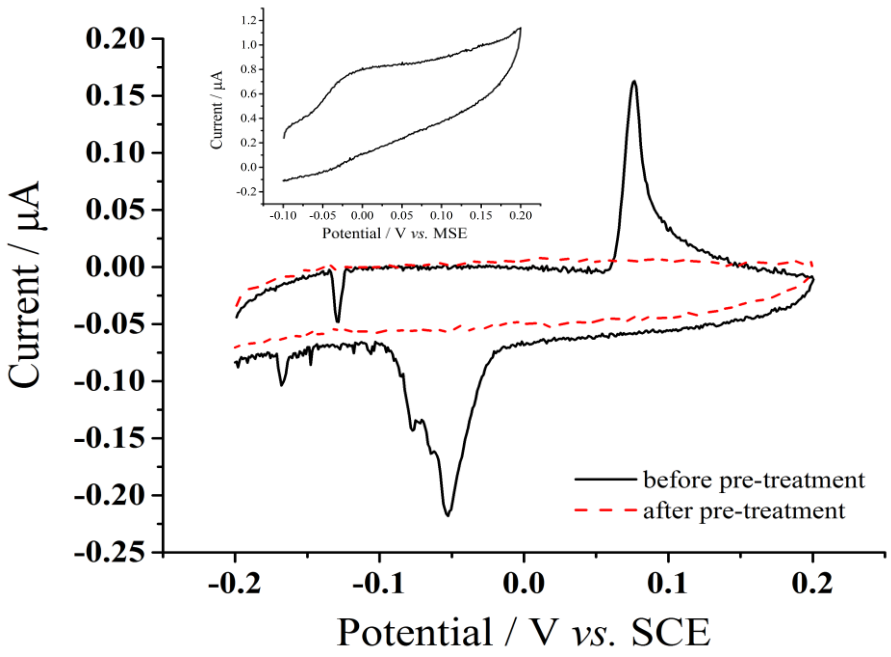

Figure 3.2: Cyclic voltammograms (50 mV s^{-1}) of screen-printed electrodes in 0.15 M PBS (pH 7.0, 20°C) of before (solid line) and after (dashed line) electrochemical pre-treatment. Inset: CV of screen-printed electrode in 0.1 M sodium nitrate solution prior to electrochemical pre-treatment.

3.3.4 Electroanalysis

3.3.4.1 Standard Addition Method

Standard addition method is a general method for measuring an unknown analyte concentration in a complex matrix sample. Such matrices contain species that have chemical properties similar to the target analyte and therefore become difficult to measure. This is known as the 'matrix effect' and occurs in samples [126], such as biological fluids. The standard addition method is a useful procedure to determine the desire analyte concentration in such matrices as it eliminates the 'matrix effect' in the complex solution. The method consists of spiking a sample with known amounts of a standard solution. The response before and after the additions are measured, then

plotted onto a calibration curve, which the concentration of the desired species is then determined. [126] This method assumes the response of the concentration to signal to be linear. This method should be repeated several times to ensure confidence.

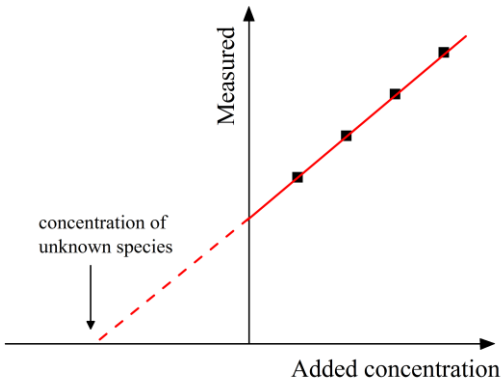

Figure 3.3. General representation of a standard addition plot for an analyte in an unknown sample.

3.3.4.2 Limit of detection

The term, limit of detection (LOD) refers to the smallest concentration of analyte that produces a signal, with reasonable confidence, which is significantly different from the blank signal, depending on the chosen analytical technique. This value is useful in comparing methods and/or instruments. For a method that requires a calibration curve, the limit of detection, consistent with the IUPAC definition, is defined as [127, 128]:

$$C = \frac{ks_B}{S} \tag{3.1}$$

where C refers to the concentration of the measured analyte, k is a numerical constant, s_B is the standard deviation of the blank measured, and S is the sensitivity of the method. The sensitivity of the method can also be referred to the slope of the calibration curve. The value of k is equal to 3, this constant is "strongly recommended" by IUPAC as it is three times the standard deviation units above the zero analyte equates to a 98.3 % confidence level. [126, 129, 130]

Chapter 4

Ortho-quinone reactions with thiol-containing molecules: Moderate overview

As mentioned in Section 2.3 this thesis focuses on discussing thiol detection using an *ortho*-quinone moiety. This short chapter will describe a general overview of two possible reaction mechanisms involving an *ortho*-quinone and a thiol-containing molecule along with their respective electrochemical behaviour. Scheme 4.1 outlines the two reaction pathways: A. electrocatalytic reaction and B. 1,4-Michael addition reaction. [37, 38, 52, 65, 87, 131-138]

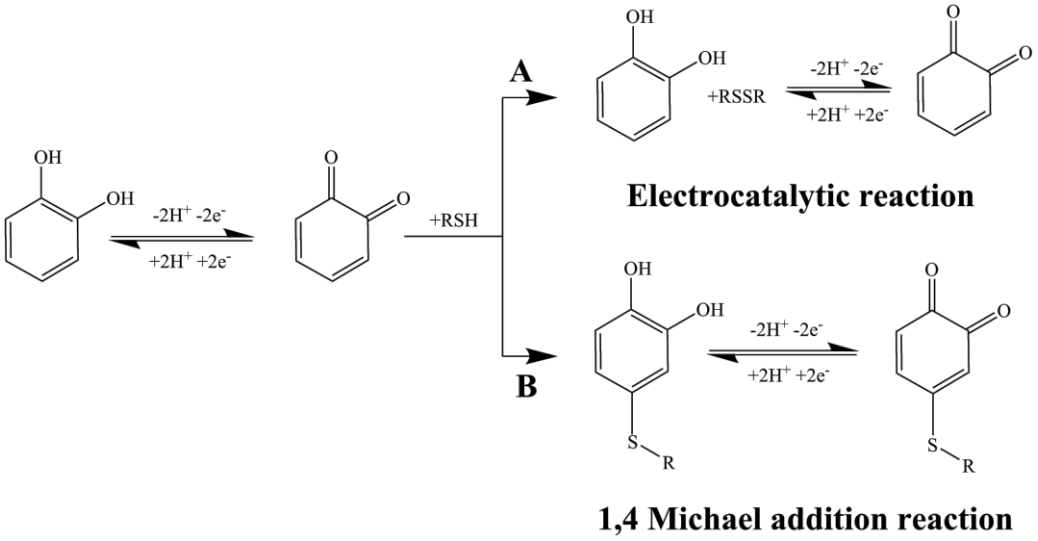

Scheme 4.1: Reaction mechanism of an *ortho*-quinone reaction with a thiol-containing molecule via A. electrocatalytic reaction or B. 1,4-Michael addition reaction.

4.1 Electrocatalytic reaction

In an electrocatalytic reaction, 1,2-dihydroxyquinone (catechol) undergoes a two-electron, two-proton electrochemical oxidation to form an *ortho*-benzoquinone (*o*-quinone) which then can mediate the reduction of a thiol species, RSH, to form a disulfide, RSSR. [52, 65, 135, 139-142]

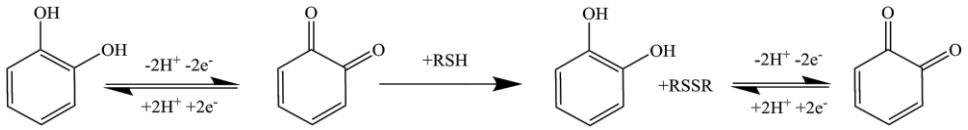

(4.1)

This type of reaction continually involves two electrons and two protons per RSSR formed as the reaction can regenerate itself to the starting species from the electrons at the electrode. As a result, the amperometric current can be monitored to give an analytical signal. [140] A typical cyclic voltammogram will show an increase in forward peak current as the back peak current decreases with increasing thiol concentration (Scheme 4.2). For this type of mechanism, no new signal will appear in the voltammogram due to the continuous involvement of a two electron process. [52, 137]

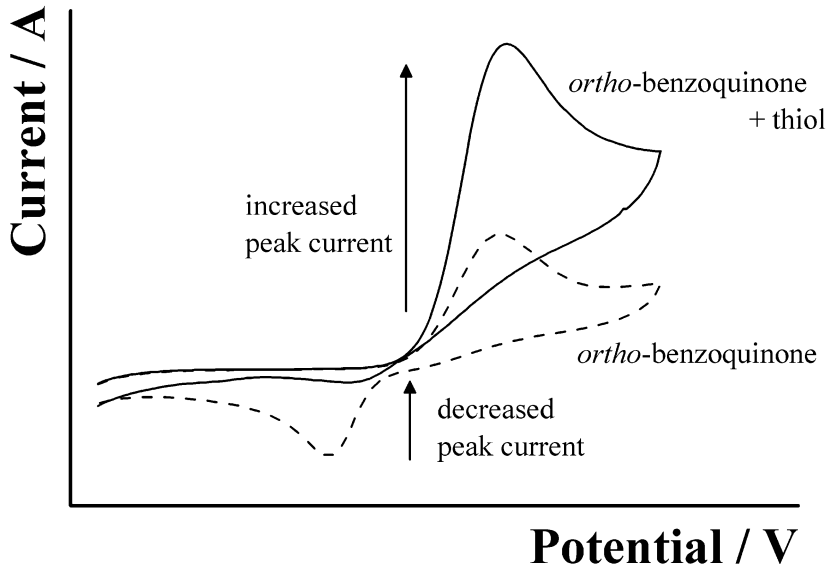

Scheme 4.2: General voltammogram representation of an electrocatalytic reaction of an *ortho*-benzoquinone with a thiol.

4.2 1,4-Michael addition reaction

The second possible pathway is through a 1,4-Michael addition reaction. In this reaction, the 1,2-dihydroxyquinone (catechol) is first electro-oxidized to form an *ortho*-benzoquinone (*ortho*-quinone). Then the *ortho*-benzoquinone undergoes nucleophilic attack from a thiol, resulting in a new electrochemically active species. [37, 131, 133, 143] This type of reaction will initially involve a two electron, two proton process to oxidize the 1,2-dihydroxyquinone then an additional two electrons will be required for the nucleophillic attack to take place with the thiol-containing molecule, thus involving a net total of four electron process. [37, 38, 65, 131, 136] During the nucleophilic attack, the *ortho*-quinone regenerates back to a hydroquinone entity, which can be re-oxidized again with two electrons and two protons.

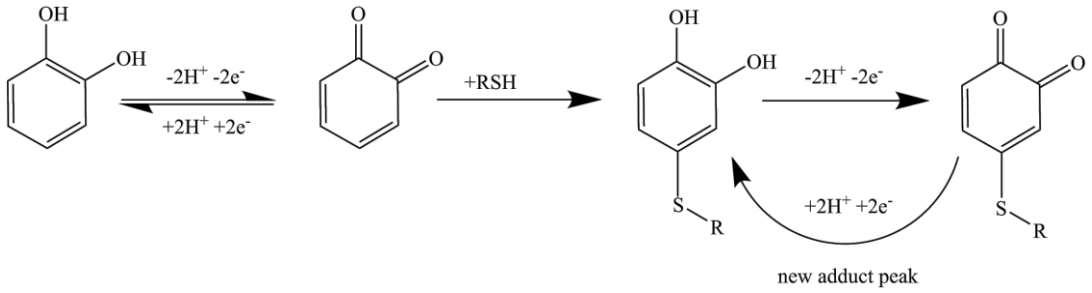

(4.2)

Scheme 4.3 depicts a typical cyclic voltammogram for this type of reaction; as it will typically show an increase in forward peak current as the back peak current decreases with increasing thiol concentration. In addition, a new peak potential away from the parent quinone peak can emerge due to the addition reaction. [37, 131, 133, 143] In this reaction pathway, the adduct signal is analytically useful the peak current increases with concentration of thiol species. [37] This new adduct peak signal in this reaction can present an analytical basis for thiol detection.

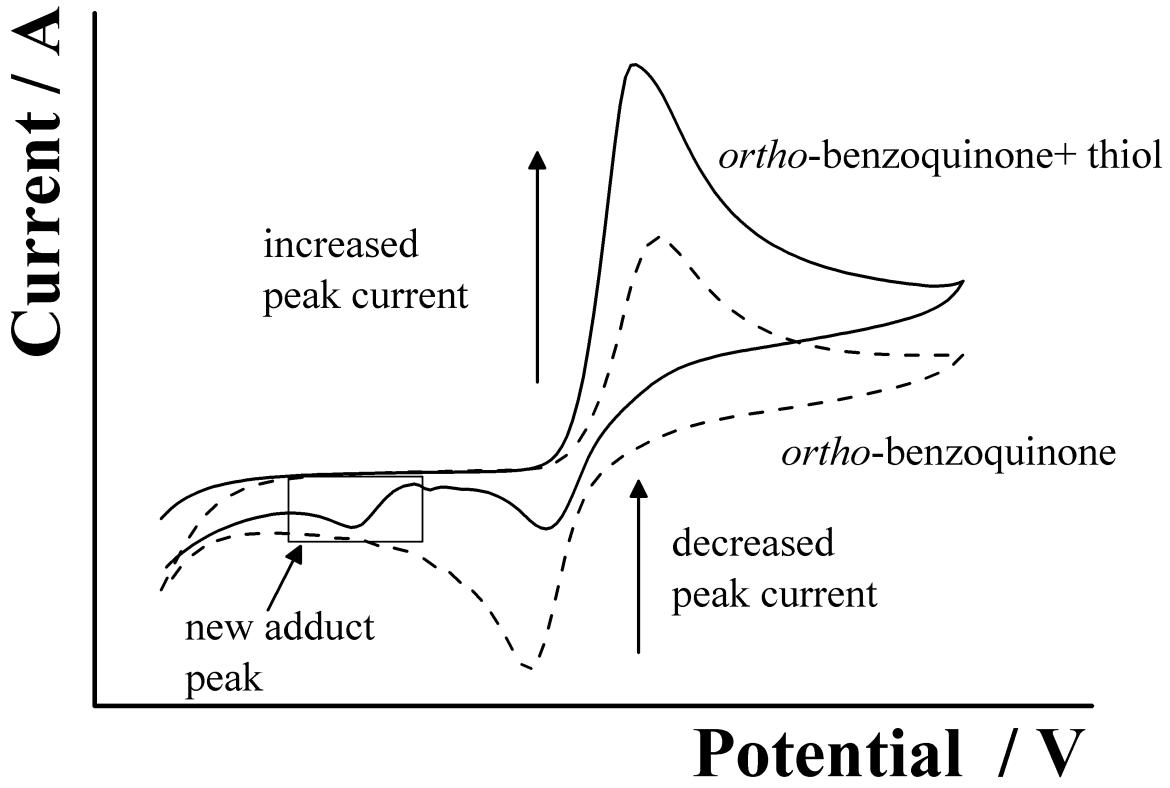

Scheme 4.3: General voltammogram representation of an 1,4-Michael addition reaction of an *ortho*-quinone with a thiol.

Chapter 5

Thiol detection via electrocatalytic reaction

This chapter will focus on the electroanalysis of thiol species via the electrocatalytic reaction, introduced in the previous chapter. This will be investigated using different *ortho*-quinone precursor in combination with different forms of carbon electrode to determine the best method for thiol detection. The proof-of–concept methodology discussed herein will then be preliminary tested in such samples typically used in the bio-medical research community.

The work presented in this chapter has been published in *Electroanalysis* [137, 141, 144] and *Analyst* [134]. This chapter includes *o*-quinone based mediators, poly(caffeic acid) and cyclotricatechylene, modified onto a glassy carbon electrode. The precursor to cyclotricatechylene discussed in Sections 5.3 and 5.4 was synthesized by Ms. Athanasia Karina, Dr. James E. Thomson and Professor Steve G. Davies. Characterization using scanning electron microscopy was performed by Mr. Chris Salter and Dr. Colin Johnston.

5.1 Electrochemical detection of NADH, cysteine, or glutathione using caffeic acid modified glassy carbon electrodes

5.1.1 Introduction

The development for a fast, sensitive, robust, cost effective sensor with low detection limits has been a main focus in the bioanalytical sciences for the past two decades. [110, 111, 113, 145] Carbon-based electrodes are often one of the many types of electrodes to satisfy these requirements towards developing an effective sensor. [146] In particular, amperometric based sensors are popular because they can offer high sensitivity over a linear range. [111, 147] This type of detection is especially important in bioanalytical sciences when it comes to detecting low concentrations (submolar range) of specific biomarkers, such as β-nicotinamide adenine dinucleotide (NADH), cysteine, and glutathione, to monitor conditions that may alter the cellular metabolic redox reactions required to regulate normal biological activities. [35, 39, 40]

For the interest of this section, poly(caffeic acid) (Figure 5.1) has been chosen to facilitate in the direct electron-transfer between the target biological molecule and the carbon electrode via the *ortho*-quinone moiety through surface immobilization using electropolymerization methods. There have been other reports on the immobilization of catechol being used in detecting biological molecules, varying in detection range as low as 0.50 μM to as high as 1.0 mM. [145, 146, 148] In this section, we will demonstrate the possibilities of having an *ortho*-quinone group as the sensing molecule for detection of specific biomarkers, β-nicotinamide adenine dinucleotide (NADH), cysteine, and glutathione, through electrocatalytic oxidation.

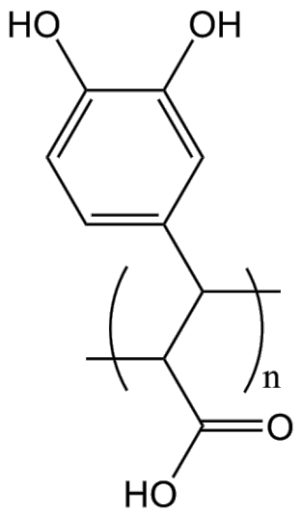

Figure 5.1: Chemical structure of poly(caffeic acid).

5.1.2 Experimental Procedures

5.1.2.1 Electrode preparation

The poly(caffeic acid) modification onto a glassy carbon electrode, GCE, is similar to that reported by Zare et al [148] but with alternatives to the solutions used. The GCE electrode was first polished accordingly to Section 3.3.1. The freshly alumina polished electrode was then electrochemically activated, by placing the three-electrode system in 0.10 M sodium bicarbonate solution and applying a continuous potential cycle from −1.10 V to +1.60 V with a sweep rate of 100 mV s^{-1} until a stable voltammogram was achieved, *ca.* 8 cycles. After carefully rinsing the electrode with deionized water, the deposition of polycaffeic acid was achieved in a solution of 2.0 mM caffeic acid mixed with 0.15 M phosphate buffer (pH 4.0) through cycling between +0.10 V to +0.90 V, at a sweep rate of 20 mV s^{-1}, for an optimum time in the solution of 5 minutes (*ca.* 4 scans). The electrode was rinsed and dried carefully before proceeding with all electrochemical experiments.

5.1.3 Results and discussion

This section first describes the optimization of the electrodeposition of the mediator, poly(caffeic acid), by changing the deposition parameters such as time, caffeic acid concentration, and cationic supporting electrolyte. Secondly, an understanding of the voltammetric behaviour of the redox species at the electrode surface is necessary before detection of any kind. Then finally, an investigation of the electrochemical determination of NADH, cysteine, and glutathione was conducted.

5.1.3.1 Characterization of CAF-GCE

Prior to the electrochemical detection of the target analyte, an electrochemical characterization of the poly(caffeic acid) modified glassy carbon electrode was undertaken. The poly(caffeic acid) film was electrodeposited onto the activated glassy carbon electrode at an optimal deposition condition of potential cycling for 5 minutes in a solution of 2.0 mM caffeic acid (pH 4.0). To determine this optimum condition, a range of different deposition time (2 - 20 mins.) was applied at different concentrations of caffeic acid (1.0 - 3.0 mM) for the surface coverage of the poly(caffeic acid) film to be calculated and compared against each other. The surface coverage (Γ) was calculated using,

$$\Gamma = \frac{Q}{nFA} \tag{5.1}$$

where the charge (Q) was determined by integrating the anodic peak current, n is the number of electrons (n=2), and A is the surface area of the glassy carbon electrode. As a result, as shown in inset to Figure 5.2, the trend shows that with all concentrations of caffeic acid, the surface coverage increases to a maximum at a certain deposition time

and then decreases afterwards. In comparison with all three concentrations, it is with 2.0 mM of caffeic acid at 5 minutes where the greatest coverage and signal is observed under these modification conditions, *ca.* 9 x 10^{-10} mol cm^{-2} at a scan rate of 100 mV s^{-1}. This surface coverage ensures the greatest coverage and signal. This section will report analytical experiments under this deposition condition.

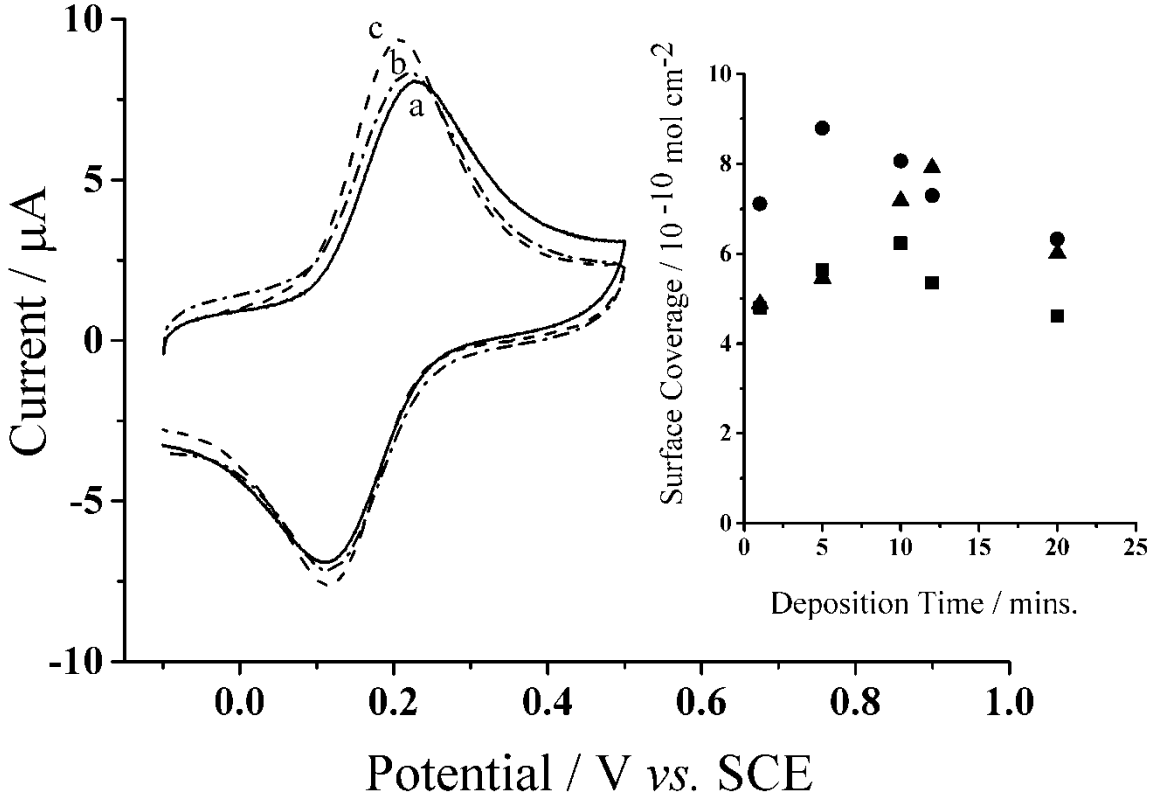

Figure 5.2: Resulting cyclic voltammograms of CAF-GCE in PBS (pH 7.0) at maximum surface coverage at maximum deposition time of concentration of caffeic acid, pH 4.0, at scan rate of 100 mV s^{-1}: a. 1.0 mM, 10 minutes, b. 2.0 mM, 5 minutes, and c. 3.0 mM, 12 minutes. *Inset*: surface coverage of poly(caffeic acid) on GCE deposited from various [CAF] at different deposition time: ■ 1.0 mM, ● 2.0 mM, ▲3.0 mM.

Cyclic voltammograms of the poly(caffeic acid) were taken in 0.15 M phosphate buffer, pH 7.0, at different scan rates (25 mV s^{-1} - 400 mV s^{-1}) to determine its voltammetric behaviour at the optimum deposition condition mentioned above, seen in

Figure 5.3. In the inset of Figure 5.3, it illustrates that there is a proportional correlation between the anodic peak current versus scan rate to each other thus showing that the redox process is surface bound. This response coincides with what has been reported on the behaviour of CAF-GCE elsewhere. [148]

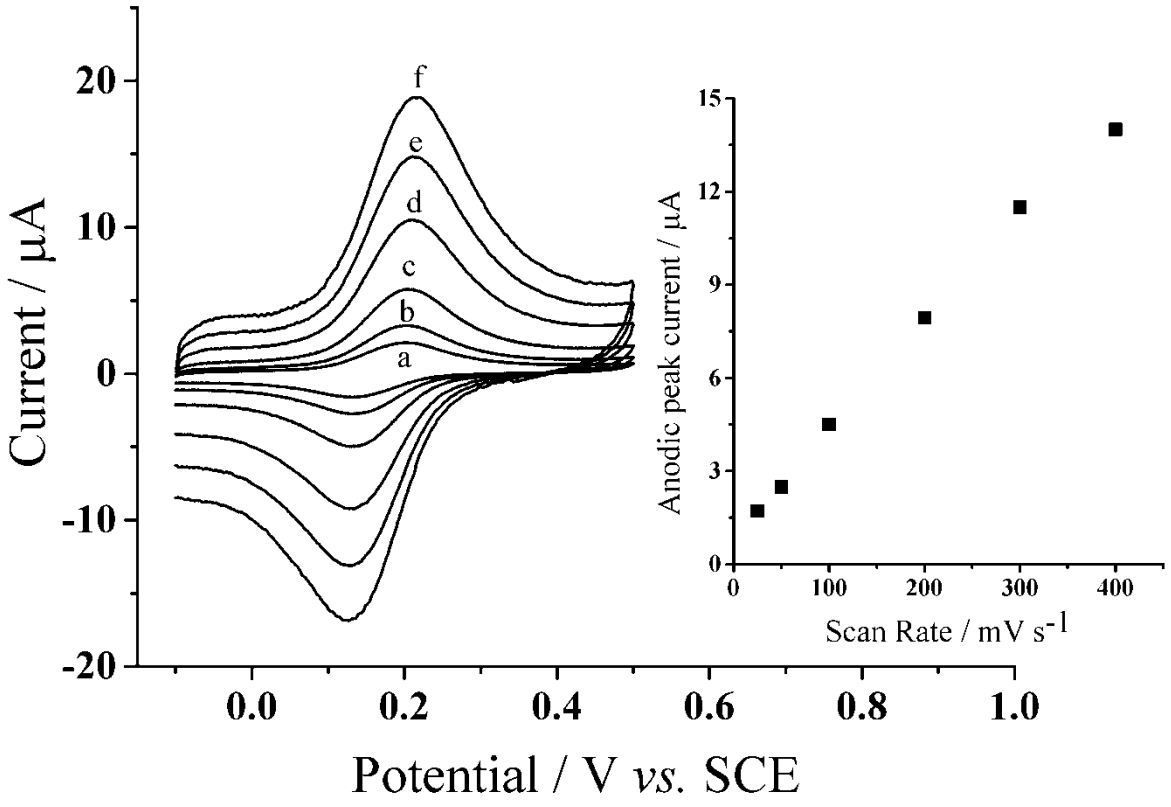

Figure 5.3: Cyclic voltammograms of 2.0 mM CAF-modified GCE in PBS (pH 7.0). a. 25 mV s^{-1}, b. 50 mV s^{-1}, c. 100 mV s^{-1}, d. 200 mV s^{-1}, e. 300 mV s^{-1}, and f. 400 mV s^{-1}. *Inset*: Anodic peak current, I_{pa}, *vs.* scan rate of CAF-GCE in PBS, pH 7.0.

5.1.3.2 Optimization of CAF-GCE

Sensitive electroanalytical detection is essential towards the development of sensors used in the detection of specific biological targets at low concentrations. For polymer based amperometric sensors, it has been reported that the thickness of the polymer film leads to higher sensitivity. [27, 149] The effects of supporting electrolyte

on polymer films have been discussed in literature as being one of the attributes to achieving film thickness. [150-152] To attain higher sensitivity on the poly(caffeic acid) modified electrode, further optimization of the polymer in respect to the film thickness were carried out through experiments using a series of different cationic supporting electrolytes while keeping the concentration of caffeic acid at its optimum 2.0 mM in phosphate buffer solution (PBS, pH 4.0). Sodium nitrate ($NaNO_3$), ammonium nitrate (NH_4NO_3), tetrabutylammonium nitrate ($(CH_3CH_2CH_2CH_2)_4N(NO_3)$), tetraethylammonium nitrate ($(C_2H_5)_4N(NO_3)$) and potassium nitrate (KNO_3) were all used to bring comparison to the current supporting electrolyte mentioned above, potassium chloride (KCl). 0.10 M of KCl supporting electrolyte was added to the 0.15 M KH_2PO_4/H_3PO_4 buffer solution, pH 4.0, used during the deposition of the poly(caffeic acid) polymer film. To ensure that the cation from the buffering system will have limited to no affect on the results, the supporting electrolyte for this experiment was increased to 0.20 M. Also to make certain that the anionic counterpart of the supporting electrolyte does not bring variance, KNO_3 was tested and used as a direct comparison to KCl. As shown in Figure 5.4, all supporting electrolytes, with the exception of tetrabutyl ammonium nitrate, observed a similar trend in comparison to potassium chloride, where the surface coverage gradually increases and maximizes at a deposition time of 5 minutes then decreases afterwards. The surface coverage in respect to sodium nitrate, tetraethyl ammonium nitrate, potassium nitrate, and potassium chloride all show a maximum surface coverage of *ca.* 9×10^{-10} mol cm^{-2}. A greater signal and surface coverage was observed having ammonium nitrate as supporting electrolyte to the caffeic acid of *ca.* 10^{-9} mol cm^{-2} at the same deposition time. However, the deposition with tetrabutyl ammonium nitrate seemed to maximize at 10 minutes with a surface

coverage of *ca.* 7 x 10^{-10} mol cm^{-2} which is lesser than of the rest due to the large molecule size that may limit the coverage and thickness of the poly(caffeic acid) film.

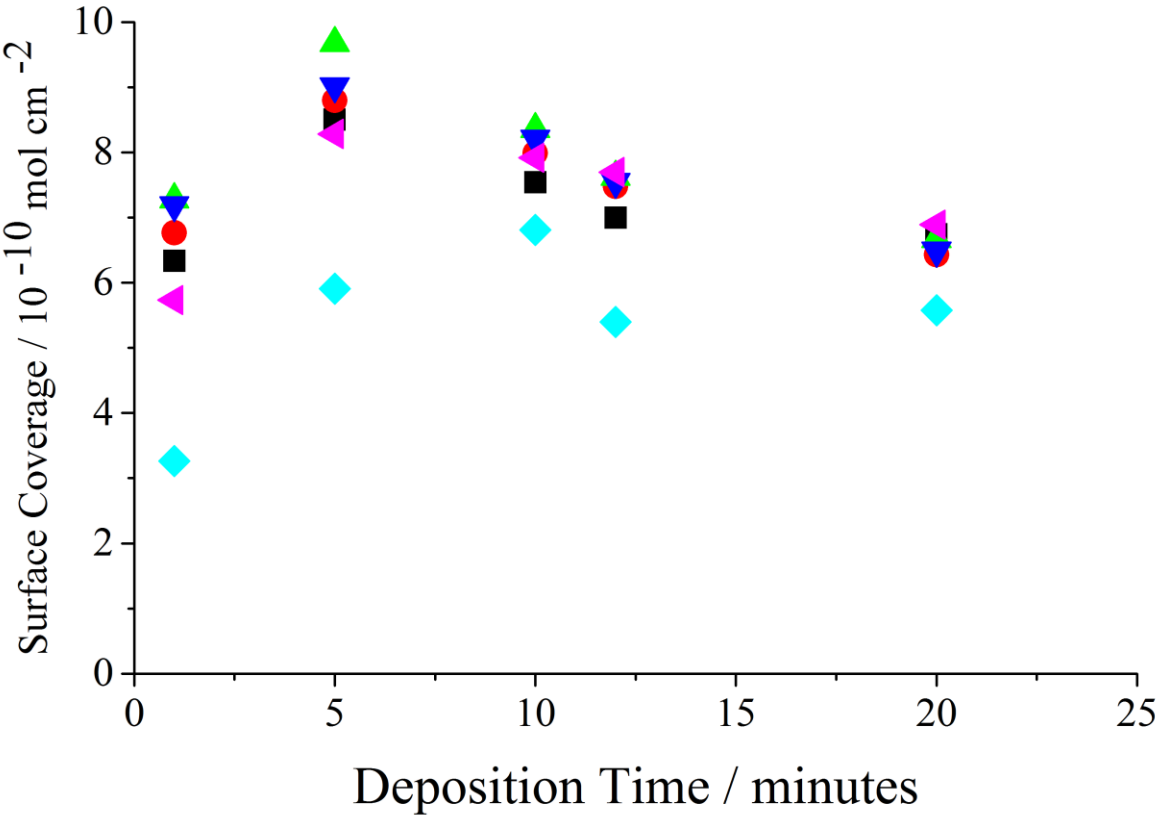

Figure 5.4: Surface coverage of poly(caffeic acid) on GCE varying supporting electrolyte in PBS, pH 7.0. ■ KCl, ● $NaNO_3$, ▲ NH_4NO_3, ▼ KNO_3, ◆ $(CH_3CH_2CH_2CH_2)_4N(NO_3)$, and ◀ $(C_2H_5)_4N(NO_3)$.

5.1.3.3 Catalytic oxidation of biological molecules: NADH, Cysteine, & Glutathione

Cyclic voltammograms of the freshly deposited poly(caffeic acid) polymer film were recorded at varying concentrations, of the targeted co-enzymes, β-nicotinamide adenine dinucelotide (NADH), cysteine, and glutathione, all in the presence of 0.15 M PBS (pH 7.0) which is shown in Figure 5.5, Figure 5.6, and Figure 5.7 respectively. The cyclic voltammogram of the polymer seen detecting the presence of the biological

molecule shows a larger anodic peak current and a lower cathodic peak current than of the one without in the buffer solution at 0 mM target concentration in curve a of Figure 5.5, Figure 5.6, and Figure 5.7, indicating that there is an electrocatalytic oxidation reaction. An average of three cyclic voltammograms was taken consecutively after each deposition and a calibration curve was determined for each target by taking the calculated average ratio of the forward and backward peak current (I_F/I_B) and plotted against the concentration of the target biomolecule at pH 7.0, illustrated in Figure 5.8, Figure 5.9, and Figure 5.10 respectively for NADH, cysteine, and glutathione.

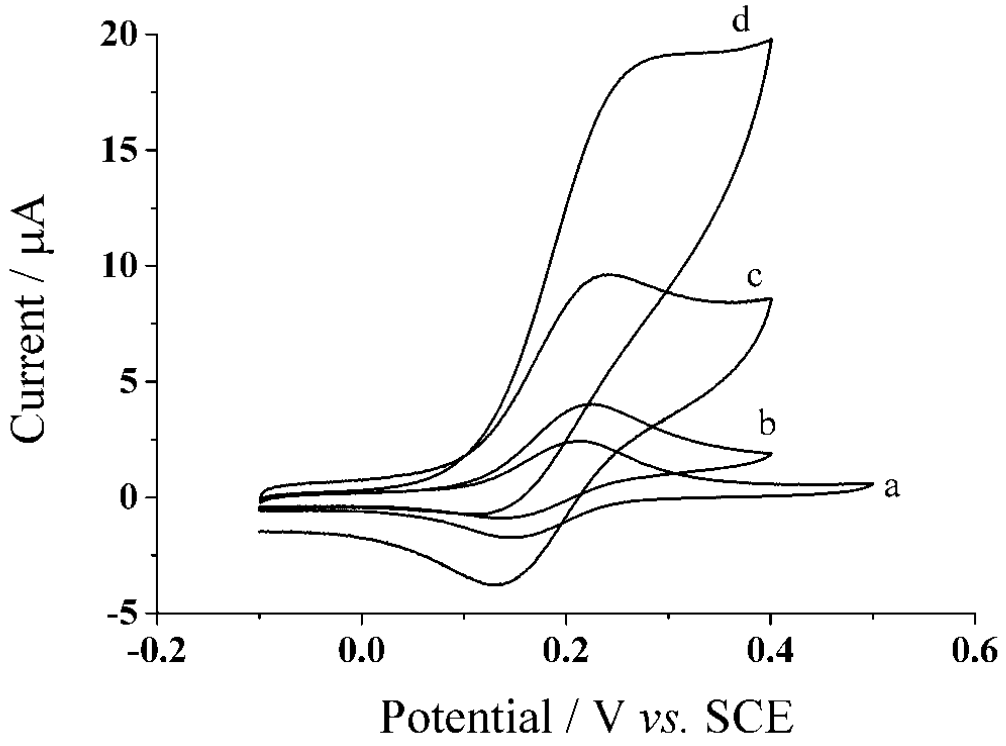

Figure 5.5: Cyclic voltammogram of CAF-GCE in varying concentrations of NADH, pH 7.0, at scan rate 25 mV s^{-1}. NADH concentration of a. 0 mM, b. 0.3 mM, c. 1.0 mM, and d. 5.0 mM.

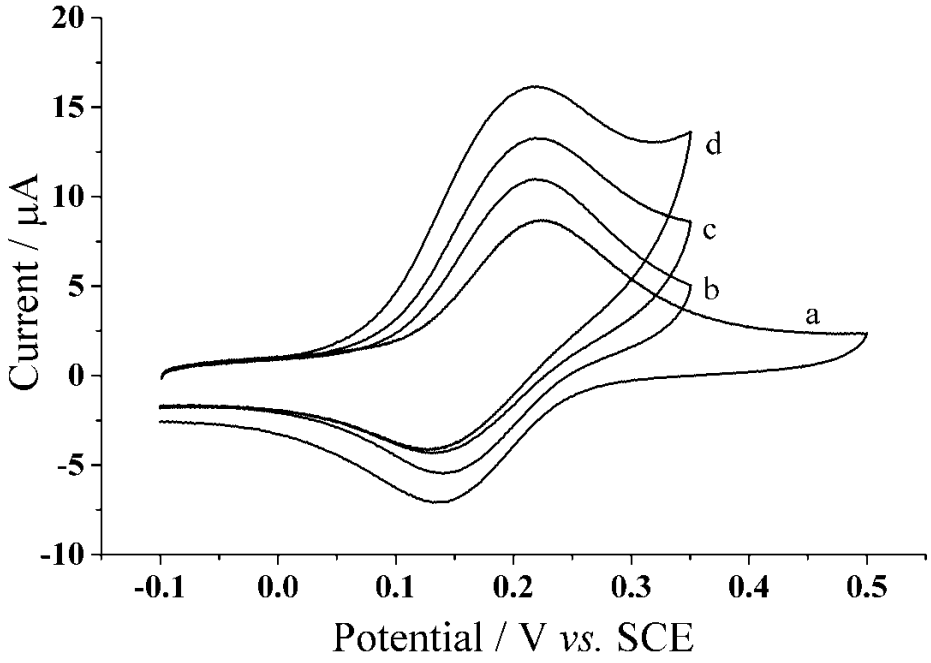

Figure 5.6: Cyclic voltammogram of CAF-GCE in varying concentrations of cysteine, pH 7.0, at scan rate of 100 mV s^{-1}. Cysteine concentration at a. 0 mM, b. 0.1 mM, c. 1.0 mM, and d. 5.0 mM.

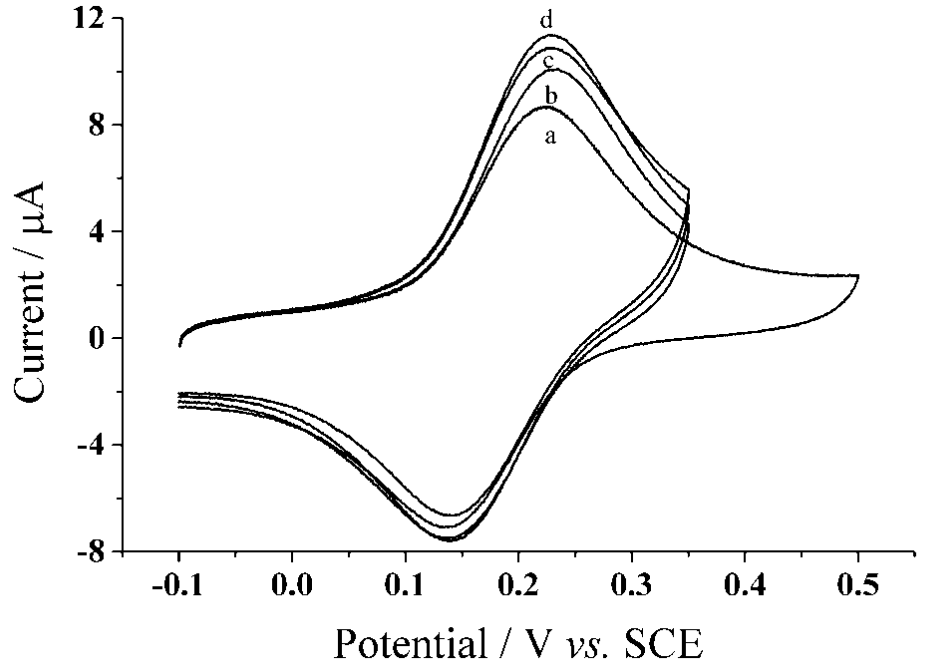

Figure 5.7: Cyclic voltammogram of CAF-GCE in varying concentrations of glutathione, pH 7.0, at scan rate 100 mV s^{-1}. Glutathione concentration at a. 0 mM, b. 3.0 μM, c. 100 μM, and d. 1.0 mM.

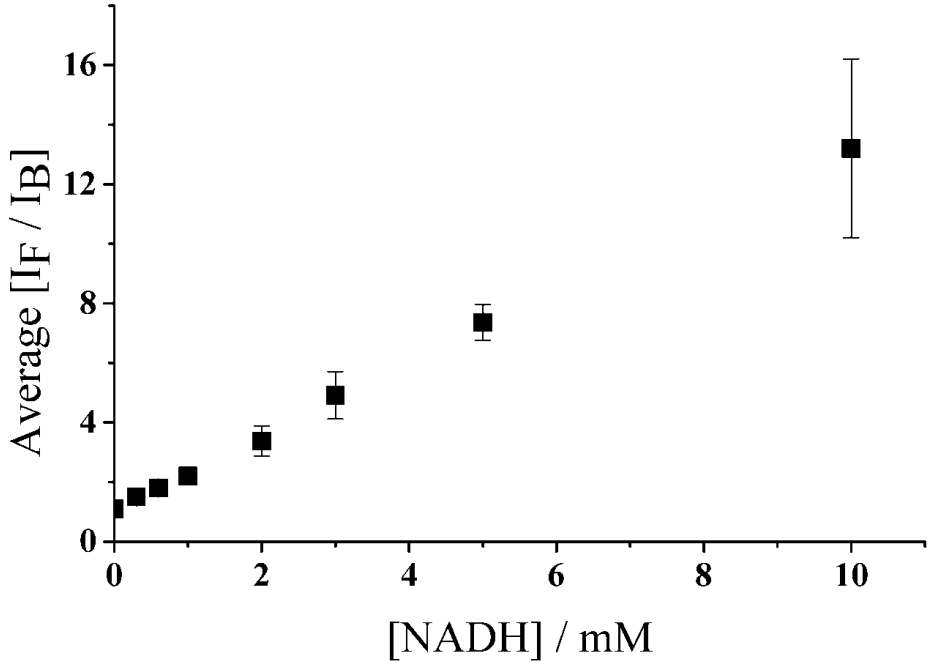

Figure 5.8: Averaged forward and backwards peak current ratio, I_F/I_B, *vs.* [NADH] of CAF-GCE in 0.15 M PBS (pH 7.0). [NADH] at 0.30, 0.60, 1.0, 2.0, 3.0, 5.0, and 10.0 mM.

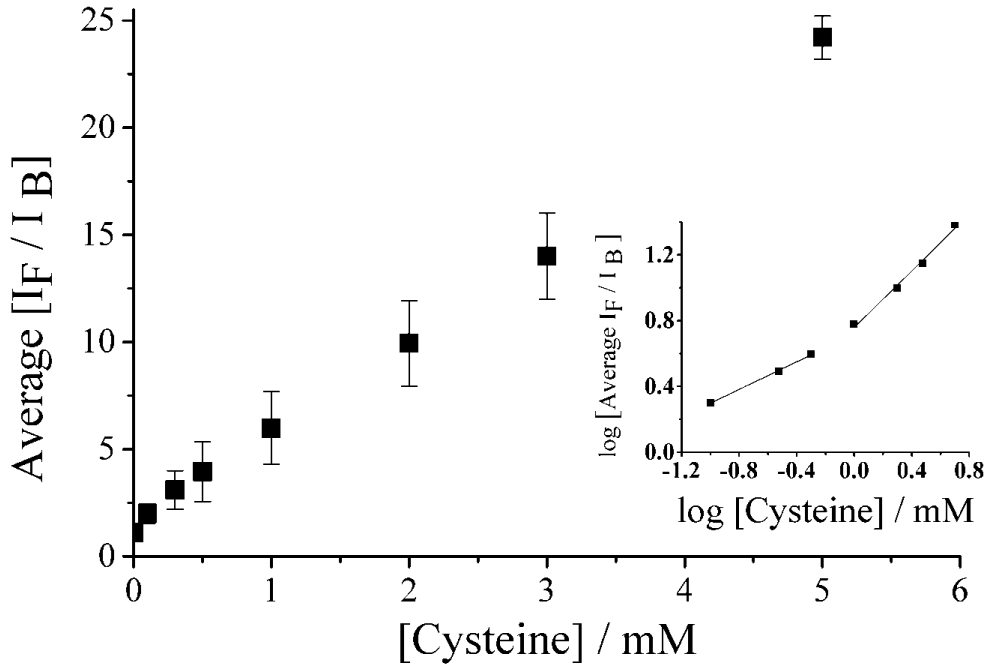

Figure 5.9: Average forward and backwards peak current ratio, I_F/I_B, *vs*. [cysteine] of CAF-GCE in 0.15 M phosphate buffer, pH 7.0. [Cysteine] at 0.10, 0.30, 0.50, 1.0, 2.0, 3.0, and 5.0 mM. *Inset*: log average peak current ratio *vs*. log [cysteine] of CAF-GCE.

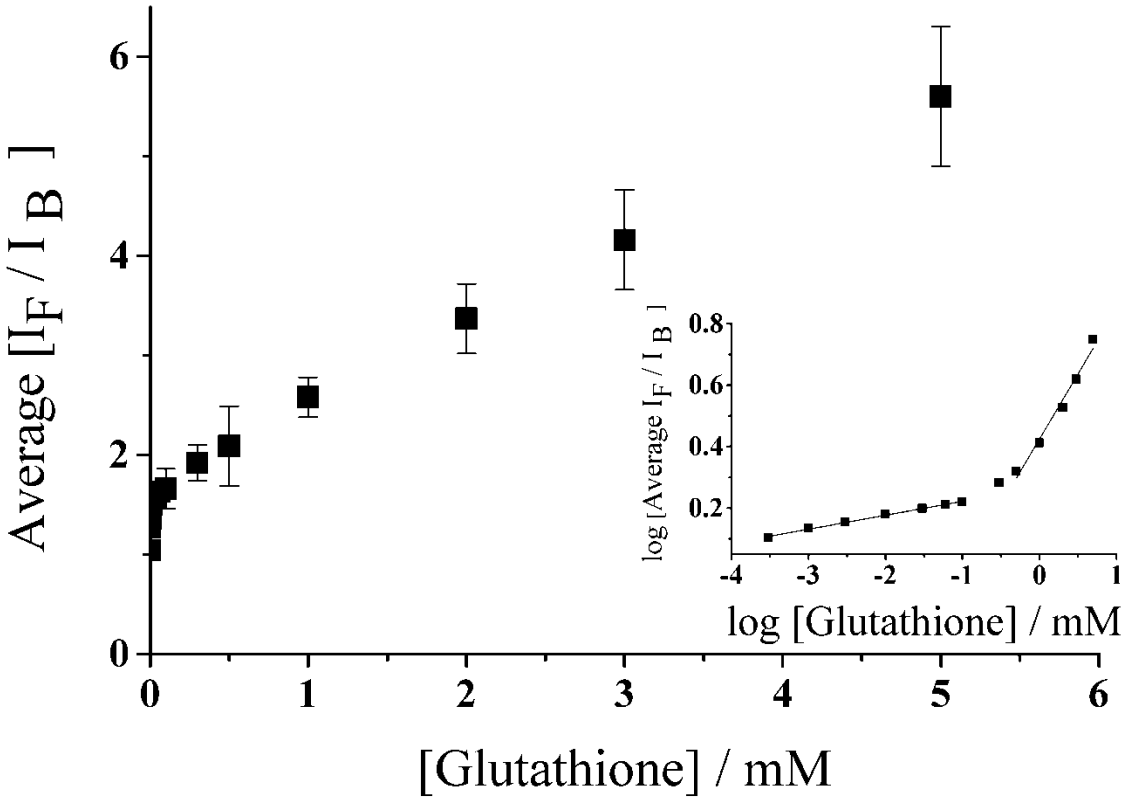

Figure 5.10: Average forward and backwards peak current ratio, I_F/I_B, *vs*. [glutathione] of CAF-GCE in 0.15 M phosphate buffer, pH 7.0. [Glutathione] at $3.0\text{x}10^{-4}$, $1.0\text{x}10^{-3}$, 0.01, 0.03, 0.06, 0.10, 0.30, 0.50, 1.0, 2.0, 3.0, and 5.0 mM. *Inset*: log average peak current ratio *vs*. log [glutathione] of CAF-GCE.

5.1.3.4 Detection of β-nicotinamide adenine dinucelotide (NADH)

To observe the response behaviour of CAF-GCE in respect to NADH at different concentrations, cyclic voltammetry of a fresh poly(caffeic acid) polymer film was recorded over a wide range of NADH concentrations, from 0.30 mM to 10 mM (Figure 5.5). A linear relationship was established when the average ratio of the forward and backward peak currents was plotted with the concentration of NADH (Figure 5.8). The limit of detection (LOD) was determined using the equation, $3S_B/S$, where S_B stands for the standard deviation of the peak current ratio CAF-GCE at the zero target concentration in the buffer solution, and S is the sensitivity at low concentration for

linear calibrations. [129] The LOD at the poly(caffeic acid) modified glassy carbon electrode for the detection of NADH is (246 $\pm$ 0.09) μM and the sensitivity was determined by the gradient of the calibration curve at (1.22 $\pm$ 0.3) μA mM^{-1}.

5.1.3.5 Detection of Cysteine

Figure 5.6 shows the detection of cysteine using CAF-GCE at a scan rate of 100 mV s^{-1}. The electrocatalytic effect of cysteine (Figure 5.6) is less pronounced than of CAF-GCE in NADH but nonetheless; similar characteristics of catalytic oxidation were observed. A similar calibration curve of average peak current ratio was plotted against cysteine concentration, shown in Figure 5.9. A linear relationship was observed with cysteine concentration up to 5.0 mM. The detection of CAF-GCE at concentrations below 1.0 mM is illustrated in Figure 5.9's inset, where a linear relationship can be determined when log [cysteine concentration] is plotted with calculated log value of average ratio of the forward and backward peak current, log [average I_F/I_B]. The limit of detection was calculated using the linear relationship within the submolar region of (99.0 $\pm$ 0.7) μM and with a sensitivity of (4.9 $\pm$ 0.1) μA mM^{-1}.

5.1.3.6 Detection of Glutathione

The detection of glutathione is also possible using CAF-GCE through cyclic voltammetry, as shown in Figure 5.7, where the concentration varies from 3.0 x 10^{-4} to 5.0 mM. A calibration curve for glutathione was established similar to the ones for NADH and cysteine. We observed a linear relationship for concentrations at 1.0 mM and above, similar to cysteine. However, to gain more insight into the trend that exists in the

concentration range of glutathione below 1.0 mM, more concentrations were tested and collected. The trend seems to show a logarithmic relationship and to determine a linear relationship at the lower concentrations, log [glutathione] was plotted against the log value of the average ratio of the forward and backwards peak current, log [average I_F/I_B], (Figure 5.10 inset) where it is helpful to determine the LOD and sensitivity of the CAF-GCE in the buffer solution containing glutathione. The LOD for CAF-GCE detecting glutathione is (2.2 ± 0.8) μM with a sensitivity of (213 ± 14) μA mM^{-1}.

5.1.4 Conclusions

We have found that a caffeic acid polymer film can be immobilized onto the surface of an activated glassy carbon electrode using electrodeposition methods. The redox species of poly(caffeic acid) polymer film was determined to be surface bound and it could be further optimized by increasing the polymer film coverage to 10^{-9} mol cm^{-2}, which is anticipated for higher sensitive analytical detection. By taking advantage of the electrocatalytic oxidation of the coenzymes: NADH, cysteine and glutathione, the modified carbon electrode show enough distinction amongst the different concentrations for a calibration curve to be determined for concentrations as low as 300 nM and as high as 10 mM. This first study shows initial promise for quantitative analysis, especially at low concentrations.

5.2 Electrochemical detection of glutathione using a poly(caffeic acid) nanocarbon composite modified electrode

5.2.1 Introduction

Electrochemical sensors have been found to be valuable in sample analysis in both biomedical and environmental applications. Over years, they have become more attractive because of the advantages they offer in size, cost, low-volume, and power requirement. [153] As observed by Murray, the electrode surface is a "powerful tool" for chemists. Using a variety of methods for attaching a redox species onto the surface allows the reaction at the electrode-solution interface to be measured with great sensitivity by applying a voltage. [110] Some of the popular methods of immobilization include covalent bonding, adsorption, and polymer films. [110, 154] As discussed in Section 5.1, electrode modifications with electroactive polymer films are often preferred over the other methods because of the advantages in the facile technical application and control over film thickness during electrochemical polymerization.

Within the last 30 years, polymer films have gained popularity over monolayer films because they have often been reported to be more stable and have a more amplified signal, which is important in analytical sensor applications. [110, 154] In this section, the focus will be to modify the electrode surface so that an amplified signal is obtained. There have been many studies focused on incorporating porous polymer films into nanomaterials at the electrode surface thus creating a composite electrode. [155-161] Others have noted that increasing the current density in the signal can lead to a more sensitive sensor for target analyte detection. [39, 162] The equation for an ideal Nernstian behaviour of surface-confined species,

$$I_p = \frac{n^2 F^2 \Gamma A \upsilon}{4RT} \tag{5.2}$$

illustrates the proportional relationship between the peak current, I_p, to the surface coverage, Γ; where n is the number of electrons involved in the redox reaction (to be discussed in a later section), F is the Faraday constant, A is the surface area of the electrode, υ is the scan rate, R is the molar gas constant, and T is the temperature. Incorporating nanomaterials onto the surface of the electrode allows more surface area for the redox species to immobilize itself onto therefore increasing its current density. This type of composite opens a promising outlet for analytical detection by creating an improved electrode with characteristics such as sensitivity, size, and stability due to the high number of active sites, and strong adherence with other complementary properties as well. [153, 163, 164]

The purpose of this section is to demonstrate an accurate and sensitive detection of glutathione using a redox polymer, poly(caffeic acid) (Figure 5.1), at a nanomaterial composite electrode. The architecture of the composite electrode will incorporate "bamboo-like" carbon nanotubes and nano-carbon (diameter = 14 nm) for their similar large surface area, thus enhance the current density of the immobilized redox species. Bamboo carbon nanotubes are carbon nanotubes that have graphene material rolled up to make up a structure that resembles a bamboo plant stem. According to Heng, their shape is comprised of a number of "transverse walls at regular intervals along the nanotubes". [165] Due to their structure, "bamboo-like" carbon nanotubes can be a new alternative to short nanotubes for their favourable electrochemical properties in both aqueous and non-aqueous solutions. Nano-carbon is the other material chosen for this study, which essentially consists of clusters of spherical carbon particles aggregated

together forming aggregates with as low as 1 particle to 100 particles per nano-carbon aggregate thus making the material porous. [166] Nano-carbon also offers a cheaper alternative over carbon nanotubes. Through a price quotation provided by the suppliers at the time of writing, nano-carbon from Cabot Corporation (Billerica, MA, USA) is £0.02 per gram whereas "bamboo-like" carbon nanotubes from NanoLab Incorporated (Waltham, MA, USA) are £78 per gram depending on purity. Incorporating these nanomaterials into the architecture of the composite electrode, their properties could be beneficial towards producing a higher sensitive system for glutathione detection.

5.2.2 Experimental procedure

5.2.2.1 Electrode preparation

The modification of the electrode is similar to that described in Section 5.1.2.1 except for the novel incorporation of nano-carbon (NC) or carbon nanotube (CNT). The GCE was first polished with sequentially 1.0, 0.3, and 0.05 μm alumina (Buehler, Germany) in water slurry on a polishing pad, and then rinsed twice with de-ionised water followed by with acetone. Then the electrode was electrochemically activated by placing the three-electrode system in 0.10 M sodium bicarbonate solution and applying a continuous potential cycle from −1.10 V to +1.60 V with a sweep rate of 100 mV s^{-1} until a stable voltammogram was achieved, *ca.* 4 scans. After carefully rinsing the electrode with deionized water and drying, the carbon material, CNT or nano-carbon, was immobilized onto the surface of the glassy carbon electrode through drop casting method. The drop casting method comprises dropping an aliquot of a carbon-ethanol suspension over the surface of the GCE. Then the volatile solvent is allowed to evaporate

at room temperature, leaving a layer of carbon material at the electrode surface. The suspension ratio of the CNT-ethanol solution was 0.1 mg/mL and for nano-carbon-ethanol, 1.0 mg/mL. To ensure a full suspension, the solutions were briefly sonicated using a sonication bath prior to drop casting. Thereafter, the electrodeposition of the poly(caffeic acid) was done electrochemically by placing the electrode into a solution of 2.0 mM caffeic acid mixed with 0.15 M phosphate buffer (pH 4.0) and applying a potential cycle between +0.10 V to +0.90 V, at a sweep rate of 20 mV s^{-1} for 5 minutes, *ca.* 4 scans. Then the electrode was rinsed and dried carefully before proceeding with all electrochemical experiments.

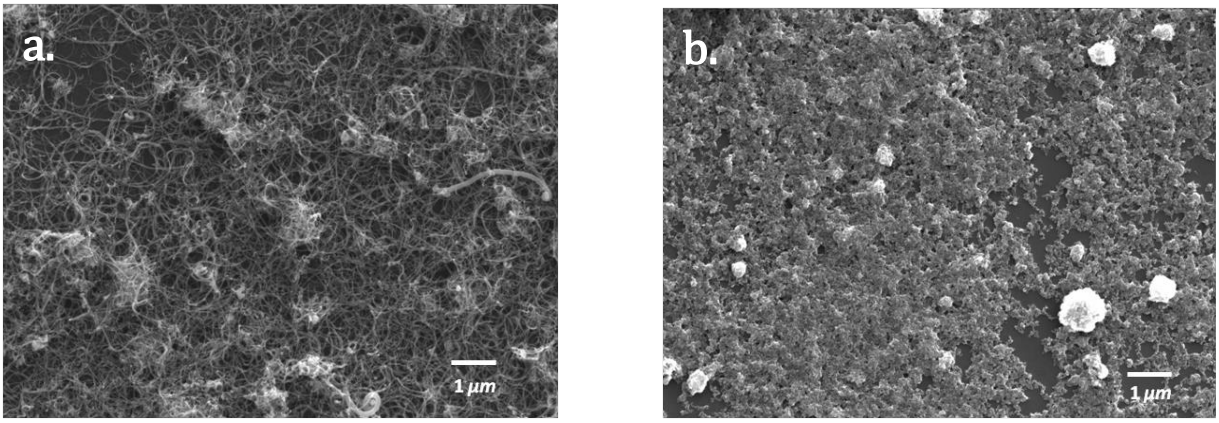

Figure 5.11: Scanning electron images of modified nanocomposite electrodes a. pCAF-CNT-GCE and b. pCAF-NC-GCE.

To characterize the morphology of the electrochemically derived polymer nanocomposite, scanning electron microscopy (SEM) analysis was performed by Dr. Kristina Tschulik and Ms. Gabriella Chapman. Secondary electron images were taken of each of the nanocomposite electrodes and are depicted in Figure 5.11 using a JSM-6500F scanning electron microscope (JEOL Ltd., UK) at an acceleration voltage of 5.0 kV. Figure 5.11a shows the mesh of the drop cast carbon nanotube coated with the electrodeposited polymer. Note that each nanotube appears coated with polymer and

that some of the polymer is more concentrated at certain zones particularly where the nanotubes are entangled. Figure 5.11b shows the surface of the polymer formed on nanocarbon particles. In the absence of the polymer [167], individual nanocarbon particles are visible but with the polymer present an open porous network is formed.

5.2.3 Results and discussion

5.2.3.1 Characterization of pCAF-CNT-GCE

Modified electrodes were prepared using different quantities of drop casted CNT-ethanol suspension ranging from 0 – 100 µL to determine the maximum signal of the poly(caffeic acid). The modified electrodes were tested in phosphate buffer solution (PBS), pH 7.0, to observe the cyclic voltammetric response from the *o*-quinone/ *o*-hydroquinone couple as in the first step of Equation 4.1. It was determined that the highest amperometric signal of poly(caffeic acid) was achieved with 6.0 µg of CNT, illustrated in Figure 5.12b. The figure shows the voltammetric response of the poly(caffeic acid) at $E_{1/2} = +0.18$ V (*vs.* SCE) which is attributed to the two electron, two proton oxidation of the *o*-hydroquinone into to the corresponding *o*-quinone species. [37, 148, 168] The surface coverage of poly(caffeic acid) with 6.0 µg CNT was calculated to be *ca.* 2.8×10^{-9} mol cm^{-2} using Equation 5.1. This surface coverage with the addition of CNT, is about three times larger than that of the poly(caffeic acid) modified glassy carbon electrode, pCAF-GCE (Figure 5.12a), reported under similar deposition conditions without the presence of CNT (*ca.* 9×10^{-10} mol cm^{-2}). [141]

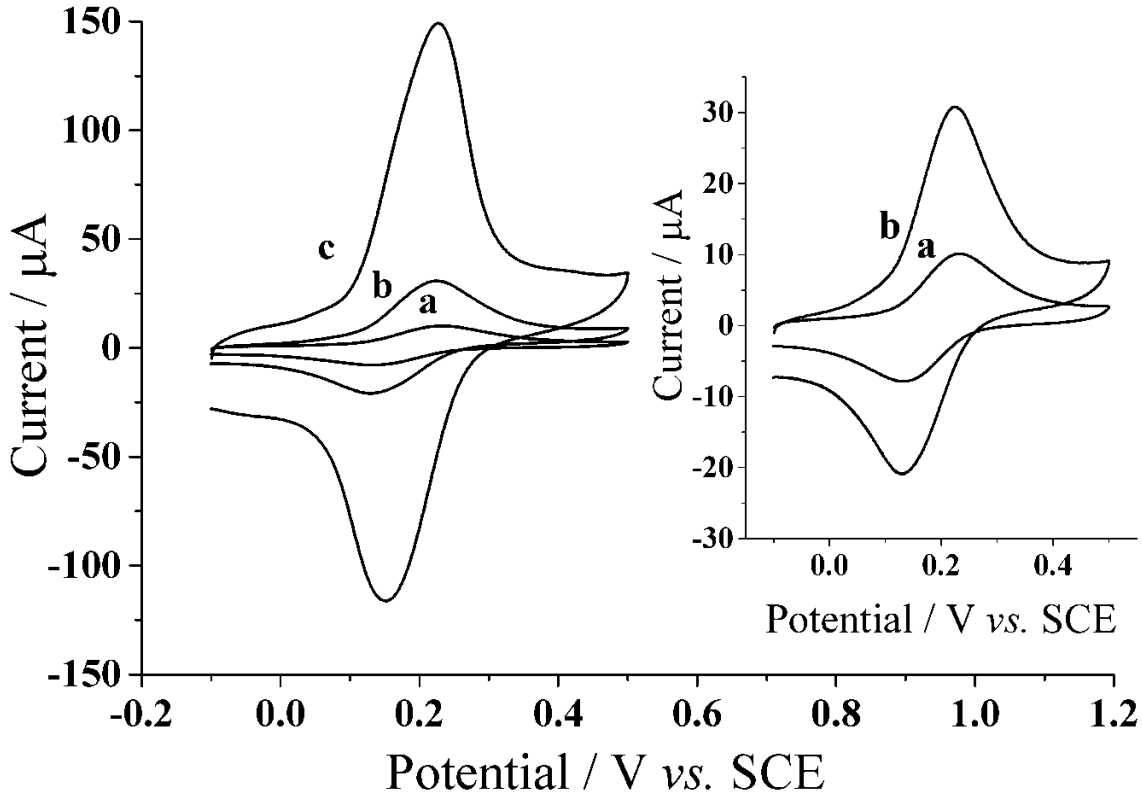

Figure 5.12: Cyclic voltammograms in 0.15 M PBS (pH 7.0) of pCAF modified electrode at a. GCE, b. 6.0 µg CNT-GCE, c. 50 µg NC-GCE. *Inset:* Enlarged view of a & b.

Cyclic voltammograms of the pCAF-CNT-GCE were also measured in 0.15 M PBS (pH 7.0) at varying scan rates (25 mV s^{-1} – 400 mV s^{-1}) to explore the factors controlling the voltammetric response (Figure 5.13). Inspection of the inset of the Figure 5.13 shows that the peak current increases apparently linearly with voltage scan rate suggests a behaviour consistent with surface confined voltammetry and corresponding 'thin layer' type voltammetry (described in Section 1.7.1.2). The slight deviation from linearity may reflect on the transport processes to/from the electrode resulting from the porosity of the nanocomposite films, as explored in similarly structured electrodes. [27, 169, 170]

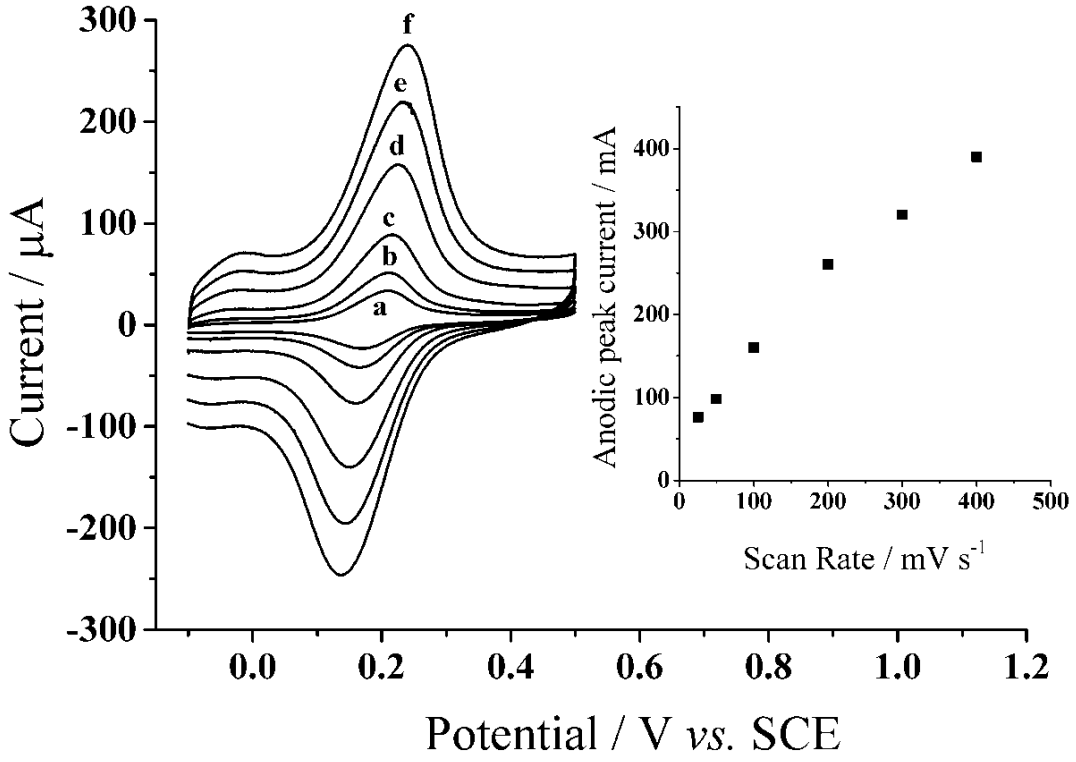

Figure 5.13: Cyclic voltammograms of pCAF-CNT-GCE in 0.15 M PBS (pH 7.0) at scan rates a. 25 mV s^{-1}, b. 50 mV s^{-1}, c. 100 mV s^{-1}, d. 200 mV s^{-1}, e. 300 mV s^{-1}, and f. 400 mV s^{-1}. *Inset:* Anodic peak current, I_{pa}, *vs.* scan rate of modified electrode

5.2.3.2 Characterization of pCAF-NC-GCE

To explore the consequences of the different surface areas of the nano-carbon materials, we next studied how the voltammetric behaviour of pCAF-NC-GCE compared with the pCAF-CNT-GCE and the pCAF-GCE. A maximum signal of the pCAF-NC-GCE was achieved by means similar to that mentioned above for pCAF-CNT-GCE; the quantities tested ranged from 0 – 60 µL of nano-carbon-ethanol suspension. It was determined that the signal maximizes with 50 µg of nano-carbon, Figure 5.12c, with a calculated surface coverage of *ca.* 11 x 10^{-9} mol cm^{-2}. When compared to pCAF-GCE (Figure 5.12a), this surface coverage is about twelve times larger. This calculated surface coverage of pCAF-NC-GCE is the highest in comparison to that of pCAF-GCE and pCAF-CNT-GCE.

A scan rate study was performed on this modified electrode to show the voltammetric behaviour. Scan rates varying from 25 mV s^{-1} up to 400 mV s^{-1} of the modified electrode were conducted in 0.15 M phosphate buffer, pH 7.0 (Figure 5.13). The relationship between the peak current and scan rate (Figure 5.13 inset) is similar to that was observed for pCAF-CNT-GCE where the peak current is approximately proportional to the scan rate suggesting the behaviour is of a surface bound species showing 'thin layer' type voltammetry.

5.2.3.3 Detection of glutathione at the poly(caffeic acid) modified carbon electrodes: pCAF-CNT-GCE *vs.* pCAF-NC-GCE *vs.* pCAF-GCE

As mentioned, two possible mechanisms can occur between an *o*-quinone and a thiol group (Chapter 4): a 1,4-Michael addition or an electrocatalytic reaction. As the foundation of either reaction is initialized by the electrochemical oxidation of the catechol (1,2-dihydroxyquinone) involving a two proton, two electron process; the subsequent reactions with the thiol species, glutathione, at the electrode surface, can result in different voltammetric responses depending on the prevailing mechanism. Scheme 4.1B illustrates an *o*-quinone undergoing a 1,4-Michael addition with thiol species where a new signal can emerge in the voltammograms or if the quinone and adduct peaks overlap an increase in peak current indicating in a four electron process. In an electrocatalytic reaction (Scheme 4.1A), no new signal will appear in the voltammogram as the reaction is exclusively based on the quinone/hydroquinone redox reaction. However, the forward peak signal will increase and back peak signal will decrease as the concentration of thiol species increases due to the catalytic oxidation of thiols to produce disulfides. This section will distinguish the prevailing type of thiol

reaction with the *ortho*-quinone moiety at the different modification of carbon electrode with the detection of glutathione.

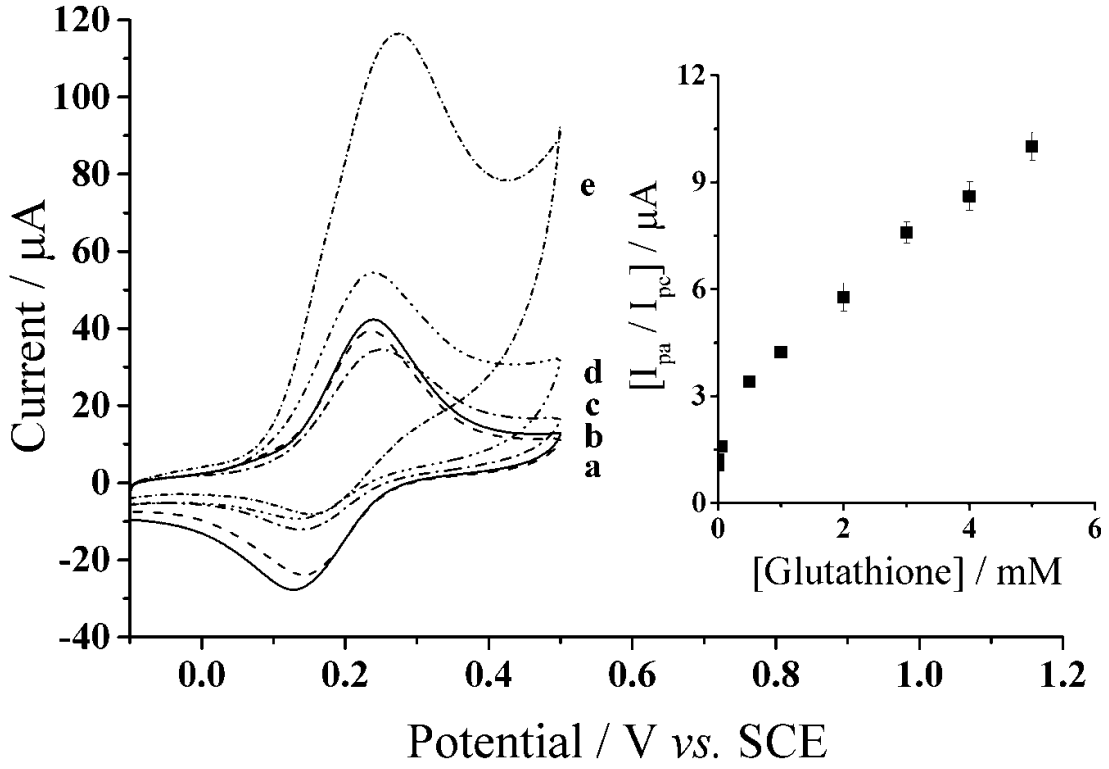

Figure 5.14: Cyclic voltammograms of pCAF-CNT-GCE in varying concentrations of glutathione, pH 7.0: a. 0 mM, b. 0.05 mM c. 0.5 mM d. 5.0 mM e. 50 mM. *Inset*: Calibration curve of pCAF-CNT-GCE for glutathione concentrations from 0 mM to 5.0 mM.

pCAF-CNT-GCE

In the detection of glutathione with the pCAF-CNT-GCE, the cyclic voltammetric response of the modified electrode was investigated in varying concentrations of glutathione (pH 7.0), 500 nM to 50 mM. Illustrated in Figure 5.14, the forward peak increases and backward peak decreases as the concentration of glutathione increases; this is an indication of an electrocatalytic reaction (Scheme 4.1A). A calculated ratio of the anodic, I_{pa}, and cathodic, I_{pc}, peak current (I_{pa}/I_{pc}) was plotted against the concentration of glutathione at pH 7.0 (Figure 5.14 inset). This calibration curve, of

pCAF-CNTs-GCE, shows a linear relationship at glutathione concentrations of 500 mM and above. At low concentrations of 500 mM and below, the trend curves and approaches towards zero analyte concentration indicating that the modified electrode is capable of detecting at these low concentrations and that separate calibration curves are needed for these concentrations.

The data in Figure 5.14 shows that the oxidative peak current in the presence of high glutathione concentration, 50 mM glutathione, is more than twice the value in its absence, with no introduction of a new peak. This indicates that the current increases beyond that corresponding to the maximum number of electrons involved on the basis of a Michael addition. Also, there is no introduction of a new peak with increasing glutathione concentration, which suggests that a nucleophilic substitution did not occur and hence that the dominating reaction is an electrocatalytic reaction.

Figure 5.15 shows the calibration curve for glutathione detection at different modified electrodes presented so far. Since the sensitivity is given by the gradient of the calibration plot [130], we can observe changes in sensitivity due to the presence or absence of nanomaterials. Just comparing pCAF-CNT-GCE with pCAF-GCE, the slope for the pCAF-CNT-GCE is higher than pCAF-GCE which suggests that the sensitivity is higher with the addition of CNT. This indicates that the carbon nanotube was able to provide additional surface area for the redox species to immobilize onto to give a larger amperometric signal, shown in the previous section, thus promoting higher sensitivity for analytical detection at these concentrations. Figure 5.15 also shows the precision of the data for pCAF-CNT-GCE, where each experiment was carried out three times for the standard deviation to be calculated at each point in the calibration curve, represented by the error bars in the plot.

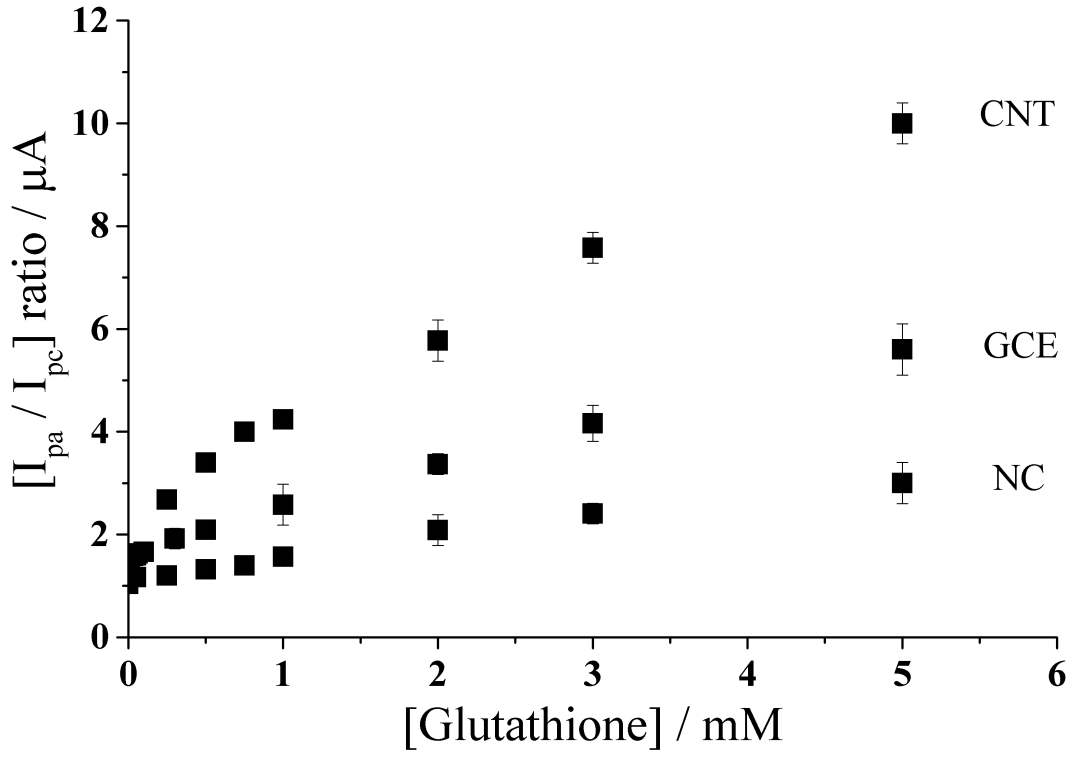

Figure 5.15: Calibration curve comparison of the electrode response to varying concentrations of glutathione (pH 7.0), 0 mM to 5.0 mM, at the different types of modified carbon electrodes (GCE, NC, and CNT).

pCAF-NC-GCE

Nano-carbon (d = 14nm) was next investigated to determine whether a more cost effective material would deliver the same or better performance over carbon nanotubes. The pCAF-NC-GCE was tested in PBS, pH 7.0, in the presence of varying concentrations of glutathione, ranging from 500 nM to 50 mM. The cyclic voltammograms (Figure 5.16) of pCAF-NC-GCE show the forward peak increases and backward peak current decreases with increasing glutathione concentration; this is evidence of an electrocatalytic reaction (Section 4.1). Next, the peak current ratio (I_F/I_B) was calculated using the forward and backward peak current and plotted with glutathione concentration, illustrated in Figure 5.16 inset. This calibration curve shows

a linear relationship over the range studied of the calculated peak current ratio with increasing glutathione concentration.

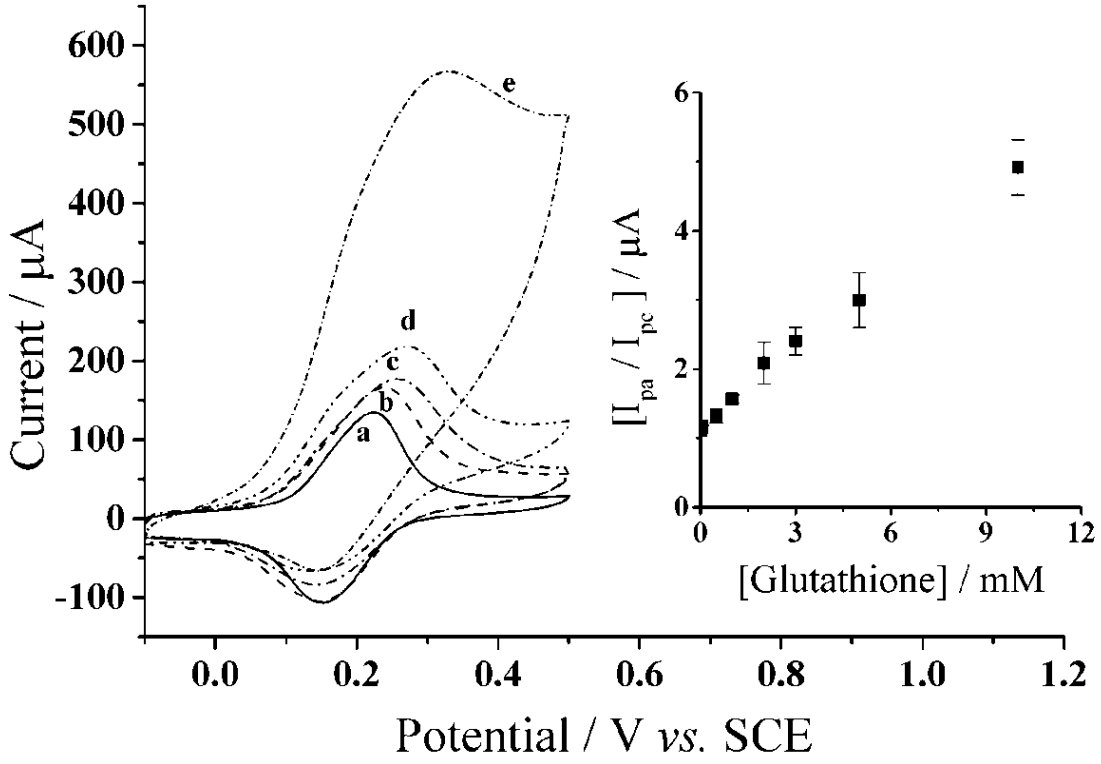

Figure 5.16: Cyclic voltammograms of pCAF-NC-GCE in varying concentrations of glutathione, pH 7.0. a. 0 mM, b. 1.0 mM, c. 5.0 mM, d. 10.0 mM, and e. 50.0 mM. *Inset*: Calibration curve of pCAF-NC-GCE for glutathione at concentrations from 0 mM to 10.0 mM.

To determine whether performance is not jeopardized with the addition of a more cost effective material, the sensitivity of the nano-carbon modified electrode is compared to the other modified electrodes mentioned alone. Shown in Figure 5.15, the calibration curve of each modified electrode is plotted with glutathione concentration ranging from 0 mM to 5.0 mM. The figure shows that the slope of the pCAF-NC-GCE is lower than that of both pCAF-CNT-GCE and pCAF-GCE. This indicates that the pCAF-NC-GCE has a low sensitivity towards glutathione detection; even though the surface coverage of the pCAF-NC-GCE is much greater than any of the presented modified

electrodes. The precision data for pCAF-NC-GCE is also depicted in Figure 5.15 for pCAF-NC-GCE, where the reproducibility of the experiment, n=3, is represented by the standard deviation of each data in the calibration curve. It was suggested by Prodromidis et al. that the effects of steric and overlapping of the molecules might affect the electrochemical behaviour due to the saturation of the redox species on the surface of a chemically modified electrode. [171] Considering that the calculated surface coverage of the caffeic acid is so large in the presence of nano-carbon, this could hinder the electrocatalytic reaction with glutathione.

5.2.4 Conclusions

We have found the use of a nanocomposite electrode comprised of nanomaterials (nano-carbon or carbon nanotubes) with poly(caffeic acid) to be encouraging in the detection of biomolecules. This nanocomposite electrode allows high concentrations of *o*-quinone precursor moiety to be deposited at the surface which then can be used for the sensitive detection of glutathione via, primarily, an electrocatalytic process allowed the determination of concentrations as low as 500 nM.

5.3 Selective electrochemical determination of cysteine with a cyclotriveratrylene modified carbon electrode

5.3.1 Introduction

Cyclotriveratrylene (CTV), shown in Scheme 5.1, is a cyclic trimer of veratrole which consists of three aromatic rings, each bearing two methoxyl substituents that are

separately fused to a cyclononatriene ring. [172, 173] CTV itself has newly gained attention in recent years in the field of supramolecular chemistry, as the number of analogues grows with potential applications in sensors, soft materials, and separations. [172, 174] One related species in particular is cyclotricatechylene (CTC) (also depicted in Scheme 5.1). As CTV can undergo an electrochemical activation to form CTC, the *tris*-catechol analogue is potentially interesting to the electrochemical community as the catechol groups are redox active and the *o*-quinone/hydroquinone system is well placed to mediated electron transfer and engage in potentially selective reaction. [175, 176] There is limited literature on the electrochemistry of CTC based derivatives [176], *in-situ* generation of CTC from CTV modified electrode and no literature on the redox chemistry of CTC alone. The present section reports on the novel use of CTC in the selective detection of cysteine in the presence of other thiols using electrochemical methods. The basis of cysteine detection with CTC is essentially a quinone-thiol interaction via electrocatalytic oxidation reaction, which has been widely studied (shown in general terms, Section 4.1). [36, 52, 65, 131, 133, 136, 137]

However, not only does this advocated methodology rely on the electrocatalytic oxidation reaction, but the different reaction rates between surface immobilized *o*-benzoquinone moieties and the different thiol-containing molecules facilitate selective measurement such that it will be seen that cysteine reacts usefully faster than glutathione or homocysteine. Application of a fast scan rate to a CTC modified electrode in the sample solution containing cysteine and the thiols, homocysteine and glutathione, excludes the unwanted thiol reactions with the *o*-benzoquinone moieties and allows only reaction with cysteine to take place, thus establishing selective cysteine detection. This novel system approach for cysteine selectivity was investigated by practical

assessment of solutions containing all three thiols (cysteine, homocysteine and glutathione) in both phosphate buffer solution and cell tissue culture media. This methodology thus establishes new diagnostic pathway for selective cysteine detection for the biomedical community.

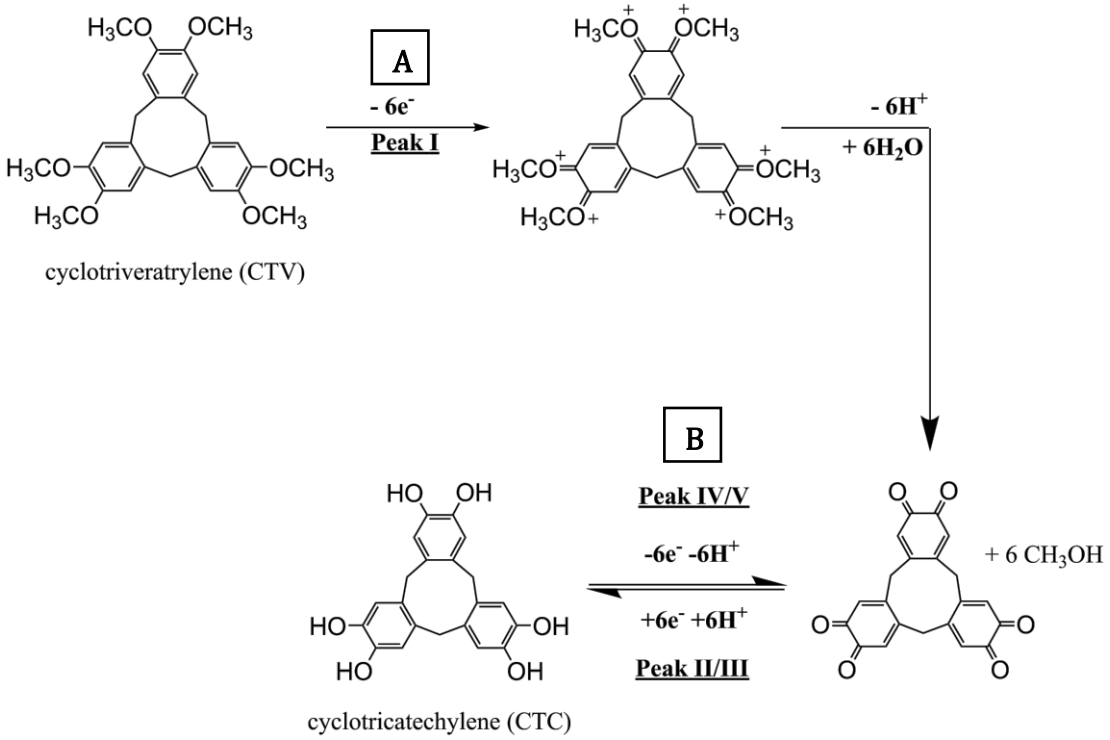

Scheme 5.1: Demethylation of cyclotriveratrylene (CTV) to form cyclotricatechylene (CTC).

5.3.2 Experimental procedure

5.3.2.1 Reagents

Dulbecco's Modified Eagles's Media (Sigma-Aldrich) was purchased and used as received without any further purification steps. CTV was synthesized according to that reported by Lindsey [173] by Ms. Athanasia Karina, Dr. James E. Thomson and Professor Steve G. Davies. Aqueous formaldehyde (38%, 40 mL) and concentrated aqueous HCl

(54 mL) was stirred at 0 °C, then veratrole (10.0 g, 72.4 mmol) was added portionwise to the mixture. The resultant mixture was stirred for 30 minutes and then stirred at room temperature for an additional 4 hours. The resulting mixture was then filtered and ice-cold water (50 mL) was used to wash the solid residue. Recrystallization with toluene was performed and the resulting white solid was dried under high vacuum to give CTV (8.22 g, 76%). Flash column chromatography was performed using silica gel (eluent hexane/EtOAc, 1:1) to give an analytically pure sample of CTV; [177] δ_H (400 MHz, $CDCl_3$) 3.87 (18H, s, O*Me*), 3.60 (3H, d, *J* 14.0, CH_AH_B), 4.82 (3H, d, *J* 14.0, CH_AH_B), 6.86 (6H, s, *Ar*); *m/z* (ESI$^+$) 473 ([M+Na]$^+$, 100%).

5.3.2.2 Electrode preparation and characterization

The electrode was modified with CTV and converted to cyclotrivatechylene (CTC) following the procedure: The glassy carbon electrode was initially polished with diamond spray (Kemet, UK) followed by a deionized water rinse and careful drying. CTV was immobilized onto the surface of the carbon electrode via drop cast method. This method consisted of dropping approximately 20 µL of a 100 µM CTV-chloroform solution onto the surface of the carbon electrode and allows the volatile solvent to dry under flowing nitrogen atmosphere.

To form CTC electrochemically, the optimal parameters were determined where the CTV modified carbon electrode is placed in a 0.05 M Britton-Robinson buffer solution (pH 1.0) and a potential sweep was applied from +1.16 V to –0.40 V (*vs.* SCE) at a sweep rate of 100 mV s^{-1}. Then the electrode was carefully rinsed with deionized water before proceeding with all electrochemical experiments. The preparation of the

CTC modified electrode was done prior to each experiment due to the solubility of CTC in aqueous systems.

Scanning electron microscopy (SEM) was used to characterize the CTV modified carbon electrode by Mr. Chris Salter and Dr. Colin Johnston. Secondary electron images were taken of CTV on glassy carbon substrate using a Merlin scanning electron microscope (Zeiss, UK) at an acceleration voltage of 5.0 kV. Shown in Figure 5.17, prism-like crystalline structures averaging *ca.* 1.0 μm x 0.15 μm, ranging from 0.3 μm x 0.05 μm to 2.2 μm x 0.4 μm, are seen scattered throughout the carbon substrate which is consistent with observations made by Steed et. al. when CTV structures of crystalline inclusion complexes are investigated with chloroform. [178]

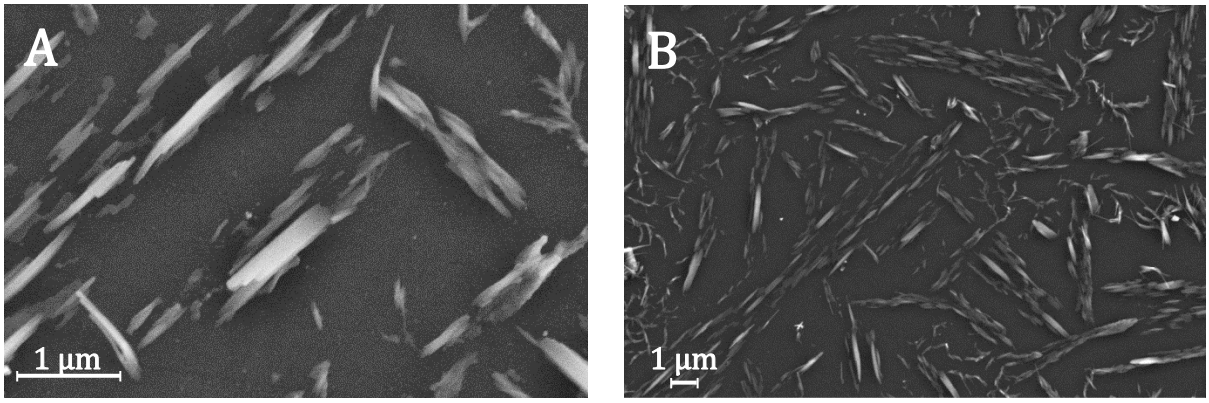

Figure 5.17: Secondary electron images of modified carbon electrode with cyclotriveratrylene (CTV) at a. high magnification and b. low magnification.

5.3.3 Results and discussion

5.3.3.1 Electrochemical characterization of cyclotricatechylene (CTC)

Cyclic voltammetry was utilized to explore the electrochemical activation of immobilized CTV to form CTC on the surface of a glassy carbon electrode. Figure 5.18 shows two successive scans of the oxidation of CTV at the glassy carbon electrode in

0.05 M Britton-Robinson buffer (pH 1.0) with a scan rate of 100 mV s^{-1}. In the first scan (dotted line) starting at –0.4 V (*vs.* SCE), a small oxidative peak (Peak I) at *ca.* +1.12 V (*vs.* SCE) is observed followed on the reverse scan, by two reduction peaks (Peak II and Peak III) *ca.* +0.4 V (*vs.* SCE) and *ca.* +0.2 V (*vs.* SCE) respectively after reversed at +1.16 V (*vs.* SCE). On the second scan (solid line), two new oxidation peaks (Peak IV and Peak V) emerge corresponding to the reduction peaks (Peak III and Peak II) respectively while the oxidative peak at *ca.* +1.12 V (*vs.* SCE) is no longer observable.

The proposed reaction for the electrochemical derivatization of CTV to form CTC is depicted in Scheme 5.1. During the first scan, the CTV undergoes a sequence of electrochemical reduction/oxidation steps with an intermediate hydrolysis of the methoxy groups forming the *o*-benzoquinone moieties. [179-181] Then, the *o*-benzoquinone species can undergo an electrochemical redox cycle (Scheme 5.1B), which can be observed in peaks III/IV and peaks II/V in Figure 5.18.

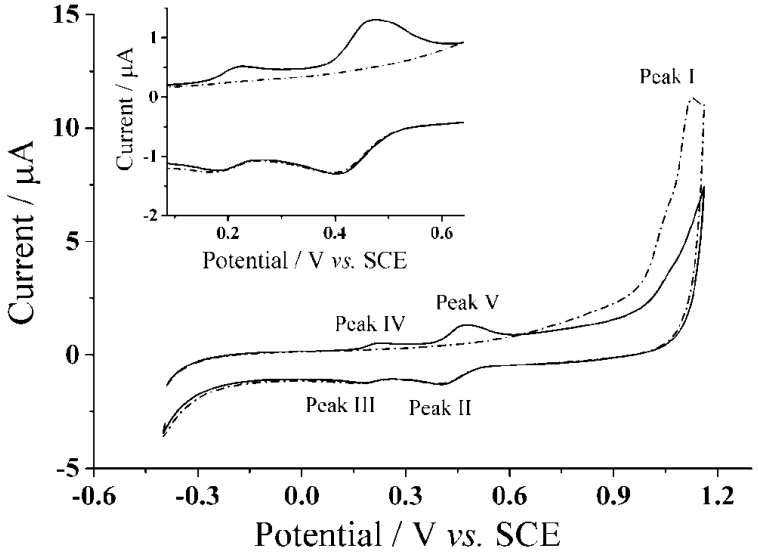

Figure 5.18: The first (dotted line) and second (solid line) scans for the de-methylation of cyclotriveratrylene (CTV) on the glassy carbon electrode in 0.05 M Britton-Robinson buffer solution (pH 1.0) to form cyclotricatechylene (CTC). Scan rate = 100 mV s^{-1}. *Inset:* Magnified view of the potential window of CTC redox reaction.

To determine this optimal condition, a range of different holding time (0 – 60 seconds) at +1.16 V (*vs*. SCE) was carried out in pH 1.0 buffer where the charge at each peak was used for comparison. It was determined that the charge remained consistent for all holding times at each peak. Therefore, there is no need for longer holding time as it is fully converted to CTC once the potential of +1.16 V (*vs*. SCE) was applied. The optimal condition for the conversion to CTC is at a potential sweep, +1.16 V to –0.40 V (vs. SCE), in 0.05 M Britton-Robinson buffer (pH 1.0) at a scan rate of 100 mV s^{-1}. The surface coverage (Γ) of CTC under the optimal condition was determined to be *ca.* 6.4 x 10^{-12} mol cm^{-2}; using Equation 5.1, $\Gamma = Q/nFA$, where the number of electrons, n=6. The CTC surface coverage observed electrochemically is estimated as *ca.* 1 % of the total theoretical coverage. This was estimated knowing that a 20 µL aliquot of 100 µM CTV solution was drop cast onto the electrode. It is likely that not all of the CTV drop casted onto the electrode was electrochemically converted to CTC and therefore the crystals, observed in the secondary electron images, may contain a mixture of CTV and CTC.

Cyclic voltammetry (100 mV s^{-1}) was next performed on the activated modified carbon electrode in 0.15 M phosphate buffer solution (pH 7.0) to observe the voltammetric response of the *o*-benzoquinone species. Figure 5.19 shows two redox process occurring at $E_{1/2} = -0.11$ V and at $E_{1/2} = +0.13$ V (*vs.* SCE) which can be attributed to a total of six electron and six proton oxidation of the three *o*-benzoquinone species (Scheme 5.1B). Note that the peak current at *ca.* +0.10 V (*vs.* SCE) is *ca.* two times larger than the peak current at *ca.* –0.10 V (*vs.* SCE). With a net total of six electrons and six proton redox process, it is proposed that a four electron, four proton process occurs at the larger peak while the other smaller peak undergoes a two electron, two proton process. It is suspected that this *might possibly* be attributed to the

crystalline structure formed during the electrode preparation step with chloroform. Steed et al. reports that CTV can self-assemble accordingly with different solvents. [178] When mixed with chloroform, it can form a weak hydrogen bond to the methoxy oxygen atoms on the CTV molecule therefore exhibiting channel structures where these molecules pack within the other along an axis to form a distinct crystalline phase. [178] Therefore it is *speculated* that when the solvent evaporates during the electrode preparation step, the CTV self-packs so that two rings overlap with others (shown in Scheme 5.2).

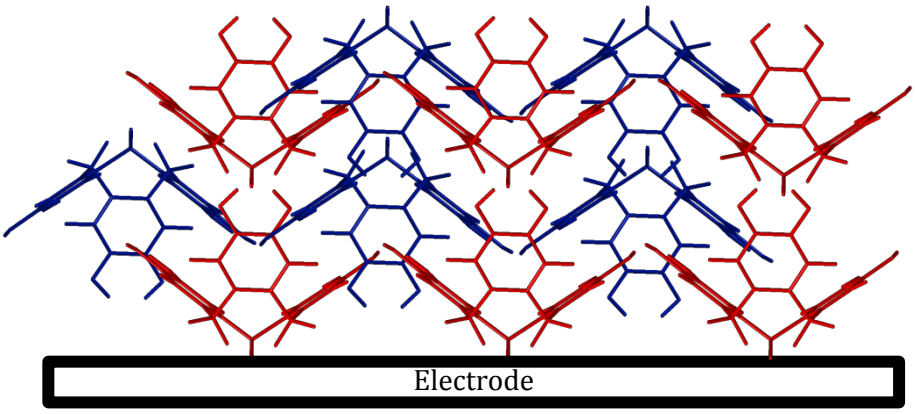

Scheme 5.2: Schematic possible representation of cyclotriveratrylene (CTV) on the electrode surface.

Lastly, a scan rate study was also carried out on the CTC modified glassy carbon electrode to show the voltammetric behaviour. Scan rates varying from 50 mV s^{-1} to 500 mV s^{-1} were run in 0.15 M phosphate buffer (pH 7.0) (Figure 5.20) on the modified electrode. The inset to Figure 5.20 shows a proportional relationship when peak current, I_p, is plotted against scan rate, ν, thus showing that the redox process is surface bound. Further characterization (i.e. pH study) of CTC using electrochemistry will be discussed in the next section (Section 5.4).

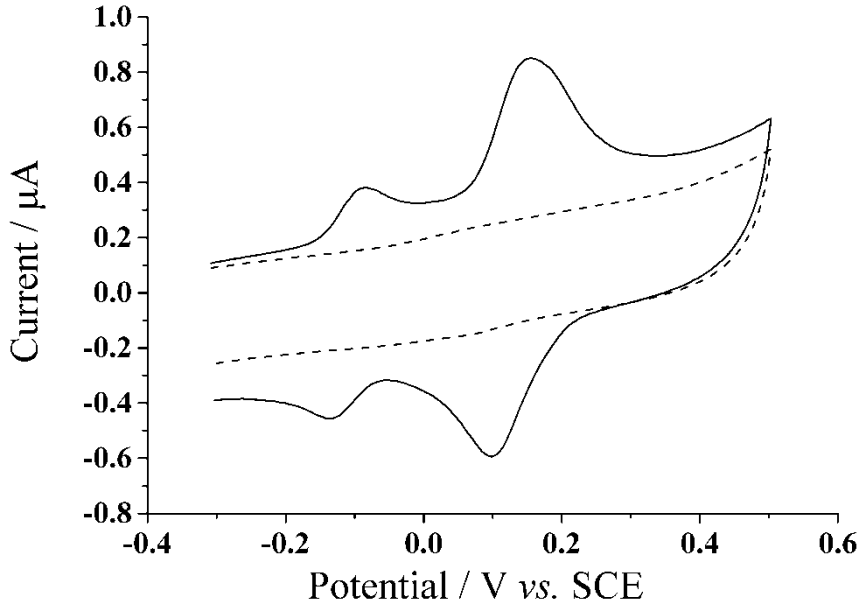

Figure 5.19: Cyclic voltammogram (100 mV s^{-1}) at a bare glassy carbon electrode (dashed line) and cyclotricatechylene (CTC) modified carbon electrode (solid line) in PBS (pH 7.0).

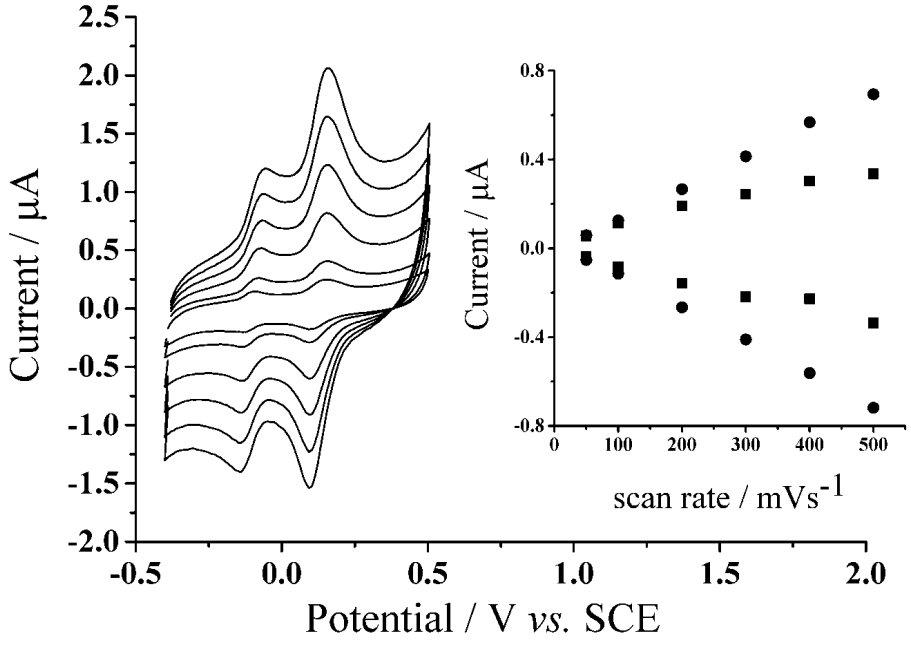

Figure 5.20: Scan rate study of cyclotricatechylene (CTC) in PBS (pH 7.0) at 20°C. *Inset:* Peak current, I_p, *vs.* scan rate, ν.

5.3.3.2 Selective cysteine detection with cyclotricatechylene (CTC)

Figure 5.21 shows the cyclic voltammograms (100 mV s^{-1}) of the CTC modified carbon electrode response to solutions containing 20 μM of each cysteine, homocysteine, and glutathione (pH 7.0). The voltammogram shows the smaller peak *ca.* −0.10 V (*vs.* SCE) appears to be unaffected by any added thiol-containing molecule whilst the larger peak *ca.* +0.10 V (*vs.* SCE) changes with added thiol. Upon a closer look at the larger peak *ca.* +0.10 V (vs SCE), the voltammogram show an increase in the forward anodic peak current, I_{pa}, while the backward cathodic peak, I_{pc}, decreases when the thiol is added to the solution thus indicating that it is an electrocatalytic oxidation reaction (Scheme 4.2); which can be analytically useful. Therefore for the purpose of quantitative analysis, the analytical parameters presented will be primarily focused on peak *ca.* +0.10 V (*vs.* SCE).

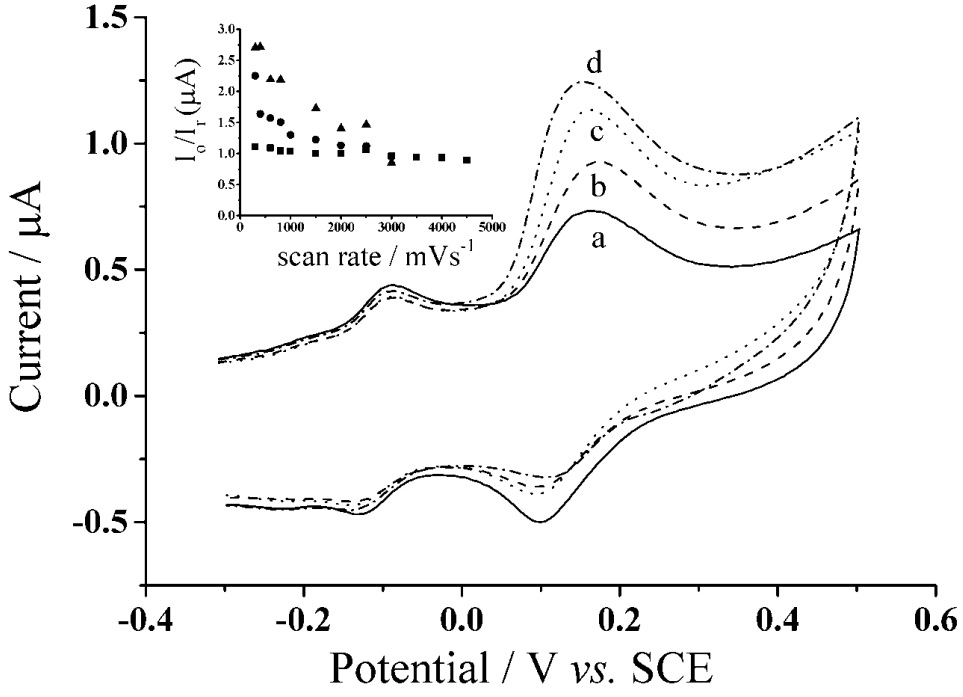

Figure 5.21: Cyclic voltammograms (100 mV s^{-1}) of cyclotricatechylene (CTC) response to a. no thiol, b. 20 μM glutathione, c. 20 μM homocysteine, and d. 20 μM cysteine. *Inset*: Plot of anodic and cathodic peak current ratio, I_o/I_r, as a function of scan rate of homocysteine (▲), glutathione (●), and no thiol analyte (■).

However, selective cysteine detection becomes an issue when all three thiols are present in the same solution as is typical in biological media. To get around this issue, increasing scan rate was applied to solutions containing 80 μM each homocysteine and glutathione (pH 7.0) where the peak current ratio, I_{pa}/I_{pc}, is calculated and then compared to the peak current ratio taken in the absence (Figure 5.21 inset). It was determined that 3.0 Vs^{-1} is the optimum scan rate where the peak current ratio taken in the absence and presence 80 μM of each homocysteine and glutathione are equal to one another. This suggests that it is possible to 'outrun' the homocysteine and glutathione reaction with the *o*-benzoquinone species but allow sufficient time for cysteine to react thus having cysteine selectivity when all three thiols are present in the solution.

Next, cyclic voltammetry (3.0 Vs^{-1}) was utilized to observe the voltammetric behaviour of CTC with varying concentrations of cysteine, from 0 μm to 100 μM (Figure 5.22). The figure shows that as the concentration of cysteine increases, the forward peak increases while the backward peak decreases thus further indicating that it is an electrocatalytic oxidation reaction, as described earlier. An analytical curve was determined for cysteine at this scan rate when the peak current ratio, I_{pa}/I_{pc}, of the peak *ca.* +0.10 V (*vs*. SCE), is plotted with respect to cysteine concentration. The analytical parameters for cysteine detection in PBS (pH 7.0) at 3.0 Vs^{-1} are tabulated in Table 5.1. The linear relationship is $[I_{pa}/I_{pc}]$ (μA) $= 0.966 + (0.023 \pm 0.001)$ [Cys/μM] (n=3) for concentrations up to 40 μM and the limit of detection is determined to be *ca.* (0.6 ± 0.02) μM.

Medium	Scan rate ($V\ s^{-1}$)	Slope ($\mu A\ \mu M^{-1}$)	I_{pa}/I_{pc}	R^2	LOD[a] (μM)	Linear Range (μM)
PBS (pH 7.0)	3.0	(0.023 ± 0.001)	0.966	0.994	0.6 ± 0.02	0.5 – 40
Dulbecco's Modified Eagles Media (pH 8.0)	3.1	(0.031 ± 0.001)	1.09	0.987	0.9 ± 0.02	1.0 – 20

[a] LOD, calculated limit of detection.

Table 5.1: Analytical parameters for selective detection of cysteine using cyclotricatechylene (CTC) modified carbon electrode.

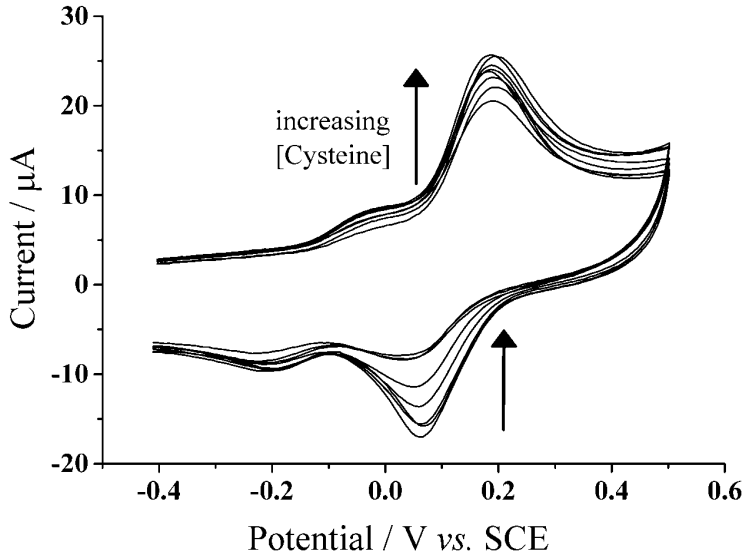

Figure 5.22: Cyclic voltammogram ($3.0\ Vs^{-1}$) of cyclotricatechylene (CTC) modified carbon electrode in varying concentrations of cysteine (pH 7.0).

Preliminary testing of several mixed solutions containing different concentrations of cysteine, homocysteine and glutathione were carried out using the CTC modified carbon electrode in PBS (pH 7.0). Concentrations in the mixed solutions are values typically seen in physiological samples. [42, 43, 46, 61, 77] Using cyclic voltammetry ($3.0\ Vs^{-1}$), the peak current ratio at *ca.* +0.10 V (*vs.* SCE) was calculated for

each mixed solution and the cysteine content can be determined through the analytical curve, mentioned above. Table 5.2 summarizes the results obtained for cysteine at each mixed solution with the CTC modified electrode. The results are well within reasonable deviation, *ca*. 15%, from the cysteine quantity present in the solution. This indicates that the selective detection of cysteine in the presence of other homologues thiols such as homocysteine and glutathione is possible.

Mixed solution			Determined [Cysteine][a] (μM) in	
Homocysteine (μM)	Glutathione (μM)	Cysteine (μM)	PBS (pH 7.0)	Dulbecco's Modified Eagle Media (pH 8.0)
10	10	10	10.1 ± 0.15	9.1 ± 0.05
10	5	5	5.4 ± 0.09	6.7 ± 0.25
10	3	15	13.1 ± 0.15	14.1 ± 0.30
10	1	20	18.4 ± 0.15	19.0 ± 0.12
5	10	5	6.7 ± 0.25	5.6 ± 0.28
3	10	15	14.7 ± 0.13	14.1 ± 0.18
1	10	30	30.2 ± 0.14	26.3 ± 0.16*

[a] Average value ± relative error (n=3). * not within the linear range.

Table 5.2: Cysteine determination in mixed solutions containing homocysteine and glutathione.

5.3.3.3 Application of selective cysteine detection in tissue culture media

A practical assessment of the proposed method was next applied to the cell tissue culture media, Dulbecco's Modified Eagle media (DMEM), as it contains a diverse variety of amino acids and vitamins, which help facilitate cell growth. [38, 182] It is thus a challenging medium for selective electroanalysis. Using the optimal parameters established above, cyclic voltammetry (3.0 Vs^{-1}) was utilized and run in 100 % cell tissue culture media (pH 8.0) with and without the modification of CTC at the carbon

electrode to ensure the window of interest for analysis is free of possible interferences from the media. Figure 5.23 shows no introduction of any new signal from the tissue culture media alone at the bare carbon electrode, which suggests that the media itself will not interfere with our analytical measurements. When the CTC modified carbon electrode is applied to the tissue culture media, two redox peaks, *ca.* –0.17 V (*vs*. SCE) and *ca*. +0.08 V (*vs*. SCE), are observed again corresponding to the two redox process of the *o*-benzoquinones. This observation is consistent with the modified electrode in PBS (pH 7.0) at the same scan rate (Figure 5.22).

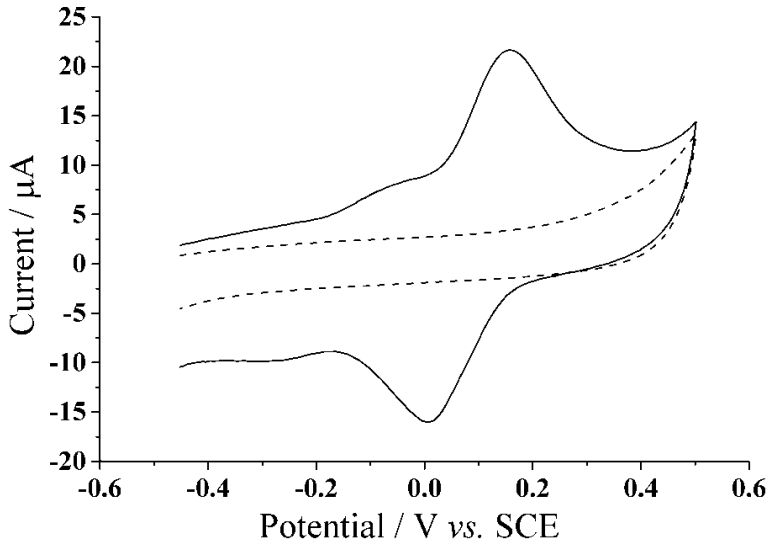

Figure 5.23: Cyclic voltammogram (3.1 Vs^{-1}) at a bare glassy carbon electrode (dashed line) and cyclotricatechylene (CTC) modified carbon electrode (solid line) in tissue culture media (pH 8.0).

To make certain that neither homocysteine nor glutathione will interfere, the media was spiked with 80 μM of each homocysteine and glutathione and the appropriate scan rate to 'outrun' these reactions were found (as described earlier). It was determined that an optimum scan rate of 3.1 Vs^{-1} was sufficient enough to 'outrun' both glutathione and homocysteine in tissue culture media. From there, an analytical

curve was determined when different concentrations of cysteine, ranging from 5 - 60 μM, were added to the media and measured at the CTC modified electrode. The linear relationship was determined to be $[I_{pa}/I_{pc}]$ (μA) = 1.09 + (0.031 ± 0.001) [Cys/μM] (n=3) for concentrations up to 20 μM and the limit of detection is determined to be *ca*. (0.9 ± 0.02) μM (Table 5.1).

To test the selective cysteine detection method in this medium, the cell tissue media was spiked with various amounts of cysteine, homocysteine and glutathione and the optimum condition described above was carried out at the modified electrode. For each spiked sample, the peak current ratio was taken at the peak *ca.* +0.08 V (*vs.* SCE) where the cysteine content was determined by the analytical curve (mentioned above). The results are summarized in Table 5.2, which shows the determined cysteine value is consistent with the spiked cysteine content and is well within reasonable deviation of *ca.* 19 % thus showing that this method for cysteine detection is reliable in the complex cell tissue media.

5.3.4 Conclusions

We have established the formation of CTC from electrode surface immobilized CTV using only electrochemical methods at a carbon electrode. The CTC generated allows selective cysteine detection in the presence of homocysteine and glutathione, at concentrations typically seen in biological samples, in both buffer solution and tissue culture media. The sensitivity is *ca.* 0.023 μA μM^{-1} and *ca.* 0.031 μA μM^{-1} with a limit of detection of *ca.* 0.6 μM and *ca*. 0.9 μM for buffer solution and tissue culture media respectively. The detection was successfully applied to several spiked sample solutions where determined values were consistent with the spiked cysteine content with an

average error acceptable for bio-medical marker applications. This method presents a potentially useful and novel way for selective detection of cysteine and opens up the use of CTC modified electrodes for electroanalysis.

5.4 Precursor modified electrodes: Electrochemical detection of captopril

5.4.1 Introduction

Electrochemical detection is not only valuable for biomolecules but for pharmaceutical drugs as well. Captopril, CAP (Figure 5.24), is an angiotensin-converting enzyme inhibitor (ACE inhibitor). [183-185] It is widely used in treatment of hypertension and other types of congestive heart diseases. [185, 186] It is marketed under the trade name, Capoten, by Bristol-Myers Squibb. [187, 188] As an orally active antihypertensive drug, it contains a terminal thiol group, which can act as a free radical scavenger. [185, 186, 189-191] Although toxicity from ingesting captopril is uncommon, undesirable side effects can occur when given in high doses to patients with collagen vascular disease or renal insufficiency. [186, 192, 193] Some side effects may include hypotension [184, 193], renal hemodyaminc dysfunction [193], dry cough [183, 184, 193], angioedema [184, 193], bone marrow suppression [194], rash [183, 185], and proteinuria. [183, 194] Therefore determination of thiol-based drugs, such as captopril, can also be desirable in the biomedical and pharmacology community as a way to monitor patients and/or for pharmaceutical formulation quality control purposes.

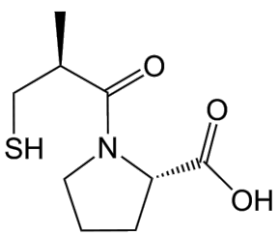

Figure 5.24: Chemical structure of thiol-containing drug captopril.

While many of the analytical methods mentioned in Section 2.2 are also used to determine captopril concentrations, the possible drawbacks remain unchanged. Once again, electrochemical methods can offer the contrary. Table 5.3 summarizes a number of methods developed for captopril determination via electrochemistry. In this section, the same principle described in the previous section on thiol detection via cyclotricatechylene (CTC, Scheme 5.1) will be adapted into carbon paste electrodes (CPE). Typically, CPEs are usually comprised of a mixture of carbon powder, and a nonelectrolytic binder. [122, 123] The use of CPEs can offer a number of advantages, as they can be facile, relatively cheap to fabricate, and easy to use. [122, 123] In fact, one of the most frequently articulated advantage of carbon paste is the diverse applicability of the substrate. [122-124] Herein, this section will demonstrate the incorporation of the precursor to CTC, cyclotriveratrylene (CTV, depicted in Scheme 5.1), into a simple carbon paste electrode first; then, electrochemically activated to form its *o*-quinone derivative, CTC. [134] Thus, the method presented in this section will be primarily focused on the quinone-thiol reaction via electrocatalytic oxidation in the detection of thiol group containing drug, captopril.

Electrode	Electrochemical Method	Sensitivity	LOD (μM)	Ref.
NiO NP modified (9,10-dihydro-9,10-ethanoanthracene-11,12-dicarboximido)-4-ethylbenzene-1,2-diol carbon paste electrode [a]	SWV	29.968 μA μM^{-1}	0.0037	[195]
N-(4-hydroxyphenyl)-3,5-dinitrobenzamide modified ZnO/CNT-CPE [a]	SWV	26.54 μA μM^{-1}	0.01	[196]
nano-TiO_2/ferrocene carboxylic acid modified CPE [b]	CV	0.0037 μA mM^{-1}	0.01	[197]
1,4-phenylene-N,N′-bis (O,O-diphenylphoramidate), L-cysteine capped CdS quantum dots/MWCNT-GCE [c]	CA	N/A	0.015	[198]

BDD [c]	SWV	0.082 $\mu A\ mg^{-1}\ L^{-1}$	0.017	[199]
p-aminophenol CNT-CPE [a]	CV/ CA/ SWV	18.5266 $\mu A\ \mu M^{-1}$	0.02	[200]
benzoylferrocene CNT-CPE [b]	CV / SWV/ CA	N/A	0.03	[201]
N-(3,4-dihydroxyphenethyl)-3,5-dinitrobenzamide modified CNT-CPE [a]	DPV	5.547 $\mu A\ \mu M^{-1}$	0.034	[202]
ZnO nanoparticle modified carbon paste electrode [a]	SWV	14.7610 $\mu A\ \mu M^{-1}$	0.04	[203]
(E)-3-((2-(2,4-dinitrophenyl)hydrazono)methyl)benzene-1,2-diol modified CNT-CPE [c]	CV	0.216 $\mu A\ \mu M^{-1}$	0.07	[204]
vinylferrocene modified carbon nanotubes paste electrode [a]	SWV	0.1091 $\mu A\ \mu M^{-1}$	0.08	[205]
ferrocenedicarboxylic acid modified CPE [a]	SWV	355 $\mu A\ \mu M^{-1}$	0.091	[206]
Mn-nanoparticles decorated organo-functionalized SiO_2-Al_2O_3 mixed-oxide [a]	CV	1.2720 $\mu A\ \mu M^{-1}$	0.095	[207]
ferrocene CNT-CPE [b]	DPV	0.23 $\mu A\ \mu M^{-1}$	0.15	[208]
iron oxide nanoparticles modified CPE [c]	CV	2.9 $\mu A\ \mu M^{-1}$	0.2	[209]
ferrocenemonocarboxylic acid modified carbon nanotubes paste electrode [a]	CV	0.2638 $\mu A\ \mu M^{-1}$	0.3	[210]
cobalt-5-nitrolsalophen CPE [c]	DPV	0.013 $\mu A\ \mu M^{-1}$	1.1	[211]
copper hexacyanoferrate/ordered mesoporous carbon-modified glassy carbon electrode [b]	CV	N/A	1.2	[212]
2,2′-[1,7-heptanediylbis(nitrilomethylidene)]-bis(4-hydroxyphenol) modified CNT-CPE [b]	DPV	N/A	2.43	[213]

4, 4'-Biphenol modified GCE [c]	LSV	0.0019 $\mu A\ \mu M^{-1}$	3.34	[214]
chlorpromazine at GCE [a]	CV	14.72 $\mu A\ mM^{-1}$	4.8	[215]
Au electrode modified with graphene-AuAg nanocomposites [b]	DPV	10^{-3} $A\ M^{-1}$	6	[216]
platinum electrode modified with iron (III) hexacyanoferrate (II) film [c]	CV	0.003 $\mu A\ M^{-1}$	7	[217]

[a] Limit of detection (LOD) = $Y_B + 3S_B$, [b] Limit of detection (LOD) = $3S_B$, [c] Limit of detection (LOD) = $3S_B/S$. CA, chronoamperometry; CV, cyclic voltammetry; DPV, differential pulse voltammetry; LSV, linear sweep voltammetry; SWV, square-wave voltammetry; NiO, nickel (II) oxide; ZnO, zinc oxide; CNT, carbon nanotube; CPE, carbon paste electrode; TiO_2, titanium dioxide; CdS, cadmium sulfide; BDD, boron doped diamond; Mn, manganese; SiO_2, silicon dioxide; Al_2O_3, aluminium oxide; GCE, glassy carbon electrode; Au, gold; Ag, silver.

Table 5.3: Literature on the electrochemical detection of captopril.

5.4.2 Experimental procedure

5.4.2.1 Reagents

Captopril (≥ 98 %, Cambridge Biosciences Ltd., Cambridge, UK), graphite powder (>20 µm synthetic, Sigma-Aldrich, Dorset, UK), and mineral oil (Sigma-Aldrich, Dorset, UK) was purchased and as used received without any further purification steps. CTV was synthesized previously according to the method reported by Lindsey (see Section 5.3.2.2 for details). [173] Analysis and characterization of the CTV material was reported in Section 5.4.2.2. [134] Buffer solutions, 0.05 M, were prepared accordingly to Section 5.4.2.2.

5.4.2.2 Electrode preparation

Cyclotriveratrylene modified carbon paste electrodes (CTV-CPE) were prepared accordingly, where cyclotriveratrylene (CTV) solids were dissolved in chloroform to

make up a solution of 1.0 mM. Afterwards, 3.0 mL of the cyclotriveratrylene-chloroform solution was mixed with 2.0 g of graphite powder, by hand, and then allow the solvent to evaporate overnight. This allows the cyclotriveratrylene solid to be distributed onto the graphite powder. Then, a modified CTV-graphite paste was prepared by hand mixing 70 μL of mineral oil per 200 mg of CTV-graphite powder. The resulting carbon paste was packed into 4 mm diameter x 1 mm depth well cavity working electrode. The working electrode consisted of a Teflon tube with a copper rod as the electrical contact.

Cyclotricatechylene (CTC) in the modified carbon paste was electrochemically activated using the method reported in Section 5.1.2.1. [134] A potential cycle from +0.05 V to +1.20 V (*vs*. SCE) with a sweep rate of 100 mV s^{-1} was applied to the CTV modified carbon paste electrode in 0.05 M Britton-Robinson buffer solution (pH 1.0). Afterwards, the electrode was rinsed with deionized water carefully before proceeding with all electrochemical experiments. Due to the solubility of the CTC, a new modified electrode was prepared before each experiment. Each experiment was repeated at least five times with a fresh, flat surface. The reproducibility of the current at each new electrode had a relative standard deviation of *ca.* (1.5 $\pm$ 0.5) %.

5.4.3 Results and discussion

In this section, the electrochemical activation of cyclotriveratrylene (CTV) to form cyclotricatechylene (CTC) via the modified carbon paste electrode (CPE) is described and optimized. Then the CTC-CPE is characterized using voltammetric methods. Thereafter, the electrochemical determination of captopril is investigated and parameters optimized for versatile, simple detection.

5.4.3.1 Electrochemical characterization of cyclotricatechylene (CTC)

The cyclotriveratrylene (CTV) in the modified carbon paste electrode (prepared as above) was electrochemically converted to cyclotricatechylene (CTC) through potential cycling (*ca.* 2 scans) in 0.05 M Britton-Robinson buffer solution (pH 1.0) (Scheme 5.1). Figure 5.25 shows two successive cyclic voltammetric scans at a voltage scan rate of 100 mV s^{-1} of the electrochemical activation of CTV to form CTC at the carbon paste electrode. During the first scan (solid line), oxidative peaks *ca.* +1.0 V and +1.1 V (*vs.* SCE), peaks I and II respectively, are first observed. Then, two reduction peaks *ca.* +0.43 V and +0.21 V (*vs.* SCE), peaks III and IV respectively, are observed on the reverse scan. During the second cycle, two new oxidation peaks, V and VI, at *ca.* +0.21 V and +0.45 V (*vs.* SCE) respectively, emerged and are due to the oxidation of the products formed at peaks III and IV; a significant decrease in the oxidative peaks I and II are simultaneously observed. These observations can be rationalized by the reaction mechanism for this electrochemical activation of CTC from its precursor, CTV, at the modified carbon paste electrode depicted in Scheme 5.1. [134] A sequence of electrochemical oxidation and reduction steps are required for the methoxy groups to undergo an intermediate hydrolysis to form the quinone moieties. [134] Subsequently, each of the quinone species undergoes a combination of an electrochemical two-proton, two-electron or four-proton, four-electron redox cycle, seen in peaks IV/V and III/VI (Figure 5.25) corresponding to *o*-quinone/hydroquinone redox processes.

To ensure that the graphite paste itself has no contribution to the signals observed, a graphite paste electrode was made without added cyclotriveratrylene and subjected to the same electrochemical steps as described above. Figure 5.26 shows cyclic voltammogram overlay for the carbon paste electrode with and without the

added precursor in Britton-Robinson buffer (pH 1.0) at a scan rate of 100 mV s^{-1}. The figure shows that the graphite paste alone has no contribution to the signals associated with the *o*-quinone species. Therefore the two redox process observed at *ca.* +0.21 V and +0.43 V (*vs*. SCE) can be attributed to the total six electron and six proton oxidation of the three *o*-quinone species on the CTC molecule (Figure 5.26). Square-wave voltammetry (frequency, 25 Hz; amplitude, 5.0 mV; step potential, 4.0 mV) was utilized at the CTC-CPE in 0.05 M Britton-Robinson Buffer (pH 1.0) to obtain a more sensitive approach to investigating the peak current relationship at the CTC-CPE (Figure 5.27). Note that the peak current in peak I is about half the size of peak II, this suggests that with an overall of a six electron and six proton redox process (Figure 5.26); a two electron, two proton process may be observed in the smaller peak (*ca.* +0.21 V *vs*. SCE) while a four electron and four proton process is observed in the larger peak (*ca.* +0.43 V *vs*. SCE) this observation is consistent with Section 5.3.

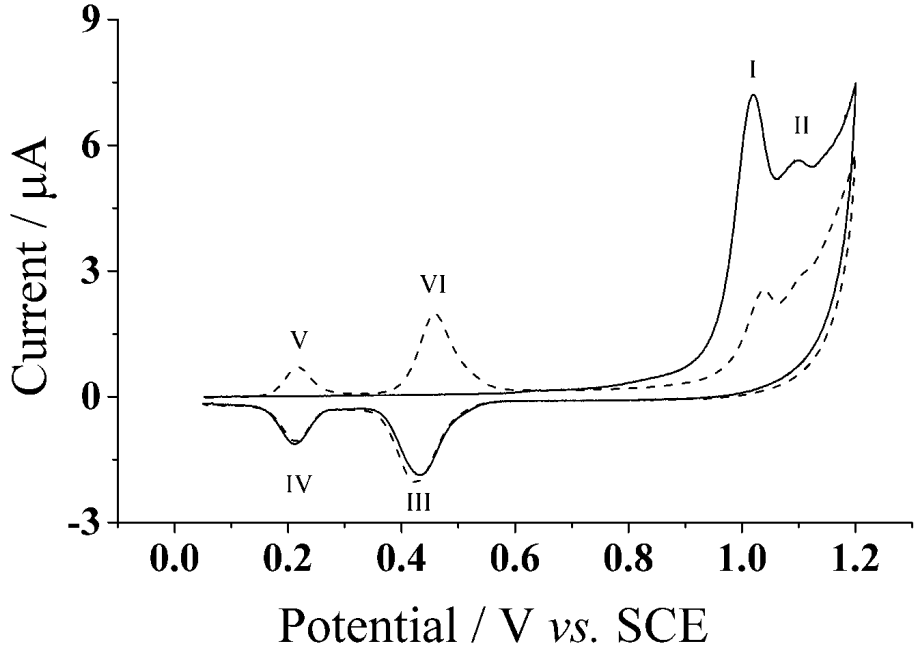

Figure 5.25: First (solid line) and second (dotted line) scans for the de-methylation of cyclotriveratrylene (CTV) to form cyclotricatechylene (CTC) at carbon paste electrode

(CPE) in 0.05 M Britton-Robinson buffer (pH 1.0). Scan rate = 100 mV s^{-1}.

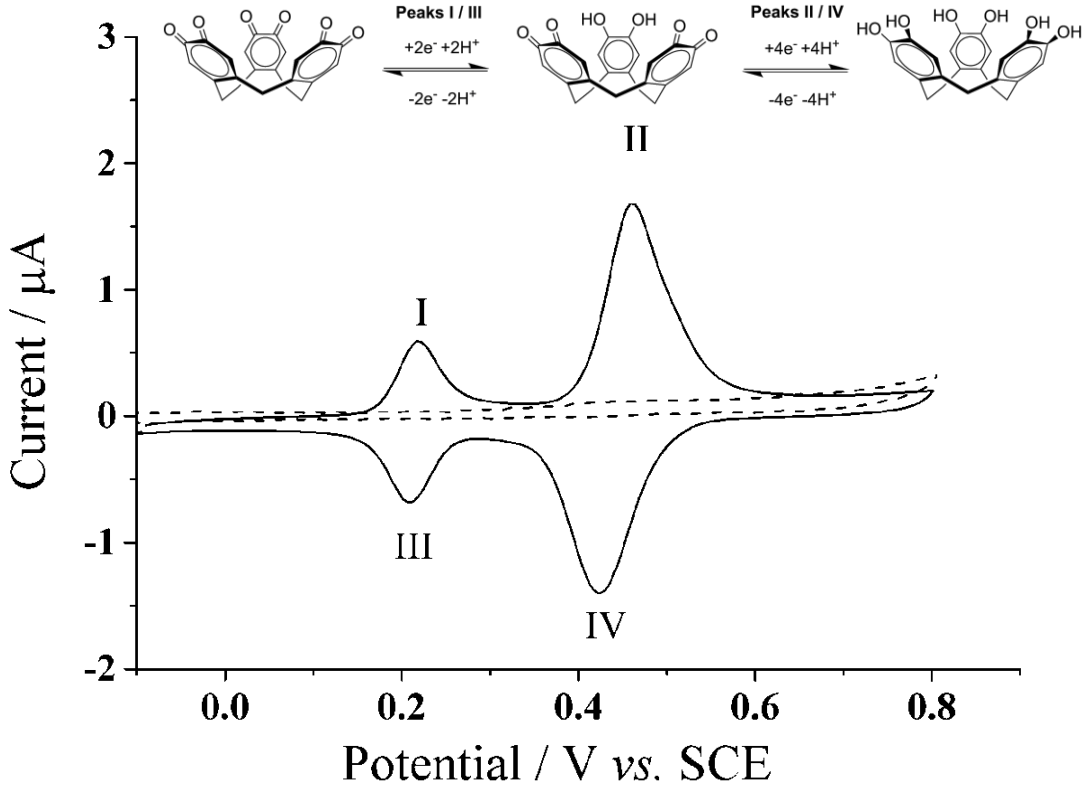

Figure 5.26: Cyclic voltammogram at bare carbon paste electrode (dash line) and CTC-CPE (solid line) in 0.05 M Britton-Robinson Buffer (pH 1.0). Scan rate = 100 mV s^{-1}. *Top:* Redox reaction of CTC.

Next, the voltammetric behaviour of the activated CTV was investigated in acidic conditions after electrochemical activation of the modified carbon paste electrode. Using cyclic voltammetry, a scan rate study was carried out at the CTC-CPE in pH 1.0 buffer. Figure 5.28 shows the voltammetry of the CTC-CPE at varying scan rates from 25 mV s^{-1} to 500 mV s^{-1}. When the peak currents, I_p, of each peak is plotted against scan rate, ν, a linear proportional relationship is observed thus indicating that the process is surface bound (Figure 5.28 inset), as expected for reactants immobilized with a carbon paste electrode.

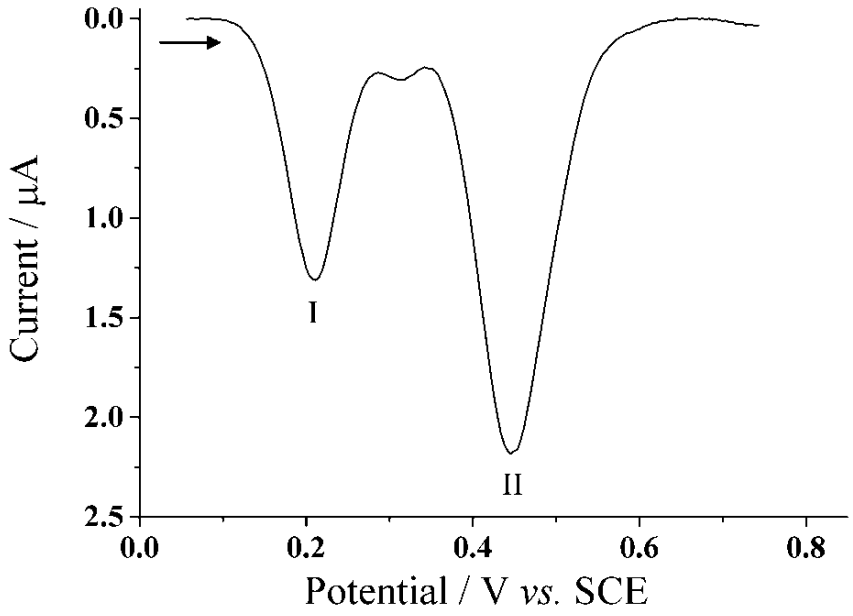

Figure 5.27: Squarewave voltammogram of cyclotricatechylene (CTC) in 0.05 M Britton-Robinson Buffer (pH 1.0). (frequency, 25 Hz; amplitude, 5.0 mV; step potential, 4.0 mV)

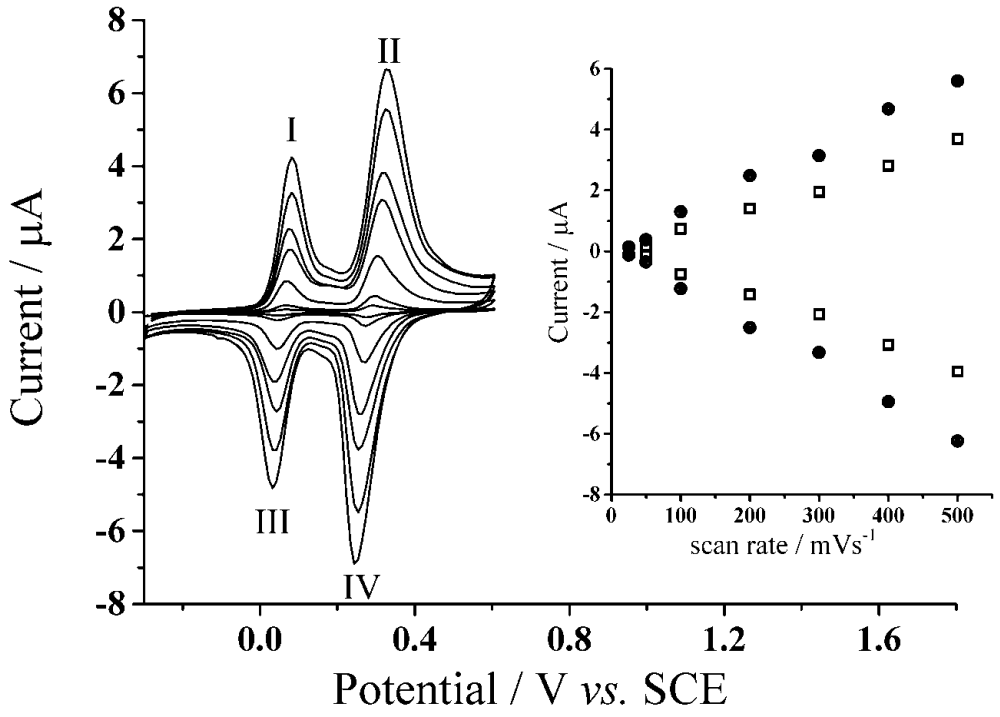

Figure 5.28: Scan rate study of CTC-CPE in 0.05 M Britton-Robinson Buffer (pH 1.0). *Inset*: Peak current, I_p, versus scan rate, v, of □ Peak I/III, ● Peak II/IV

5.4.3.2 pH study of cyclotricatechylene (CTC)

Cyclic voltammetry (100 mV s^{-1}) was utilized to investigate the effect of pH at the activated modified electrode. A range of pH buffers (pH 2−12) was made and tested to determine the voltammetric response. Figure 5.29 shows the cyclic voltammetric response at the activated precursor (CTC) modified electrode from pH 2 to 9. The figure shows that as the pH increases, the peaks shift towards negative potentials and a decrease of peak current is evident. The signals for the CTC were inconclusive for pH buffers beyond 9 due to poorly resolved signals and working potential window. However, when the anodic peak potentials is plotted against pH (Figure 5.30a), the plot shows a linear relationship between the peak potential with respect to pH unit for both set of redox couple. The gradient is (58 ± 0.8) mV/pH and (57 ± 0.9) mV/pH for peaks I/III and peaks II/IV respectively, which is close to the Nernstian value for a two-electron, two-proton process. When the anodic peak currents were plotted against pH unit, illustrated in Figure 5.30b, it was observed that peaks I and II have a 1:2 ratio at pH range 2 – 4 and then the ratio decreases towards a 1:1 ratio in neutral to basic conditions. This suggests that the CTC redox couple is limited by the available protons in the solutions. Therefore, acidic solutions would be the best condition for this mediator. The 1:2 peak current ratio in acidic solutions can be rationalized by the distribution of the net total six-electron, six-proton redox process of the CTC. It is proposed that a two-electron, two-proton process occurs during the smaller peak while a four-electron, four-proton process occurs during the larger peak. [134]

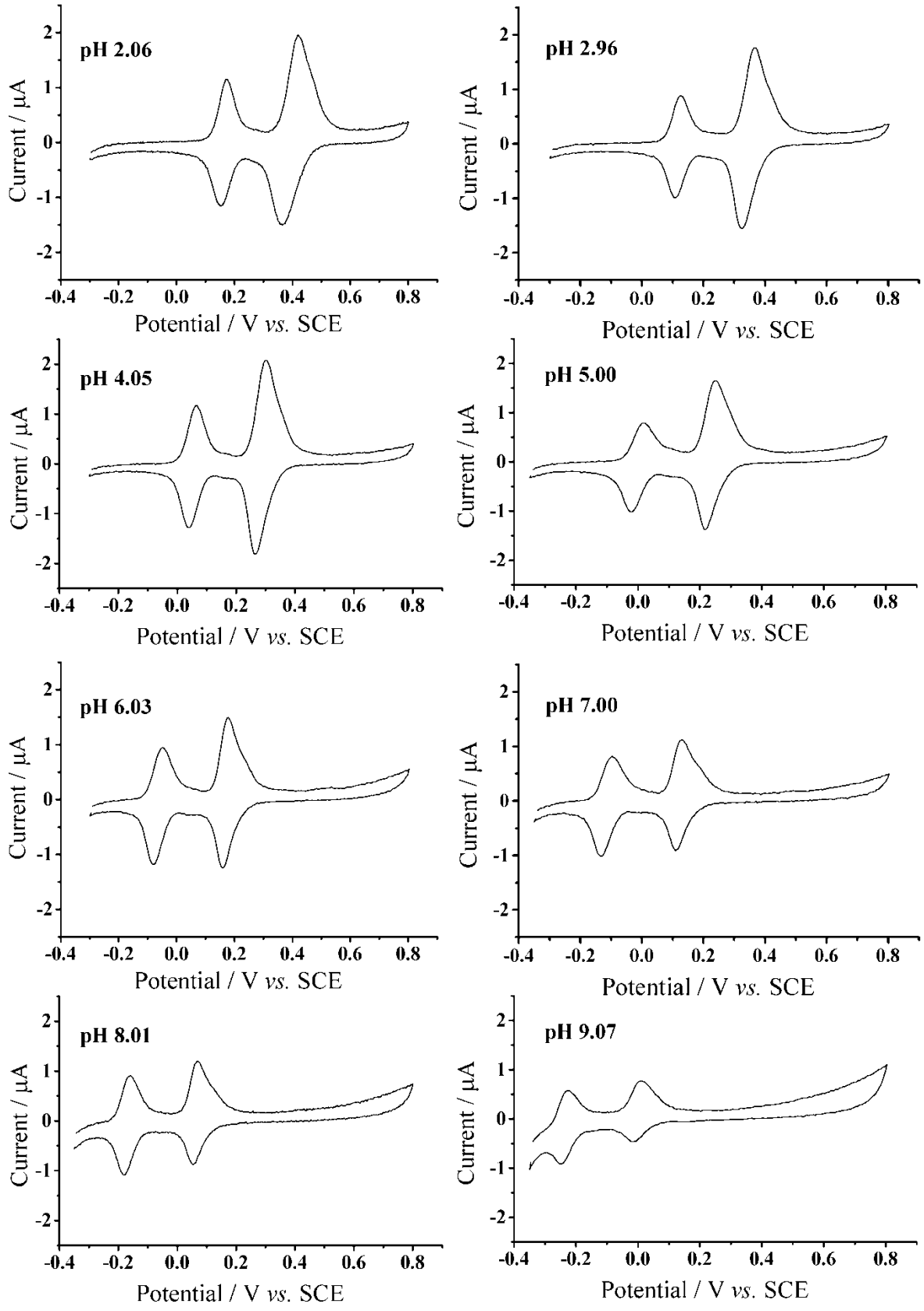

Figure 5.29: Cyclic voltammetry of CTC-CPE in varying pH buffers (pH 2- 9) at 20°C. Scan rate = 100 mV s^{-1}.

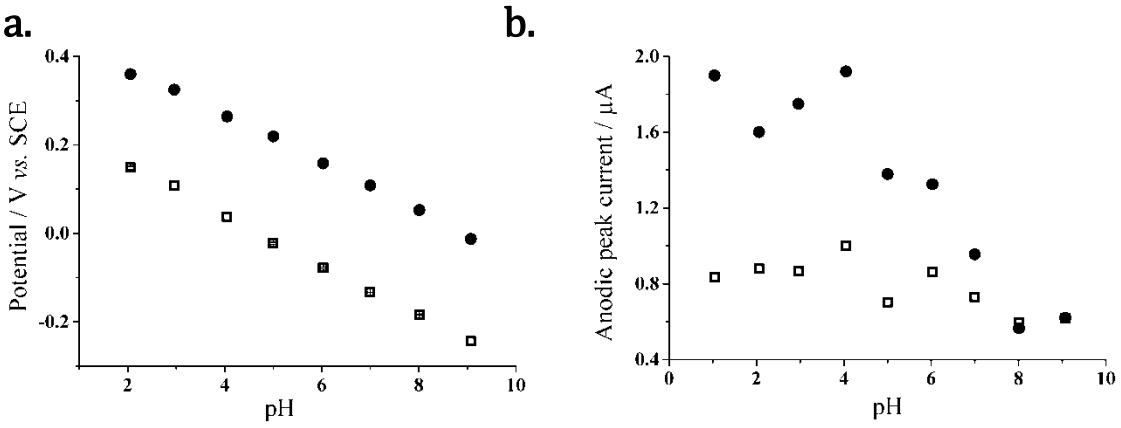

Figure 5.30: a. Peak potential, *E*, vs. pH of □ Peak I and ● Peak II. b. Anodic peak current, I_{pa}, vs. pH.

5.4.3.3 Electrochemical determination of captopril

Cyclic voltammetry (100 mV s^{-1}) was carried out at the activated modified electrode for varying concentrations of captopril, 0.5 – 100 μM, in the presence of 0.05 M citrate buffer (pH 4.0) at 20°C (Figure 5.31). This buffer solution was first chosen to investigate the detection of captopril at the activated modified carbon paste electrode under mild acidic conditions. The figure shows that with increasing concentration of the thiol containing drug, both forward peaks increase as the backward peaks decrease. This suggests that the *o*-quinone species within the cyclotricatechylene undergo electrocatalytical oxidation reaction with the captopril as described in Section 4.1. Though the anodic / cathodic peaks to peaks II/III and peaks I/IV seem to increase / decrease respectively together with increasing target thiol concentration, analytical determination of captopril was not possible using square-wave voltammetry. This is because of the variable mediator loading at the carbon substrate as each new surface was prepared, the relative standard deviation was found to be *ca.* (10 $\pm$ 2.0) %. However, it was successfully and sensitively determined when each forward signal was

normalized to its respective backward signal; the reproducibility had a low relative standard deviation of *ca.* (1.5 ± 0.5) %.

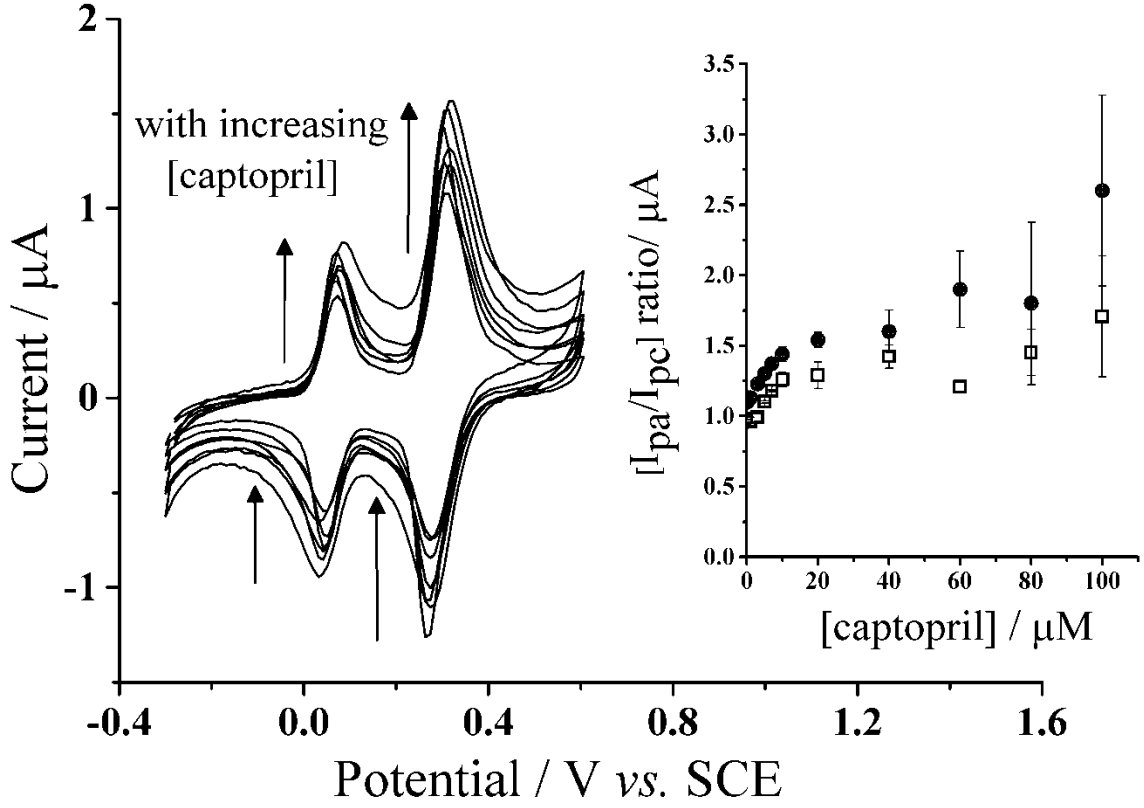

Figure 5.31: Cyclic voltammetry at CTC-CPE in varying concentrations of captopril, 0.5 – 100 μM (pH 4.0). *Inset:* Peak current ratio, I_{pa} / I_{pc}, versus varying concentrations of captopril. □ Peak I/III and ● Peak II/IV.

Therefore, cyclic voltammetry was utilized once again to determine the analytical parameters for this system. The inset to Figure 5.31 shows that when the forward peak currents are normalized to their corresponding backward peak currents, a linear relationship was determined. The linear relationship for peaks I/III is $[I_{pa} / I_{pc}]_{I/III}$ (μA) = 0.91 + (0.036 ± 0.003) [CAP/μM] (n=5) for concentrations from 4 to 10 μM; with a sensitivity of (0.036 ± 0.003) μA μM^{-1} and an experimental determining limit of detection of (4.0±0.2) μM. The linear relationship for peaks II/IV is given as $[I_{pa} / I_{pc}]_{II/IV}$ (μA) = 1.11 + (0.036 ± 0.002) [CAP/μM] (n=5); where the sensitivity is also (0.036 ±

0.002) μA μM^{-1} and an experimental limit of detection of (1.0±0.1) μM. The limit of detection for both set of redox peaks was determined experimentally and is the real limit value for this system. Given that the experimental limit of detection is much lower for redox couple at peaks II/IV than at peaks I/III, it is best to focus on the redox couple II/IV for the analytical determination of captopril at the activated modified carbon paste electrode. A summary of the analytical parameters for captopril detection at the CTC-CPE is tabulated in Table 5.4.

Condition for Captopril detection	Sensitivity (μM μA^{-1})	Linear Regression	Linear Range (μM)	Experimental LOD [a] (μM)
pH 1	0.051 ± 0.003	0.996	1.0 – 7	1.0 ± 0.2
pH 4	0.036 ± 0.002	0.988	1.0 – 10	1.0 ± 0.1
pH 7	0.038 ± 0.010	0.966	3 – 7	3.0 ± 0.2
pH 4 with 50% reduction of mediator	0.045 ± 0.005	0.983	0.5 – 3	1.0 ± 0.1

[a] LOD, limit of detection

Table 5.4: Summary of analytical parameters for captopril detection at CTC-CPE (Peak II/IV)

Next, we investigated whether it was possible to optimize the conditions of the detection method to obtain a more sensitive response at the CTC-CPE. One variable is to change the loading of the CTC precursor, CTV, at the graphite prior to making the paste. To do this, the concentration of the CTV was reduced by 50 % but the volume of the total solvent remained constant to maintain the same paste mix consistency. As a result, different concentrations of captopril were tested using the same experimental conditions as described above. A linear relationship was determined when the peak current ratio of peaks II/IV was plotted with concentration of captopril. Also tabulated

in Table 5.4, the linear relationship for captopril at the CTC-CPE with reduced mediator loading is $[I_{pa} / I_{pc}]_{II/IV,\ 50\ \%}$ (μA) = 1.10 + (0.045 ± 0.005) [CAP/μM] (n=5) at the linear range of 0.05 – 3 μM; with a sensitivity of (0.045 ± 0.005) μA μM^{-1} and an experimental limit detection of (1.0 ± 0.1) μM. The analytical parameters of the reduced mediator did not make a significant difference in sensitivity and limit of detection; however, the range for linear detection decreased as we decreased the quantity of mediator.

The next variable we investigated was the change in pH buffer solution. Captopril detection at the CTC-CPE was tested separately in pH 1.0 and 7.0 buffer solutions using cyclic voltammetry (100 mV s^{-1}) at 20°C; the loading of the mediator on the carbon still remained the same as described in Section 5.4.2.2. Analytical parameters were determined and compared with those parameters determined at pH 4.0, described at the beginning of this section. The forward and backward peak current ratio of peaks II/IV was plotted with respect to captopril concentration at each buffer solution tested. The linear relationship for captopril detection at the CTC-CPE under buffer solution at pH 1.0 is $[I_{pa} / I_{pc}]_{II/IV,\ pH\ 1}$ (μA) = 1.19 + (0.051 ± 0.003) [CAP/μM] (n=5); where the sensitivity is (0.051 ± 0.003) μA μM^{-1} and the experimental limit of detection is (1.0±0.2) μM. For pH 7.0 buffer, a linear relationship was determined to be $[I_{pa} / I_{pc}]_{II/IV,\ pH\ 7}$ (μA) = 0.97 + (0.038 ± 0.01) [CAP/μM] (n=5) with a narrow linear range of 3.0 – 7.0 μM. The sensitivity is (0.038 ± 0.01) μA μM^{-1} with an experimental limit of detection of (3.0±0.2) μM. These values are tabulated in Table 5.4 and compared against each other. As the parameters determined in pH 7.0 buffer solution give a poor response due to the reduced number of available protons in the solution. The parameters under acidic conditions are comparable; as pH 1.0 has a higher sensitivity, while pH 4.0 has a wider linear range. Therefore, depending on the required application, this simple method for captopril detection can be versatile in most acidic medium.

5.4.4 Conclusions

The determination of the thiol-based drug, captopril, was developed using cyclotricatechylene (CTC) from a simple carbon paste electrode modified with its precursor, cyclotriveratrylene (CTV), using only electrochemical methods. The electrochemical generated CTC allows selective detection of the thiol containing drug compound, captopril, via electrocatalytic oxidation reaction. By taking advantage of this reaction, optimization of this detection method was undertaken. Comparison of the analytical parameters at different variables tested determined that acidic conditions are best suited for this with a real (measurable) experimental limit of detection at 1 μM. This facile, easy method of detection via electrocatalytical reaction is shown to be also useful towards applications in pharmaceutical and/or biological assays. Thus now concludes the work on the electrochemical detection of thiol containing compounds via electrocatalytic reaction, the following chapter will discuss thiol detection via 1,4-Michael addition reaction.

Chapter 6

Thiol detection via 1,4-Michael addition reaction

This chapter will continue its investigation into selective thiol determination at various modified carbon electrode. Its contents will discuss thiol detection using an *ortho*-quinone based mediator, specifically catechol (Figure 6.1), via 1,4-Michael addition reaction. This second mechanistic route initially involves the electro-oxidation of the hydroquinone to form *ortho*-quinone thus allowing a nucleophilic reaction to take place (Section 4.2). The development of the methodology is further refined by employing screen-printed electrodes. The work presented in this chapter has been published in *Electroanalysis* [218], *Analyst* [143], and *Sensors* [133]; where they were done in collaboration with Professor Denise Lowinsohn.

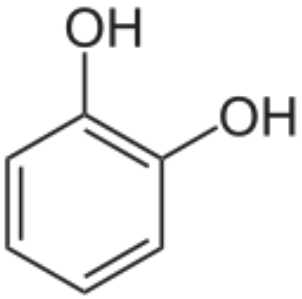

Figure 6.1: Chemical structure of catechol.

6.1 Simultaneous detection of homocysteine and cysteine in the presence of ascorbic acid and glutathione using a nanocarbon modified electrode

6.1.1 Introduction

As mentioned in Chapter 2, concentrations of thiol-based antioxidants are critical to maintaining regular function of the biological system as they have particular physiological roles. When alteration of these concentrations occurs at the physiological level, it may lead to certain disorders, such as cyntiosis and hyperhomocysteinemia. [35, 73] Cystinosis is a disorder that can occur when cysteine concentrations in the plasma are above 30 μM which can cause formation of cysteine crystals in the cornea and/or kidneys. [42, 43, 55, 64, 219] Hyperhomocystienemia is another disorder when levels of homocysteine are elevated to 15 μM or more, which can cause brittle bones. [42, 220] Unfortunately in some rare cases, these disorders can occur at the same time in a patient. [84, 221] Thus the necessity for an analytical methodology to detect compounds, such as homocysteine and cysteine, simultaneously and selectively would be beneficial to be used as a quick diagnostic tool. Yet, the current type of detection methods, especially electrochemical, requires the use of a separation technique. [48, 93, 136, 222, 223] Therefore this section will report on the simultaneous and selective electrochemical detection of homocysteine and cysteine using a nanocarbon modified carbon electrode *without* the use of separation techniques and sample pretreatment.

Previously in Section 5.2, the use of nanocarbon showed that the porous material allows more surface area for the redox species to immobilize itself onto therefore increasing current density. This results in a type of composite electrode with characteristics such as sensitivity, size, and high volume of active sites. For this section, nanocarbon was modified onto the electrode surface again to investigate the

electrochemical behaviour of thiol detection with an electro-oxidised catechol via 1,4-Michael addition reaction. [137, 167, 224, 225]

6.1.2 Electrode preparation

The electrodes were prepared accordingly to Section 3.3.1.1

6.1.3 Results and discussion

6.1.3.1 Electrochemical characterization of catechol on nanocarbon modified glassy carbon electrode

Initial characterization of catechol using a nanocarbon modified glassy carbon electrode (NC-GCE) was performed using cyclic voltammetry to determine the electrochemical behaviour. Cyclic voltammograms of the modified electrode were recorded in a solution containing 0.1 mM catechol (PBS, pH 7.0) at 20˚C at varying scan rates, ranging from 25 mV s^{-1} to 300 mV s^{-1} (shown in Figure 6.2). The figure shows that the catechol undergoes a redox process *ca.* +0.14 V (*vs*. SCE). This is attributed to the two electron, two proton oxidation of the catechol to the corresponding *ortho*-quinone species [38, 52, 142], refer to the first step in Equation 4.2. The voltammograms in Figure 6.2 show the catechol peak, *ca.* +0.14 V (*vs*. SCE), splits with increasing scan rate. Inspection of inset to Figure 6.2 shows that anodic peak current, I_{pa}, increases approximately linearly with voltage scan rate, ν, which suggests behaviour consistent with surface confined voltammetry. [2]

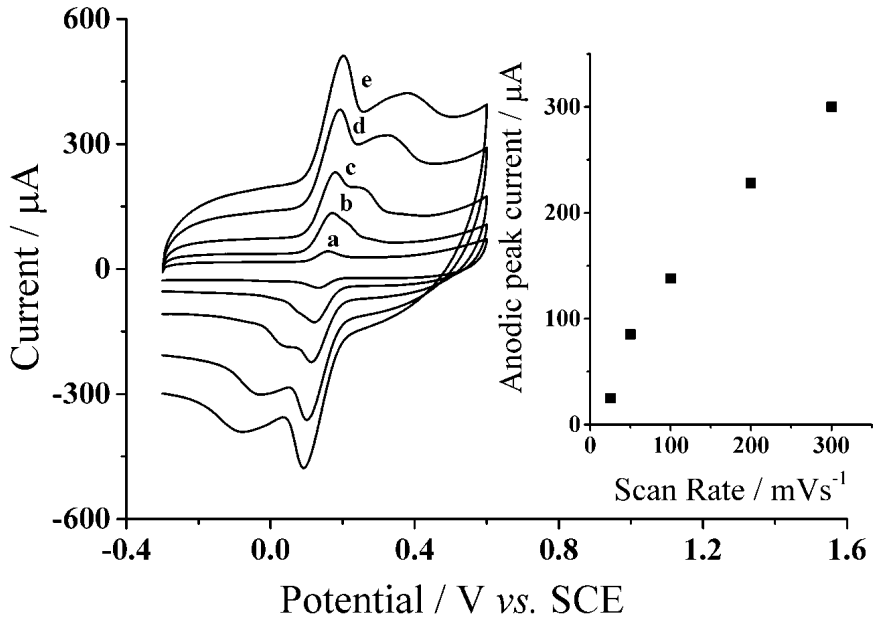

Figure 6.2: Cyclic voltammograms of NC-GCE in 0.1 mM catechol (PBS, pH 7.0) at a. 25 mV s^{-1} b. 50 mV s^{-1} c. 100 mV s^{-1} d. 200 mV s^{-1} e. 300 mV s^{-1}. *Inset:* Anodic peak current, I_{pa}, *vs.* scan rate, ν.

Furthermore, the porous structure of nanocarbon on the NC-GCE was investigated in relation to the electrochemical response of catechol. The electrode was pretreated by dipping the NC-GCE into a solution containing 0.1 mM catechol (PBS, pH 7.0) for *ca.* 43 seconds. Next, the dipped electrode, CAT-NC-GCE, was transferred into PBS (pH 7.0) and a cyclic voltammetry was obtained and to compare to the NC-GCE when catechol is in solution (pH 7.0), shown in Figure 6.3. The cyclic voltammograms of the NC-GCE with catechol present in solution (curve a) compared to in CAT-NC-GCE in PBS (pH 7.0) (curve b) are similar to one another. The measured peak current of the catechol in solution at the NC-GCE is (2.04 $\pm$ 0.07) μA, while the peak current of the catechol at the NC-GCE dipped in PBS containing catechol prior to experiments is (2.03 $\pm$ 0.25) μA; this is in good agreement with each other. This suggests that the catechol is physisorbed onto the porous nanocarbon, which further indicates that the catechol on the NC-GCE is surface bound. One can suggest that the electrode can have the option of

having the catechol present in solution or immobilized onto the surface of the electrode depending on application. This electrode would be best suited for one time use as it has *ca.* 30% reproducibility (n=3) due to the drop cast method. The variability of using drop casting can be seen in the capacitance differences seen in the cyclic voltammograms. Hence the presented work will report the data on the catechol-nanocarbon modified glassy carbon electrode, CAT-NC-GCE, with errors bars representing the precision as a new modified electrode is done for each experiment.

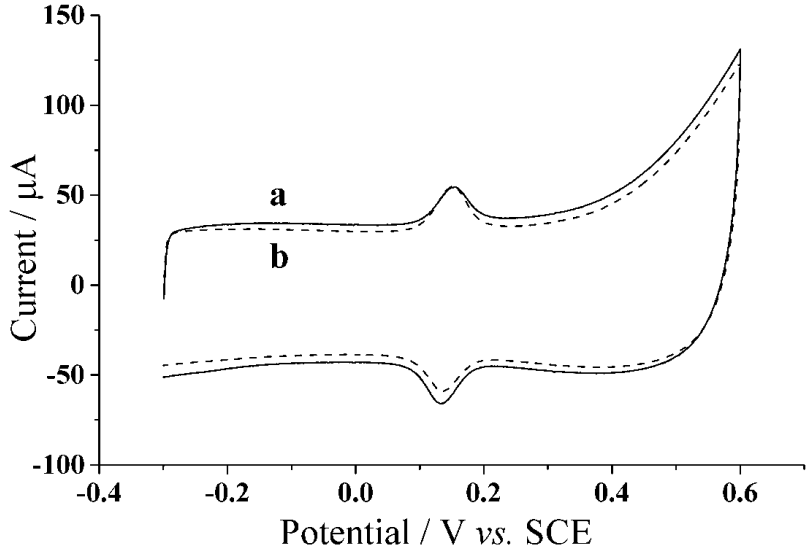

Figure 6.3: Cyclic voltammograms (50 mV s^{-1}) NC-GCE in PBS (pH 7.0) of a. 0.1 mM catechol in solution and b. dipped in 0.1 mM catechol solution prior to test.

6.1.3.2 Electrochemical characterization of homocysteine (HCys)

Figure 6.4 shows cyclic voltammograms (50 mV s^{-1}) of the electrochemical behaviour of the catechol (curve a) when 0.1 mM homocysteine is present in the solution (curve b). The figure illustrates that when homocysteine is added to the solution, an introduction of a new peak potential emerges (*ca.* −0.16 *vs.* SCE). This is due to the addition reaction of a thiol-containing molecule to the *ortho*-quinone

mentioned earlier. Next, various concentration of homocysteine was added to PBS (pH 7.0), ranging from 0 to 0.1 mM (Figure 6.5). The inset to the figure shows that the adduct peak (*ca.* −0.16 *vs.* SCE) increases linearly, I_{pHcys} (nA) = (0.033±0.001)[HCys/nM] (n=3).

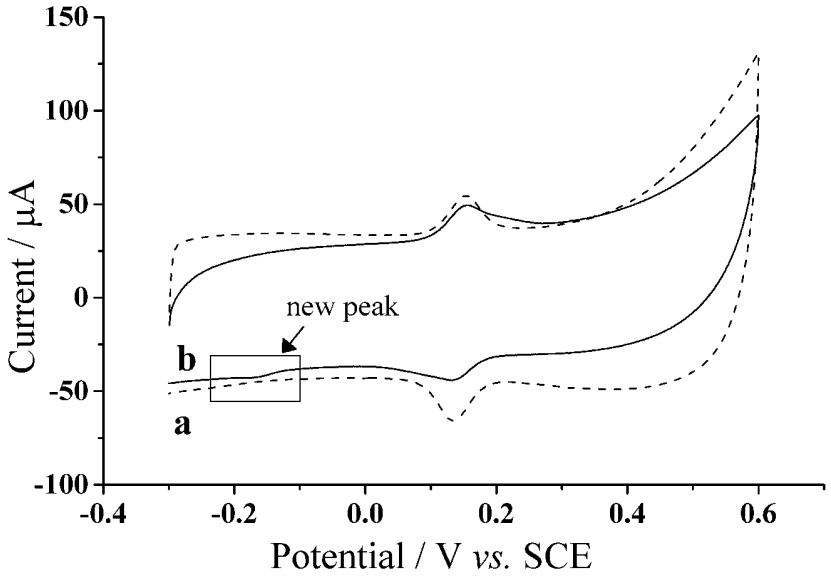

Figure 6.4: Cyclic voltammogram (50 mV s^{-1}) of CAT-NC-GCE in a. PBS (pH 7.0) (dotted) and b. 0.1 mM homocysteine (solid) (pH 7.0).

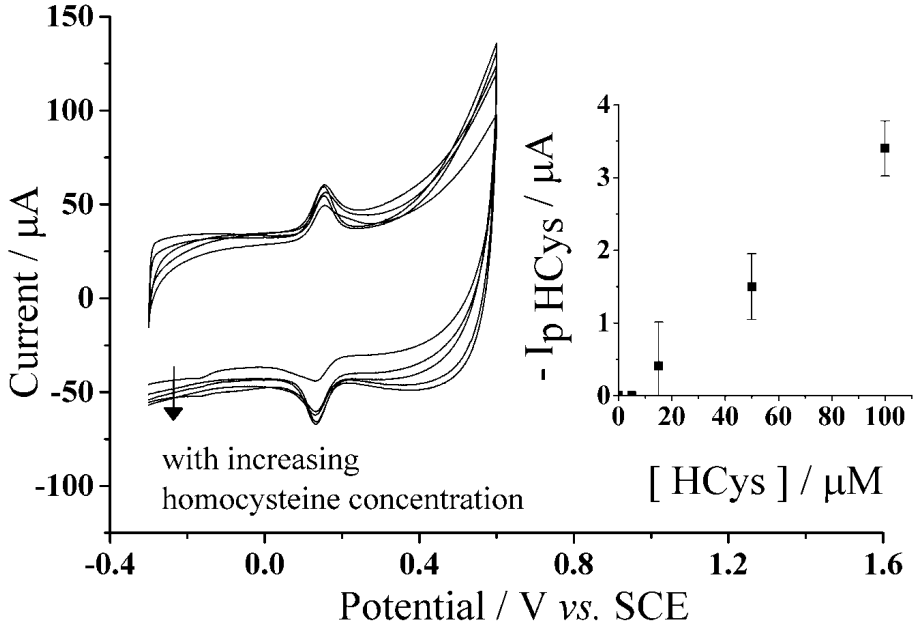

Figure 6.5: Cyclic voltammogram (50 mV s^{-1}) of CAT-NC-GCE in PBS (pH 7.0) with varying concentration of homocysteine. *Inset:* peak current of homocysteine product peak, I_{pHCys}, *vs.* homocysteine concentration.

Next, square wave voltammetry was applied to increase the sensitivity towards homocysteine detection. The parameters were optimized at frequency 25 Hz, amplitude 50 mV and step potential 8.0 mV. Figure 6.6 shows the product peak current of homocysteine (*ca.* −0.16 *vs.* SCE) increases with increasing homocysteine concentration. The inset to Figure 6.6 indicates that there is a linear response, I_{pHCys} (nA) = 1.13 [HCys/nM], (standard deviation is 3.2%, n=3) when the current of the homocysteine product peak, I_{pHCys}, is plotted with homocysteine concentration. The limit of detection (LOD) was determined to be *ca.* (8.0 ± 0.1) nM, using $3S_B/S$ where SD is the standard deviation at zero analyte concentration and S is the sensitivity given by the gradient of the calibration curve. [129, 130] Using square wave voltammetry, the sensitivity of homocysteine detection, 1.13 nA nM^{-1}, was increased about thirty times compared to cyclic voltammetry.

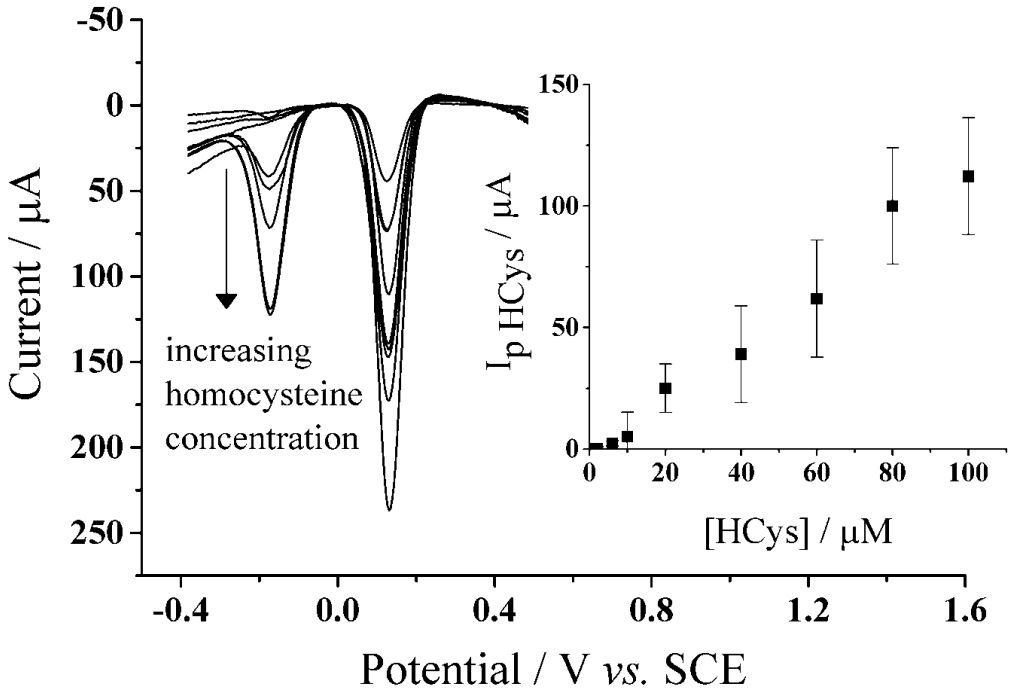

Figure 6.6: Square wave voltammetry (freq. 25 Hz, amp. 50 mV, and step pot. 8.0 mV) response of CAT-NC-GCE with varying concentration of homocysteine, pH 7.0, ranging from 0 – 0.1 mM. *Inset:* Peak current at *ca.* −0.30 V (*vs.* SCE) plotted against concentration of homocysteine.

6.1.3.3 Electrochemical characterization of cysteine (Cys)

A solution containing 0.1 mM cysteine, Cys, (pH 7.0) was initially tested using cyclic voltammetry (50 mV s^{-1}) at the CAT-NC-GCE. Figure 6.7, shows that a product peak appears *ca.* +0.30 V (*vs.* SCE). This is rationalized by cysteine being a thiol-containing compound can therefore also react with catechol via 1,4-Michael addition reaction as in Equation 4.2. To see the influence of different cysteine concentrations, cyclic voltammetry (50 mV s^{-1}) was applied to different concentrations ranging, 0 – 0.1 mM (Figure 6.8). The inset to Figure 6.8 show that cysteine product peak (*ca.* +0.30 V *vs. SCE*) increases also linearly with cysteine concentration, I_{pCys} (mA) = 3.96[Cys/μM] with a standard deviation of 3.8% (n=3).

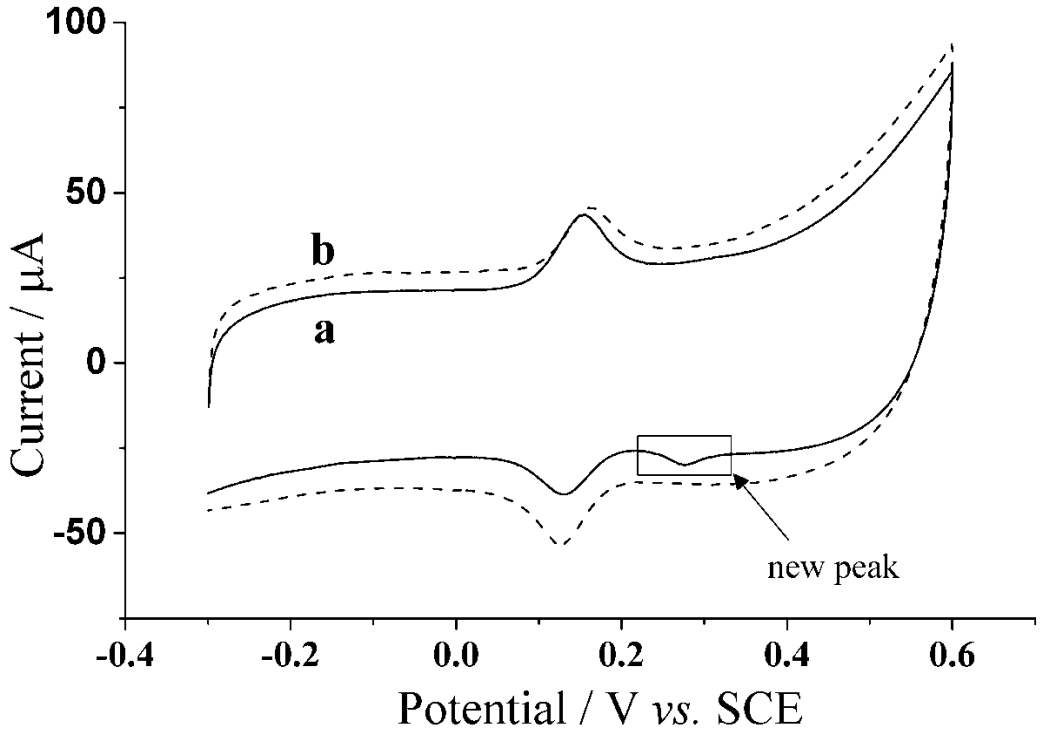

Figure 6.7: Cyclic voltammogram (50 mV s^{-1}) of CAT-NC-GCE in a. PBS (pH 7.0) (dotted) and b. 0.1 mM cysteine (solid) (pH 7.0).

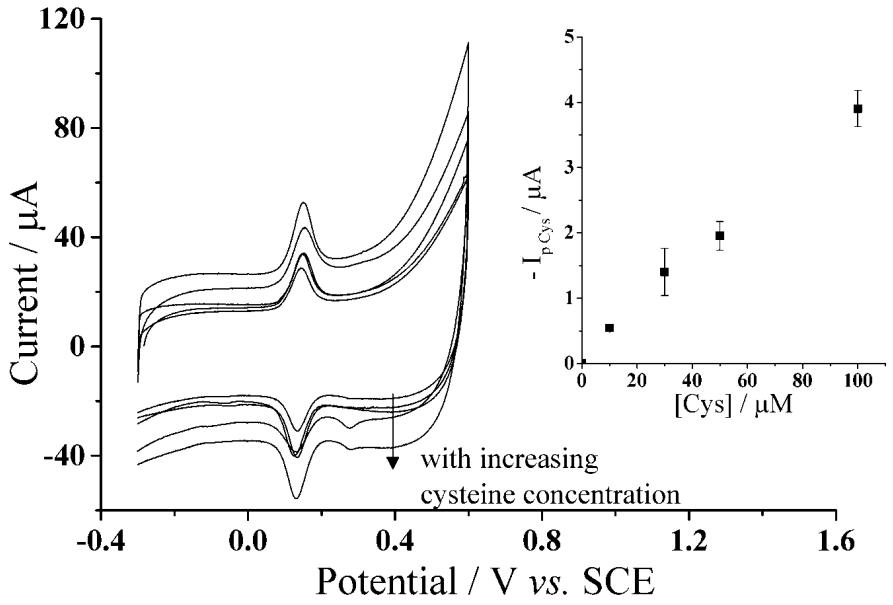

Figure 6.8: Cyclic voltammogram (50 mV s^{-1}) of CAT-NC-GCE in PBS (pH 7.0) with varying concentration of cysteine. *Inset:* Peak current of cysteine product peak, I_{pCys}, *vs.* cysteine concentration.

The same square wave voltammetry parameters as optimized during the homocysteine detection (mentioned earlier) were also applied to the electrochemical system of cysteine because the aim is to detect both homocysteine and cysteine in the same experiment. Figure 6.9 shows the voltammogram of the CAT-NC-GCE at varying cysteine concentrations, 0 – 0.1 mM. The figure illustrates there is small product peak that emerges at *ca.* +0.28 V (*vs.* SCE) with increasing cysteine concentration; this is a result of the thiol containing molecule, cysteine, reacting with catechol (as described above). The inset to Figure 6.9 further shows that there is a linear relationship, I_{pCys} (mA) = 9.71 [Cys/µM] with a standard deviation of 1.5% (n=3), when cysteine concentration is plotted with product peak current of cysteine, I_{pCys}. The determined LOD is *ca.* (4.0±0.1) µM. However, sensitivity, 9.71 µM mA^{-1}, towards cysteine detection using square wave voltammetry is four times less. The reasoning will be discussed below.

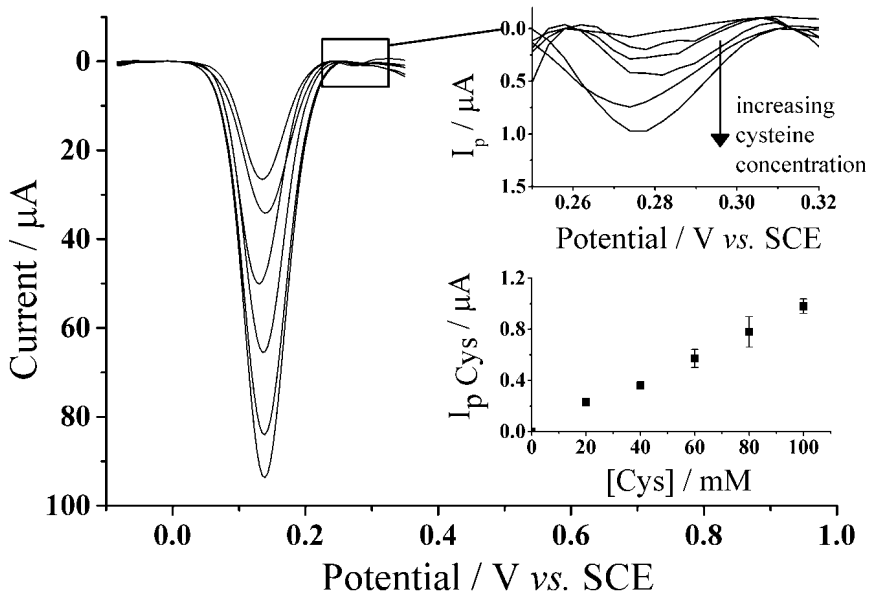

Figure 6.9: Square wave voltammetry (freq. 25 Hz, amp. 50 mV, and step pot. 8.0 mV) response of CAT-NC-GCE with varying concentration of cysteine, pH 7.0, ranging from 0 – 0.1 mM. *Inset:* Peak current at *ca.* +0.30 V (*vs.* SCE) plotted against concentration of cysteine.

6.1.3.4 Interference studies

The selectivity of homocysteine and cysteine detection was investigated in PBS (pH 7.0) with the presence of other antioxidants, such as glutathione (GSH) and/or ascorbic acid (AA), as they can interfere by possibly interacting with the catechol. The interaction between catechol and the possible interfering analytes, GSH and AA, was investigated first. Figure 6.10 shows the voltammograms of CAT-NC-GCE in PBS (pH7.0) (curve a) with the presence of 0.1 mM antioxidants (curve b): GSH (i), and AA (ii). In the presence of glutathione (Figure 6.10i), there is an introduction of a new product peak *ca.* –0.20 V (*vs.* SCE). While in Figure 6.10ii, the peak at *ca.* -0.10 V (*vs.* SCE) is due to the oxidation of AA at the electrode. Under inspection, GSH can interfere with the detection of HCys given that their peak positions are close to each other; thus making it difficult to quantify HCys in the presence of GSH.

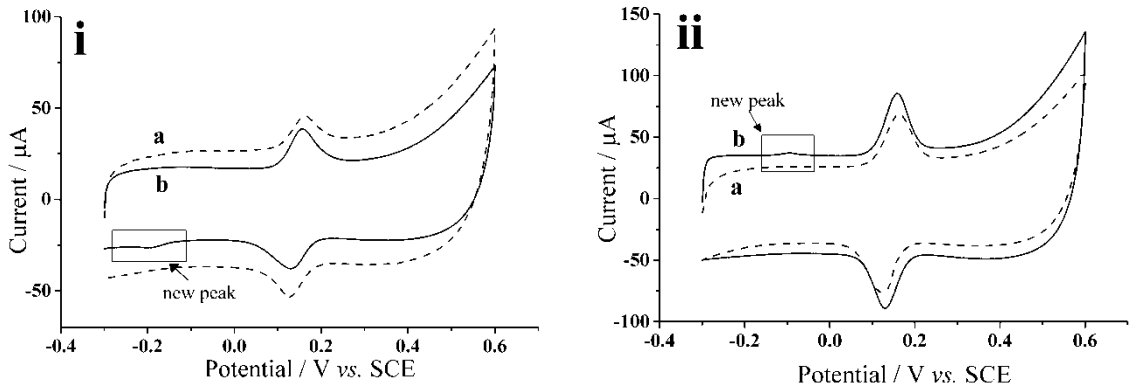

Figure 6.10: Cyclic voltammograms (50 mV s^{-1}, pH 7.0) for CAT-NC-GCE in an absence a. and presence b. of 0.1 mM concentration of i. glutathione and ii. ascorbic acid.

One method for homocysteine selectivity in the presence of glutathione is to take advantage of their reaction rates and molecular size by increasing the scan rate. The aim is to possibly outrun the catechol reaction with, the larger molecule, glutathione at a higher scan rate but be able to allow the catechol to react with homocysteine. In Figure 6.11, an optimum faster scan rate of 200 mV s^{-1} was applied to a solution containing a mixture of 0.1 mM Cys and AA with the presence of 0.1 mM GSH (curve a) and 0.1 mM HCys (curve b). Notice that there is no observable peak in the presence of glutathione when a higher scan rate is applied (curve a). Then when the same scan rate was applied to a solution containing homocysteine, there is slight indication of the homocysteine product peak (curve b). These voltammograms show that a peak at *ca.* –0.20 V (*vs.* SCE) at the higher scan rate corresponds to the reaction of homocysteine-catechol. Consequently, the cysteine product peak (*ca.* +0.30 V *vs.* SCE) current decreases significantly as a result of the higher scan rate. This value is consistently seen at the square wave voltammograms mentioned above (scan rate at 200 mV s^{-1}) for the cysteine-catechol product peak.

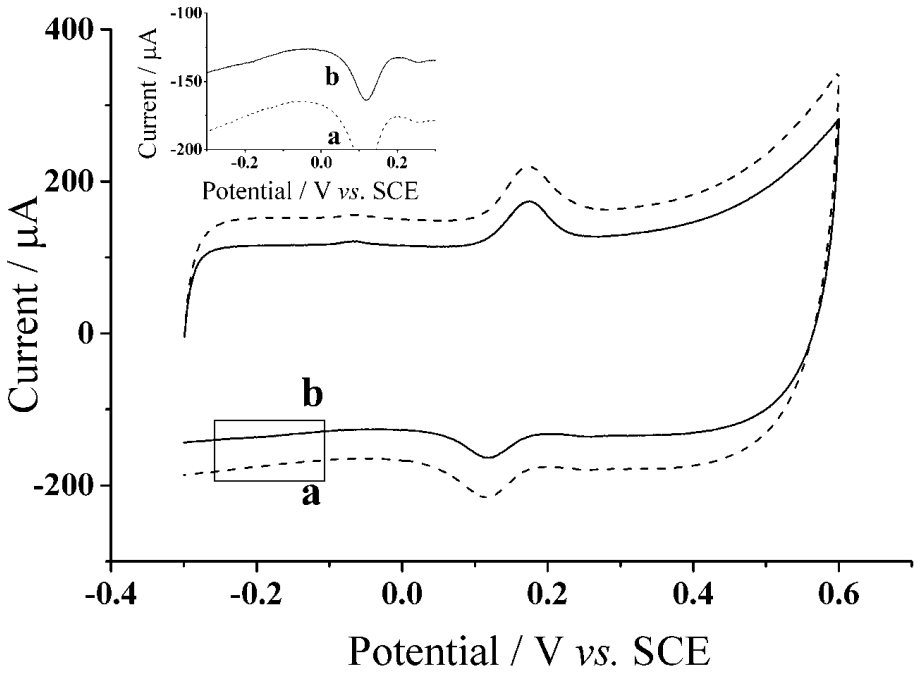

Figure 6.11: Cyclic voltammetry (200 mV s^{-1}) of CAT-NC-GCE in a. 0.1 mM GSH, Cys, AA and b. 0.1 mM HCys, Cys, and AA (pH 7.0).

The same square wave parameters mentioned above were also applied to obtain simultaneous electrochemical detection of both homocysteine and cysteine in the presence of ascorbic acid and glutathione. Glutathione and ascorbic acid have been reported to be as high as 0.1 mM in biological samples and/or media, this concentration is considered to be the abnormal range for high risk for the diseases mentioned earlier. [31, 34, 41-43, 52, 54, 55, 58, 65, 226-229] Therefore, testing at these high concentrations presents the likely worst-case scenario in a sample. Figure 6.11 shows a reductive square wave voltammogram of a solution containing 0.1 mM of each cysteine, homocysteine, glutathione, and ascorbic acid (pH 7.0) at the CAF-NC-GCE. The figure shows peaks with potentials at *ca.* -0.10 V, +0.10 V, and −0.20 V (*vs.* SCE) for cysteine product, catechol and homocysteine product respectively. The different peak potentials make it possible to detect both homocysteine and cysteine in the presence of all of the analytes mentioned above simultaneously.

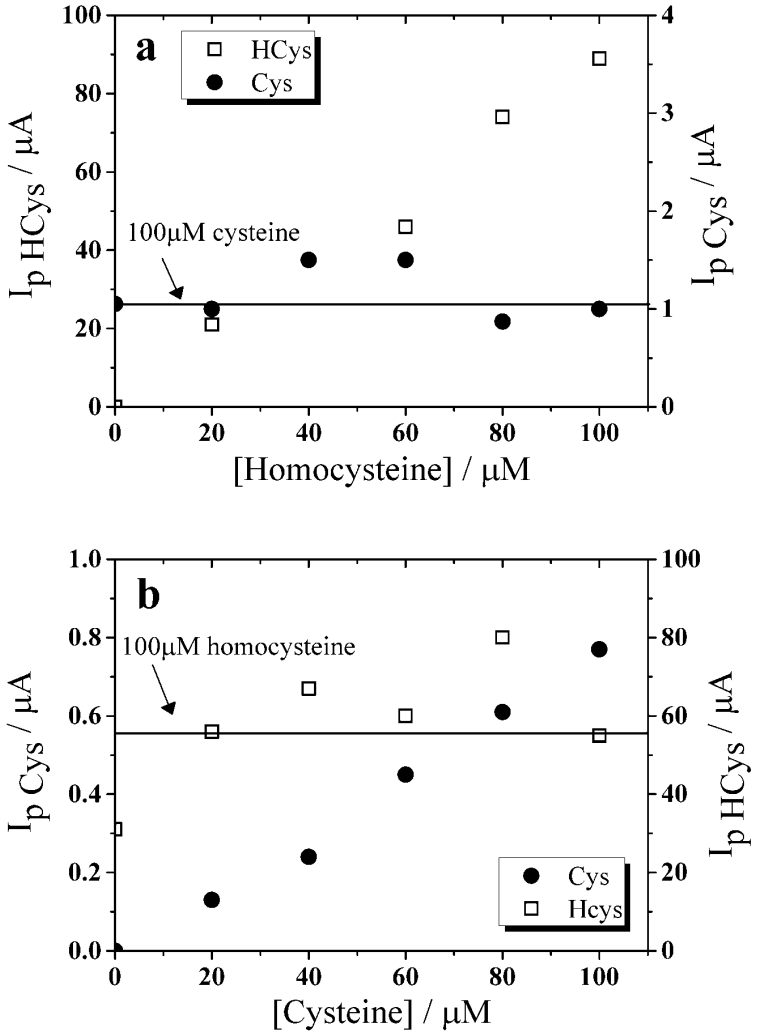

Figure 6.12: Calibration plot of independent and simultaneous detection of a. homocysteine and b. cysteine in the presence of glutathione, and ascorbic acid PBS (pH 7.0) at the CAT-NC-GCE.

An experiment was carried out in order to detect homocysteine and cysteine independently and simultaneously in the presence of both AA and GSH. A concentration of one analyte was held constant at 0.1 mM while the other varied, ranging from 0 to 0.1 mM. First, Figure 6.12 shows a linear trend of peak current versus concentration of homocysteine (Figure 6.12a) and cysteine (Figure 6.12b) when in the presence of other analytes. The linear relationship of homocysteine with peak current in the presence of the other analytes is I_{pHCys} $(nA) = 0.88$ [HCys/nM] with a determined LOD of *ca.* (11 $\pm$

0.09) nM. Cysteine has a linear relationship at I_{pCys} (mA) = 7.50 [Cys/μM] with a LOD of *ca.* (5.0 ± 0.04) μM. The standard deviation in respect of the sensitivity is 3.3% and 2.7% respectively (n=3). These values are similar to the sensitivity of pure homocysteine and cysteine. The horizontal line drawn across each plot indicates the median of the analyte that was held constant. The "error" of the analyte being held constant is due to limited reproducibility of the nanocarbon loading done to each electrode surface (minimum error, *ca.* 30%), mentioned above. Nonetheless, these values are comparative to these seen when GSH and AA are absent from the solution.

6.1.4 Conclusions

Catechol was immobilized onto a porous matrix of the nanocarbon modified glassy carbon electrode in order to facilitate in the reaction of oxidized catechol with two thiol-containing molecules, homocysteine and cysteine. A simultaneous electrochemical detection of both homocysteine and cysteine was achieved separately first and then second in the presence of glutathione and ascorbic acid to determine their calibration curves. The sensitivity of homocysteine detection is (0.882 ± 0.296) nA nM^{-1} with a LOD of *ca.* (11 ± 0.09) nM and sensitivity of cysteine is (7.501 ± 0.202) mA μM^{-1} with a LOD of *ca.* (5.0 ± 0.04) μM. These values are well within the concentration range of analytes, 0 – 0.1 mM, reported in biological samples. [31, 34, 41-43, 52, 54, 55, 58, 65, 226-229] This section demonstrates the possibility of having simultaneous quantitative detection of homocysteine and cysteine in the presence of each other, glutathione and ascorbic acid.

6.2 The selective electrochemical detection of homocysteine in the presence of glutathione, cysteine, and ascorbic acid using carbon electrodes

6.2.1 Introduction

Carbon electrodes are widely used in electroanalysis as they have a relatively low cost when compared to the precious metal electrode, chemical inertness, and provide a wide potential range in aqueous solutions. [110, 230] In the last section, we discussed thiol detection at a nanocarbon modified glassy carbon electrode. The porous nature of the nanocarbon material allowed more sites for the mediator to physisorbed itself onto thus relating to higher current density. This section will continue on the investigation of thiol detection using catechol at two more forms of carbon electrodes; bare glassy carbon electrode (GCE), and the multi-walled carbon nanotube modified glassy carbon electrode (CNT-GCE).

The complexity of in-vitro studies lies in the biological matrix; as they may contain homologous compounds. Often, a separation technique or sample derivatization is necessary to obtain an exclusive chemical determination. However, with the ultimate aim of a point-to-care sensor in clinical applications, thus having a separation technique before analysis is not ideal. The other approach to gaining selectivity and/or sensitivity is sample derivatization. Salehzadeh et al. [87] were the first to report the selective detection of homocysteine in the presence of cysteine and glutathione in a partly *non-aqueous* system only using 3,5-di-tert-butylcatechol at glassy carbon and carbon nanotube modified carbon electrodes. They observed that cysteine did not interfere but used 3,5-di-tert-butylcyclohexa-3,5-diene-1,2-dione to react with glutathione to eliminate it as an interference. Though, Salehzadeh's approach to homocysteine selectivity was achieved, it required a great deal of complex sample pre-treatment.

Hence, the purpose of this section is to present a simple electrochemical method to selectively detect homocysteine in the presence of cysteine and glutathione. In contrast to Salehzadeh et al., the detection was achieved solely in the presence of catechol, which is readily soluble in 100% aqueous systems, again using glassy carbon and carbon nanotube modified carbon electrodes. Cyclic voltammetry and square wave voltammetry were thus used without the need for extensive pre-treatment to the sample. Further, we extend the method to embrace screen-printed electrodes.

6.2.1.1 Electrode preparation

A glassy carbon electrode was modified with multi-walled carbon nanotube (CNT-GCE) was used and is described in Section 3.3.1.2. The use of multi-walled carbon nanotube screen-printed electrodes (CNT-SPE) was also used and is described in Section 3.3.3

6.2.2 Results and discussion

6.2.2.1 Electrochemical characterization of catechol

Cyclic voltammograms of the system were taken at different scan rates ranging from 25 mV s^{-1} to 400 mV s^{-1} in PBS, pH 7.0 at 20°C (Figure 6.13) to initially characterize the electrochemical behaviour of 0.1 mM catechol using at both CNT-GCE and GCE. The figure shows the redox process of catechol at $E_{1/2} = +0.15$ V (*vs.* SCE). This is attributed to the two electron, two proton oxidation of the catechol to the

corresponding *ortho*-quinone species (described in the first step of Equation 4.2) [37, 38, 52, 231]:

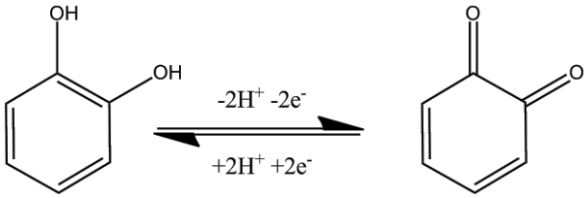

(6.1)

The inset in Figure 6.13 shows that there is a linear correlation when the anodic peak current, I_{pa}, is plotted with the square root of scan rate, $\nu^{1/2}$, suggesting a diffusional process of catechol at either electrode. The diffusion coefficient was estimated using the Randle-Ševčik equation, as being (7.0 ± 1.0) x 10^{-6} cm^2s^{-1} for the CNTs-GCE and 7.5 x 10^{-6} cm^2s^{-1} for GCE, this is reasonably consistent with the literature value [38, 232], 7.7 x 10^{-6} cm^2s^{-1}.

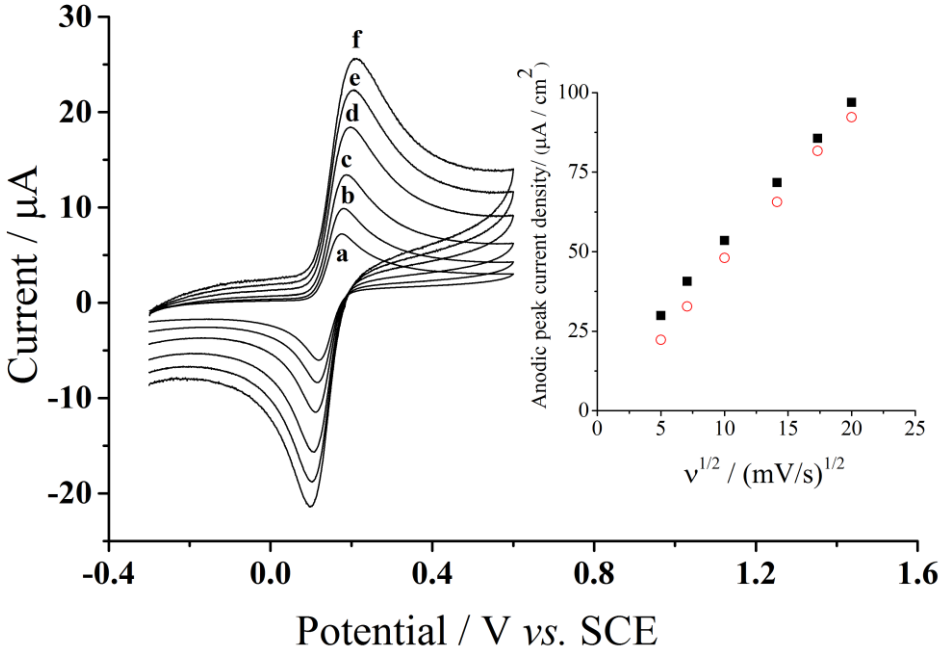

Figure 6.13: Cyclic voltammograms of CNT-GCE in 0.1 mM catechol (PBS, pH 7.0) at a. 25 mV s^{-1}, b. 50 mV s^{-1}, c. 100 mV s^{-1}, d. 200 mV s^{-1}, e. 300 mV s^{-1}, and f. 400 mV s^{-1}. *Inset:* Anodic peak current, I_{pa}, *vs.* square root of scan rate, $\nu^{1/2}$. ■ CNT-GCE and ○ GCE.

6.2.2.2 Catechol electrochemical characterization in the presence of homocysteine

Cyclic voltammetry (50 mV s^{-1}) was used to observe the electrochemical response of 0.1 mM catechol (pH 7.0, PBS) in a presence of HCys. Figure 6.14 shows the comparison of the voltammetric response of the catechol in the absence (dotted line) and presence (solid line) of 0.1 mM HCys at the CNT-GCE (i) and GCE (ii). In the presence, the voltammogram shows the forward peak increases as the back peak decreases and a new product peak emerges at *ca.* −0.20 V (*vs.* SCE). This peak is due to the reduction of substituted catechol molecule, as described above in Scheme 4.3. [137]

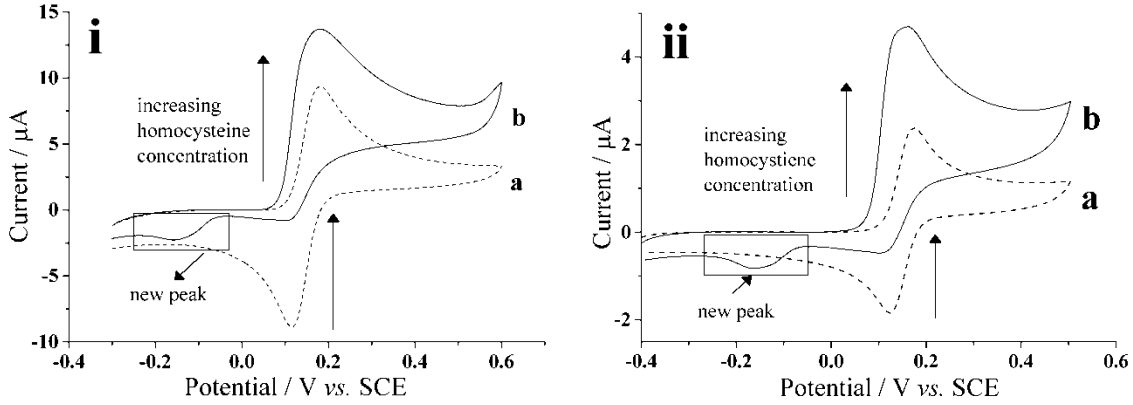

Figure 6.14: Cyclic voltammograms (50 mV s^{-1}, pH 7.0, PBS) illustrating the 0.1 mM catechol response in an absence (dotted) and presence of 0.1 mM homocysteine (solid) at the i. CNT-GCE and ii. GCE.

6.2.2.3 Electrochemical detection of homocysteine

To observe the electrochemical behaviour of catechol with different concentrations of homocysteine, cyclic voltammetry (scan rate of 50 mV s^{-1}) was carried out with a solution containing 0.1 mM catechol at varying homocysteine concentrations ranging from 0 – 0.1 mM. Figure 6.15 shows that as the concentration of homocysteine increases, the forward and new product peak, *ca.* −0.20 V (*vs.* SCE), increases as the

back peak decreases. When the peak current of the new product peak is plotted with concentration of homocysteine (Figure 6.15 inset), the linear trend increases up to 60 μM and then decreases at 0.1 mM homocysteine. This suggests that there is a maximum concentration of homocysteine that will be able to react with the concentration of catechol available in solution. However, the systematically increasing trend shows the possibility of homocysteine detection.

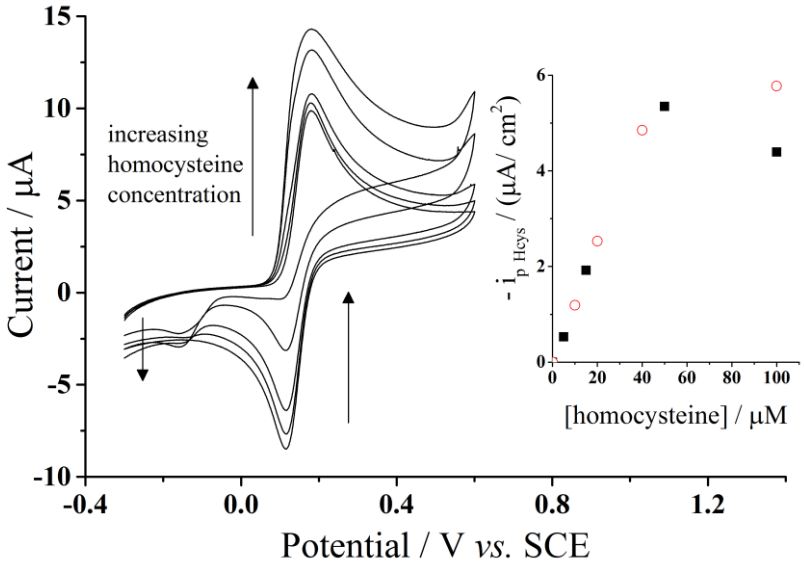

Figure 6.15: Cyclic voltammograms (50 mV s^{-1}, pH 7.0 phosphate buffer) illustrating the 0.1 mM catechol response to homocysteine concentrations ranging from 0 – 0.1 mM. *Inset:* peak current of the new peak plotted against the concentration of homocysteine. ■ CNT-GCE and ○ GCE.

To increase the sensitivity of HCys detection in the presence of 0.1 mM catechol (PBS, pH 7.0), square wave voltammetry was utilized. The parameters were optimized for CNT-GCE and GCE at frequency 50 Hz, step potential 4.0 mV, and amplitude 50 mV. Figure 6.16 shows the square wave voltammograms of the catechol response to different concentrations of homocysteine at the CNT-GCE as we observe similar response at GCE. The results obtained with square wave voltammetry are consistent with the results obtained with cyclic voltammetry for both electrodes; where the

catechol peak (*ca.* +0.14 V *vs.* SCE) decreases and the new product peak at *ca.* −0.20 V (*vs.* SCE) emerges and grows with increasing homocysteine concentration. There is a linear relationship when the peak current of the product, *ca.* −0.20 V (*vs.* SCE), is plotted with concentration of homocysteine. For CNT-GCE, the linear relationship is I_{pHCys} (μA) = 0.2[HCys/μM] with concentrations up to 80 μM (Figure 6.16 inset) and the limit of detection (LOD) was determined to be (120 ± 8.5) nM. For GCE, the linear relationship is I_{pHCys} (μA) = 0.2 [HCys/μM] at homocysteine concentration up to 40 μM and a determined LOD of (90 ± 1.5) nM.

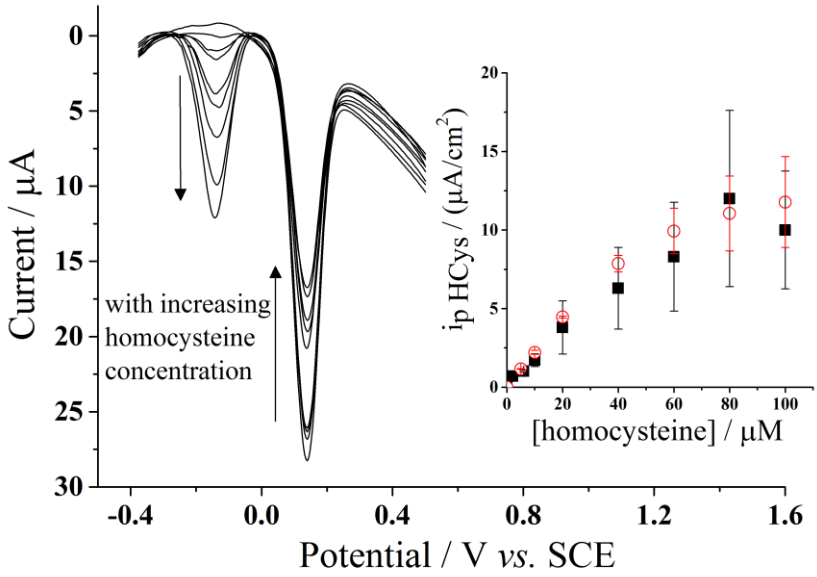

Figure 6.16: Square wave voltammetry response of 0.1 mM catechol at the CNT-GCE with varying concentration of homocysteine (PBS, pH 7.0) ranging from 0 – 0.1 mM. *Inset:* Peak current at *ca.* –0.20 V (*vs.* SCE) plotted against concentration of homocysteine. ■ CNT-GCE and ○ GCE.

6.2.2.4 Interference studies

Towards the use of homocysteine detection in authentic biological samples and media, the selectivity of the system was next investigated at each electrode. First, an individual assay with 0.1 mM catechol (PBS, pH 7.0) was done with the separate

additions of 0.1 mM of each antioxidant: glutathione (GSH), cysteine (Cys), and ascorbic acid (AA) at each CNT-GCE and GCE. These antioxidants were chosen because they are commonly found in biological samples at high concentrations (Table 1) [31, 34, 41-43, 52, 54, 55, 58, 65, 226-229] and have a high propensity to interact with *ortho*-quinones [37, 65, 107, 131, 142]. In addition, 0.1 mM of each analyte was use to present the worst-case scenario of possibly having abnormally high concentrations present in biological samples. [31, 34, 41-43, 52, 54, 55, 58, 65, 226-229]

Antioxidant Name	Normal Range (μM)	Abnormal Range (μM)
Homocysteine	5 - 15	≥ 100
Cysteine	10 – 30	≥ 100
Glutathione	2 – 12	≥ 100
Ascorbic Acid	30 - 80	0 – 30, 80 - 200

Table 6.1: Tabulated values of antioxidants found in human plasma. [31, 34, 41-43, 52, 54, 55, 58, 65, 226-229]

6.2.2.4.1 Interference study at the glassy carbon electrode

Cyclic voltammograms (50 mV s^{-1}) were recorded of 0.1 mM catechol (PBS, pH 7.0) solutions containing 0.1 mM of each GSH, Cys, and AA. Figure 6.17 shows a cyclic voltammogram comparison in the absence (curve a) and presence (curve b) of these antioxidants: GSH (i), Cys (ii) and AA (iii) reacting with catechol. For GSH and Cys, the voltammograms show the forward peak increases and back peak decreases but only in the case with GSH, a new peak emerges at *ca.* −0.20 V (*vs.* SCE) due to the catechol-thiol interaction favouring the 1,4-Michael addition reaction. In the case with the catechol interaction with Cys at the GCE, the favouring reaction seems to be electrocatalytic at the GCE. With AA, the voltammogram shows that the forward peak increases slightly

and new peak emerges *ca.* 0 V (*vs.* SCE) indicating that it is the oxidation of pure ascorbic acid at the GCE. Upon examining all the voltammograms, there can be difficulties measuring HCys when in the presence of GSH at GCE because the peak potentials of their adduct with oxidized quinones are close to each other.

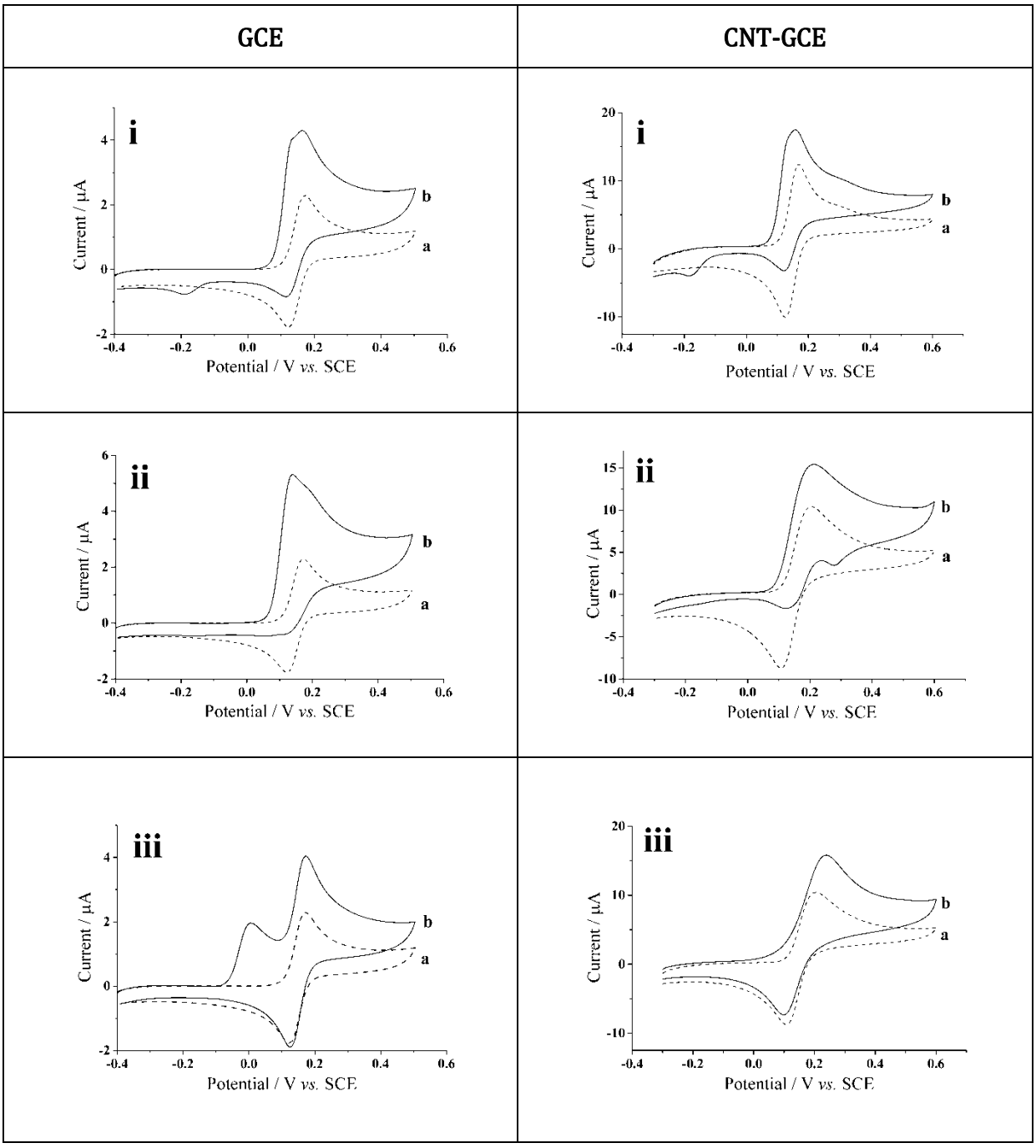

Figure 6.17: Cyclic voltammograms (50 mV s^{-1}, pH 7.0, PBS) for 0.1 mM catechol in an absence a. and presence b. of 0.1 mM concentration of i. glutathione ii. cysteine iii. ascorbic acid at CNT-GCE and GCE.

6.2.2.4.2 Interference study at the carbon nanotube modified carbon electrode

Figure 6.17 shows the electrochemical response at each electrode of 0.1 mM catechol (dotted line) in a presence of 0.1 mM of each antioxidants (solid lines): GSH (i), Cys (ii), and AA (iii) at the CNT-GCE. Voltammograms show an increase in forward peak with a decrease in the back peak for catechol reacting with GSH (i) and Cys (ii), with an introduction of a new product peak at *ca.* −0.200 V, and +0.300 V respectively. This introduction of a new product peak indicates a 1,4-Michael addition reaction is favoured and occurs with the thiols at the CNT-GCE. While there was no new product peak for the presence of ascorbic acid, the voltammogram show a slight increase in the forward peak, which is similarly seen with GCE. By examining the peak potentials of the new product peak, the presence of glutathione can be a possible interference towards the detection of homocysteine as the product peak potentials are close to each other. For the case with cysteine, the product peak emerges at a different peak potential further away from the reaction with homocysteine and glutathione. It is suspected that the catechol reaction with each different thiol reacts to form new and different electrochemical species thus having different peak potentials.

6.2.2.5 Homocysteine selectivity

At this point, it would be difficult to quantify homocysteine in the presence of glutathione with the square wave voltammetry parameters presented above (Section 6.2.2.3) at either electrodes. Figure 6.18 shows the behaviour of catechol in the presence of homocysteine (curve a), glutathione (curve b), and both (curve c) at 50 mV s^{-1}, similar behaviour is also seen at GCE. Notice that in the presence of both HCys and GSH (Figure 6.18c); the new product peaks for both analytes are close which makes

it difficult to determine changes in peak current between the two analytes, if it should occur. As an attempt to optimize the single homocysteine signal, one proposed method can be to take advantage of the different molecular size and reaction rates of either analytes with catechol. The aim would be to apply a higher scan rate to outrun the glutathione-catechol reaction but still be able to allow the homocysteine-catechol interaction to take place.

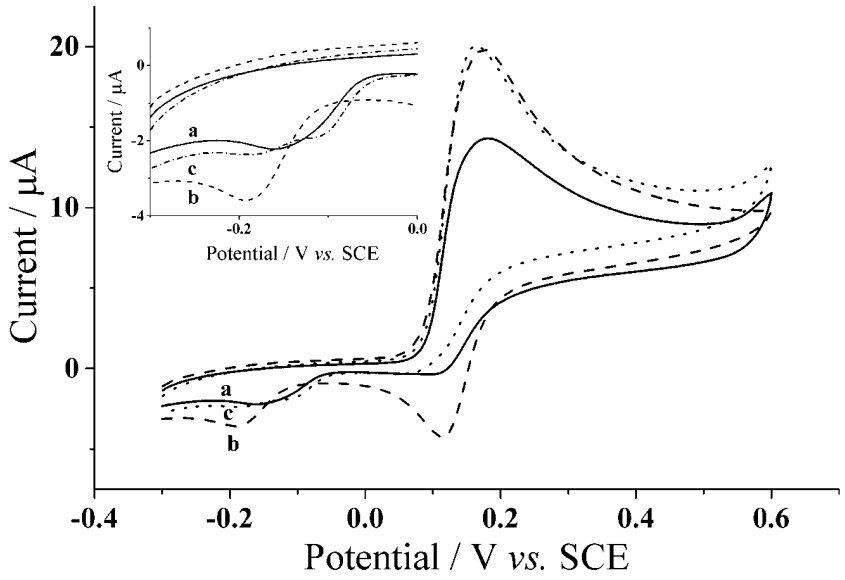

Figure 6.18: Cyclic voltammograms (50 mV s^{-1}, pH 7.0 PBS) at CNT-GCE of 0.1 mM catechol containing a. 0.1 mM homocysteine b. 0.1 mM glutathione and c. 0.1 mM homocysteine and glutathione.

Figure 6.19 shows cyclic voltammetry at an optimum scan rate of 1.5 V s^{-1} for GCE (i) and 500 mV s^{-1} for CNTs-GCE (ii) of a solution containing catechol with the presence of glutathione (curve a) and homocysteine (curve b) (PBS, pH 7.0). This is done separately to see the possibility of homocysteine selectivity. There is no significant signal for the product peak of the glutathione-catechol reaction (curve a) while for the homocysteine-catechol reaction (curve b), the product peak (*ca.* −0.20 V *vs.* SCE) emerges for both systems. This indicates that it is possible to detect homocysteine in the

presence of glutathione at the higher scan rate. As mentioned before, AA and Cys were not interferences to the homocysteine product signal and now, it can be possible to have homocysteine detection in the presence of AA, Cys and GSH using cyclic voltammetry.

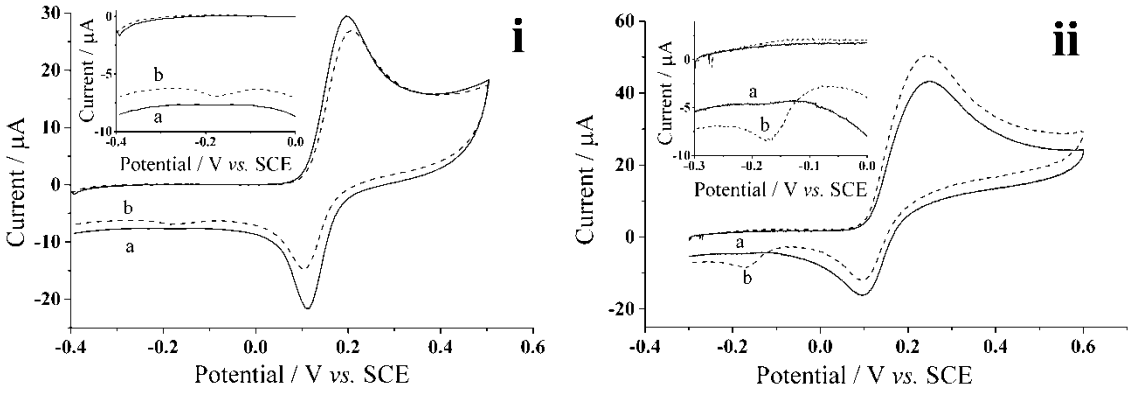

Figure 6.19: Cyclic voltammograms at i. GCE (at 1.5 Vs^{-1}) and ii. CNT-GCE (at 500 mV s^{-1}) of 0.1 mM catechol containing a. 0.1 mM glutathione and b. 0.1 mM homocysteine (PBS, pH 7.0).

Square wave voltammetry (optimized for CNT-GCE at frequency 50 Hz, amplitude 50 mV, and step potential 10 mV and GCE at frequency 50 Hz, amplitude 75 mV, and step potential 30 mV) was applied to a solution containing various HCys concentrations, 0 – 0.1 mM, in a presence 0.1 mM of each catechol, GSH, Cys, and AA. Figure 6.20 shows the square wave voltammograms of different homocysteine concentration in the presence of cysteine, glutathione and ascorbic acid at the CNT-GCE. The inset to Figure 6.20 shows the homocysteine-catechol product current peak increases with homocysteine concentration at both electrodes. Homocysteine selectivity was not achieved at GCE under the optimized square wave voltammetry parameters presented because the result shows a signal in the absence of homocysteine due to catechol-glutathione product. While the selectivity of homocysteine was successfully achieved at CNT-GCE as no signal appeared in the absence of homocysteine when the

other antioxidants are present. The differences in selectivity can be rationalized by the diffusion changes at the electrode surfaces, bare glassy carbon electrode versus porous layer of carbon nanotube modified electrode. [27, 28] The porous layer is likely to promote the glutathione and quinone reaction. Under linear diffusion semi-infinite diffusion conditions the reaction is too slow to be usefully observed whereas the 'thin layer' like environment in the porous layer slows the transport and hence help aide the reaction. Therefore, the CNT-GCE is the best electrode at this time to obtain selective homocysteine detection in the presence of glutathione, cysteine and ascorbic acid.

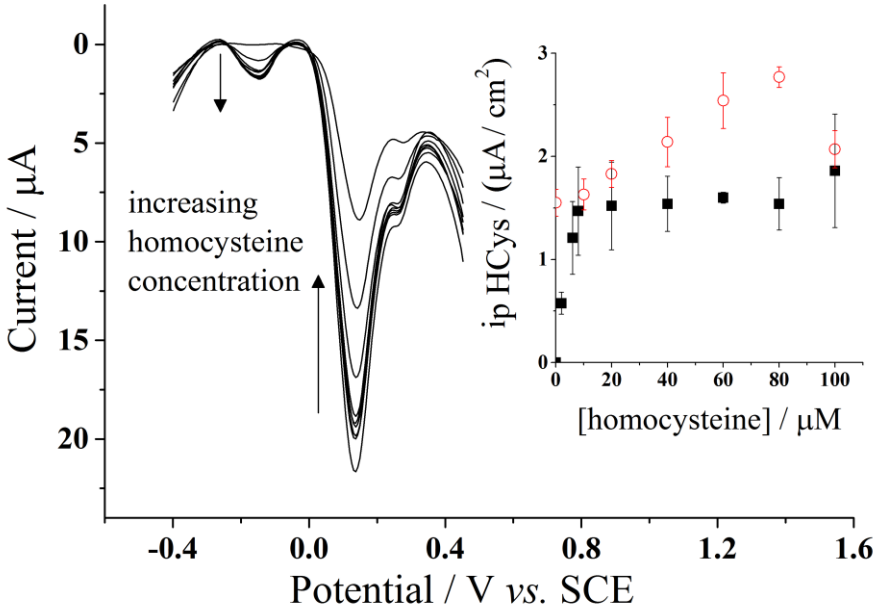

Figure 6.20: Square wave voltammograms of CNT-GCE in solution containing 0.1 mM glutathione-cysteine-ascorbic acid-catechol with varying homocysteine concentration (0 - 0.1 mM). *Inset:* Homocysteine peak current at *ca.* −0.20 V (*vs.* SCE) plotted against concentration of homocysteine. ■ CNT-GCE and ○ GCE.

Sensitivity of homocysteine at CNT-GCE was obtained in the presence of these analytes, at the range 0 – 10 µM, is (0.20 ± 0.02) µA μM^{-1} and the limit of detection is determined to be (660 ± 4.5) nM. It is suspected that the narrow working range is due to the antioxidants present; including homocysteine, undergo a competition reaction

with the available catechol in solution. In spite of the antioxidant present undergoing a reaction we can still observe no change in peak current up to 10 μM homocysteine in the presence of 0.1 mM analytes. However, there is a possibility that the dynamic range might be extended if those concentrations were lower.

6.2.2.6 Homocysteine detection using carbon nanotube screen-printed electrodes (CNT-SPE)

The use of readily available commercial carbon nanotube screen-printed electrodes, CNT-SPE, was applied to this system. CNT-SPE was tested in a solution containing 0.1 mM of catechol and all of the other analytes mentioned above while varying the concentration of homocysteine (pH 7.0, PBS) at 20˚C. To ensure the same potential and conditions used previously, SCE was used as the reference electrode in the testing for comparison to the CNT-GCE. Figure 6.21 shows a calibration curve of the tested CNT-SPE plotted in comparison with the other calibration curves of homocysteine concentration up to 10 μM. The figure shows the linear range up to 10 μM, with using CNT-SPE is similar to CNT-GCE in the presence of the other analytes. The sensitivity for HCys at CNT-SPE is (0.20 ± 0.02) μA μM^{-1}, which is the same in the absence and presence of the analytes at CNT-GCE. Graphite screen-printed electrode was also applied to the same system. However, a signal appeared in the absence of homocysteine due to catechol-glutathione product showing that homocysteine selectivity is not possible under these conditions. To conclude, the commercially available carbon nanotube screen-printed electrodes was shown to be applicable towards homocysteine detection.

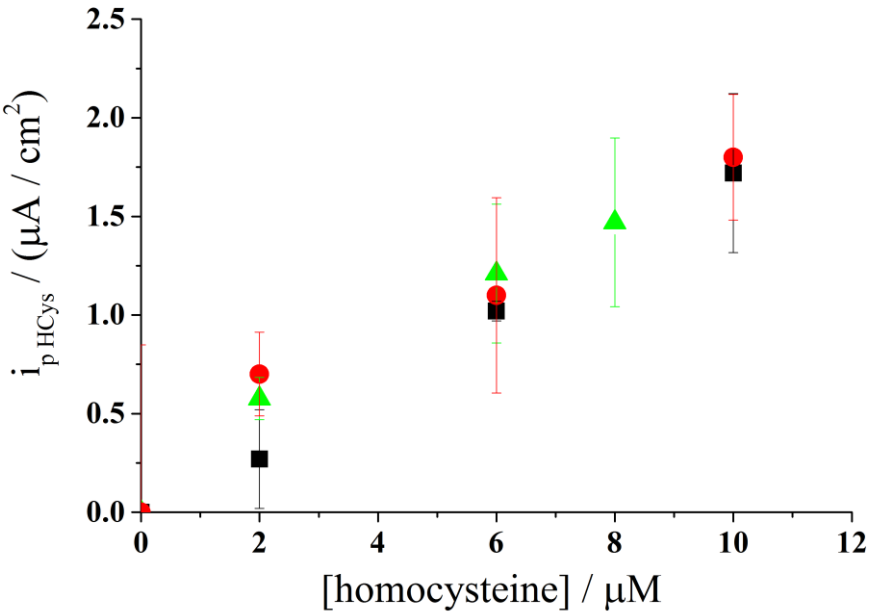

Figure 6.21: Calibration plot of detection of homocysteine (pH 7.0, PBS) with 0.1 mM catechol present in solution at ■ CNT-GCE. Homocysteine detection in the presence of cysteine, glutathione, and ascorbic acid (PBS, pH 7.0) at ● CNT-GCE, ▲ CNT-SPE.

6.2.3 Conclusions

We have demonstrated that the detection of pure homocysteine is able to take place at two different carbon electrodes, bare glassy carbon electrode and carbon nanotube modified carbon electrode. Though, in the presence of other antioxidants, glutathione, cysteine and ascorbic acid, homocysteine selectivity was not possible at the glassy carbon electrode. The selective detection of homocysteine was achieved using a carbon nanotube modified electrode with a sensitivity of (0.20 ± 0.02) μA μM^{-1} and a limit of detection (660 ± 4.5) nM at a linear range up to 10 μM in the absence and presence of other antioxidants: glutathione, ascorbic acid, and cysteine. In addition, the use of commercially available carbon nanotube screen-printed electrodes was applied and it was shown that it can be applicable towards facile, fast and disposable electrodes for selective homocysteine detection.

6.3 The use of screen-printed electrodes in a proof of concept electrochemical estimation of homocysteine and glutathione in the presence of cysteine using catechol

6.3.1 Introduction

Screen-printing technology is a well-known and established technology for capabilities of mass producing screen-printed electrodes. [113, 233, 234] The attractiveness of screen printing technology lies in the production process, for it being fast and simple to fabricate. A general screen-printed electrode can comprise from any number of electrodes from as low as one to an array of working electrodes on a supporting material with integrated circuitry to satisfy the desire application. [112] Though there are some difficulties with commercializing screen-printed array electrodes, the market for the single working electrode is well established and is very advantageous for it being compact, low in cost, versatile, robust and disposable. [112, 113] Especially with carbon-based electrodes, the inks used are usually comprised of graphite and/or carbon nanotube, they have attributes similar to the conventional carbon based electrode by being low in cost, possessing a low background current and a wide window of working potential. [233, 235] To satisfy the growing technology of present and future applications, screen-printed electrodes are becoming more attractive and ideal for applications that require high throughput screening or do not require the need for complex and expensive equipment, such as bio-applications. [113, 233] Therefore it is desirable to provide a *simple* electrochemical method that allows for access to easy sample preparation with a unit that can possibly promote point-of-care applications. [57, 87, 97]

This section reports on the use of disposable screen-printed electrodes to facilitate in the determination of homocysteine and glutathione in the presence of each other by utilizing the same hydroquinone/*o*-quinone mediator, as presented in the last section, in a pure aqueous system. Building upon a procedure previously described in Section 5.3, the exclusive quantification will essentially take advantage of the different reaction rates of homocysteine and/or glutathione with the electrochemically oxidized catechol with the use of voltammetric methods. Allowing the faster reaction with homocysteine to initially take place by applying a high voltage scan rate, this makes it possible to 'outrun' the slower reaction with glutathione resulting in an analytically useful adduct peak possible for pure homocysteine detection. Thereafter, a slower scan rate is applied giving sufficient time for both analytes to react thus relating the contents to the new adduct peak at low scan rate. The glutathione content can then be determined by subtracting the determined homocysteine value from the total adduct peak obtained at the slower scan rate. This proof of concept work was applied to buffered solutions spiked with both analytes (glutathione and homocysteine) and then later applied to the same solutions spiked with another added thiol compound, cysteine, to further emphasize the value in this proposed procedure towards possible practical applications on physiological fluids (i.e. urine and/or plasma). Carbon nanotubes screen printed electrodes were used throughout this study as it has been previously, Section 6.2 [143], emphasized that the use of an electrode with a porous surface layer promotes 'thin-layer' like diffusion [27, 28, 143, 169, 170] rather than semi-infinite diffusion. Under this diffusion condition, the porous layer reduces the rate of transport of the thiols and therefore facilitates observation of the chemical reaction in the voltammetry. With conventional carbon electrodes (i.e. glassy carbon electrode) that offer semi-infinite planar diffusion [28, 143], the thiol reaction with *ortho*-quinone may be too slow for

any useful observations to take place. The use of screen-printed electrodes continues to add upon the proposed idea of presenting a possible alternate portable sensor solution, whether it is for a space-saving equipment in the lab or a point-of-care system for a medical facility.

6.3.2 Experimental procedure

The electrochemical experiments were carried out in a three electrode system using a saturated calomel electrode, SCE, reference electrode (Hach Lange, UK), a platinum mesh 99.99% (Goodfellow, UK) counter electrode and multi-walled carbon nanotube disposable screen printed electrodes (DropSens, Spain) as the working electrode. Due to the silver quasi-reference electrode built into the screen-printed electrodes is prone to large variation with up to, *ca.* estimated 40 mV shifts in reference potential. The purpose of using an external reference electrode is to ensure that all potentials are the same in every condition to compare with previous studies described in this thesis. To ensure little to no change in the resistance, the distance among the electrodes were fixed to each other. The details on the screen-printed electrode are described in Section 3.3.3.

6.3.3 Results and discussion

6.3.3.1 Homocysteine selectivity in the presence of glutathione

The determination of homocysteine with catechol at a carbon nanotube modified electrode (CNT-GCE) was reported in Section 6.2. [143] Shown in the Figure 6.22, the cyclic voltammetric response of electro-oxidized catechol when homocysteine is

present in solution shows an increase in the forward peak, decrease in the back peak and an appearance of a new adduct peak; thus indicating a 1,4-Michael addition reaction between homocysteine and oxidized catechol (discussed above). Experiments were next carried out to investigate the determination of *both* homocysteine and glutathione using catechol solution at the CNT-SPE.

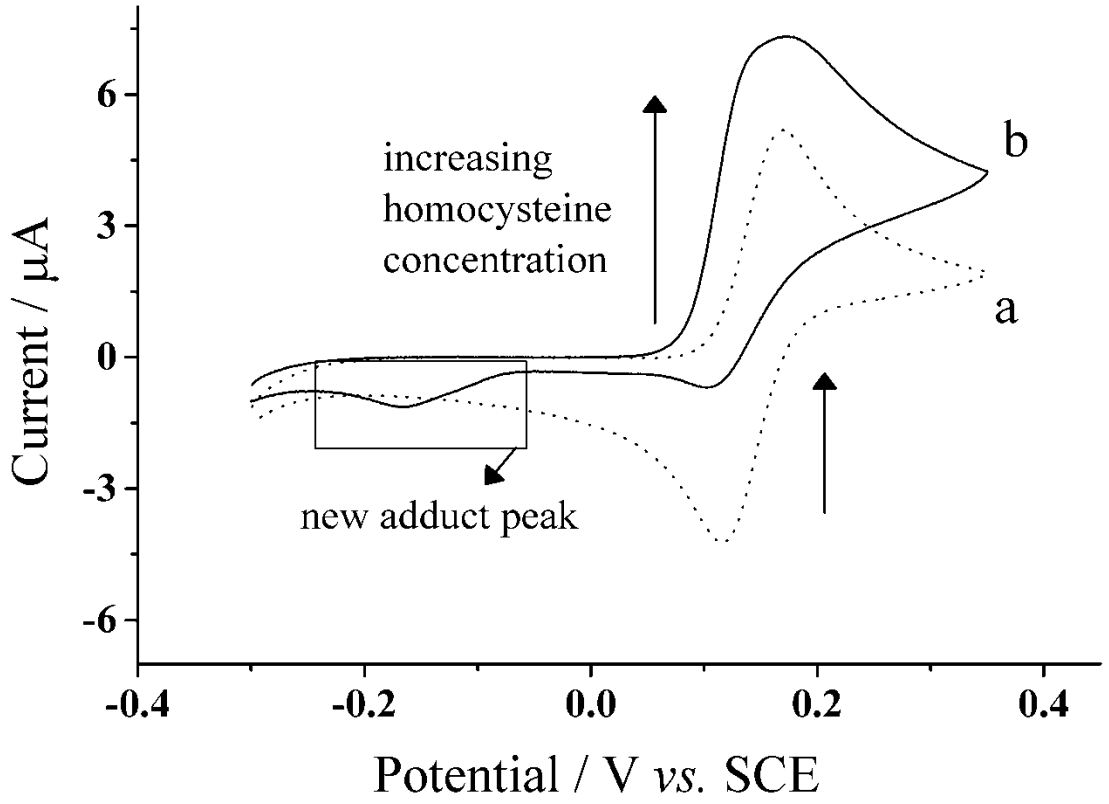

Figure 6.22: Cyclic voltammograms (50 mV s^{-1}) of 100µM catechol (PBS, pH 7.0) in the a. absence and b. presence of 100 µM homocysteine.

Initial results (Figure 6.23) showed that upon applying a low scan rate using cyclic voltammetry (50 mV s^{-1}) to a solution containing 100 µM of each catechol (PBS, pH 7.0) (Figure 6.23a), homocysteine (Figure 6.23b) and glutathione (Figure 6.23c), an adduct peak appears reflecting the oxidized catechol reaction with both glutathione and homocysteine thus making it difficult for quantification when both are present in the solution. This is due to the slow scan rate, allowing sufficient time for both

homocysteine and glutathione to react with the electrochemically oxidized catechol. The new adduct peak observed in the voltammogram is due to the 1,4-Michael addition reaction, as described above, of *ortho*-quinone taking place with both glutathione and homocysteine at the electrode. This simple electrochemical behaviour at the CNT-SPE presents a problem with quantifying either homocysteine or glutathione in the presence of each other. Accordingly, the following two-step procedure is proposed.

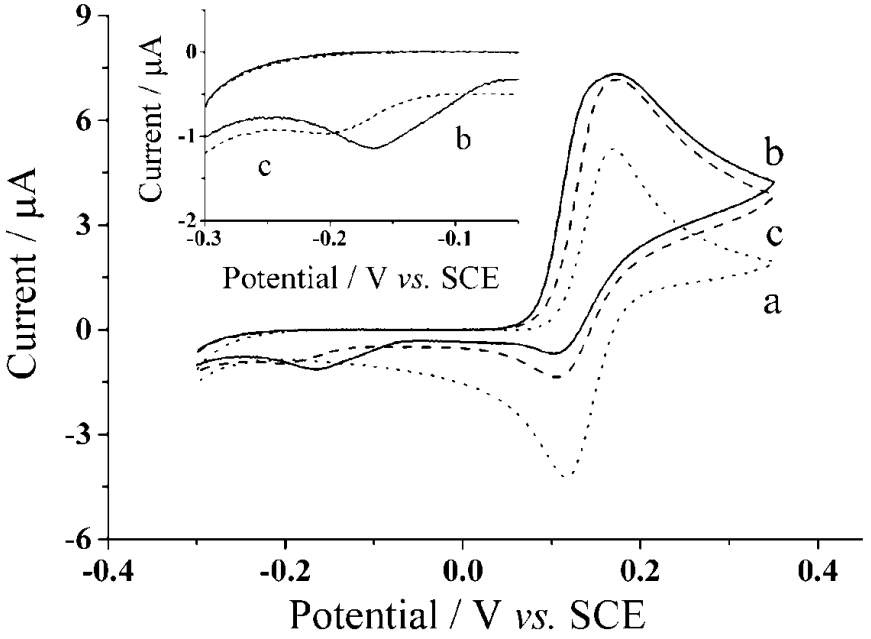

Figure 6.23: Cyclic voltammetry (50 mV s^{-1}) 100 μM catechol (0.15 M PBS, pH 7.0) a. absence and presence of b. 100 μM homocysteine, and c. 100 μM glutathione (0.15 M PBS) at CNT-SPE. *Inset:* Magnified view of adduct peaks.

First, homocysteine selectivity was investigated by examining the reaction rates of glutathione and homocysteine with electro-oxidized catechol at the CNT-SPE. A higher voltage scan rate was applied with the aim to 'outrun' the glutathione-catechol reaction but allow the homocysteine-catechol reaction to still take place. The optimized scan rate of 500 mV s^{-1} [143] was applied using cyclic voltammetry of a solution containing 100 μM of each catechol, glutathione and/or homocysteine (PBS, pH 7.0)

using the CNT-SPE (Figure 6.24). The results show little to no product peak appearance when the high scan rate is applied to a solution containing glutathione while an analytically useful adduct peak appears in the presence of homocysteine. This suggests that the higher scan rate was fast enough to preclude the catechol reaction with glutathione but still allow the reaction to take place with homocysteine thus allowing selective determination of homocysteine to also take place at CNT-SPE. Thus using 100 µM of catechol (PBS, pH 7.0), an analytical curve was obtained for homocysteine (Figure 6.25) as, $I_{pHCys\ 500mV\ s^{-1}}$ (µA) = (0.0201 ± 0.000076) [HCys/µM] (n=3), at homocysteine concentrations up to 60 µM. This measurement at high scan rate thus allows the selective measurement of homocysteine in the presence of glutathione at the screen-printed electrode.

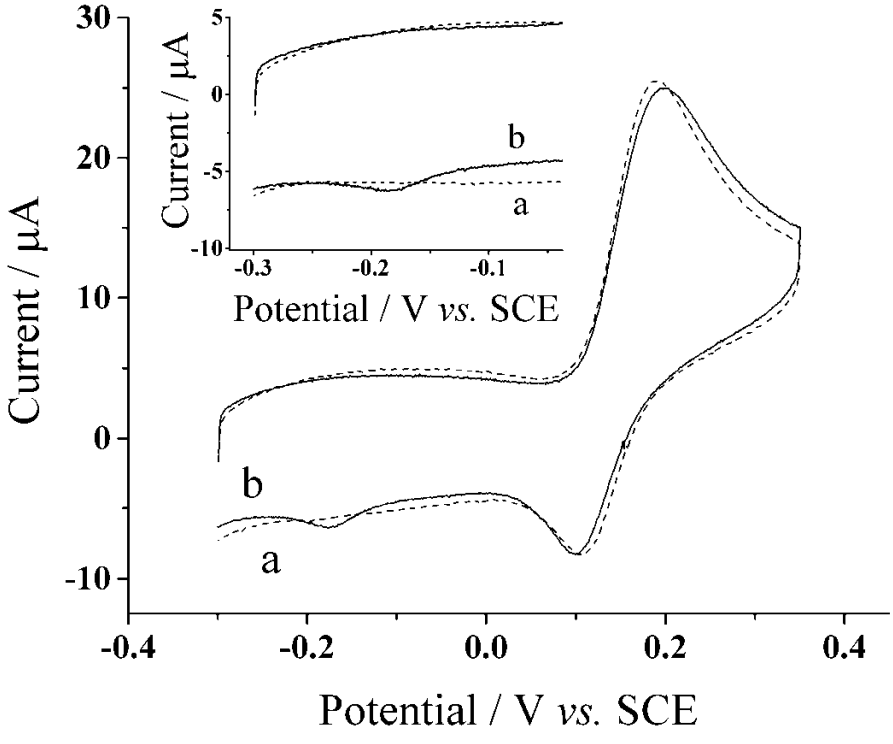

Figure 6.24: Cyclic voltammetry (500 mV s^{-1}) at CNT-SPE of 100 µM catechol containing a. 100 µM glutathione b. 100 µM homocysteine (PBS, pH 7.0)

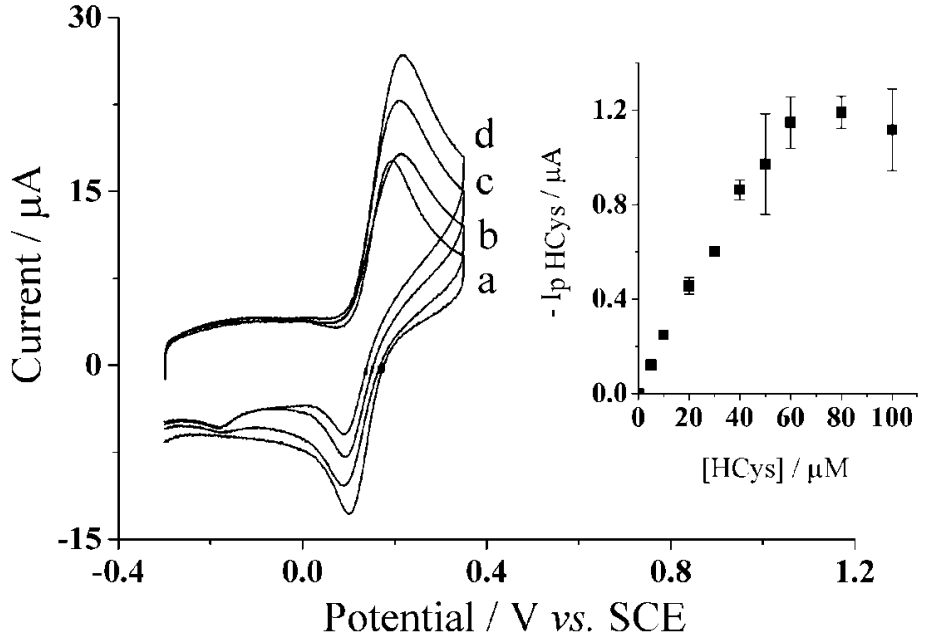

Figure 6.25: Cyclic voltammograms (500 mV s^{-1}) of 100 µM catechol (PBS, pH 7.0) at varying homocysteine concentrations, a. 0 M, b. 20 µM, c. 60 µM, and d. 100 µM, at CNT-SPE. *Inset:* Peak current of homocysteine adduct peak *vs.* concentration of homocysteine.

6.3.3.2 Determination of glutathione in the presence of homocysteine

Though the selective detection of homocysteine is achievable at high scan rate, 500 mV s^{-1}, the further concept towards glutathione determination within the same sample is proposed in the following as the second step procedure. The same sample solution is agitated and then a low scan rate of 50 mV s^{-1} [143] using cyclic voltammetry is applied. As discussed above, the low scan rate allows the reaction of both homocysteine and glutathione to take place with the electro-oxidized catechol thus resulting in the same peak potential for the adduct peak; consequently, the adduct peak will contain contents of both analytes (Figure 6.23). By this means, homocysteine is being measured at both scan rates and the adduct peak of pure homocysteine can then be subtracted from the total adduct peak obtained at low scan rate, containing HCys and GSH, thus resulting in a concentration of glutathione alone. Furthermore, calibration

curves need to be obtained at the low scan rate, 50 mV s^{-1}, for each homocysteine and glutathione in the presence of 100 µM catechol (PBS, pH 7.0) using cyclic voltammetry. First shown in Figure 6.26, the calibration curve for homocysteine at a scan rate of 50 mV s^{-1} shows a linear relationship, $I_{pHCys\ 50mV\ s^{-1}}$ (µA) = (0.013 ± 0.00013) [HCys/µM], with a linear range up to 30 µM. Second, Figure 6.27 shows another calibration curve at low scan rate of 100 µM catechol (PBS, pH 7.0) at varying concentrations of glutathione, 0 – 100 µM. The figure also shows that peak current is proportional to concentration at the low scan rate, $I_{pGSH\ 50\ mV\ s^{-1}}$ (nA) = (3.5 ± 0.066) [GSH/µM] with a linear range up to 60 µM of glutathione. Once all the appropriate calibration curves are determined, the proposed method can be applied and tested.

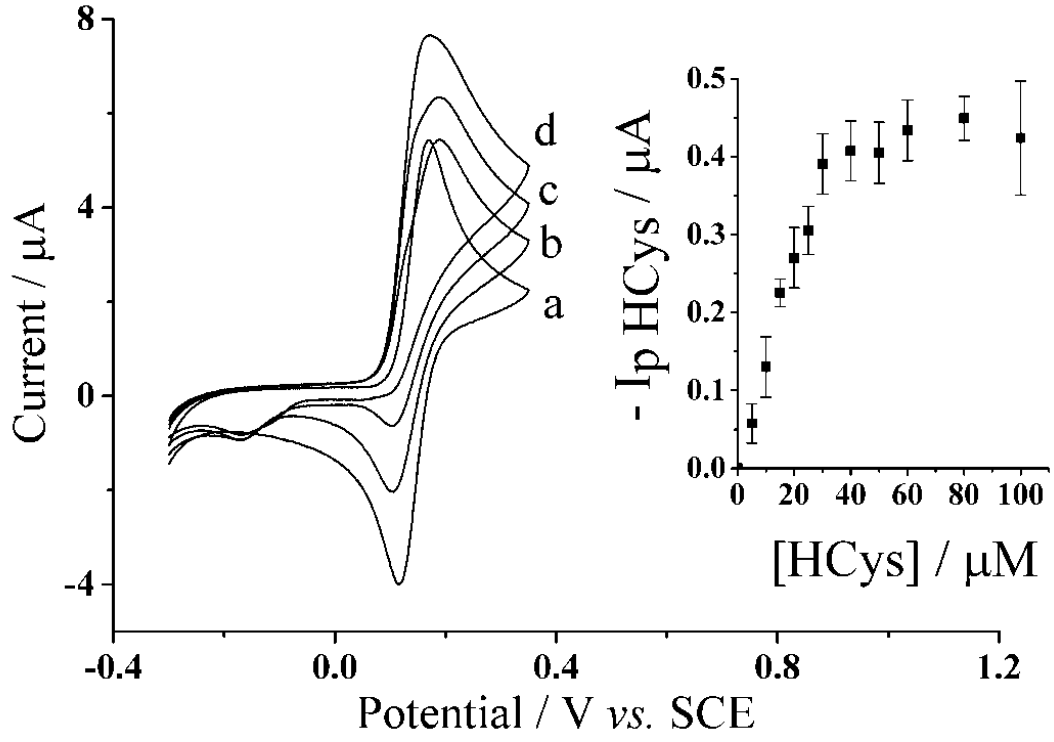

Figure 6.26: Cyclic voltammograms (50 mV s^{-1}) of 100 µM catechol (PBS, pH 7.0) at varying homocysteine concentrations, a. 0 M, b. 20 µM, c. 60 µM, and d. 100 µM, at CNT-SPE. *Inset:* Peak current of homocysteine adduct peak *vs.* concentration of homocysteine.

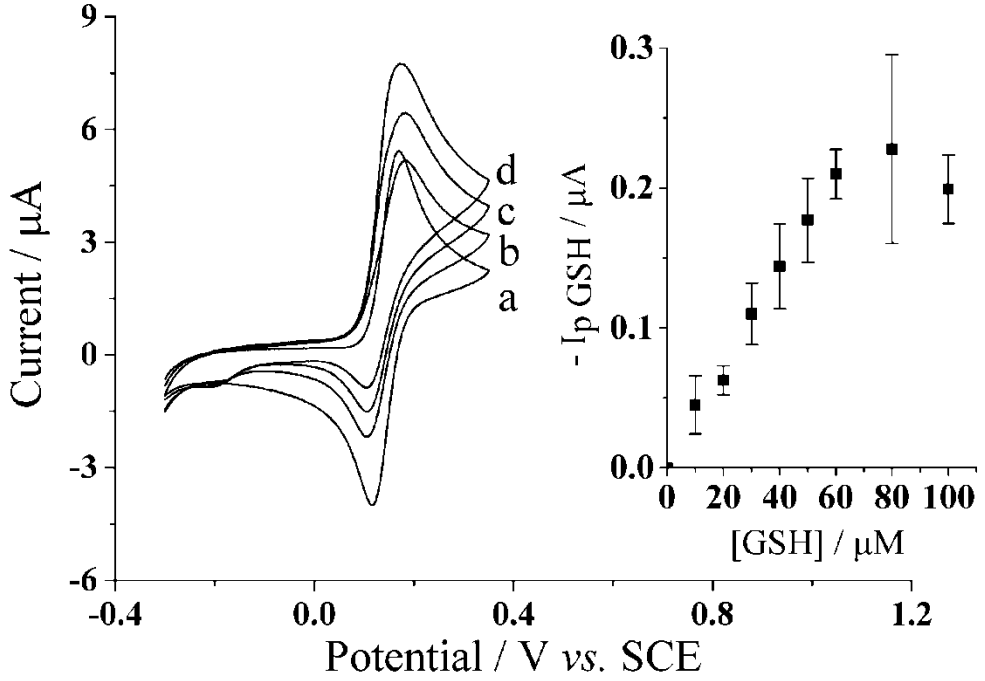

Figure 6.27: Cyclic voltammograms (50 mV s^{-1}) of 100 µM catechol (PBS, pH 7.0) at varying glutathione concentrations, a. 0 M, b. 20 µM, c. 60 µM, and d. 100 µM, at CNT-SPE. *Inset:* Peak current of glutathione adduct peak *vs.* concentration of glutathione.

A preliminary experiment using a number of pre-determined mixed solutions with varying amounts of each homocysteine and glutathione, ranging from 1.0 µM to 10 µM, with 100 µM catechol (PBS, pH 7.0 at 20˚C) using CNT-SPE was carried out using the following two-step procedure. First, the concentration of homocysteine present in solution was determined using the peak current at high scan rate, 500 mV s^{-1}, using the analytical curve at this scan rate mentioned in Section 6.3.3.1, $I_{pHCys\ 500\ mV\ s^{-1}}$ (µA) = (0.0201 ± 0.000076) [HCys/µM] at the CNT-SPE. Next knowing the homocysteine concentration, using a different corresponding linear relationship for homocysteine, we calculate the peak current at a lower scan rate, 50 mV s^{-1}, $I_{pHCys\ 50\ mV\ s^{-1}}$(µA) = (0.013 ± 0.00013) [HCys/µM] (Figure 6.26). We can subtract this value from the total adduct peak current at the low scan rate thus providing the current for glutathione-catechol reaction. The glutathione concentration can then be determined using the

corresponding calibration curve at 50 mV s^{-1}, $I_{pGSH\ 50\ mV\ s^{-1}}$ (nA) = (3.5 ± 0.0066) [GSH/μM] (Figure 6.27). Accordingly, the results can be seen in the Table 6.2, where most of the determined analyte values correspond to the real mix. At low concentrations, such as 1.0 μM homocysteine, there were difficulties measuring the correct peak current due to the peak current for the adduct peak being small to evaluate. Nonetheless, these results initially show that this procedure provides good agreement with the real mixture at an average detection standard deviation *ca.* 23 % as the estimated value is compared to the real values in the mixture. The proposed method will work generally providing both glutathione and homocysteine are of much lower concentration then the added catechol.

Mixed solution		Determined content [a]	
Homocysteine (μM)	Glutathione (μM)	[Homocysteine] (μM)	[Glutathione] (μM)
10	10	10.02 ± 0.01	9.83 ± 0.23
5	10	5.05 ± 0.35	8.90 ± 0.85
10	5	9.40 ± 0.10	5.75 ± 0.15
10	3	9.30 ± 0.10	2.90 ± 0.20
3	10	3.30 ± 0.01	10.05 ± 0.65
1	10	1.60 ± 0.10	11.45 ± 0.25
10	1	10.30 ± 0.60	0.84 ± 0.01

[a] Average value ± standard deviation (n=2).

Table 6.2: Determination of homocysteine and glutathione in mixed solution containing homocysteine, glutathione and 100 μM catechol (PBS, pH 7.0).

6.3.3.3 Selective determination of homocysteine and glutathione in the presence of cysteine

As mentioned above, we were able to show the viability of a procedure for estimating both glutathione and homocysteine in the presence of each other. However, cysteine is another thiol that can also be present in biological media and can act as a possible interferrent since it is a homologue to homocysteine. To investigate whether cysteine interferes with the electrochemical measurement in the proposed method, an experiment was carried out at the CNT-SPE in a solution containing 100 μM catechol (PBS, pH 7.0, at 20°C) and 30 μM cysteine using cyclic voltammetry (50 mV s^{-1} and 500 mV s^{-1}). The concentration of 30 μM cysteine was used as reports have shown that 30 μM of cysteine can be a higher limit observed with certain body fluids such as urine. [42, 236, 237] Figure 6.28 shows the voltammograms of the electro-oxidized catechol in the absence (dotted line) and presence of cysteine (solid line) at scan rates 50 mV s^{-1} (Figure 6.28i) and 500 mV s^{-1} (Figure 6.28ii). The figures show that in the presence of cysteine at either scan rates, the forward peak increases while the back peak decreases but show no evidence of a new adduct peak. This suggests that the reaction between the electrochemically oxidized catechol and cysteine is not a 1,4,- Michael addition but an electrocatalytic reaction [137, 141] and will not interfere with the signal for homocysteine and/or glutathione provided the concentration of cysteine is low compared to that of electro-oxidized catechol. Thus this method using CNT-SPE can enable the possible determination of homocysteine and glutathione in the presence of each other and cysteine.

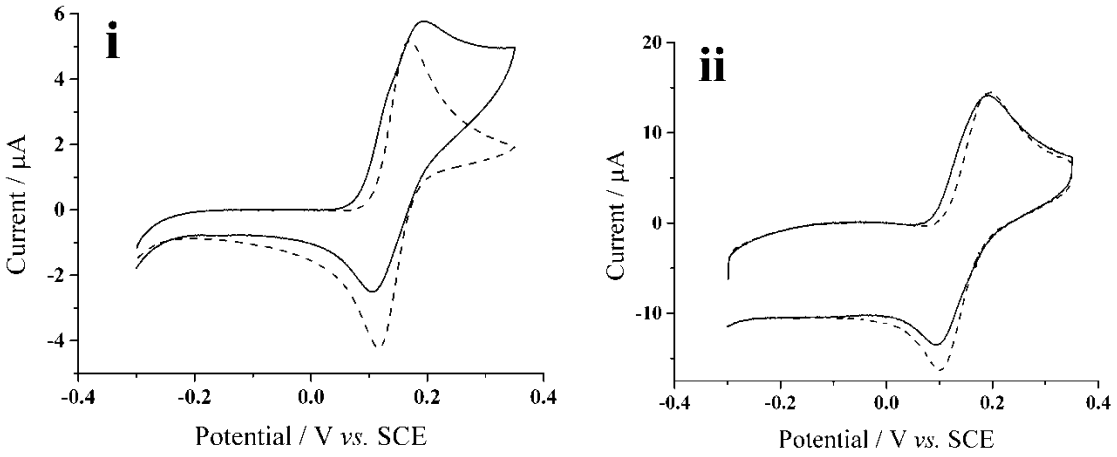

Figure 6.28: Cyclic voltammogram i. 50 mV s^{-1} and ii. 500 mV s^{-1} of 100 μM catechol in the absence (dotted line) and presence (solid line) of 30 μM cysteine (PBS, pH 7.0) at CNT-SPE.

To further validate the proposed method, experiments were performed just as the described above in the presence of 30 μM cysteine. Calibration curves were determined using cyclic voltammetry for homocysteine (scan rates at 500 mV s^{-1} and 50 mV s^{-1}) and glutathione (scan rate at 50 mV s^{-1}) all in the presence of 30 μM cysteine and 100 μM catechol (PBS, pH 7.0 at 20°C), shown in Figure 6.29. The linear relationship of homocysteine at the high scan rate is $I_{pHCys\ 500\ mV\ s^{-1}}$ (μA) = (0.019 ± 0.00029) [HCys/μM] with the linear range up to 40 μM. The linear range and the sensitivity of homocysteine detection at the high scan rate are relatively close when compared to values in the absence of cysteine. This suggests that there is no significant interference during the detection of homocysteine at high scan rate while in the presence of both cysteine and/or glutathione, provided the catechol concentration is sufficiently high. Next, the homocysteine relationship at the lower scan rate is, $I_{pHCys\ 50\ mV\ s^{-1}}$ (μA) = (0.077 ± 0.00029) [HCys/μM] with a linear range up to 25 μM. The linear range and sensitivity for this case at the low scan rate is slightly lower when compared to the absence of cysteine. This is rationalized again provided that the concentration of

the catechol is higher than the amount of thiol present in solution. Lastly, the linear relationship for glutathione at the low scan rate is, $I_{pGSH\ 50\ mV\ s^{-1}}$ (μA) = (0.0019 ± 0.000047) [GSH/μM] with a linear range up to 60 μM. The sensitivity for glutathione detection in the presence of cysteine is also lower than in the absence; where similar to the detection of homocysteine at low scan rate; again, more catechol can be added to increase those values. The limit of detection (LOD) for this proposed method was determined using the following, $3S_B/S$ where S_B is the standard deviation given in the presence of zero analyte and S is the sensitivity, given by the gradient of the calibration curve. In the presence of 30 μM cysteine, the LOD for homocysteine at the high scan rate is *ca.* (1.2 ± 0.1) μM and since the determination of glutathione is dependent on the homocysteine detection, the LOD was determined for homocysteine at the low scan rate, therefore the LOD is *ca.* (0.11 ± 0.2) μM. The determined LOD to the respected analytes are all within reasonable range of detection needed for biological samples.

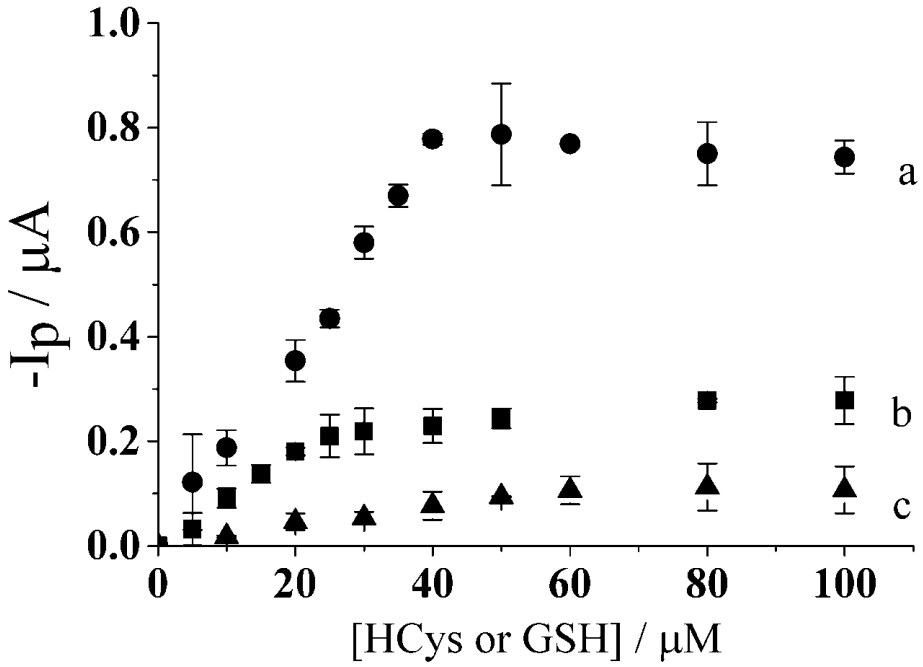

Figure 6.29: Calibration curve of 100 μM catechol (PBS, pH 7.0) in the presence of 30 μM cysteine of a. homocysteine at 500 mV s^{-1}, b. homocysteine at 50 mV s^{-1}, and c. glutathione at 50 mV s^{-1}.

An experiment was carried out, similar to the preliminary test described in Section 6.3.3.2 but with the addition of 30 μM cysteine to further validate this method in solutions containing all three thiol analytes. A number of pre-determined mix solutions containing different quantities of homocysteine and glutathione, varied from 1.0 μM to 10 μM, were combined with a constant amount of catechol (100 μM, PBS, pH 7.0) and cysteine (30 μM, PBS, pH 7.0); thereafter, the proposed method described above was applied using CNT-SPE. The results are then summarized in Table 6.3 where the values are within reasonable deviation, *ca.* 28%, from the pre-determined quantities present in the solutions. It should be noted that there were difficulties with quantifying 1.0 μM homocysteine concentration due to the low peak current produced at the high scan rate and confirms with the calculated LOD value of the system. Nevertheless, the values obtained in this test are within reason to match with the real contents of the mixture.

Mixed solution		Determined content [a]	
Homocysteine (μM)	Glutathione (μM)	[Homocysteine] (μM)	[Glutathione] (μM)
10	10	10.45 ± 0.85	11.35 ± 0.05
5	10	5.75 ± 0.35	9.70 ± 0.40
10	5	11.05 ± 0.15	4.60 ± 0.10
10	3	10.15 ± 0.25	3.15 ± 0.65
3	10	3.55 ± 0.15	10.16 ± 1.14
1	10	2.05 ± 0.15	10.40 ± 0.50
10	1	10.80 ± 0.40	1.30 ± 0.80

[a] Average value ± standard deviation (n=2).

Table 6.3: Determination of homocysteine and glutathione in mixed solution containing homocysteine, glutathione, 30 μM cysteine and 100 μM catechol (PBS, pH 7.0).

6.3.4 Conclusions

The electrochemical estimation of homocysteine and glutathione was shown to be achievable in the absence and presence of cysteine using the proposed two-step procedure at the commercial carbon nanotube screen-printed electrode. This method takes advantage of the different reaction rates of homocysteine and glutathione with the electrochemically oxidized catechol taking place at the surface of the screen printed working electrode via 1,4-Michael addition reaction. It was shown that this method can be easily adaptable to real world applications by having low limit of detections within reasonable range seen in real samples. In addition, the proof of concept method was further proven to be successful as the determined values of homocysteine and glutathione were comparable to the real mix sample solution contents using the two-step method. An average standard deviation *ca.* 28% of the determined values was obtained when evaluated with the real contents in spiked solutions containing the presence of cysteine. This value, which derived from the ten-fold difference in sensitivity towards glutathione and homocysteine, is sufficient for medical applications where threshold values are typically required as 'biomarker' signals. This easy two-step procedure involves little to no extensive sample pre-treatment, which enables possible real-world application towards healthcare or medicinal research; this is to be discussed in more detail in the following chapter.

Chapter 7

Electrochemical methodology applied for the detection of thiols in biological media

We have discussed the thiol detection with *ortho*-quinone derived mediators via two mechanisms: Electrocatalytic and 1,4-Michael addition reaction. The results have shown that a simple *selective* thiol determination is made possible by means of the thiol 1,4-Michael addition reaction with an electro-oxidized catechol at a carbon nanotube screen-printed electrode. Initial proof-of-concept work showed successful exclusive thiol quantification in buffered system containing its homologue species. So ultimately this chapter discusses the practical assessment of the developed methodology into synthetic and real biological samples. The work presented in this chapter has been published in *Analytical Sciences* [238] and *Sensors and Actuators: B* [132, 239]. The work published in *Sensors and Actuators: B* [239] was done in collaboration with Dr. Luis M. Goncalves.

7.1 Selective thiol detection in authentic biological samples with the use of screen-printed electrodes

7.1.1 Introduction

To better understand the biological processes at the cellular level, clinicians and researchers use a variety of available physiological fluids and tissues samples. [30-33, 41, 42, 44-58] Often, these samples are used as a diagnostic medium [41, 42, 44, 55, 82, 117, 240-242], as the intrinsic information gained from the medium can be substantial. As discussed in the previous sections, a developed methodology was conceived for selective thiol detection in the presence of other thiol-containing molecules in a controlled buffered system. Therefore, this section will show a continuation of our proof-of-concept work into typical 'real world' samples, notably tissue cell culture media and human plasma in order to emphasize the authentic practical application and viability of this single two-step method. [133] With the added use of disposable screen-printed electrodes, the selective detection of homocysteine and glutathione in 'real' world biological samples (i.e. human plasma and cell culture tissue media) brings nearer realization of the notion of presenting a viable sensor in the form of a point-of-care system.

To re-iterate the concept, the electrochemical reaction of *ortho*-quinone with thiol compounds is measured at a carbon nanotube screen-printed electrode by utilizing a simple two-step electroanalytical procedure. The single two-step method takes advantage of the different reaction rates of the homocysteine and glutathione with the electrochemically oxidized catechol with the later reacting more slowly (Scheme 7.1). Initially, a faster scan rate is applied, allowing a rapid reaction with homocysteine to take place, and thus 'outrunning' the reaction with glutathione. This subsequently

leaves an analytically useful signal for homocysteine only detection. Next, a slower scan rate is applied that allows both analytes to react, thus relating the contents of both analytes in the adduct peak. Thereafter, the determined homocysteine concentration is subtracted from the concentration obtained at a low scan rate, and thus resulting in the concentration of glutathione.

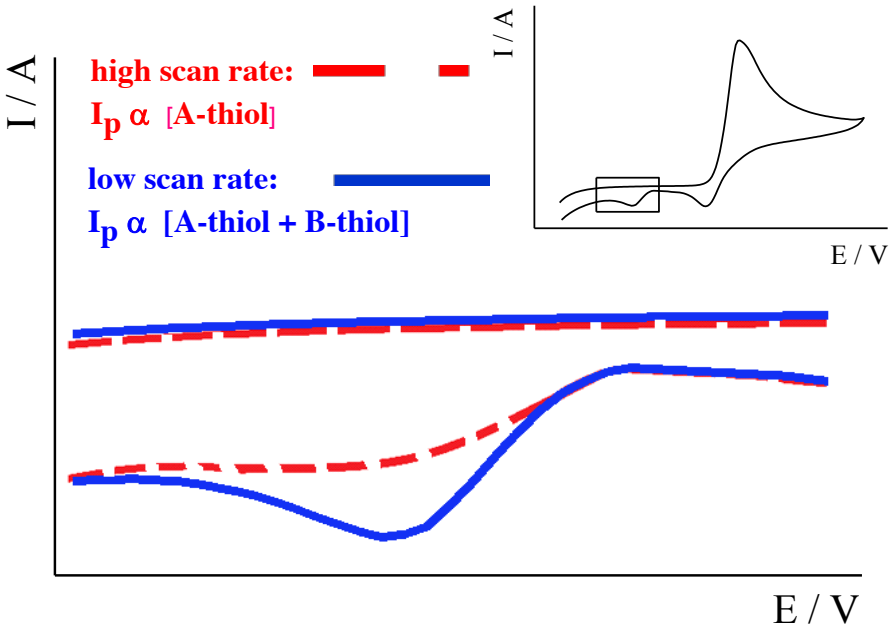

Scheme 7.1: Schematic representation of a two-step method for the selective electrochemical detection of homocysteine and glutathione at the adduct peak.

7.1.2 Experimental procedure

7.1.2.1 Biological media

Dulbecco's Modified Eagle Media (DMEM), and human plasma were purchased through Sigma-Aldrich at their highest purity, and were used as received without any further purification steps.

7.1.2.2 Electrochemical experiments in biological media

Electrochemical experiments involving the tissue culture media, Dulbecco's Modified Eagle Medium (DMEM), were carried out in a three-electrode system using a saturated calomel reference electrode (SCE) from Hach Lange, UK, a platinum mesh (99.99%) counter electrode from Goodfellow, UK, and multi-walled carbon nanotube disposable screen-printed electrodes from DropSens as the working electrode. The initial use of the calomel reference electrode in the tissue culture media was to ensure that all potentials are reliably comparable to that seen in earlier studies, described in this thesis. [133, 143]

Experiments involving human plasma were fully carried out on the screen-printed electrode, accordingly to Section 3.3.3 due to the small volume of available human plasma samples. An approximately 50 μL drop of plasma sample was deposited onto the ceramic chip such that all three electrodes are covered.

7.1.3 Results and discussion

7.1.3.1 Detection in tissue culture media

Tissue culture media contains a variety of amino acids and vitamins to help facilitate in the nourishment and maintenance of cell growth. [38, 182] Some of its contents may be electro-active, and other possible interferences can arise when catechol is added to the medium. Before applying the single two-step analytical procedure, an investigation of possible interferences from the cell tissue culture medium was carried out. Cyclic voltammetry was utilized in 100 % tissue culture media, Dulbecco's Modified Eagle's medium (DMEM), at a scan rate of 50 mV s^{-1} in both the

absence and presence of 0.1 mM catechol (Figure 7.1). The figure shows that within the potential window of interest for analysis, the media alone will not interfere with the measurement. When catechol is added to the media, a redox process at $E_{1/2} = +0.15$ V (*vs.* SCE) is observed, which corresponds to the two-electron, two-proton oxidation of the *ortho*-quinone species. [37, 38, 143] This observation of catechol is consistent with literature reports that the media alone will not interfere with the electrochemical reaction of catechol. [37, 133, 143]

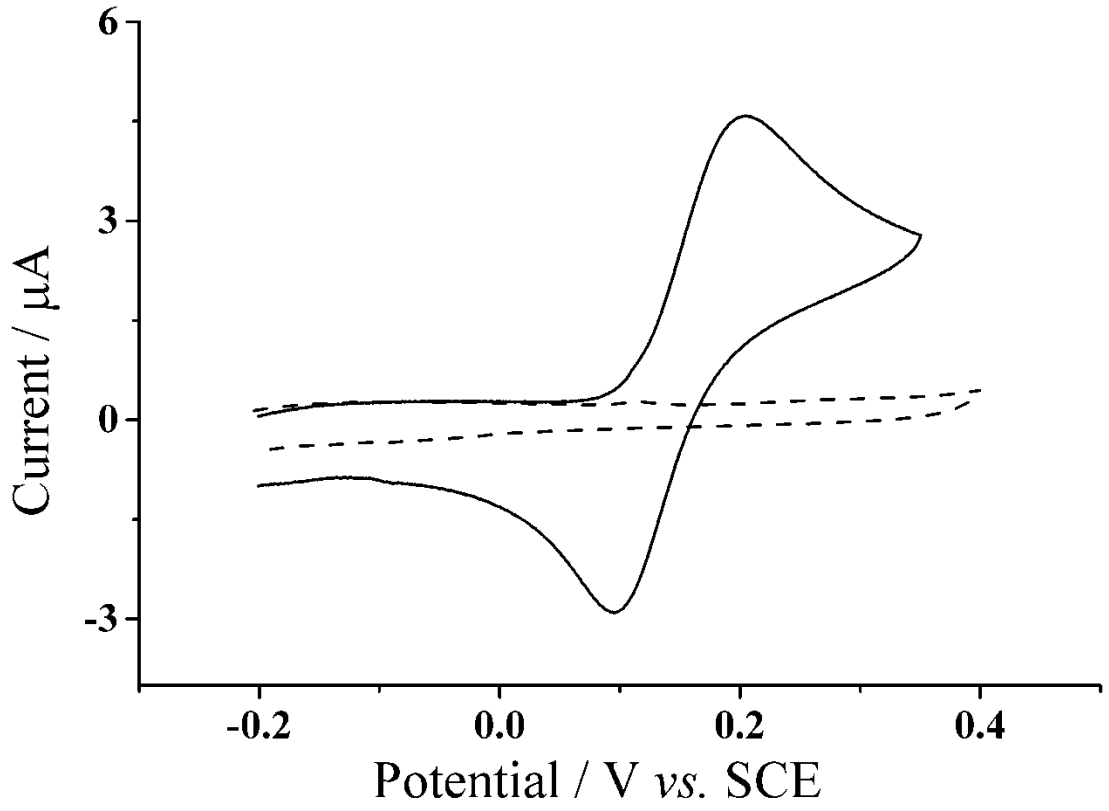

Figure 7.1: Cyclic voltammograms (50 mV s^{-1}) at a CNT-SPE in Dulbecco's Modified Eagle Media (DMEM) in the absence (dashed line) and presence (solid line) of 0.1 mM catechol.

Cyclic voltammetry was applied to tissue media in the presence of catechol and thiols. Figure 7.2 shows the voltammetric behaviour at 50 mV s^{-1} of 0.1 mM catechol for different concentrations of either homocysteine or glutathione. The figure shows that

with each addition of the thiol analyte, a new adduct peak emerges (*ca.* −0.2 *vs.* SCE), and increases along with the forward peak, while the backward peak decreases. This is consistent with a 1,4-Michael addition reaction, as described above and elsewhere. [37, 38, 133, 143] Analytical curves were then obtained at this scan rate; specifically, the adduct peak current for thiol species, I_p, was plotted against the concentration of each thiol analyte. The analytical parameters tabulated in Table 7.1 show a linear relationship for homocysteine at 50 mV s^{-1} is $I_{pHCys\ 50\ mV\ s^{-1}}$ (nA) = (6.59 ± 0.019) [HCys/μM] (n=3) for concentrations of up to 20 μM. The limit of detection (LOD) is determined to be *ca.* (0.5 ± 0.01) μM. For glutathione, the linear relationship at the same scan rate is $I_{pGSH\ 50\ mV\ s^{-1}}$ (nA) = (1.02 ± 0.462) [GSH/μM] (n=3) for concentrations ranging up to 10 μM; the LOD is *ca.* (1.0 ± 0.3) μM. Due to the complexity of the tissue culture media [133], we can expect to observe lower sensitivities for homocysteine and glutathione compared to a pure aqueous system, 19 and 1.9 nA μM^{-1} respectively. Nonetheless, the relationships among those values are consistent with their reaction rates for catechol. [133] However, at a low scan rate the observed adduct peak will reflect the reaction of the electro-oxidized catechol with both homocysteine and glutathione, thus making selective quantification difficult when both thiols are present in the same solution.

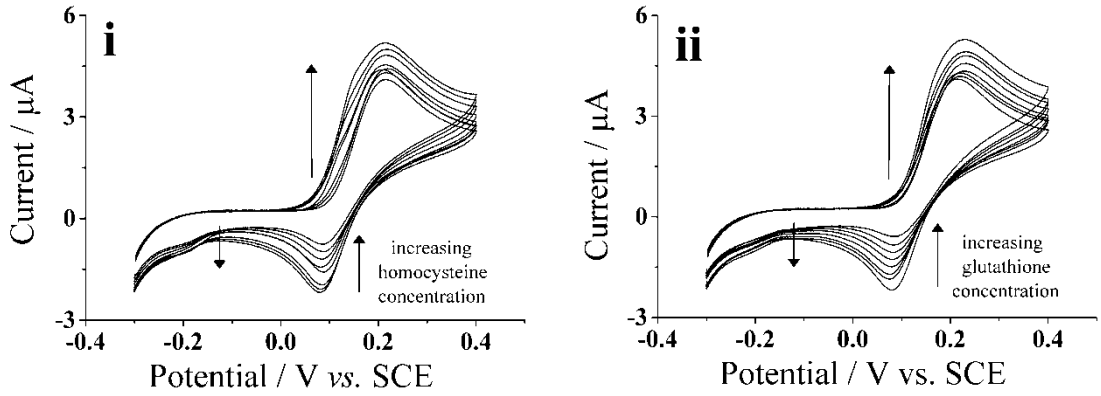

Figure 7.2: Cyclic voltammograms (50 mV s^{-1}) at a CNT-SPE of 0.1 mM catechol (Dulbecco's Modified Eagle Media) with varying concentrations, 0 - 60 µM, of each i. homocysteine or ii. glutathione.

Thiol	Scan rate ($mV\ s^{-1}$)	Slope ($nA\ \mu M^{-1}$)	R^2	LOD [a] (µM)	Linear Range (µM)
Homocysteine	300	(2.96 ± 0.021)	0.981	2.0 ± 0.02	2.0 – 20
Homocysteine	50	(6.59 ± 0.019)	0.997	0.5 ± 0.01	0.5 – 20
Glutathione	50	(1.02 ± 0.462)	0.994	1.0 ± 0.3	1.0 - 10

[a] LOD, calculated limit of detection.

Table 7.1: Analytical parameters for the detection of homocysteine and glutathione in cell tissue culture media (pH 8.0)

An optimum scan rate of 300 mV s^{-1} was found for the homocysteine selectivity in a tissue culture media. Figure 7.3 shows voltammogram of the electro-oxidized catechol in the presence of glutathione (dotted line) and in the presence of homocysteine (solid line). The figure shows that in the presence of glutathione, the adduct peak ceased to exist when a faster scan rate was applied; however, the adduct peak (*ca*. –0.2 V *vs.* SCE) appears in the presence of homocysteine. This indicates that the faster scan rate 'outruns' the *ortho*-quinone reaction with glutathione, but is still sufficient to allow the reaction with homocysteine to take place; similarly described in

Section 6.3. [133] Thus perhaps the selective detection of homocysteine is achievable in the presence of glutathione in tissue culture media at the screen-printed electrode when a higher scan rate is applied. Next, a calibration curve was obtained that indicated a linear relationship of homocysteine at 300 mV s^{-1}, $I_{pHCys\ 300\ mV\ s^{-1}}$ (nA) = (2.96 ± 0.021) [HCys/μM] (n=3), for concentrations of up to 20 μM, and the LOD being *ca.* (2.0 ± 0.02) μM (also summarized in Table 7.1). Finally, at this point, all of the appropriate calibration curves have been determined, and the method can be fully applied and tested in the tissue culture media.

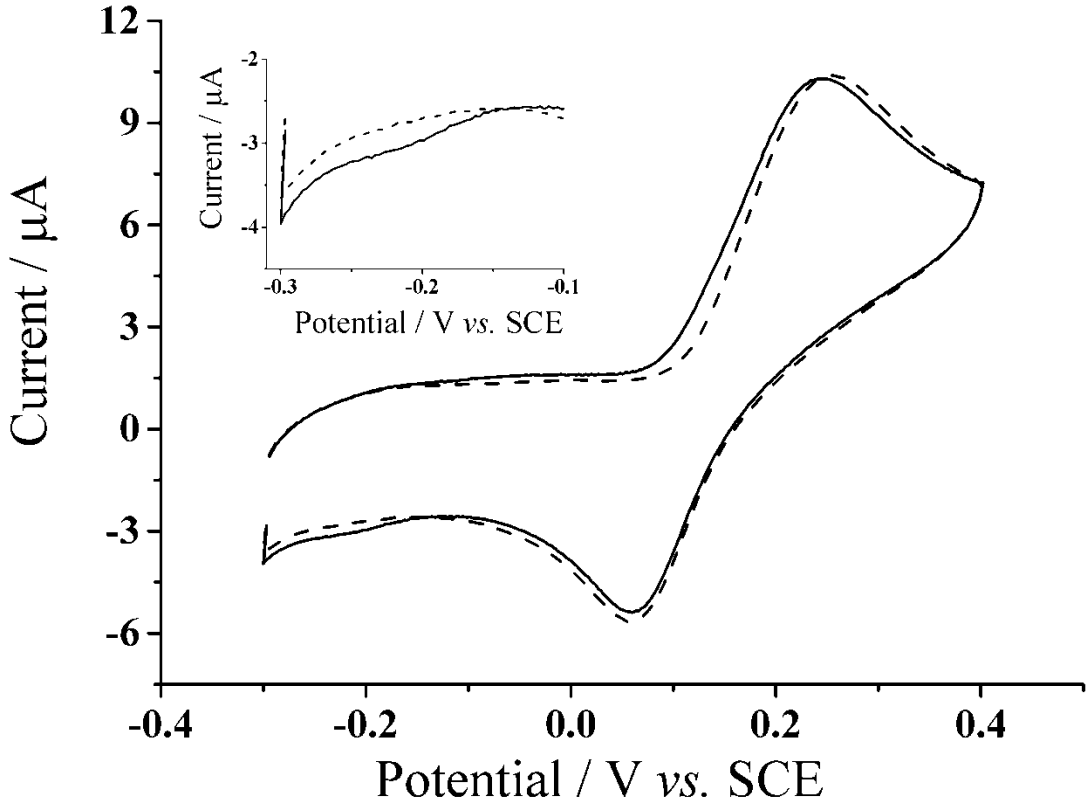

Figure 7.3: Cyclic voltammograms (300 mV s^{-1}) at a CNT-SPE in Dulbecco's Modified Eagle Media with 0.1 mM catechol in the presence of 20 μM homocysteine (solid line) and 20 μM glutathione (dash line). *Inset:* Enlarge view of the thiol adduct peak.

A number of pre-determined mixed solutions containing varying spiked amounts of homocysteine and glutathione, ranging from 1.0 to 10.0 μM, were examined with the

presence of 0.1 mM catechol (Dulbecco's Modified Eagle Media, pH 8.0) using the carbon nanotube screen-printed electrode. Upon applying the two-step method, a peak current at a scan rate of 300 mV s^{-1} was obtained from the Dulbecco's Modified Eagle Media mixture, where the homocysteine content can be determined from the analytical curve, $I_{pHCys\ 300\ mV\ s^{-1}}$ (nA) = (2.96 ± 0.021) [HCys/μM]. Then by knowing the homocysteine concentration present, the peak current for homocysteine can be calculated at the low scan rate by using the analytical curve, $I_{pHCys\ 50\ mV\ s^{-1}}$ (nA) = (6.59 ± 0.019) [HCys/μM]. Next, we can subtract this value from the total adduct peak current at a low scan rate, which results in the peak current corresponding to the reaction of glutathione-catechol. Lastly, the glutathione content can be determined from the respective calibration curve, $I_{pGSH\ 50\ mV\ s^{-1}}$(nA) = (1.02 ± 0.462) [GSH/μM].

Table 7.2 gives the measurement results of different combinations of the thiol mixture in the tissue culture media using the two-step procedure. The table shows that the determined values correlate well within a reasonable error, with the spiked thiol contents of the tissue culture media mixture. The average standard deviation for the detection measurement in comparison to the spiked values is *ca.* 10% which is acceptable for bio-marker applications. Given that the two-step method is limited by the capacity of the fast scan rate in order for the determination of glutathione to work, the limit of detection of the procedure in tissue culture media is *ca.* (2.0 ± 0.02) μM. This value is within the range of thiols typically seen in human physiological samples. [55, 82] Therefore, this two-step method for quantifying homocysteine and glutathione works well in tissue cell culture media.

Mixed solution		Determined content [a]	
Homocysteine (μM)	Glutathione (μM)	[Homocysteine] (μM)	[Glutathione] (μM)
10	10	10.5 ± 0.150	9.4 ± 1.7
10	5	9.0 ± 0.60	5.1 ± 1.1
10	3	10.1 ± 0.100	2.1 ± 0.10
10	1	10.9 ± 0.800	1.0 ± 0.30
5	10	4.9 ± 1.4	10.1 ± 0.100
3	10	2.6 ± 0.01	10.7 ± 1.00
1	10	1.2 ± 0.05	10.4 ± 0.250

[a] Average value ± standard deviation (n=2).

Table 7.2: Determination of homocysteine and glutathione in mixed solutions containing homocysteine, glutathione and 100 μM catechol (Dulbecco's Modified Eagle Media, pH 8.0)

7.1.3.2 Detection in human plasma

Human plasma, itself, has a complex matrix containing different analytes and species. [243, 244] A partial list of constituents in human plasma is given in Table 7.3. Therefore, a selective determination for a specific analyte in human plasma is a challenge for the electroanalytical community, since many of its constituents may be redox active, or impede the electroanalysis. [38, 41, 119, 243] Consequently, reports that focus on electrochemical detection in human plasma are usually coupled with a separation technique, such as HPLC. [41, 42, 72, 82, 95, 117, 223, 236, 245, 246] In our experiments, human plasma was diluted to 25% with 0.15 M PBS (pH 7.2), and an optimal catechol concentration of 1.0 mM was used, because higher concentrations resulted in coagulation. Lastly, all three electrodes on the disposable screen-printed electrode, itself, were fully used due to the small quantity of available human plasma.

Constituent(s)	Normal range	Units	Reference(s)
Aldosterone	100 – 450	pmol/L	[247, 248]
Ammonia	0 – 54	µmol /L	[247, 249]
Aspartic Acid	0.1 – 0.14	mg/mL	[242]
Arginine	1.5 – 2.5	µg/mL	[242]
Calcitonin	0 – 4.5	ng/L	[247]
Cortisol	80 – 700	nmol/L	[250, 251]
Creatinine	50 - 100	µmol /L	[252, 253]
Cysteine	10 - 30	µmol /L	[42, 43]
Glucose	4.1 – 6.0	mmol/L	[252]
Glutamic acid	0.4 – 1.15	µg/mL	[95, 242]
Glutathione	2 - 12	µmol /L	[31, 33, 34, 43, 55, 58]
Hemoglobin	120 - 160	g/L	[252]
Homocysteine	5 - 15	µmol /L	[42, 43, 61, 82]
Lactate	0.5 - 2.22	mmol/L	[252]
Lysine	2.2 – 3.0	µg/mL	[242]
Magnesium	1.7 - 2.3	µg/mL	[244, 252]
Methionine	0.2 – 1.0	µg/mL	[117, 222, 242]
Potassium	12.1 – 25.4	µg/mL	[252]
Sodium	300 - 330	mg/dL	[252]
Uric Acid	0.18 – 0.48	mmol/L	[254, 255]
Vitamin A	30 - 65	µg /dL	[241, 256]
Vitamin C	23 - 85	µmol /L	[226, 229]
Vitamin D	20 – 150	nmol/L	[257-259]

Table 7.3: Table of some constituents of human plasma

Initially, to investigate any interference that may arise from human plasma alone, cyclic voltammetry was run in both the absence and presence of catechol. Figure 7.4 shows cyclic voltammograms (100 mV s^{-1}) of human plasma with and without the addition of 1.0 mM catechol (pH 7.2). This figure shows that in the absence of catechol, an anodic process occurs at *ca.* +0.4 V (*vs.* Ag), and a cathodic process occurs *ca.* −0.6 V (*vs.* Ag). These processes can be attributed to be a result of an unknown electroactive species in human plasma. [54, 55, 243] With the presence of 1.0 mM catechol in human plasma, a new redox process is observed, $E_{1/2} = +0.2$ V (*vs.* Ag), which is attributed to the two-electron oxidation of the catechol forming the *ortho*-quinone. [37, 38, 143]

Since analytically we are concerned with the reductive scan, the cathodic signal from the human plasma *ca.* −0.6 V (*vs.* Ag) should not hinder the adduct peak signal, because the adduct signal should appear near to the catechol signal. However, because no observable thiol-catechol signal was seen in the cyclic voltammetry, the square wave was utilized to increase the sensitivity of the measurements in the plasma.

Figure 7.5a shows a reduction scan in square-wave voltammetry (optimized to a frequency of 10 Hz; amplitude, 5.0 mV; step potential, 10 mV) of human plasma containing 1.0 mM catechol (pH 7.2) at the CNT-SPE. The scan rate under these optimized parameters is 100 mV s^{-1}. Three signals are observed in the figure corresponding to the reductive wave of the catechol (*ca.* +0.2 V *vs.* Ag), the thiol-catechol adduct peak (*ca.* −0.1 V *vs.* Ag), and the unknown electroactive species within the plasma (*ca.* −0.5 V *vs.* Ag). The shift of the unknown electroactive species was attributed to the silver quasi-reference electrode built into the screen-printed electrode.

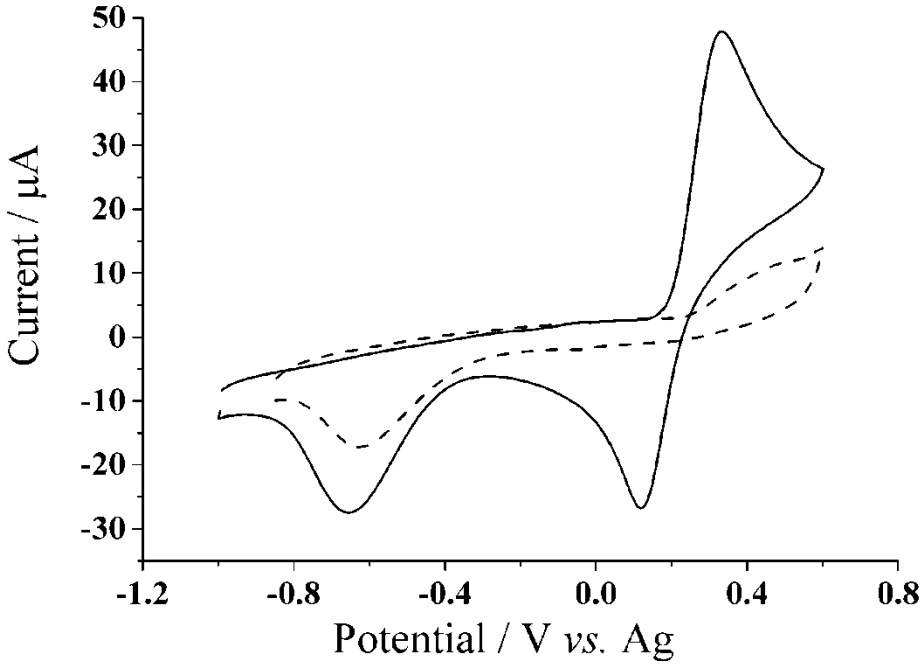

Figure 7.4: Cyclic voltammogram (100 mV s^{-1}) at a CNT-SPE in 25% human plasma diluted with 0.15 M PBS (pH 7.2) with both the presence (solid line) and absence (dashed line) of 1.0 mM catechol.

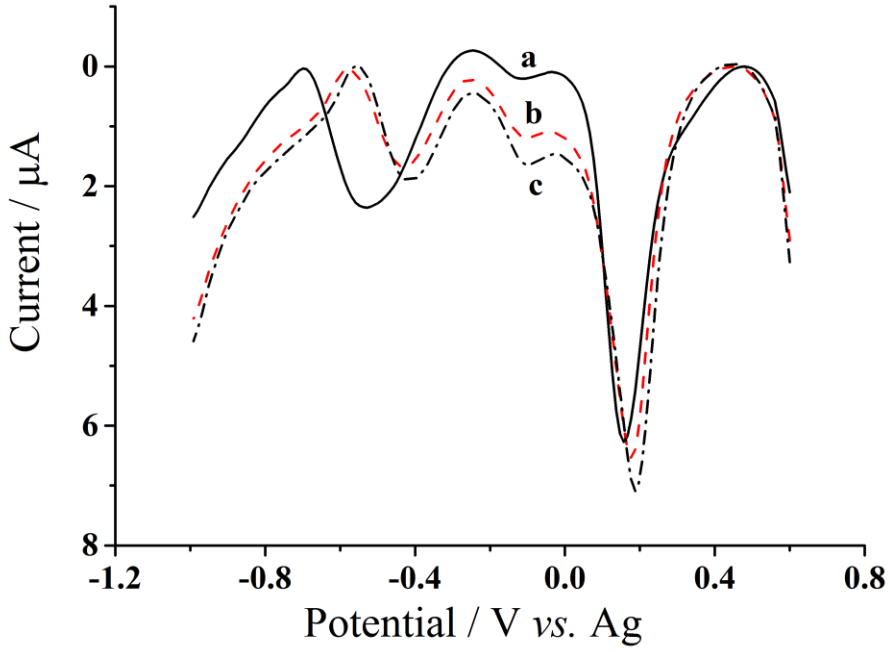

Figure 7.5: Square-wave voltammograms of 25% human plasma with 1.0 mM catechol containing a. no thiol, b. 20 μM homocysteine, and c. 20 μM glutathione. (frequency, 10 Hz; amplitude, 5.0 mV; step potential, 10 mV).

Since human plasma alone contains contents of homocysteine and glutathione, [41, 43, 52, 54, 55, 69, 82, 223] we can expect to see an adduct peak signal associated with the thiol-catechol reaction. To definitively determine the peak observed at *ca.* −0.1 V (*vs.* Ag) is the thiol interaction with catechol, the human plasma was spiked with 20 μM of each homocysteine and glutathione. As can be observed in Figure 7.5, the peak at *ca.* −0.1 V (*vs.* Ag) increases with the spiked content, thus indicating that the peak of interest represents the thiol-catechol interaction. Next, different concentrations of either homocysteine or glutathione, ranging from 0 to 20 μM, were added separately to the human plasma in the presence of 1.0 mM catechol. By using square-wave voltammetry, a linear relationship, I_{pHCys} (nA) = 625 + (59.96 ± 4.256) [HCys/μM] (n=3), was determined for homocysteine with a linear range of up to 15 μM, and the LOD was determined to be *ca.* (0.6 ± 0.2) μM. For glutathione, the linear relationship is

I_{pGSH} (nA) = 588 + (39.1 ± 2.22) [GSH/μM] (n=3) within a linear range up to 15 μM, and the LOD is *ca.* (0.8 ± 0.4) μM.

Furthermore, square-wave voltammetry was again applied to the plasma to determine if homocysteine selectivity was possible in the presence of glutathione. The square-wave parameters were changed and the signal was optimized to a frequency of 50 Hz, amplitude of 5.0, and step potential of 12 mV, increase in scan rate to 600 mV s^{-1}. Thereafter, the square-wave was applied to plasma spiked with 20 μM of each homocysteine and glutathione. Figure 7.6 shows the thiol-catechol signal, *ca.* −0.1 V (*vs.* Ag). An increase appears in the peak current in the presence of spiked homocysteine, while the peak current remains unchanged in the plasma sample spiked with glutathione, thus showing that homocysteine selectivity is possible in the human plasma sample. Once again, a linear relationship was determined for homocysteine at a higher scan rate, I_{pHCys} (nA) = 104 + (93.7 ± 11.4) [HCys/μM] (n=3) with a linear range up to 15 μM. The LOD is *ca.* (0.8 ± 0.4) μM. At this point, the analytical parameters reflect the homocysteine and glutathione sourced from the human plasma sample in addition to that added. In order for the two-step method to be applied, the calibration curves need to be corrected so as to allow for the intercept of the linear plot to be zero, which is here tabulated in Table 7.4. The analytical parameters show the possibility for homocysteine and glutathione detection with catechol in a human plasma sample.

Thiol	Scan rate (mV s^{-1})	Slope (nA μM^{-1})	R^2	LOD[a] (μM)	Linear Range (μM)
Homocysteine	600	(93.7 ± 11.4)	0.957	0.8±0.4	0.5 - 15
Homocysteine	100	(59.96 ± 4.256)	0.985	0.6±0.2	0.5 - 15
Glutathione	100	(39.1 ± 2.22)	0.990	0.8±0.4	0.5 - 15

[a] LOD, calculated limit of detection.

Table 7.4: Two-step method analytical parameters for the detection of homocysteine and glutathione in 25 % human plasma (pH 7.2)

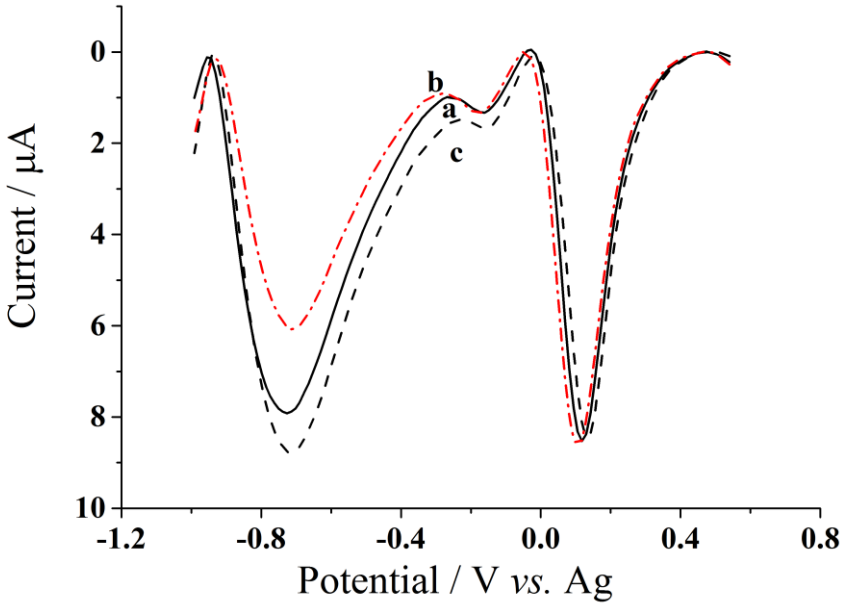

Figure 7.6: Square wave voltammograms of 25% human plasma with 1.0 mM catechol containing a. no thiol, b. 20 μM glutathione, and c. 20 μM homocysteine. (frequency, 50 Hz; amplitude, 5.0 mV; step potential, 12 mV).

The two-step method for homocysteine and glutathione detection was applied to a human plasma medium using catechol at the CNT-SPE. As described above, a high scan rate of 600 mV s^{-1} was first applied to a human plasma sample also containing catechol in order to determine the homocysteine content using the sensitivity of the corresponding analytical curve. Then, the homocysteine content could be used to determine the peak current corresponding to the low scan rate. Thereafter, the peak current associated with homocysteine at a low scan rate was subtracted from the total adduct peak at the same low scan rate. This resulted in the peak current associated with the glutathione content, which could then be calculated using the next corresponding gradient. The results of the determined homocysteine and glutathione content in human plasma via two-step method are tabulated in Table 7.5. As described above, the limit of detection for this two-step method is dictated by the limitation of the first step, and thus the LOD for the procedure in human plasma is (0.8 ± 0.4) μM. This value is reasonable

and practical for the range thiols that are typically seen in human plasma. [55, 61, 69, 82, 246]

Thiol	Standard addition method [a] (μM)	Two-step method [a] (μM)
Homocysteine	10.4 ± 0.70	11.1 ± 1.40
Glutathione	15.0 ± 0.90	16.7 ± 1.80

[a] Average value ± standard deviation (n=3).

Table 7.5: Determination of homocysteine and glutathione in 25 % human plasma via a two-step procedure compared to a standard addition

The standard addition method was also performed on the plasma sample in the presence of 1.0 mM catechol (pH 7.2). Using the square-wave parameters (frequency, 10 Hz; amplitude, 5.0 mV; step potential, 10 mV) the human plasma was spiked separately with either homocysteine or glutathione at different concentrations of up to 20 μM. Then, a calibration curve of those multiple additions was used to calculate the unknown analyte concentrations. [126] The results from the standard addition are also tabulated in Table 7.5, where they can be compared to those obtained via the two-step method. The table shows that the values are in good agreement with one another, and are well within the deviation of each other, which further validates the application of the two-step method in such biological samples. The average error of the two-step method when compared to the standard addition method is *ca.* 10%, which is acceptable for biological applications. These results of 'real' world sample offer good promise for using the two-step method. It encourages a fast, simple, facile method towards bio-applications in the selective determination of homocysteine and glutathione.

7.1.4 Conclusions

We have established a successful adaptation of the single two-step method for the selective electrochemical detection of homocysteine and glutathione in two common 'real' world biological samples. The parameters for the simple two-step method were optimized for applications in both tissue culture media and human plasma using disposable carbon screen-printed electrodes. The limit of detection for the system in cell tissue media and human plasma is *ca.* 2 μM and *ca.* 1 μM, respectively, and with an average error of *ca.* 10% when compared to control experiments for either biological sample. These values are acceptable for bio-marker applications, and may allow for the development of a system for medical use.

7.2 Selective electrochemical detection of thiol biomarkers in saliva using multiwalled carbon nanotube screen-printed electrodes

7.2.1 Introduction

Though typical biological fluids in clinical applications include human plasma, obtaining the sample is invasive to the patient. In recent reports, investigators propose the use of saliva as an alternative diagnostic medium to blood plasma. [44, 75, 260, 261] The reason for this is that analysis of saliva from several apparently healthy individual show thiol concentrations are within the same range of that observed in human blood plasma (Table 7.6). Since saliva sampling is both easy and non-invasive, its use in clinical applications is potentially very appealing. [44, 46, 76, 77, 240] This in turn, cascaded into a number of diagnostic studies on saliva in the biomedical field; in particular, reports showing the diagnostic use in case studies relating different levels of

homocysteine (HCys) [46, 75, 76, 240] and glutathione (GSH) [46, 53, 76, 77, 79-81, 262] concentrations to having *possible* implications to deleterious conditions.

Physiological Fluid	Homocysteine (μM)	Glutathione (μM)	Reference(s)
Saliva	2 – 5	5 – 30	[46, 53, 77, 79, 240]
Blood Plasma	5 – 15	2 – 12	[42, 59, 61, 82, 223, 242, 246]

Table 7.6: Literature of homocysteine and glutathione found in natural human saliva and blood plasma.

To the best of our knowledge to date, there is no literature reporting thiol detection in saliva without the use of expensive instrumentation or elaborate prior separation. [44-46, 53, 75, 77, 81, 88, 240, 260, 263, 264] Accordingly, the precursor of a versatile, simple, clear diagnostic pathway in clinical applications in a form of a point-of-care sensor is highly desirable. As previously mentioned in Section 6.3 and 7.1, selectivity of homocysteine and glutathione in the reaction with oxidized catechol can be achieved through their different reaction rates with the *ortho*-quinone leading to different responses as a function of voltage scan rate. [133] Proof of concept of the single two-step electrochemical method showed a quantitative performance in buffer and in typical biological media such as cell tissue media and human plasma. [133, 238] Again, human plasma can be quite intrusive; so, ultimately the purpose of this chapter is to expand the application of this technique for not only use of blood plasma but beyond, namely to saliva. Herein, the reported data is of synthetic saliva spiked with glutathione and homocysteine for selective measurement of those biomolecules.

7.2.2 Synthetic saliva

Synthetic saliva was purchased from Synthetic Urine e.K (Germany). The proprietary formulation of the synthetic saliva reflects the standardized production process of DIN 53160-1 [120], which contains no added thiol compound.

7.2.3 Carbon nanotube screen-printed electrode

The three electrode screen-printed electrochemical chip, described in Section 3.3.3 was fully used in this section to show the capability of using a disposable unit for this method. For each experiment carried out, a new electrode was used to prevent any cross contamination of the synthetic saliva sample. Different electrodes from the same batch were tested and show good reproducibility in the synthetic saliva, $\geq$ 90 %.

7.2.4 Results and discussion

The compatibility of this two-step detection method with synthetic saliva was investigated using cyclic voltammetry at CNT-SPEs. Initially, the synthetic saliva was tested in the presence and absence of catechol to show the reproducibility of the mediator voltammetry in the biological fluid (Section 7.2.4.1). Next, different concentrations of each homocysteine and glutathione were separately spiked into synthetic saliva containing catechol to ensure the electrochemical behaviour is consistent with the expected behaviour at low scan rates (Section 7.2.4.2). As detection of both analytes is attainable at low scan rate, homocysteine selectivity was next investigated through a variable scan rate study (Section 7.2.4.3). With all the appropriate calibration curves known, the two-step method for selective homocysteine

and glutathione determination is shown feasible in synthetic saliva using a combination of data obtained at a high scan rate first followed by a low scan rate (Section 7.2.4.3).

7.2.4.1 Catechol in synthetic saliva

Saliva contains a number of proteins, enzymes, hormones, ions, and other molecules including homocysteine and glutathione (Table 7.7). Although the pure, unspiked synthetic saliva contains no thiol compounds, other analytes within the media *may* be electro-active. Cyclic voltammetry was undertaken to investigate this possibility. Figure 7.7 shows the voltammetry (50 mV s^{-1}) at a CNT-SPE in a solution consisting of 95 % synthetic saliva and 5 % buffer solution with or without catechol (100 µM, pH 7.3). The figure shows that in the absence of catechol, there is no signal thus suggesting no electro-activity from the synthetic saliva alone in the potential range studied.

Constituent(s) name	Reference(s)
Albumin	[260, 261]
Ammonia	[260]
Amylase	[44, 260]
Ascorbic acid	[81, 260, 261]
Aspartate aminotransferase	[79, 81, 260]
ß-glucuronidase	[260]
Carbohydrates	[260]
Chloride	[260]
Creatinine	[260]
Glucose	[260]
Glutathione	[76, 77, 79-81, 260]
Histatins	[260]
Homocysteine	[46, 76, 240, 260]
Immunoglobulin A, G, & M	[44, 260]
Lactic acid dehydrogenase	[79, 81, 260]
Lipase	[260]

Lipids	[44, 260]
Lysozyme	[260]
Mucins	[46, 260]
Sialic acid	[260]
Urea	[260]
Uric Acid	[46, 80, 81, 260, 261]

Table 7.7: Literature reference on some constituents in natural human saliva.

In the presence of catechol (100 μM), a redox process was observed in synthetic saliva showing an oxidation peak at *ca.* +0.28 V (*vs.* Ag) followed by a reduction peak at *ca.* +0.12 V (*vs.* Ag) attributed to the two electron and two proton oxidation/reduction of the catechol-benzoquinone couple (Scheme 4.3). [37, 65, 131, 133] Repetitive voltammetric cycling of catechol in *pure* synthetic saliva was also carried out at the CNT-SPE for five minutes (*ca.* 18 scans) and it sustained no significant loss of the redox peak current suggesting suitability of this redox mediator for thiol studies in this media.

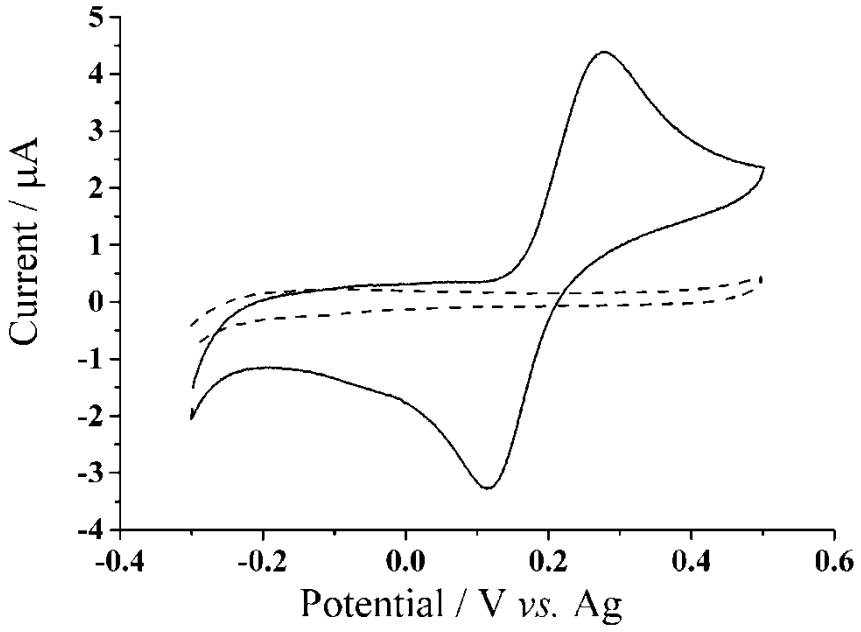

Figure 7.7: Cyclic voltammetry (50 mV s^{-1}) at CNT-SPE of 95 % synthetic saliva in the absence (dotted line) and presence of 100 μM catechol (solid line).

7.2.4.2 Thiol detection in synthetic saliva

Cyclic voltammetry (50 mV s^{-1}) was next carried out in 95 % synthetic saliva (as above) containing 100 μM catechol (pH 7.3) to observe the behaviour at different concentrations of homocysteine and glutathione (ranging from 5 μM to 100 μM). Figure 7.8 shows that with increasing concentration of each homocysteine and glutathione, the anodic peak current increases, the cathodic peak current decreases and an introduction of a new peak emerges at *ca.* −0.15 V (*vs.* Ag). This observation is consistent with nucleophilic attack on the electro-oxidized catechol by the thiol containing molecule thus resulting in a new adduct peak (Scheme 4.3), in agreement with the literature. [37, 131, 133] Note that there is a slight change in the adduct peak potential compared with studies done with a SCE reference electrode; this is attributed to slight drift of the quasi-silver reference electrode provided on the screen-printed electrode.

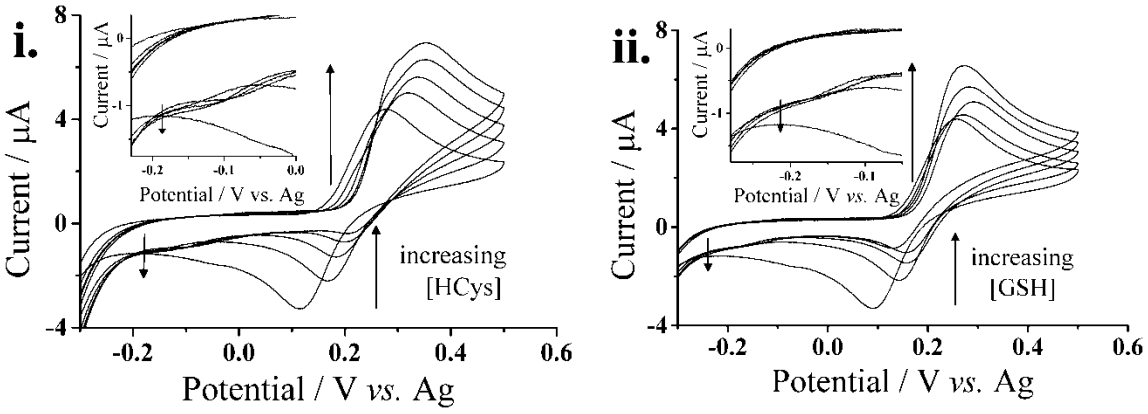

Figure 7.8: Cyclic voltammogram (50 mV s^{-1}) at CNT-SPE of 100 μM catechol (95 % synthetic saliva, pH 7.3) at varying concentrations (0 – 100 μM) of i. homocysteine and ii. glutathione. *Insets:* Magnified view of adduct peak regions.

Upon examination of the adduct peak for thiol species x (x = HCys or GSH), the peak current, I_{px}, increases with increasing concentration of both homocysteine and

glutathione. When a calibration curve is plotted separately for both homocysteine and glutathione, it was found that there is a linear relationship between the adduct peak current and the thiol concentration. The empirical equation for homocysteine at 50 mV s^{-1} is $I_{pHCys\ 50\ mV\ s^{-1}}$ (nA) = (2.8 ± 0.2) [HCys/μM] (n=3) at a linear range up to 20 μM and a limit of detection, LOD, was determined to be *ca*. (2.0 ± 0.1) μM. For glutathione, the linear relationship at 50 mV s^{-1} is $I_{pGSH\ 50\ mV\ s^{-1}}$ (nA) = (2.1 ± 0.2) [GSH/μM] (n=3) with a linear range up to 20 μM and a limit of detection is *ca.* (3.0 ± 0.3) μM. These analytical parameters are tabulated in Table 7.8 where values are found suitable for concentrations typically seen in natural human saliva.

Target Thiol	Scan Rate ($mV\ s^{-1}$)	Slope ($nA\ \mu M^{-1}$)	R^2	Range (μM)	LOD [a] (μM)
Glutathione	50	(2.1 ± 0.2)	0.973	5 – 20	3.0±0.3
Homocysteine	50	(2.8 ± 0.2)	0.978	5 – 20	2.0±0.2
Homocysteine	300	(13.2 ± 0.42)	0.995	5 – 20	0.9±0.01

[a] LOD, calculated limit of detection.

Table 7.8: Analytical parameters for homocysteine and glutathione detection in synthetic saliva, pH 7.3.

7.2.4.3 Selective thiol detection in synthetic saliva

The observations reported above show that homocysteine and glutathione can be detected separately via catechol oxidation in synthetic saliva using cyclic voltammetry at a CNT-SPE. However, *selective* detection of either or both thiols is required for the analysis of authentic saliva, which will contain both species. Different scan rates (≥ 50 mV s^{-1}) were applied to 100 μM catechol (synthetic saliva, pH 7.3) solutions containing additions of 20 μM of both analytes: homocysteine and glutathione.

The aim was to outrun one thiol's reaction with the *ortho*-quinone. Figure 7.9 shows a magnified view of the adduct peak region of the cyclic voltammogram at the optimal high voltage scan rate of 300 mV s^{-1}. The figure shows, no evidence of an adduct peak in the presence of glutathione (Figure 7.9i) whilst the adduct appears in the presence of homocysteine (Figure 7.9ii) at this scan rate. This suggests that a scan rate of 300 mV s^{-1} is adequate to exclude the electro-oxidized catechol reaction with glutathione but still allow the reaction with homocysteine thus permitting selective homocysteine detection in the presence of glutathione in saliva.

Using these optimal voltammetric parameters for selective homocysteine detection, varying concentrations of homocysteine (5 – 100 μM) were tested in the presence of 100 μM catechol (synthetic saliva, pH 7.3) at the CNT-SPE (Figure 7.10). The figure shows an increase in forward peak, a decrease in backward peak and a new adduct peak as the concentration of homocysteine increases; again suggesting the nucleophilic attack on the *ortho*-quinone by the thiol, described previously in the case of 1,4-Michael addition reaction. The inset to Figure 7.10 shows a magnified view of the adduct peak (*ca.* −0.15 *vs.* Ag), where the peak current increases with increasing concentration of homocysteine. Again, this analytically useful adduct peak is well-suited for selective homocysteine detection under these conditions. Next, an analytical curve was determined when the adduct peak current, I_p, was plotted with homocysteine concentration. The linear relationship at 300 mV s^{-1} was determined to be $I_{pHCys\ 300\ mV\ s^{-1}}$ (nA) = (13.2 ± 0.42) [HCys/μM] (n=3) with a linear range up to 20 μM and the LOD is *ca*. (0.9 ± 0.01) μM (Table 7.8). These values are also within reasonable limits suited for bio-marker sensing in human saliva.

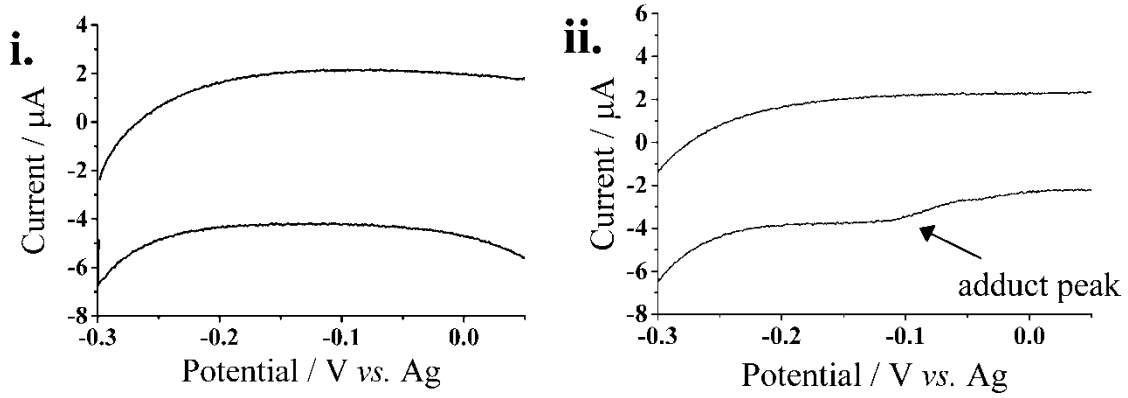

Figure 7.9: Magnified view of adduct peak region (scan rate = 300 mV s^{-1}) at CNT-SPE of 100 µM catechol (95 % synthetic saliva, pH 7.3) with 20 µM i. glutathione and ii. homocysteine.

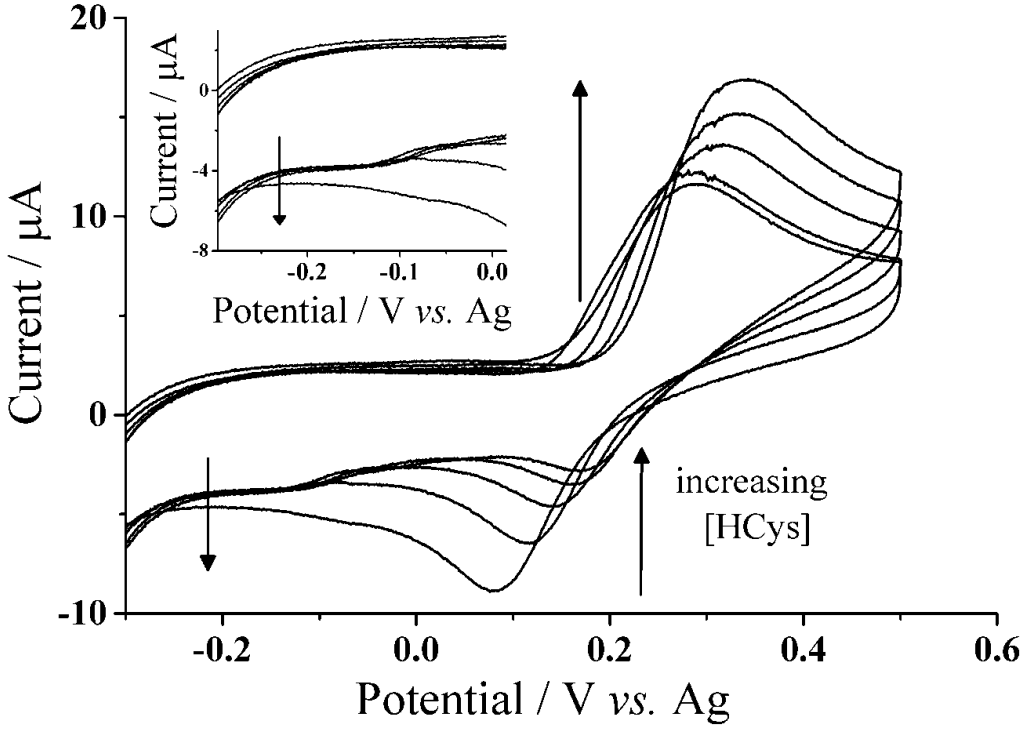

Figure 7.10: Cyclic voltammogram (300 mV s^{-1}) at CNT-SPE of 100 µM catechol (95 % synthetic saliva, pH 7.3) with varying concentrations of homocysteine (0 – 100 µM). *Inset:* Magnified view of adduct peak region.

The above shows that we can selectively evaluate the concentrations of both homocysteine and glutathione by applying a combination of high and low scan rates to

the synthetic saliva sample. The adopted procedure entails application of a high scan rate initially to obtain the homocysteine content using the empirical equation, $I_{pHCys\ 300\ mV\ s^{-1}}$ (nA) = (13.2 ± 0.42) [HCys/μM]. With the determined homocysteine concentration, the corresponding peak current at low scan rate can be calculated using, $I_{pHCys\ 50\ mV\ s^{-1}}$ (nA) = (2.8 ± 0.2) [HCys/μM]. This latter value can be subtracted from the total adduct peak current measured at low scan rate thus resulting in the peak current corresponding to the glutathione reaction with *ortho*-quinone. Finally, the glutathione content can be determined using the analytical curve $I_{pGSH\ 50\ mV\ s^{-1}}$ (nA) = (2.1 ± 0.2) [GSH/μM]. Next, the application of this method was entirely assessed in synthetic saliva solutions (pH 7.3) containing 100 μM catechol spiked with different concentrations of glutathione and homocysteine using CNT-SPEs. The spiked values in these solutions are within typical range observed in natural human saliva. [46, 76, 77, 79, 80] Table 7.9 shows the summary of the determined homocysteine and glutathione values of these spiked synthetic saliva samples using this method. The determined values correspond well to the spiked content and have reasonable error, *ca.* 18% and *ca.* 8% for homocysteine and glutathione respectively. The average error for homocysteine detection is relatively high due to the low peak current produced at the high scan rate, which leads to some difficulties quantifying at low concentrations. Nonetheless, the low concentrations tested are close to the calculated limit of detection of the system. It should be noted that the determination of glutathione is dependent on the homocysteine detection at the low scan rate. So, the analytical limit for glutathione detection should be considered accordingly with homocysteine at the same low scan rate, *ca.* (2.0 ± 0.1) μM. In addition, as this procedure has an approximate assay time *ca.* 5 minutes, which is much faster than the conventional analytical methodologies,

mentioned in Section 2.2, this illustrates the adaptability and versatility of this method on saliva using only screen-printed electrodes.

Spike content		Determined content [a]	
Homocysteine (μM)	Glutathione (μM)	[Homocysteine] (μM)	[Glutathione] (μM)
5	5	5.5 ± 1.8	4.9 ± 1.2
5	15	5.1 ± 0.9	17.2 ± 0.07
10	5	8.1 ± 0.3	4.3 ± 0.1
2	30	3.4 ± 0.5	34.5 ± 1.25
2	15	3.5 ± 0.5	17.7 ± 0.04
5	30	4.5 ± 0.3	29.1 ± 0.68

[a] Average value $\pm$ standard deviation. (n=3)

Table 7.9: Summary of determined homocysteine and glutathione content in spiked synthetic saliva, pH 7.3.

7.2.5 Conclusions

The selective determination of homocysteine and glutathione was successfully carried out in synthetic saliva using screen-printed electrodes, with limit of detections of *ca*. 0.9 μM and *ca.* 2.0 μM for homocysteine and glutathione respectively. Concentration ranges seen in natural human saliva of homocysteine and glutathione were successfully determined in synthetic saliva. Accordingly, this electroanalytical technique is shown to be well suited for biomarker sensing applications in 'real' saliva, as it demonstrates good versatility and easy utilization from a non-invasive sampling approach.

7.3 Electrochemical determination of free and total glutathione in authentic human saliva samples

7.3.1 Introduction

This section will now discuss the application progression of this two-step methodology on *real* human saliva samples. Until now, the focus had been on reduced thiol species detection. However, not only will the results be based on detection of the reduced thiol species but of both, the reduced and the oxidized species, as both are present in real saliva. As thiol-containing molecules are prevalent in many biological systems, they have their own role in maintaining metabolism throughout the cells. [32] Often, regular systematic function at the cellular level requires the biosynthesis of the thiol in order to limit the number of harmful free radicals in the cell. In particular, glutathione, in its reduced form (GSH), can oxidize to form a dissulfide (GSSG, Figure 7.11). Then, GSH can be regenerated by the combination of the glutathione reductase enzyme and nicotamide adenine dinucleotide phosphate (NADPH). [32] Therefore, this continuous conversion of glutathione is important in sustaining regular healthy function of the cell. However, glutathione not only acts as a reducing agent but a major antioxidant within the cells, it also acts as a mediator for many physiological reactions from cellular signaling to metabolism of xenobiotic. [50] Unsurprisingly, it is a key player in the pathophysiology of many diseases. [50] This can often be the effect of an imbalance in the GSH:GSSG ratio. Thus, suggesting that the GSH:GSSG chemical pair is an important indicator for cellular toxicity.

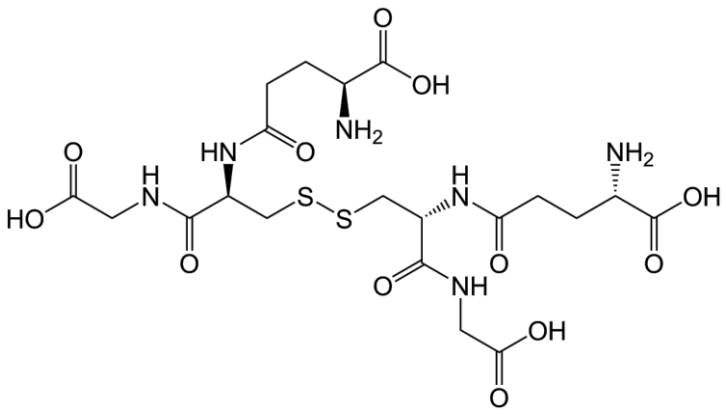

Figure 7.11: Chemical structure of oxidized glutathione.

There have been a number of growing interests among investigators linking the GSH:GSSG ratio to subject topics such as illnesses [33, 45, 47, 50, 58], metabolism [30-32, 52, 54, 58], and aging. [32, 41] Consequently, its quantitative analysis as individuals and/or as a ratio can be valuable to measure oxidative stress. [56] Recent publications show normal GSSG is maintained at concentrations lower than 5% of the total glutathione in humans. [265] However, oxidative stress can deplete GSH, thus increasing the GSSG by 50% or higher. [47, 53, 265] To determine these levels analytically, methodologies often incorporate reducing agents to break the disulfide bond in order to determine the total GSH. [47, 53, 58, 265] The GSSG content can thus be inferred from the difference between the free and total GSH. Some typical reducing agents used in the analytical detection of glutathione may include glutathione reductase, dithioerythritol, dithiothreitol, mercaptoethanol, phosphines or sodium borohydride. [58]

This section will present a simple method of determining free reduced and total GSH, which embraces the 1,4-Michael addition reaction with or without prior reduction treatment to the sample. To obtain a determination of the free reduced form, the

electro-analytical measurement is first performed on a sample containing catechol, which is then electro-oxidized to form *ortho*-quinone. Then to get the total GSH value, a chemical reduction pre-treatment is performed on the sample followed by a similar sample analysis in the presence of the mediator. The procedure will be first applied to a buffer solution to investigate the viability of the method in a control setting then followed by an application onto real human saliva. The free and total glutathione levels in human saliva samples are analysed as a proof-of-concept of this method; while the classical Ellman's test was done in parallel. [266] Moreover, commercially available electrochemical chips will be fully utilized again to demonstrate a point-of-care technology available for glutathione, GSH:total GSH, quantification. [233, 234]

7.3.2 Reagents and samples

For the reduction procedure, sodium borohydride ($NaBH_4$, technical grade, Fisher Scientific), and hydrochloric acid (37%, Fisher Scientific) were used as received without any further purification steps. Saliva samples were kindly donated by laboratory colleagues without any known pathological conditions.

The chemicals listed in the Sigma-Aldrich Glutathione Enzyme Assay Kit were purchased individually from Sigma-Aldrich (UK). They are comprised of ethylenediaminetetraacetic acid (EDTA, ≥ 98 %), glutathione reductase, reduced glutathione (98%), 5,5'-dithiobis(2-nitronezoic acid) (≥ 98 %, DTNB), 5-sulfosalicyclic acid dihydrate (≥ 99 %), β-nicotinamide adenine dinucleotide 2′-phosphate reduced tetrasodium salt hydrate (≥ 95 %, NADPH), and dimethyl sulfoxide (≥ 99.9 %, DMSO).

7.3.3 Commercially available Glutathione Enzyme Assay Kit

The Sigma-Aldrich Glutathione Assay Kit procedure was performed as described but with two slight modifications. First, the phosphate buffer solution was prepared in-house, described in Section 2.1. Second, a double beam single sample UV-vis spectrophotometer (Hitachi U-2001, Germany) was used instead of a UV-vis spectroscopy microplate reader.

The procedure from the Sigma-Aldrich Glutathione Assay Kit was carried out as follows: mix 750 µL of a working reacting solution with 100 µL of GSH standards (for the calibration curve) or 100 µL of the saliva samples; after 5 minutes of reaction, 50 µL of NADPH (0.16 mg mL^{-1}) were further added. The working reacting solution was comprised of 8 mL of PBS with 1 mmol L^{-1} EDTA and 228 µL of DTNB (1.5 mg L^{-1}). For total GSH, 20 µL of glutathione reductase (400 units mL^{-1}) were added to the working solution. Then, the solutions underwent spectrophotometric quantification, at 412 nm, of the product formed in the reaction between the DTNB and GSH. [121]

7.3.4 Carbon nanotube screen-printed electrode

The three electrode screen-printed chip, described in Section 3.3.3, was fully used in this section to show the capability of using a disposable unit for this method. These potentials were measured relative to the Ag pseudo-reference electrode on the chip. For each experiment carried out, a new electrode was used to prevent any cross contamination of the saliva samples. Different electrodes from the same batch were tested and show good reproducibility in the saliva, ≥ 90 %.

7.3.5 Results and discussion

In this section, an optimized procedure to reduce the GSSG is described. Then the determination of free and total GSH contents is carried out in solutions containing a mixture of the reduced and oxidized GSH. Lastly, the method to determine free and total GSH is applied to healthy human saliva samples.

7.3.5.1 Reduction of oxidized glutathione

The determination of total glutathione in many physiological fluids often requires the reduction of the disulfide bond. [42, 55, 58, 85, 117] The selection of the reducing agent strongly depends on the desired separation and/or the detection system one intends to use. For electro-analytical measurements, these common reducing agents may contain a redox active sulfhydryl-containing group and thus can interfere with the window of analysis or foul the electrode surface. [32, 58] Sodium borohydride ($NaBH_4$), in particular, is a strong reductant and has been selected for this study to reduce the oxidized glutathione due to its lack of electrochemical activity and inability to foul the electrode surface. [58] The reaction with $NaBH_4$ is quick in comparison to the other reducing agents [58] and slight effervescence was observed. An optimized procedure was developed to reduce the oxidized glutathione in phosphate buffer solution and is as follows: 2 wt% of $NaBH_4$ is added and dissolved in 3.0 mL of solution containing the dimer (PBS, pH 7.0). Then the solution is neutralized to *ca.* pH 7.0 with approximately 2.0 mL of 1.0 mol L^{-1} hydrochloric acid. Finally, a 1.0 mL aliquot of the solution was added to a vial containing 1.0 mL catechol (final catechol concentration is 100 μmol L^{-1}, PBS, pH 7.0).

To ensure that no interference arises from the $NaBH_4$ treatment alone, an experiment was carried out in PBS (0.15 mol L^{-1}, pH 7.0) only. Then, cyclic voltammetry (50 mV s^{-1}) was performed on the treated buffer in the absence and presence of catechol (100 µmol L^{-1}, pH 7.0). Figure 7.12 shows no observable redox signal from the $NaBH_4$ treated buffer alone, therefore establishing no interference from the reducing agent within the window of analysis. While in the presence of catechol, a redox couple $E_{1/2} = +0.2$ V (*vs.* Ag) is observed; corresponding to the reported two electron, two proton oxidation of the *ortho*-quinone species. [132, 133, 238] This redox couple is consistent with literature and therefore shows that the disulfide reduction method using $NaBH_4$ will not interfere with the redox process of the *ortho*-quinone. [37]

The reduction procedure, described above, was next applied to a buffer solution containing 25 µmol L^{-1} GSSG (PBS, pH 7.0) to form GSH. Figure 7.13 shows the cyclic voltammogram at a scan rate of 50 mV s^{-1} of the *ortho*-quinone at the CNT-SPE with and without the $NaBH_4$ treatment to the GSSG solution. This figure shows neither a change in the forward and backward peaks nor appearance of the adduct peak when the non-treated GSSG solution was tested. While with the $NaBH_4$ treated solution, an adduct peak *ca.* −0.1 V (*vs.* Ag) emerges suggesting the GSSG was reduced to GSH via $NaBH_4$ and therefore available to react with the *ortho*-quinone. This signifies that the reduction of the dimer was successful and it is possible to detect total GSH as well as free GSH using this method.

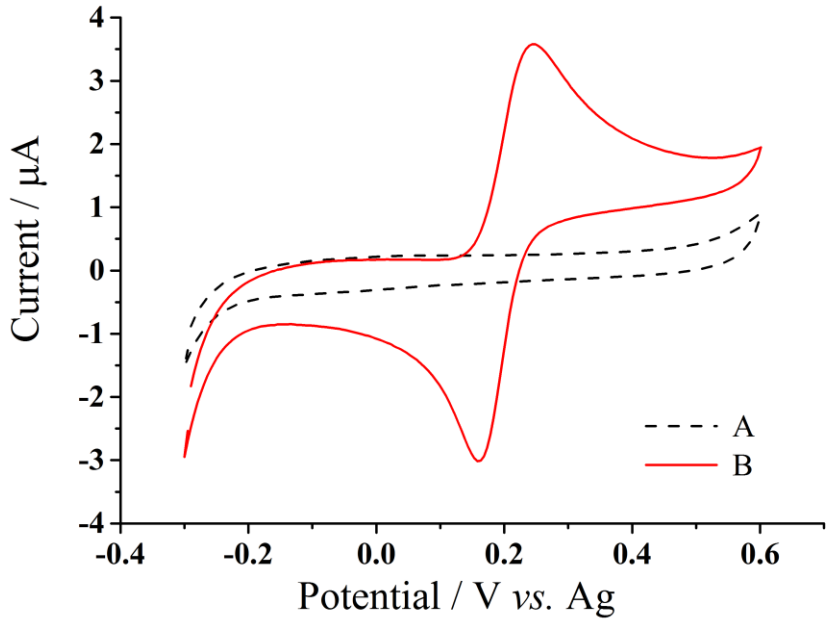

Figure 7.12: Cyclic voltammetry (50 mV s^{-1}) at CNT-SPE of PBS (pH 7.0) with $NaBH_4$ treatment with the A. absence and B. presence of 0.1 mol L^{-1} catechol.

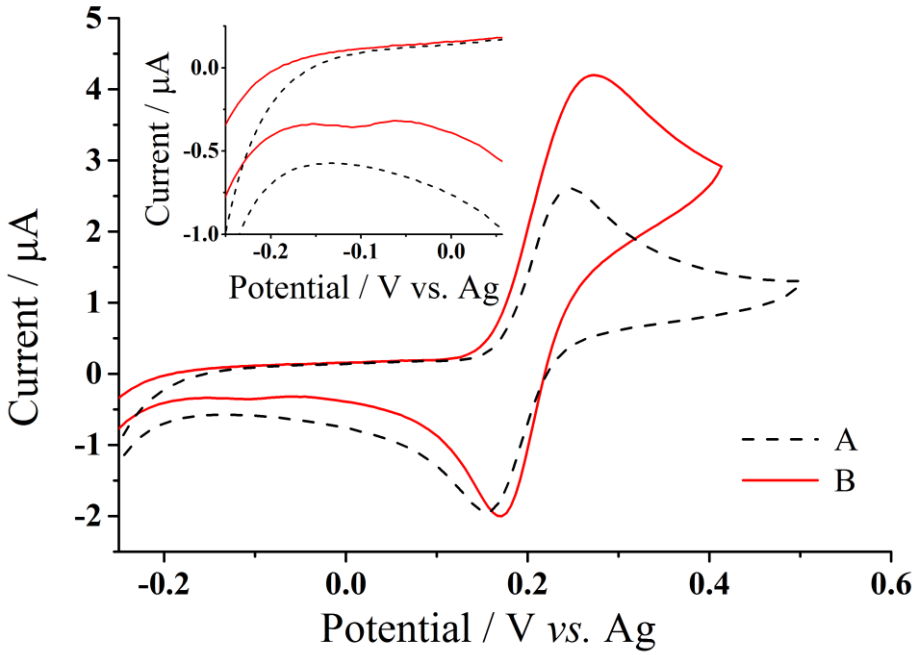

Figure 7.13: Cyclic voltammetry (50 mV s^{-1}) at CNT-SPE of 0.1 mol L^{-1} catechol and 25 µmol L^{-1} GSSG A. without and B. with $NaBH_4$ treatment. *Inset.* Magnified view of adduct peak.

7.3.5.2 Determination of free and total glutathione

Based on the results of the GSH detection from GSSG, analytical parameters were next determined. Cyclic voltammetry (50 mV s^{-1}) was again utilized to show the voltammetric behaviour of 100 µmol L^{-1} catechol (PBS, pH 7.0) at different concentrations, from 10 to 100 µmol L^{-1}, of reduced glutathione from its dimer. Figure 7.14 shows that with each increasing concentration, the forward (*ca.* +0.4 V *vs.* Ag) and the adduct peaks (*ca.* −0.04 V *vs.* Ag) increase as the backward peak decreases thus indicating the nucleophilic attack on the *ortho*-quinone by the thiol group. Also shown in Figure 7.14, a linear relationship was determined for the GSH formed from GSSG, $I_{pGSH\ from\ GSSG}$ (nA) = (0.64 ± 0.008) [GSH/µmol L^{-1}] (n = 3) for concentrations up to 60 µmol L^{-1}. The limit of detection was determined to be *ca.* (3.0 ± 0.07) µmol L^{-1} using $3S_B/S$, where S_B is the standard deviation and S is the sensitivity of the system. [130] The sensitivity of the GSH formed from GSSG is a lower in comparison to the sensitivity of the direct detection of the reduced form, reported in previous literature. [133] This is most likely due to the change in the environment provoked by the reducing steps in the methodology, i.e. the addition of the reducing agent and posterior neutralization. Nonetheless, it is still possible to detect GSH formed from its dimer as well as the free GSH.

To test whether it is possible to detect the free and total GSH, a number of solutions spiked with different percentages of the GSH and GSSG were made accordingly to reported values typically seen in physiological fluids, Table 7.10. To determine the free GSH content first, 100 µL of catechol (100 µmol L^{-1}, PBS, pH 7.0) was added to a 100 µL aliquot of the mixed solution and then tested using cyclic voltammetry. From the adduct peak current obtained from the voltammogram, the free GSH content was determined using the calibration curve obtained for this buffer system, reported in

[133]. Subsequently, the mixed solution sample underwent the $NaBH_4$ reduction procedure (as described above) to determine the total GSH content. An aliquot (100 µL) of the reduced sample was added to 100 µL of catechol (100 µmol L^{-1}, PBS, pH 7.0). The total GSH content can then be determined using the analytical parameters determined earlier, $I_{pGSH\ from\ GSSG}$ (nA) = (0.64 ± 0.008) [GSH/µmol L^{-1}]. Figure 7.15 shows a summary of the determined values in comparison to their expected values of several spiked solutions. The figure shows that with this proposed method, the determined free and total GSH matches well to the expected values with the average relative standard errors of *ca.* 0.9% for free GSH and *ca.* 2% for the total GSH. Therefore, it is possible to determine different percentages of the free and total GSH in solutions containing both reduced and oxidized glutathione using the presented method of detection.

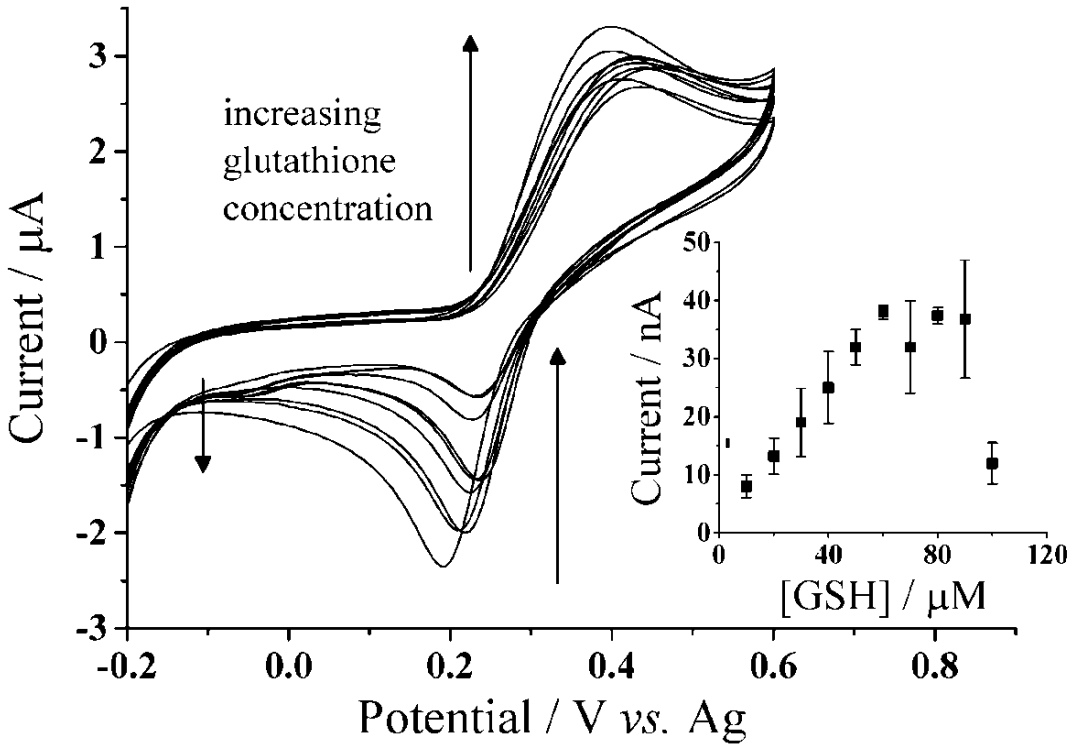

Figure 7.14: Cyclic voltammetry (50 mV s^{-1}) at CNT-SPE of 0.1 mol L^{-1} catechol with different concentrations of GSH from GSSG after $NaBH_4$ treatment.

Physiological fluid(s)	Free [GSH] (µmol L^{-1})	Total [GSH] (µmol L^{-1})	Reference(s)
Human plasma	2.2 - 12	0.91 – 20	[42, 58]
Whole human blood	400 - 800	343 – 1100	[41, 58]
Saliva	2 - 15	7 - 30	[46, 53, 79]

Table 7.10: Literature values of free and total glutathione in various physiological fluids.

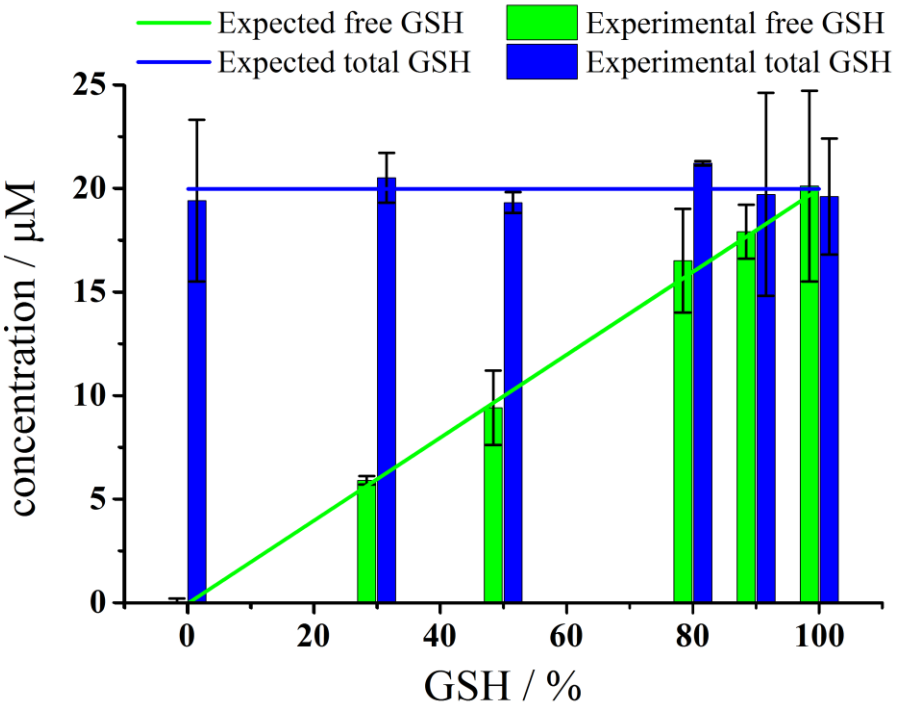

Figure 7.15: Plot comparing the expected and experimental values of free and total GSH at several solutions.

7.3.5.3 Determination of free and total glutathione in human saliva

Application of this method to determine free and total glutathione was next applied to saliva samples from human subjects without any known pathological condition. Cyclic voltammetry (50 mV s^{-1}) was first carried out on the saliva sample

before and after the $NaBH_4$ treatment to determine whether saliva itself has any inherent redox active species. Figure 7.16a and Figure 7.16b show the voltammograms of *pure* saliva at the CNT-SPE with and without the $NaBH_4$ treatment, respectively. The figure shows a redox process at *ca.* +0.3 V (*vs.* Ag) is observed revealing an electroactive species in the human saliva, possibly uric acid. [45, 263, 267-270] To overcome this interference, catechol was added to the saliva sample where the forward and backward peaks currents of the *ortho*-quinone (at *ca.* $E_{1/2}$ = +0.2 V *vs.* Ag) both become observable (Figure 7.16c and Figure 7.16d). It was determined that 300 and 800 µmol L^{-1} of catechol were enough to determine the free and total GSH, respectively, in the saliva samples. However, cyclic voltammetry was not sensitive enough to see the adduct peak so, square wave voltammetry was utilized for higher sensitivity so as to quantify GSH in saliva.

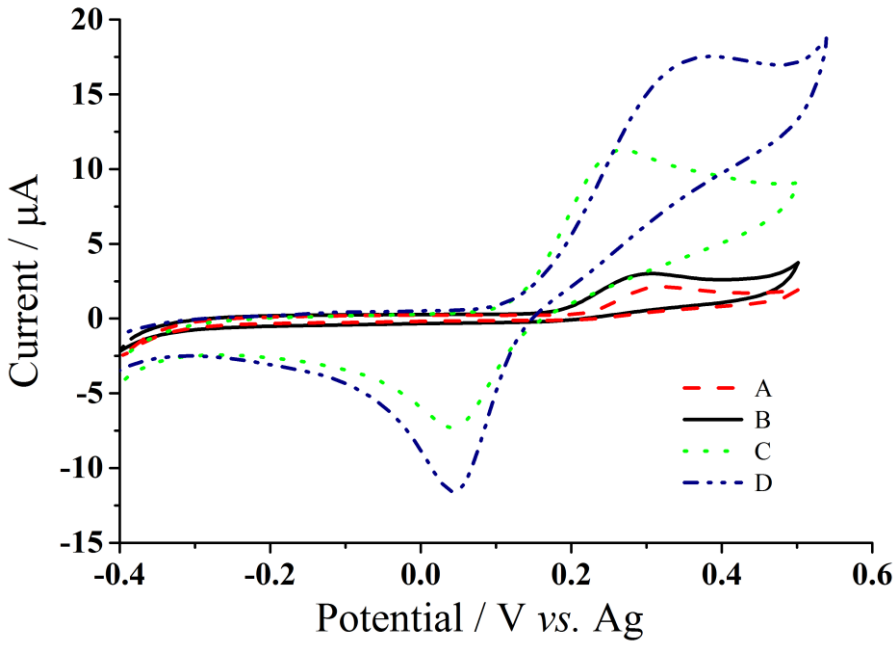

Figure 7.16: Cyclic voltammetry (50 mV s^{-1}) at CNT-SPE of apparently healthy human saliva sample A. untreated, B. $NaBH_4$ treated, C. untreated with 300 µmol L^{-1} catechol, and D. $NaBH_4$ treated with 800 µmol L^{-1} catechol.

First, square wave voltammetry was carried out on the saliva sample containing 300 µmol L^{-1} catechol to determine whether the adduct peak is visible (see experimental section for parameters). Figure 7.17a shows two peaks; one at *ca.* +0.10 V (*vs.* Ag) and the second at *ca.* −0.13 V (*vs.* Ag). To differentiate the peaks, the saliva sample was spiked with 15 µmol L^{-1} GSH. In comparison to the non-GSH spiked saliva sample, the peak *ca.* +0.10 V (*vs.* Ag) decreases while the peak at *ca.* −0.13 V (*vs.* Ag) increases with the added GSH. Therefore, the peak at *ca.* +0.10 V (*vs.* Ag) is likely to correspond to the reductive wave of the *ortho*-quinone species while the second peak at *ca.* –0.13 V (vs. Ag) relates to the GSH adduct peak. This is consistent with the 1,4-Michael addition reaction mentioned above.

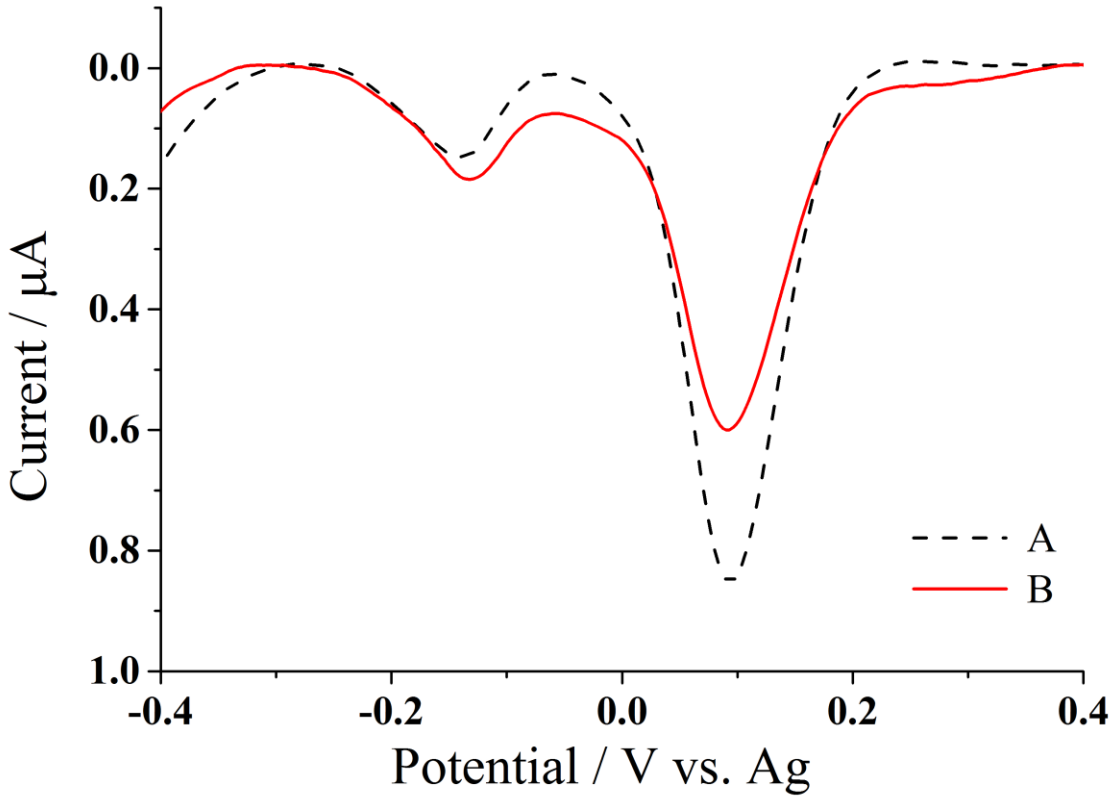

Figure 7.17: Square wave voltammetry of A. healthy human saliva with 300 µmol L^{-1} catechol at CNT-SPE and B. saliva sample spiked with 15 µmol L^{-1} GSH.

Next, standard additions of GSH, up to 20 μmol L^{-1}, were carried out before and after $NaBH_4$ treatment (as described above) to determine the respective free and total GSH contents in several saliva samples. The reduction procedure was adjusted to accommodate for the small saliva samples available. To compare the results determined via this method are reasonable, a commercially available glutathione enzyme assay test was run in parallel on the same saliva samples. The results are summarized in Table 7.11; which shows they are in good agreement with each other. It should be noted that variability within the results *can* be due to the rapid oxidation of the free GSH prior to testing or sample condition after collection. Nonetheless, both tests were carried out in parallel and testing procedures were conducted accordingly. The average error for % GSH of the presented method is *ca.* 8.6 % while the enzyme assay had *ca.* 10%. This suggests that the results determined by the presented method on *real* human saliva are comparable to the commercially available assay test for glutathione.

	Proposed Methodology [a]			**Enzyme Assay Test [a]**		
	Free GSH(μM)	**Total GSH (μM)**	**% GSH**	**Free GSH (μM)**	**Total GSH (μM)**	**% GSH**
Saliva sample-1	9.6 ± 0.9	9.0 ± 1.4	**106 ± 10**	9.2 ± 1.7	11.4 ± 2.7	**81 ± 24**
Saliva sample-2	3.3 ± 1.3	11.1 ± 2.7	**30 ± 13**	2.3 ± 0.4	11.4 ± 1.4	**20 ± 4**
Saliva sample-3	1.0 ± 0.2	15.4 ± 2.9	**6 ± 2**	1.5 ± 0.3	14.9 ± 1.4	**10 ± 2**

[a] average ± standard deviation (n =3).

Table 7.11: Summary of the free and total glutathione in saliva samples from several apparently healthy human subjects.

7.3.6 Conclusions

This section concludes the work on thiol quantification using catechol at a disposable electrochemical chip. The work herein, describes a simple, fast and easy method for determining not only the free reduced glutathione content but also the total glutathione content in *real* human saliva. The application on *real* human saliva shows that the glutathione values and error are analogous to the commercially available enzyme assay test. Hence for that reason, this demonstrates a suitable alternative for clinicians and/or researchers.

Overall summary

The state-of-the-art methodologies discussed herein were developed for the selective electrochemical analysis of cysteine, glutathione, and homocysteine in the presence of each other in buffer solution then successfully realized in complex media and 'real' world samples. The analytical methods are tabulated in Table OS1 and OS2.

Cysteine detection

For selective cysteine detection, the approaches include techniques such as cyclic voltammetry and square wave voltammetry measured at an activated precursor modified electrode, CTC-GCE, and a modified nanocarbon composite electrode, CAT-NC-GCE. The basis for cysteine detection at the activated precursor electrode, CTC-GCE, is via electrocatalytic reaction. In order to obtain selective detection, a higher voltage scan rate was applied to the electrode to exclude the *ortho*-quinone reaction with other thiol containing molecules, such as homocysteine and glutathione. Then the peak currents of the forward and backward peaks are measured to give a ratio corresponding to the quantity of cysteine present. The sensitivity for this method at the CTC-GCE is (0.023 ± 0.001) μM μA^{-1} with a determined limit of detection *ca.* (0.6 ± 0.02) μM in a buffered system. This system was also tested in complex media, cell tissue culture media, where the sensitivity was determined to be (0.031 ± 0.001) μM μA^{-1} and a limit of detection of (0.9 ± 0.02) μM. This system exhibits a potential and novel way to selectively detect cysteine using the supramolecule *ortho*-quinone derivative, CTC. However, the analytical parameters may differ with different complex solutions.

The next presented case for cysteine determination is at the CAT-NC-GCE via 1,4-Michael addition reaction. For this electrode, a simultaneous and selective detection of both cysteine and homocysteine is possible, in the presence of each other, glutathione, and ascorbic acid, as two different adduct peaks emerge at potentials away from each other and the parent *ortho*-quinone peak. The quantitative evaluation of cysteine using square wave voltammetry at the CAT-NC-GCE had a sensitivity of (7.501 $\pm$ 0.202) mA μM^{-1} and a determined limit of detection of *ca.* (5.0 $\pm$ 0.04) µM. However, due to the porous nature of the nanocarbon, it may adsorb unwanted analytes contained in the complex solution. Nonetheless, the thiol determination at this electrode exemplifies the possibility of having a simultaneous quantitative detection of two thiols molecules, cysteine and homocysteine.

Homocysteine detection

In addition to selective homocysteine determination at the CAT-NC-GCE, homocysteine can also be selectively determined at the CNT-GCE in the presence catechol via 1,4-Michael addition reaction in solutions containing other analytes, such as glutathione, cysteine, and ascorbic acid. Similarly to the method at the CAT-NC-GCE, the methodology at the CNT-GCE in the presence of catechol requires an application of a high scan rate during the cyclic voltammetry in order to 'outrun' the *ortho*-quinone reaction with glutathione as the corresponding adduct peak potentials are close to each other. The homocysteine sensitivity for this system at the CNT-GCE, is (20.1 $\pm$ 0.076) nA μM^{-1} with a limit of detection determined to be *ca.* (0.11 $\pm$ 0.20) µM; whereas the homocysteine sensitivity at the CAT-NC-GCE is (0.882 $\pm$ 0.296) nA nM^{-1} with a limit of detection of *ca.* (11.0 $\pm$ 0.090) nM. The best approach for exclusive detection of

homocysteine is with catechol via 1,4-Michael addition reaction at the CNT-GCE. The carbon nanotube layers provide a more porous surface to facilitate in the enhanced voltammetry and when compared to the nanocarbon material, the CNTs are less likely to adsorb unwanted interfering analytes present in the solution. Therefore, the methodology at the CNT-GCE with catechol was carried out in such biological samples such as cell tissue culture media, human plasma, and synthetic saliva where the sensitivity is (2.96 $\pm$ 0.021) nA μM^{-1}, (93.7 $\pm$ 11.4) nA μM^{-1}, and (13.2 $\pm$ 0.42) nA μM^{-1} respectively and the limit of detection was determined to be (2.0 $\pm$ 0.02) µM, (0.8 $\pm$ 0.4) µM, and (0.9$\pm$0.01) µM respectively. It is to be taken note that for the CNT-GCE, the exact amount of catechol mediator best suited for each complex solution *may* differ, thus the analytical parameters may change with the quantity of the mediator.

Glutathione detection

Finally, the best approach for selective glutathione detection is cyclic voltammetry carried out at the CNT-GCE with catechol via 1,4-Michael addition reaction in the presence of homocysteine, cysteine, and ascorbic acid. This reaction results in an analytically useful adduct peak; such that the potential is far from the parent *ortho*-quinone peak. A single two-step procedure was developed to suitably quantify homocysteine and glutathione selectively in the presence of each other, cysteine, and ascorbic acid by using a combination of high and low scan rates. The analytical parameters were determined for glutathione using cyclic voltammetry, where the sensitivity is (3.50 $\pm$ 0.066) nA μM^{-1} and a determined limit of detection of *ca.* (0.11 $\pm$ 0.20) µM. This method was then realized in biological samples such as cell tissue culture media, human plasma, and synthetic saliva; where the sensitivities are (1.02 $\pm$ 0.462)

nA μM^{-1}, (39.1 $\pm$ 2.22) nA μM^{-1}, and (2.1 $\pm$ 0.2) nA μM^{-1} respectively and the limit of detection determined to be (1.0 $\pm$ 0.3) µM, (0.8 $\pm$ 0.4) µM, and (3.0$\pm$0.3) µM respectively. Similar to homocysteine detection at the CNT-GCE with catechol, the analytical parameters will change accordingly to the amount of catechol utilized.

Electrode	Reaction mechanism	Electrochemical method	Targeted thiol compound	Tested in the presence of	Voltage scan rate (mVs^{-1})	Sensitivity	Limit of detection [a]	Linear range
CTC-GCE	EC	CV	Cys	GSH, HCys	3000	(0.023 ± 0.001) $\mu A\ \mu M^{-1}$	(0.6 ± 0.02) µM	0-40µM
CAT-NC-GCE	MA	SWV	Cys	HCys, GSH, AA	–	(7.501 ± 0.202) $mA\ \mu M^{-1}$	(5.0 ± 0.04) µM	0-100mM
			HCys	Cys, GSH, AA	–	(0.882 ± 0.296) $nA\ nM^{-1}$	(11.0 ± 0.09) nM	0-100mM
CNT-GCE with catechol [b]	MA	CV	GSH	Cys, AA	50	(3.50 ± 0.066) $nA\ \mu M^{-1}$	(0.11 ± 0.20) µM	0-10µM
			HCys	Cys, AA	500	(20.1 ± 0.076) $nA\ \mu M^{-1}$	(0.11 ± 0.20) µM	0-10µM

[a] calculated limit of detection. [b] requires single two-step method. EC, electrocatalytic oxidation reaction; MA, 1,4-Michael addition reaction; CV, cyclic voltammetry; SWV, square wave voltammetry; Cys, cysteine; GSH, glutathione; HCys, homocysteine; AA, Ascorbic acid; CTC-GCE, cyclotricatechylene modified glassy carbon electrode; CAT-NC-GCE, catechol modified nanocarbon glassy carbon electrode; CNT-GCE, carbon nanotube modified glassy carbon electrode.

Table OS1. Tabulated summary of analytical parameters presented in this thesis for selective homocysteine, glutathione, and/or cysteine detection in buffered systems.

		Cysteine			*Homocysteine*			*Glutathione*		
Electrode	**Biological sample**	**Sensitivity**	**Limit of detection [a]**	**Linear range**	**Sensitivity**	**Limit of detection [a]**	**Linear range**	**Sensitivity**	**Limit of detection [a]**	**Linear range**
CTC-GCE	Cell tissue media	(0.031 ± 0.001) $\mu M\ \mu A^{-1}$	(0.9 ± 0.02) μM	0-40 µM	–	–	–	–	–	–
CNT-GCE with catechol [b]	Cell tissue media	–	–	–	(2.96 ± 0.021) $nA\ \mu M^{-1}$	(2.0 ± 0.02) μM	0-20 µM	(1.02 ± 0.462) $nA\ \mu M^{-1}$	(1.0 ± 0.3) μM	0-10 µM
	Human plasma	–	–	–	(93.7 ± 11.4) $nA\ \mu M^{-1}$	(0.8 ± 0.4) μM	0-15 µM	(39.1 ± 2.22) $nA\ \mu M^{-1}$	(0.8 ± 0.4) μM	0-15 µM
	Saliva	–	–	–	(13.2 ± 0.42) $nA\ \mu M^{-1}$	(0.9 ± 0.01) μM	0-20 µM	(2.1 ± 0.2) $nA\ \mu M^{-1}$	(3.0 ± 0.3) μM	0-20 µM

[a] calculated limit of detection. CTC-GCE, cyclotricatechylene modified glassy carbon electrode; CNT-GCE, carbon nanotube modified glassy carbon electrode.

Table OS2. Tabulated summary of analytical parameters presented in this thesis for selective homocysteine, glutathione, and/or cysteine detection in 'real' world samples.

Overall conclusions

This thesis has addressed several electrochemical methods of detecting thiol-containing molecules using different derivatives of the *ortho*-quinone/ hydroquinone species. These methods exploit either the electrocatalytic or 1,4-Michael addition reaction of the *ortho*-quinone moiety with the thiol-containing molecule at different forms of carbon electrodes. Studies described herein show that for either *ortho*-quinone reactions with thiol-containing molecules, selectivity and sensitivity is feasible with a combination of a nanomaterial modified carbon electrode and an electrochemical method utilizing variable voltage scan rates.

Whilst thiol detection is viable via electrocatalytic reaction, both selective and sensitive quantification of multiple thiols is better achieved via 1,4-Michael addition reaction as the appearance of the new 'adduct' peak is analytically useful. The assessment of the state-of-the-art concept was carefully executed in buffer, then realized in synthetic and real world samples. These results were shown to be analogous to the commercially available enzyme test. Commercially available electrochemical chips were employed to emphasize the ultimate aim of developing a fast, easy, facile, and cheap sensor for selective thiol detection with little to no sample preparation. Thus, the reasons and results discussed in this thesis emphasize the potential of this method for the biomedical and clinical community as an alternative and simple analytical approach.

Bibliography

[1] A.J. Bard, L.R. Faulkner, Electrochemical Methods: Fundamentals and Applications, 2nd ed.: Wiley; 2001.

[2] R.G. Compton, C.E. Banks, Understanding Voltammetry, 2nd ed.: Imperial College Press; 2007.

[3] J.A.V. Butler, Studies in heterogeneous equilibria: Part II - The kinetic interpretation of the Nernst theory of electromotive force, Trans. Faraday Soc., 19 (1923) 729-733.

[4] R. Guidelli, R.G. Compton, J.M. Feliu, E. Gileadi, J. Lipkowski, W. Schmickler, S. Trasatti, Defining the transfer coefficient in electrochemistry: An assessment (IUPAC Technical report), Pure Appl. Chem., 86 (2014) 245-258.

[5] R. Guidelli, R.G. Compton, J.M. Feliu, E. Gileadi, J. Lipkowski, W. Schmickler, S. Trasatti, Definition of the transfer coefficient in electrochemistry (IUPAC Recommendations 2014), Pure Appl. Chem., 86 (2014) 259-262.

[6] J.I. Crabtree, The nature of overvoltage, Trans. Faraday Soc., 9 (1913) 125-131.

[7] R. Guidelli, Thermodynamic consideration on the various contribution to overpotential. Part 2 Trans. Faraday Soc., 66 (1969) 1194-1202.

[8] A.C. Cummings, The elimination of potential due to liquid contact: Part II. A simple equation for the calculation of diffusion potential, Trans. Faraday Soc., 8 (1912) 86-93.

[9] J.A.V. Butler, Studies in heterogeneous equilibria. Part III. A kinetic theory of reversible oxidation potentials at inert electrodes, Trans. Faraday Soc., 19 (1924) 734-739.

[10] T. Erdey-Gruz, M. Volmer, The theory of hydrogen high tension, Z. Physik. Chem., 150 (1930) 203-213.

[11] M.C. Henstridge, E. Laborda, N.V. Rees, R.G. Compton, Marcus–Hush–Chidsey theory of electron transfer applied to voltammetry: A review, Electrochim. Acta, 84 (2012) 12-20.

[12] R.A. Marcus, On the Theory of Oxidation-Reduction Reactions Involving Electron Transfer. I, J Chem. Phys., 24 (1956) 966.

[13] R.A. Marcus, N. Sutin, Electron transfers in chemistry and biology, Biochim. Biophys. Acts, 811 (1985) 265-322.

[14] N.S. Hush, Adiabatic Rate Processes at Electrodes. I. Energy-Charge Relationships, J Chem. Phys., 28 (1958) 962.

[15] N.S. Hush, Electron transfer in retrospect and prospect 1: Adiabatic electrode processes, J. Electroanal. Chem., 470 (1999) 170-195.

[16] C.W. Tobias, M. Eisenberg, C.R. Wilke, Diffusion and convection in electrolysis-a theoretical review, J. Electrochem. Soc., 99 (1958) 359C-365C.

[17] A. Fick, Über diffusion, Poggendorff's Annel. Physik, 94 (1855) 59-86.

[18] D.R. Gabe, F.C. Walsh, The rotating cylinder electrode: A review of development, J. Appl. Electrochem., 13 (1983) 3-21.

[19] R.G. Compton, J.C. Eklund, F. Marken, Sonoelectrochemical processes: A review, Electroanal., 9 (1997) 509-522.

[20] H. Helmholtz, Ueber einige Gesetze der Vertheilung elektrischer Ströme in körperlichen Leitern mit Anwendung auf die thierisch-elektrischen Versuche, Ann. Phys., 165 (1853) 211-233.

[21] H. Helmholtz, Studien über electrische Grenzschichten, Ann. Phys., 243 (1879) 337-382.

[22] D.J.G. Ives, G.J. Janz, Reference Electrodes, New York: Academic; 1961.

[23] R.H. Gerke, A Summary of Electrode Potentials, Chem. Rev., 1 (1925) 377-395.

[24] J.E.B. Randles, A cathode ray polargraph. Part II. The current-voltage curves, Trans. Faraday Soc., 44 (1948) 327-338.

[25] K.B. Oldham, Analytical expressions for the reversible Randles-Sevcik function, J. Electroanal. Chem., 105 (1979) 373-375.

[26] A. Ševčík, Oscillographic polargraphy with periodical triangular voltage, Collect. Czech. Chem. Commun., 13 (1948) 349-377.

[27] M.C. Henstridge, E.J.F. Dickinson, M. Aslanoglu, C. Batchelor-McAuley, R.G. Compton, Voltammetric selectivity conferred by the modification of electrodes using conductive porous layers or films: The oxidation of dopamine on glassy carbon electrodes modified with multiwalled carbon nanotubes, Sensors Actuat. B-Chem., 145 (2010) 417-427.

[28] M.C. Henstridge, E.J.F. Dickinson, R.G. Compton, Mass transport to and within porous electrodes. Linear sweep voltammetry and the effects of pore size: The prediction of double peaks for a single electrode process, Russ. J. Electrochem., 48 (2012) 629-635.

[29] L.M. Gonçalves, C. Batchelor-McAuley, A. A.A. Barros, R.G. Compton, Electrochemical Oxidation of Adenine: A Mixed Adsorption and Diffusion Response on an Edge-Plane Pyrolytic Graphite Electrode, J. Phys. Chem. C, 114 (2010) 14213-14219.

[30] M.L. Circu, T.Y. Aw, Glutathione and apoptosis, Free Radical Res., 42 (2008) 689-706.

[31] S.M. Deneke, B.L. Fanburg, Regulation of cellular glutathione, Am. J. Physiol., 257 (1989) L163-L173.

[32] A. Meister, M.E. Anderson, Glutathione, Annu. Rev. Biochem., 52 (1983) 711-760.

[33] M. Reid, F. Jahoor, Glutathione in disease, Curr. Opin. Clin. Nutr., 4 (2001) 65-71.

[34] H. Sies, Glutathione and its role in cellular functions, Free Radical Bio. Med., 27 (1999) 916-921.

[35] Y.M. Go, D.P. Jones, Cysteine/cystine redox signaling in cardiovascular disease, Free Radical Bio. Med., 50 (2011) 495-509.

[36] G. Hignett, S. Threlfell, A.J. Wain, N.S. Lawrence, S.J. Wilkins, J. Davis, R.G. Compton, M.F. Cardosi, Electroanalytical exploitation of quinone-thiol interactions: application to the selective determination of cysteine, Analyst, 126 (2001) 353-357.

[37] E.H. Seymour, S.J. Wilkins, N.S. Lawrence, R.G. Compton, Electrochemical detection of glutathione: an electrochemically initiated reaction pathway, Anal. Lett., 35 (2002) 1387-1399.

[38] N.S. Lawrence, J. Davis, R.G. Compton, Electrochemical detection of thiols in biological media, Talanta, 53 (2001) 1089-1094.

[39] I. Katakis, E. Dominguez, Catalytic electrooxidation of NADH for dehydrogenase amperometric biosensors, Mikrochim. Acta, 126 (1997) 11-32.

[40] A.S. Kumar, P. Swetha, Simple adsorption of anthraquinone on carbon nanotube modified electrode and its efficient electrochemical behaviors, Colloids Surface A, 384 (2011) 597-604.

[41] F. Michelet, R. Gueguen, P. Leroy, M. Wellman, A. Nicolas, G. Siest, Blood and plasma glutathione measured in healthy subjects by HPLC: relation to sex, aging, biological variables and life habits, Gen. Clin. Chem., 41 (1995) 1509-1517.

[42] A. Pastore, R. Massoud, C. Motti, A.L. Russo, G. Fucci, C. Cortese, G. Federici, Fully automated assay for total homocysteine, cysteine, cysteinylglycine, glutathione, cysteamine, and 2-mercaptopropionylglycine in plasma and urine, Clin. Chem., 44 (1998) 825-832.

[43] M.A. Mansoor, A.M. Svardal, P.M. Ueland, Determination of the in vivo redox status of cysteine, cysteinylglycine, homocysteine, and glutathione human plasma, Anal. Biochem., 200 (1992) 218-229.

[44] I.D. Mandel, The diagnostic uses of saliva, J. Oral Pathol. Med., 19 (1990) 119-125.

[45] G. Almadori, F. Bussu, J. Galli, A. Limongelli, S. Persichilli, B. Zappacosta, A. Minucci, G. Paludetti, B. Giardina, Salivary glutathione and uric acid levels in patients with head and neck squamous cell carcinoma, Head Neck, 29 (2007) 648-654.

[46] E. Bald, R. Glowacki, Analysis of saliva for glutathione and metabolically related thiols by liquid chromatography with ultraviolet detection, Amino Acids, 28 (2005) 431-433.

[47] L. Cao, D. Waldon, Y. Teffera, J. Roberts, M. Wells, M. Langley, Z. Zhao, Ratios of biliary glutathione disulfide (GSSG) to glutathione (GSH): a potential index to screen drug-induced hepatic oxidative stress in rats and mice, Anal. Bioanal. Chem., 405 (2013) 2635-2642.

[48] F.D. Carvalho, F. Remião, P. Valet, J.A. Timbrell, M.L. Bastos, M.A. Ferreira, Glutathione and cysteine measurement in biological samples by HPLC with a glassy carbon working detector, Biomed. Chromatogr., 8 (2005) 134-136.

[49] J. Chen, Z. He, H. Liu, C. Cha, Electrochemical determination of reduced glutathione (GSH) by applying the powder microelectrode technique, J. Electroanal. Chem., 588 (2006) 324-330.

[50] R. Franco, O.J. Schoneveld, A. Pappa, M.I. Panayiotidis, The central role of glutathione in the pathophysiology of human diseases, Arch. Physiol. Biochem., 113 (2007) 234-258.

[51] F. Gu, V. Chauhan, A. Chauhan, Glutathione redox imbalance in brain disorders, Curr. Opin. Clin. Nutr., 18 (2015) 89-95.

[52] J.C. Harfield, C. Batchelor-McAuley, R.G. Compton, Electrochemical determination of glutathione: a review, Analyst, 137 (2012) 2285-2296.

[53] Y. Iwasaki, M. Hoshi, R. Ito, K. Saito, H. Nakazawa, Analysis of glutathione and glutathione disulfide in human saliva using hydrophilic interaction chromatography with mass spectrometry, J. Chromatogr. B, 839 (2006) 74-79.

[54] D.P. Jones, J.L. Carlson, J. V. C. Mody, J. Cai, M.J. Lynn, J. P. Sternberg, Redox state of glutathione in human plasma, Free Radical Bio. Med., 28 (2000) 625-635.

[55] W.A. Kleinman, J.P. Richie, Status of glutathione and other thiols and disulfides in human plasma, Biochem. Pharmacol., 60 (2000) 19-29.

[56] M. Meloni, J.F. Nicolay, Dynamic monitoring of glutathione redox status in UV-B irradiated reconstituted epidermis: effect of antioxidant activity on skin homeostasis, Toxicol. In Vitro, 17 (2003) 609-613.

[57] E.J. Pacsial-Ong, R.L.McCarley, E. Wang, R.M. Strongin, Electrochemical detection of glutathione using redox indicators, Anal. Chem., 78 (2006) 7577-7581.

[58] A. Pastore, G. Federicia, E. Bertinib, F. Piemonte, Analysis of glutathione: implication in redox and detoxification, Clin. Chim. Acta, 333 (2003) 19-39.

[59] W.A. Kleinman, J.P. Richie, Status of gutathione and other thiols and disulfides in human plasma, Biochem. Pharm., 60 (2000) 19-29.

[60] B. Zappacosta, A. Manni, S. Persichilli, S. Scribano, A. Minucci, D. Lazzaro, P.D. Sole, B. Giardina, HPLC analysis of some sulphur compounds in saliva: comparison between healthy subjects and periodontopathic patients, Clinica Chimica Acta, 338 (2003) 57-60.

[61] H. Refsum, P.D. Ueland, P. Nygård, S.E. Vollset, Homocysteine and cardiovascular disease, Annu. Rev. Med., 49 (1998) 31-62.

[62] W. Leesutthiphonchai, W. Dungchai, W. Siangproh, N. Ngamrojnavanich, O. Chailapakul, Selective determination of homocysteine levels in human plasma using a silver nanoparticle-based colorimetric assay, Talanta, 85 (2011) 870-876.

[63] B. Hultberg, A. Andersson, A. Isaksson, The cell-damaging effects of low amounts of homocysteine and copper ions in human cell line cultures are caused by oxidative stress, Toxicology, 123 (1997) 33-40.

[64] T. Toyo'oka, recent advances in separation and detection methods for thiol compounds in biological samples, J. Chromatogr. A, 877 (2009) 3318-3330.

[65] P.C. White, N.S. Lawrence, J. Davis, R.G. Compton, Electrodetermination of thiols: a perspective, Electroanal., 14 (2002) 89-98.

[66] E.L. Mayer, D.W. Jacobsen, K. Robinson, Homocysteine and coronary atherosclerosis, J. Am. Coll. Cardiol., 27 (1996) 517-527.

[67] G.N. Welch, J. Loscalzo, Homocysteine and Atherothrombosis, N. Engl. J. Med, 336 (1998) 1042-1043.

[68] K.S. McCully, Vascular pathology of homocysteine: implications for the pathogenesis of arteriosclerosis, Am. J. Pathol., 56 (1969) 111-128.

[69] O. Nekrassova, N.S. Lawrence, R.G. Compton, Analytical determination of homocysteine: a review, Talanta, 60 (2003) 1085-1095.

[70] W. Wang, O. Rusin, X. Xu, K.K. Kim, J.O. Escobedo, S.O. Fakayode, K.A. Fletcher, M. Lowry, C.M. Schowalter, C.M. Lawrence, F.R. Fronczek, I.M. Warner, R.M. Strongin, Detection of Homocysteine and Cysteine, J. Am. Chem. Soc., 127 (2005) 15949-15958.

[71] W. Wang, J.O. Escobedo, C.M. Lawrence, R.M. Strongin, Direct detection of homocysteine, J. Am. Chem. Soc., 126 (2003) 3400-3401.

[72] H. Refsum, F. Wesenberg, P.M. Ueland, Plasma homocysteine in children with acute lymphoblastic leukemia: changed during a chemotherapeutic regimen including methotrexate, Cancer Res., 51 (1991) 828-835.

[73] G.J. Hankey, J.W. Eikelboom, Homcysteine and vascular disease, Lancet, 354 (1999) 407-413.

[74] D.C. Matthews, The Relationship Between Diabetes and Periodontal Disease, J. Can. Dent. Assoc., 68 (2002) 161-164.

[75] M. Boulot-Tolle, B. Chadefaux, P. Kamoun, Salivary Homocyst(e)ine Concentrations, Clin. Chem., 38 (1992) 1504-1505.

[76] S. Persichilli, J. Gervasoni, M. Castagnola, C. Zuppi, B. Zappacosta, A Reversed-Phase HPLC Fluorimetric Method for Simultaneous Determination of Homocysteine-Related Thiols in Different Body Fluids, Lab. Med., 42 (2011) 657-662.

[77] B. Zappacosta, A. Manni, S. Persichilli, D. Scribano, A. Minucci, D. Lazzaro, P. De Sole, B. Giardina, HPLC analysis of some sulphur compounds in saliva: comparison between healthy subjects and periodontopathic patients, Clin. Chim. Acta, 338 (2003) 57-60.

[78] S. Koshimune, S. Awano, K. Gohara, E. Kurihara, T. Ansai, T. Takehara, Low salivary flow and volatile sulfur compounds in mouth air, Oral Surg. Oral Med. O., 96 (2003) 38-41.

[79] B. Zappacosta, A. Manni, S. Persichilli, A. Boari, D. Scribano, A. Minucci, L. Raffaelli, B. Giardina, P. De Sole, Salivary thiols and enzyme markers of cell damage in periodontal disease, Clin. Biochem., 40 (2007) 661-665.

[80] B. Zappacosta, S. Persichilli, P.D. Sole, A. Mordente, B. Giardina, Effect of smoking one cigarette on antioxidant metabolites in the saliva of healthy smokers, Arch. Oral. Biol., 44 (1999) 485-488.

[81] B. Zappacosta, S. Persichilli, A. Mordente, A. Minucci, D. Lazzaro, E. Meucci, B. Giardina, Inhibition of salivary enzymes by cigarette smoke and the protective role of glutathione, Hum. Exp. Toxicol., 21 (2002) 7-11.

[82] T. Fiskerstrand, H. Refsum, G. Kvalheim, P.M. Ueland, Homocysteine and other thiols in plasma and urine: automated determination and sample stability, Clin. Chem., 39 (1993) 263-271.

[83] K. Kusmierek, G. Chwatko, R. Glowacki, E. Bald, Determination of endogenous thiols and thiol drugs in urine by HPLC with ultraviolet detection, J. Chromatogr. B, 877 (2009) 3300-3308.

[84] R. Ragone, Homocystine solubility and vascular disease, FASEB J, 16 (2002) 401-404.

[85] R.A. Winters, J. Zukowski, N. Ercal, R.H. Matthews, D.R. Spitz, Analysis of glutathione, glutathione disulfides, cysteine, homocysteine, and other biological thiols by high-performance liquid chromatography following derivatization by N-(1-pyrenyl)maleimide, Anal. Biochem., 227 (1995) 14-21.

[86] S.P. Stabler, P.D. Marcell, E.R. Rodell, R.H. Allen, D.G. Savage, J. Lindenbaum, Elevation of total homocysteine in the serum of patients with cobalamin or folate deficiency detected by capillary gas chromatography-mass spectrometry, J. Clin. Invest., 81 (1988) 466-474.

[87] H. Salehzadeh, B. Mokhtari, D. Nematollahi, Selective electrochemical determination of homocysteine in the presence of cysteine and glutathione, Electrochim. Acta, 123 (2014) 353-361.

[88] W. Zhang, P. Li, Q. Geng, Y. Duan, M. Guo, Y. Cao, Simultaneous determination of glutathione, cysteine, homocysteine, and cysteinylglycine in biological fluids by ion-pairing high-performance liquid chromatography coupled with precolumn derivatization, J. Agri. Food Chem., 62 (2014) 5845-5852.

[89] I. Mefford, R.N. Adams, Determination of reduced glutathione in guinea pig and rat tissue by HPLC with electrochemical detection, Life Sci., 23 (1978) 1167-1173.

[90] R. Kand'ár, P. Žákováa, H. Lotkováb, O. Kučerab, Z. Červinkováb, Determination of reduced and oxidized glutathione in biological samples using liquid chromatography with fluorimetric detection, J. Pharmaceut. Biomed., 43 (2007) 1382-1387.

[91] S. Melnyk, M. Pogribna, I. Pogribny, R.J. Hinet, S.J. James, A new HPLC method for the simultaneous determination of oxidized and reduced plasma aminothiols using coulometric electrochemical detection, J. Nutr. Biochem., 10 (1999) 490-497.

[92] J.P. Richie Jr, C.A. Lang, The determination of glutathione, cyst(e)ine, and other thiols and disulfides in biological samples using high-performance liquid chromatography with dual electrochemical detection, Anal. Biochem., 163 (1987) 9-15.

[93] P.J. Vandeberg, D.C. Johnson, Pulsed electrochemical detection of cysteine, cystine, methionine, and glutathione at gold electrodes following their separation by liquid chromatography, Anal. Chem., 65 (1993) 2713-2718.

[94] X. Yang, Y. Guo, R.M. Strongin, Conjugate addition/cyclization sequence enable selective and simultaneous fluorescence detection of cysteine and homocysteine, Angew. Chem. Int. Edit., 50 (2011) 10690-10693.

[95] Y.V. Tcherkas, A.D. Denisenko, Simultaneous determination of several amino acids, including homocysteine , cysteine and glutamic acid, in human plasma by isocratic reversed-phase high-performance liquid chromatography with fluorimetric detection, J. Chromatogr. A, 913 (2001) 309-313.

[96] P.R. Lima, W. Santos, A.B. Oliveira, M.O.F. Goulart, L.T. Kubota, Electrocatalytic activity of 4-nitrophthalonitrile-modified electrode for the L-glutathione detection, J. Pharmaceut. Biomed., 47 (2008) 758-764.

[97] J.C. Ndamanisha, J. Bai, B. Qi, L. Guo, Application of electrochemical properties of ordered mesoporous carbon to the determination of glutathione and cysteine, Anal. Biochem., 386 (2009) 79-84.

[98] T.H. Huang, T. Kuwana, A. Warsinke, Analysis of thiols with tyrosinase-modified carbon paste electrodes based on blocking of substrate recycling, Biosens. Bioelectron., 17 (2002) 1107-1113.

[99] L. Mao, K. Yamamoto, Amperometric biosensor for glutathione based on osmium-polyvinylpyridine gel polymer and glutathione sulfhydryl oxidase, Electroanal., 12 (2000) 577-582.

[100] R.R. Moore, C.E. Banks, R.G. Compton, Electrocatalytic detection of thiols using an edge plane pyrolytic graphite electrode, Analyst, 129 (2004) 755-758.

[101] K. Gong, X. Zhu, R. Zhao, S. Xiong, L. Mao, C. Chen, Rational attachment of synthetic triptycene orthoquinone onto carbon nanotubes for electrocatalysis and sensitive detection of thiols, Anal. Chem., 77 (2005) 8158-8165.

[102] J.-B. Raoof, R. Ojani, M. Baghayeri, Simultaneous electrochemical determination of glutathione and tryptophan on a nano-TiO_2/ferrocene carboxylic acid modified carbon paste electrode, Sensors Actuat. B-Chem., 143 (2009) 261-269.

[103] P. Abiman, G.G. Wildgoose, R.G. Compton, Electroanalytical exploitation of nitroso phenyl modified carbon-thiol interactions: Application to the low voltage determination of thiols, Electroanal., 19 (2007) 437-444.

[104] R. Luz, F.S. Damos, A.A. Tanaka, L.T. Kubota, Y. Gushikem, Electrocatalysis of reduced L-glutathione oxidation by iron(III) tetra-(N-methyl-4-pyridyl)-porphyrin (FeT_4MPyP) adsorbed on multi-walled carbon nanotubes, Talanta, 76 (2008) 1097-1104.

[105] G. Ziyatdinova, L. Grigor'eva, M. Morozov, A. Gilmutdinov, H. Budnikov, Electrochemical oxidation of sulfur-containing amino acids on an electrode modified with multi-walled carbon nanotubes, Microchim. Acta, 165 (2009) 353-359.

[106] M. Mazloum-Ardakani, M.A. Sheikh-Mohseni, B.-F. Mirjalili, Selective and simulataneous voltammetric determination of glutathione, uric acid and penicillamine by a modified carbon nanotube paste electrode, Electroanal., 25 (2013) 2021-2029.

[107] W. Ren, H.Q. Luo, N.B. Li, Simultaneous voltammetric measurement of ascorbic acid, epinephrine and uric acid at a glassy carbon electrode modified with caffeic acid, Biosens. Bioelectron., 21 (2006) 1086-1092.

[108] Y. Zhang, W. Ren, S. Zhang, Simultaneous determination of epinephrine, dopamine, ascorbic acid and uric acid by polydopamine-nanogold composite modified electrode, Int. J. Electrochem. Sci., 8 (2013) 6839-6850.

[109] N.B. Li, W. Ren, H.Q. Luo, Caffeic acid-modified glassy carbon electrode for the simultaneous determination of epinephrine and dopamine, Electroanal., 19 (2007) 1496-1502.

[110] R.W. Murray, A.G. Ewing, R.A. Durst, Chemically modified electrode: molecular design for electroanalysis, Anal. Chem., 59 (1987) 379A-390A.

[111] J. Wang, Amperometric biosensors for clinical and therapeutic drug monitoring: a review, J. Pharmaceut. Biomed., 19 (1999) 49-53.

[112] H.D. Goldberg, R.B. Brown, D.P. Liu, M.E. Meyerhoff, Screen printing: a technology for the batch fabrication of integrated chemical-sensor arrays, Sensors Actuat. B-Chem., 21 (1994) 171-183.

[113] S.A. Wring, J.P. Hart, Chemically modifed, carbon-based electrode and their application as electrochemical sensors for the analysis of biologically important compounds: a review, Analyst, 117 (1992) 1215-1229.

[114] X. Chen, Y. Yang, M. Ding, Electrocatalytic oxidation and sensitve detection of cysteine at layer-by-layer assembled carbon nanotube-modified electrode, Anal. Chim. Acta, 557 (2006) 52-56.

[115] F. Arduini, C. Majorani, A. Amine, D. Moscone, G. Palleschi, Hg^{2+} detection by measuring thiol groups with a highly sensitive screen-printed electrode modified with a nanostructure carbon black film, Electrochim. Acta, 56 (2011) 4209-4215.

[116] Z.X. Gong, H. Li, Electrocatalytic and analytical responses of 10-methylphenothiazine toward reduced glutathione, J. Electrochem. Soc., 147 (2000) 238-241.

[117] P. Houze, S. Gamra, I. Madelaine, B. Bousquet, B. Gourmel, Simultaneous determination of total plasma glutathione, homocystiene, cysteinylglycine, and methionine by high-performance liquid chromatography with electrochemical detection, J. Clin. Lab. Anal., 15 (2001) 144-153.

[118] M. Scampicchio, N.S. Lawrence, A. Arecchi, S. Mannino, Electrochemical Reduction of Ellman's Reagent: A Novel Selective Detection Protocol for Thiol Compounds, Electroanal., 19 (2007) 2437-2443.

[119] O. Nekrassova, P.C. White, S. Threlfell, G. Hignett, A.J. Wain, N.S. Lawrence, J. Davis, R.G. Compton, An electrochemical adaptation of Ellman's test, Analyst, 127 (2002) 797-802.

[120] Synthetic Urine e.K. http://www.synthetic-urine.de/en/products/din-standards-iso-standarts/din-53160-1-2.html. Accessed on October 2014.

[121] Glutathione Assay Kit. https://www.sigmaaldrich.com/content/dam/sigma-aldrich/docs/Sigma/Bulletin/cs0260bul.pdf. Accessed on April 2015.

[122] I. Švancara, K. Vytřas, J. Barek, J. Zima, Carbon paste electrodes in modern electroanalysis, CRC. Cr. Rev. Anal. Chem., 31 (2001) 311-345.

[123] I. Švancara, K.A. Vytřas, K.B. Kalcher, A.C. Walcarius, J. Wang, Carbon paste electrodes in facts, numbers, and notes: a review on the occasion of the 50-year jubilee of carbon paste in electrochemistry and electroanalysis, Electroanal., 21 (2009) 7-28.

[124] R.N. Adams, Carbon paste electrodes, Anal. Chem., 30 (1958) 1576.

[125] DropSens. http://www.dropsens.com/en/home.html. Accessed on November 2013.

[126] D.A. Skoog, D.M. West, F.J. Holler, S.R. Crouch, Fundamental of Analytical Chemistry, 8th ed., USA: Brooks/Cole-Thomson Learning; 2003.

[127] G.L. Long, J.D. Winefordner, Limit of Detection A Closer Look at the IUPAC Definition, Anal. Chem., 55 (1983) 712A-724A.

[128] J. Inczedy, T. Lengyel, A.M. Ure, IUPAC Compendium of Analytical Nomenclature, 3rd ed., Oxford, UK: Blackwell Science Ltd.; 1998.

[129] A.M. Committee, Recommendation for the definition, estimation and use of the detection limit, Analyst, 112 (1987) 199-204.

[130] C.M.A. Brett, A.M.O. Brett, Electroanalysis, Oxford: Oxford University Press Inc.; 1998.

[131] P.C. White, N.S. Lawrence, J. Davis, R.G. Compton, Electrochemically initiated 1,4 additions: a versatile route to the determination of thiols, Anal. Chim. Acta, 447 (2001) 1-10.

[132] P.T. Lee, R.G. Compton, Selective electrochemical detection of thiol biomarkers in saliva using multiwalled carbon nanotube screen-printed electrodes, Sensors Actuat. B-Chem., 209 (2015) 983-988.

[133] P.T. Lee, D. Lowinsohn, R.G. Compton, The use of screen-printed electrodes in a proof of concept electrochemical estimation of homocysteine and glutathione in the presence of cysteine using catechol, Sensors, 14 (2014) 10395-10411.

[134] P.T. Lee, J.E. Thomson, A. Karina, C. Salter, C. Johnston, S.G. Davies, R.G. Compton, Selective electrochemical determination of cysteine with a cyclotricatechylene modified carbon electrode, Analyst, 140 (2015) 236-242.

[135] T. Inoue, J.R. Kirchhoff, Electrochemical detection of thiols with a coenzyme pyrroloquinoline quinone modified electrode, Anal. Chem., 72 (2000) 5755-5760.

[136] N.S. Lawrence, E.L. Beckett, J. Davis, R.G. Compton, Advances in the voltammetric analysis of small biological relevant compounds, Anal. Biochem., 303 (2002) 1-16.

[137] P.T. Lee, K.R. Ward, K. Tschulik, G. Chapman, R.G. Compton, Electrochemical Detection of Glutathione Using a Poly(caffeic acid) Nanocarbon Composite Modified Electrode, Electroanal., 26 (2014) 366-373.

[138] L. Fotouhi, L. Behrozi, M.M. Heravi, D. Nematollahi, Electrochemical oxidation of catechols in the presence of pyrimidine-2-thiol: application to electrosynthesis, Phosphorus Sulfur, 184 (2009) 2749-2757.

[139] T.R. Wendland, B.S. Muntean, J. Kaur, I. Mukherjee, J. Chen, X. Tan, D. Attygalle, R.W. Collins, J.R. Kirchoff, L.M.V. Tillekerante, In situ self assembly of thiolated ortho-quinone capped electrocatalysts for bioanalytical applications, Electroanal., 23 (2011) 2275-2279.

[140] C.Y. Lumibao, L.M.V. Tillekeratne, J.R. Kirchhoff, D.M.D. Fouchard, R.A. Hudson, Electrochemical and electrocatalytic properties of imidazole analogues of the redox cofactor pyrroloquinoline quinone, Electroanal., 20 (2008) 2177-2184.

[141] P.T. Lee, R.G. Compton, Electrochemical detection of NADH, cysteine, or glutathione using a caffeic acid modified glassy carbon electrode, Electroanal., 25 (2013) 1613-1620.

[142] P.C. White, N.S. Lawrence, Y.C. Tsai, J. Davis, R.G. Compton, Electrochemically Driven Derivatisation-Detection of Cysteine, Mikrochim. Acta, 137 (2001) 87-91.

[143] P.T. Lee, D. Lowinsohn, R.G. Compton, The selective electrochemical detection of homocysteine in the presence of glutathione, cysteine, and ascorbic acid using carbon electrodes, Analyst, 139 (2014) 3755-3762.

[144] P.T. Lee, R.G. Compton, Precursor Modified Electrodes: Electrochemical Detection of Captopril, Electroanal., (2015) DOI: 10.1002/elan.201500093.

[145] A. Chaubey, B.D. Malhotra, Mediated biosensors, Biosens. Bioelectron., 17 (2002) 441-456.

[146] E. Lorenzo, F. Pariente, L. Hernandez, F. Tobalina, M. Darder, Q. Wu, M. Maskus, H.D. Abruna, Analytical strategies for amperometric biosensors based on chemically modified electrodes, Biosens. Bioelectron., 13 (1998) 319-332.

[147] J. Janata, M. Josowicz, D.M. DaVaney, Chemical Sensors, Anal. Chem., 66 (1994) 207R-228R.

[148] H.R. Zare, S.M. Golabi, Caffeic acid modified glassy carbon electrode for electrocatalytic oxidation of reduce nicotinamide dinucleotide (NADH), J. Solid State Electr., 4 (2000) 87-94.

[149] N.F. Atta, I. Marawi, K.L. Petticrew, H. Zimmer, H.B.M. Jr., A. Galal, Electrochemistry and detection of some organic and biological molecules at conducting

polymer electrodes. Part 3. Evidence of the electrocatalytic effect of the heteroatom of the poly(hetetroarylene) at the electrode/electrolyte interface, J. Electroanal. Chem., 408 (1996) 47-52.

[150] J. Bobacka, A. Ivaska, M. Grzeszczuk, Electrochemical study of poly(3-octylthiophene) film electrodes I. Electrolyte effects on the voltammetric characteristics of the polymer. Three states of the polymer film, Synthetic Met., 44 (1991) 9-19.

[151] N.F. Atta, A. Galal, A.E. Karagozler, H. Zimmer, J.F. Rubinson, H.B.M. Jr., Voltammetric Studies of the Oxidation of Reduced Nicotinamide Adenine Dinucelotide at a Conducting Polymer Electrode, J. Chem. Soc., Chem. Commun., (1990) 1347-1349.

[152] P. Marque, J. Roncali, F. Garnier, Electrolyte Effect on the Electrochemical Properties of Poly(3-Methylthiophene) Thin Films, J. Electroanal. Chem., 218 (1987) 107-118.

[153] J. Wang, Nanomaterial-based electrochemical biosensors, Analyst, 130 (2005) 421-426.

[154] H.D. Abruña, Coordination chemistry in two dimensions: chemically modified electrodes, Coordin. Chem. Rev., 86 (1988) 135-189.

[155] L. Zhu, J. Zhai, Y. Guo, C. Tian, R. Yang, Amperometric glucose biosensors based on integration of glucose oxidase onto Prussian blue/carbon nanotubes nanocomposite electrodes, Electroanal., 18 (2006) 1842-1846.

[156] l. Zhu, R. Yang, J. Zhai, C. Tian, Bienzymatic glucose biosensor based on co-immobilization of peroxidase and glucose oxidase on carbon nanotubes electrode, Biosens. Bioelectron., 23 (2007) 528-535.

[157] X. Kang, Z. Mai, X. Zou, P. Cai, J. Mo, A novel glucose biosensor base on immobilization of glucose oxidase in chitosan on a glassy carbon electrode modified with gold-platinum alloy nanoparticles/multiwall carbon nanotubes, Anal. Biochem., 369 (2007) 71-79.

[158] X. Luo, A.J. Killard, A. Morrin, M.R. Smyth, Enhancement of a conducting polymer-based biosensor using carbon nanotube-doped polyaniline, Anal. Chim. Acta, 575 (2006) 39-44.

[159] M.C. Kum, K.A. Joshi, W. Chen, N.V. Myung, A. Mulchandani, Biomolecules-carbon nanotubes doped conducting polymer nanocomposites and their sensor application, Talanta, 74 (2007) 370-375.

[160] L. Tang, Y. Zhu, l. Xu, X. Yang, C. Li, Amperometric glutamate biosensor based on self-assembling glutamate dehydrogenase and dendrimer-encapsulated platinum nanoparticle onto carbon nanotubes, Talanta, 73 (2007) 438-443.

[161] N.K. Kang, T.S. Jun, D.-D. La, J.H. Oh, Y.W. Cho, Y.S. Kim, Evaluation of the limit of detection capability of carbon black polymer composite sensor for volatile breath biomarkers, Sensors Actuat. B-Chem., 147 (2010) 55-60.

[162] C. Kranz, H. Wohlschläger, H.-L. Schidt, W. Schuhmann, Controlled electrochemical preparation of amperometric biosensor based on conducting polymer multilayers, Electroanal., 10 (1998) 546-552.

[163] A.J.S. Ahammad, J. Lee, M.A. Rahman, Electrochemical sensors based on carbon nanotubes, Sensors, 4 (2009) 2289-2319.

[164] L. Agüí, P. Yáñez-Sedeño, J.M. Pingarrón, Role of carbon nanotubes in electroanalytical chemistry: a review, Anal. Chim. Acta, 622 (2008) 11-47.

[165] L.Y. Heng, A. Chou, J. Yu, Y. Chen, J.J. Gooding, Demonstration of the advantages of sing bamboo-like nanotubes for electrochemical biosensor applications compared with single walled carbon nanotubes, Electrochem. Comm., 7 (2005) 1459-1462.

[166] A.I. Medalia, F.A. Heckman, Morphology of aggregates-II. size and shape factors of carbon black aggregates from electron microscopy, Carbon, 7 (1969) 567-582.

[167] T.W.B. Lo, L. Aldous, R.G. Compton, The use of nano-carbon as an alternative to multi-walled carbon nanotubes in modified electrodes for adsorptive stripping voltammetry, Sensors Actuat. B-Chem., 162 (2012) 361-368.

[168] C. Giacomelli, K. Ckless, D. Galat, F.S. Miranda, A. Spinelli, Electrochemistry of caffeic acid aqueous solutions with pH 2.0 to 8.5, J. Brazil Chem. Soc., 13 (2002) 332-338.

[169] I. Streeter, G.G. Wildgoose, L. Shao, R.G. Compton, Cyclic voltammetry on electrode surfaces covered with porous layers: An analysis of electron transfer kinetics at single-walled carbon nanotube modified electrodes, Sensors Actuat. B-Chem., 133 (2008) 462-466.

[170] M.J. Sims, N.V. Rees, E.J.F. Dickinsons, R.G. Compton, Effects of thin-layer diffusion in the electrochemical detection of nicotine on basal plane pyrolytic graphite (BPPG) electrodes modified with layers of multi-walled carbon nanotubes (MWCNT-BPPG), Sensors Actuat. B-Chem., 144 (2010) 153-158.

[171] M.I. Prodromidis, A.B. Florou, S.M. Tzouwara-Karayanni, M.I. Karayannis, The importance of surface coverage in the electrochemical study of chemically modified electrodes, Electroanal., 12 (2000) 1498-1501.

[172] M.J. Hardie, R.M. Mills, C.J. Sumby, Building blocks for cyclotriveratrylene-based coordination networks, Org. Biomol. Chem., 2 (2004) 2958-2964.

[173] A.S. Lindsey, The structure of cyclotriveratrylene (10-15-dihydro-2,3,7,8,12,13-hexamethoxy-5H-tribenzo[a,d,g]cyclononene) and related compounds, J. Chem. Soc., (1965) 1685-1692.

[174] M.J. Hardie, Recent advances in the chemistry of cyclotriveratrylene, Chem. Soc. Rev., 39 (2010) 516-527.

[175] J.J. Loughrey, C.A. Kilner, M.J. Hardie, M.A. Halcrow, Six new crystalline clathrates of cyclotricatechylene (CTC) including two donor–acceptor complexes, Supramol. Chem., 24 (2012) 2-13.

[176] D.S. Bohle, D. Stasko, Extended rim redox active tris-metallodioxolene derivatives of cyclotricatechylene, Chem. Commun., (1998) 567-568.

[177] A. Warshawsky, N. Shoef, A facile synthesis of cyclotriveratrylene, J. Inclusion Phenom., 6 (1988) 647-651.

[178] J.W. Steed, H. Zhang, J.L. Atwood, Inclusion chemistry of cyclotriveratrylene and cyclotricatechylene, Supramol. Chem., 7 (1994) 37-45.

[179] R.T. Kachoosangi, G.G. Wildgoose, R.G. Compton, Carbon nanotube-based electrochemical sensors for quantifying the 'heat' of chilli peppers: the adsorptive stripping voltammetric determination of capsaicin, Analyst, 133 (2008) 888-895.

[180] L. Papouchado, J. Bacon, R.N. Adams, Potential step cyclic voltammetry for the study of electrode reaction mechanism, J. Electroanal. Chem., 24 (1969) A1-A5.

[181] M. Jonsson, J. Lind, T. Reitberger, T.E. Eriksen, G. Merényi, Redox Chemistry of Substituted Benzenes. The One-Electron Reduction Potentials of Methoxy-Substituted Benzene Radical Cations, J. Phys. Chem., 97 (1993) 11278-11282.

[182] J. Kruid, R. Fogel, J. Limson, Voltammetric investigation of complex growth media at a bare glassy carbon electrode: A case study of oxytetracycline, Electrochim. Acta, 128 (2014) 41-47.

[183] C.M. Smith, A.M. Reynard, Essentials of Pharmacology, 1st ed., Philadelphia, USA: Saunders; 1995.

[184] B.G. Katzung, Basic and Clinical Pharmacology, 9th ed., New York, USA: Lange Medical Books/McGraw-Hill; 2004.

[185] K. Florey, Analytical Profiles of Drug Substances, New Jersey, USA: Academic Press; 1982.

[186] A. Golik, D. Modai, Z. Averbukh, M. Sheffy, A. Shamis, N. Cohen, U. Shaked, E. Dolev, Zine metabolism in patients treated with captopril versus enalapril, Metabolism, 39 (1990) 665-667.

[187] National Health Service (NHS). http://www.nhs.uk/medicine-guides/pages/MedicineOverview.aspx?condition=Blood%20pressure&medicine=Capoten. Accessed on February 2015.

[188] Bristol-Myers Squibb. http://www.bms.com/products/Pages/trademark.aspx. Accessed on February 2015.

[189] E.M.V. de Cavanagh, F. Inserra, L. Ferder, L. Romano, L. Ercole, C.G. Fraga, Superoxide dismutase and glutathione peroxidase activities are increased by enalapril and captopril in mouse liver, FEBS Lett., 361 (1995) 22-24.

[190] D. Bagchi, R. Prasad, D.K. Das, Direct scavenging of free radicals by captopril, an angiotensin converting enzyme inhibitor, Biochem. Bioph. Res. Co., 158 (1989) 52-57.

[191] S.P. Andreoli, Captopril scavenges hydrogen peroxide and reduces, but does not eliminate, oxidant-induced cell injury, Am. J. Physiol., 264 (1993) F120-F127.

[192] J.I.S. Robertson, D.M. Tillman, Coverting Enzyme Inhibitors in the Treatment of Hypertension, J. Cardiovasc. Pharm., 10 (1987) 843-848.

[193] G.H. Willams, Drug Therapy: Converting-Enzyme Inhibitors in the Treatment of Hypertension, N. Engl. J. Med, 319 (1988) 1517-1525.

[194] H. Parham, B. Zargar, Square-wave voltammetric (SWV) determination of Captopril in reconstituted serum and pharmaceutical formulations, Talanta, 65 (2005) 776-780.

[195] H. Karimi-Maleh, M. Moazampour, V.K. Gupta, A.L. Sanati, Electrocatalytic determination of captopril in real samples using NiO nanoparticle modified (9,10-dihydro-9,10-ethanoanthracene-11,12-dicarboximido)-4-ethylbenzene-1,2-diol carbon paste electrode, Sensors Actuat. B-Chem., 199 (2014) 47-53.

[196] H. Bagheri, H. Karimi-Maleh, F. Karimi, S. Mallakpour, M. Keyvanfard, Square wave voltammetric determination of captopril in liquid phase using N-(4-hydroxyphenyl)-3,5-dinitrobenzamide modified ZnO/CNT carbon paste electrode as a novel electrochemical sensor, J. Mol. Liq., 198 (2014) 193-199.

[197] J.B. Raoof, R. Ojani, M. Baghayeri, Sensitive Voltammetric Determination of Captopril Using a Carbon Paste Electrode Modified with Nano-TiO_2/Ferrocene Carboxylic Acid, Chin. J. Catal., 32 (2011) 1685-1692.

[198] G. Paimard, M.B. Gholivand, M. Shamsipur, K. Gholivand, L. Mohammadi-Behzad, A. Gholami, A. Barati, Fabrication of a highly sensitive amperometric sensor using 1,4-phenylene-N,N′-bis (O,O-diphenylphoramidate)/CdS quantum dots/multi-walled carbon nanotubes for nanomolar detection of captopril, J. Electroanal. Chem., 738 (2015) 176-183.

[199] A.B.F. Vitoreti, O. Abrahao, R.A.D. Gomes, G.R. Salazar-Banda, R.T.S. Oliveira, Electroanalytical Determination of Captopril in Pharmaceutical Formulations Using Boron-Doped Diamond Electrodes, Int. J. Electrochem. Sci., 9 (2014) 1044-1054.

[200] A.A. Ensafi, B. Rezaei, Z. Mirahmadi-Zare, H. Karimi-Maleh, Highly selective and sensitive voltammetric sensor for captopril determination based on modified multiwall carbon nanotubes paste electrode, J. Brazil Chem. Soc., 22 (2011) 1315-1322.

[201] H. Beitollahi, M.A. Taher, M. Ahmadipour, R. Hosseinzadeh, Electrocatalytic determination of captopril using a modified carbon nanotube paste electrode: Application to determination of captopril in pharmaceutical and biological samples, Measurement, 47 (2014) 770-776.

[202] A.A. Ensafi, H. Karimi-Maleh, S. Mallakpour, B. Rezaei, Highly sensitive voltammetric sensor based on catechol-derivative-multiwall carbon nanotubes for the catalytic determination of captopril in patient human urine samples, Colloids Surface B, 87 (2011) 480-488.

[203] R. Seifie-Makrani, N. Sajjadi, O. Younesi, H. Bagheri, A New Strategy for Determination of Captopril as a Hypertension Drug Using ZnO Nanoparticle Modified Carbon Paste Electrode, Int. J. Electrochem. Sci., 9 (2014) 1799-1811.

[204] M. Mazloum-Ardakani, M.A. Sheikh-Mohseni, B.-F. Mirjalili, L. Zamani, Simultaneous determination of captopril, acetaminophen and tryptophan at a modified electrode based on carbon nanotubes, J. Electroanal. Chem., 686 (2012) 12-18.

[205] A.A. Ensafi, M. Monsef, B. Rezaei, H. Karimi-Maleh, Electrocatalytic oxidation of captopril on a vinylferrocene modified carbon nanotubes paste electrode, Anal. Methods, 4 (2012) 1332.

[206] H. Karimi-Maleh, A.A. Ensafi, A.R. Allafchian, Fast and sensitive determination of captopril by voltammetric method using ferrocenedicarboxylic acid modified carbon paste electrode, J. Solid State Electr., 14 (2009) 9-15.

[207] A.A. Ensafi, H. Karimi-Maleh, M. Ghiaci, M. Arshadi, Characterization of Mn-nanoparticles decorated organo-functionalized SiO_2–Al_2O_3 mixed-oxide as a novel electrochemical sensor: Application for the voltammetric determination of captopril, J. Mater. Chem., 21 (2011) 15022.

[208] M. Fouladgar, Electrocatalytic Measurement of Trace Amount of Captopril Using Multiwall Carbon Nanotubes as a Sensor and Ferrocene as a Mediator, Int. J. Electrochem. Sci., 6 (2011) 705-716.

[209] B. Rezaei, S. Damiri, Voltammetric behavior of multi-walled carbon nanotubes modified electrode-hexacyanoferrate(II) electrocatalyst system as a sensor for determination of captopril, Sensors Actuat. B-Chem., 134 (2008) 324-331.

[210] M.A. Khalilzadeh, H. Karimi-Maleh, A. Amiri, F. Gholami, R.M. Mazhabi, Determination of captopril in patient human urine using ferrocenemonocarboxylic acid modified carbon nanotubes paste electrode, Chinese Chem. Lett., 21 (2010) 1467-1470.

[211] S. Shahrokhian, M. Karimi, H. Khajehsharifi, Carbon-paste electrode modified with cobalt-5-nitrolsalophen as a sensitive voltammetric sensor for detection of captopril, Sensors Actuat. B-Chem., 109 (2005) 278-284.

[212] S. Lu, P. Lu, C. Li, C. Wang, J. Yu, Highly Improved Electrooxidation of Captopril on Copper Hexacyanoferrate/Ordered Mesoporous Carbon-Modified Glassy Carbon Electrode, Aust. J. Chem., 67 (2014) 851.

[213] M. Mazloum-Ardakani, F. Sabaghian, A. Khoshroo, M. Abolhasani, H. Naeimi, Electrochemical determination of captopril in the presence of acetaminophen, tryptophan, folic acid, and l-cysteine at the surface of modified carbon nanotube paste electrode, Ionics, 21 (2014) 239-250.

[214] A. Niazi, Z. Pourghobadi, D. Nematollahi, H. Beiginejad, Electrochemical Oxidation and Voltammetric Determination of Captopril Using 4,4'-Biphenol as a Homogeneous Mediator, J. Electrochem. Soc., 161 (2014) H284-H289.

[215] A.A. Ensafi, A. Arabzadeh, A new sensor for electrochemical determination of captopril using chlorpromazine as a mediator at a glassy carbon electrode, J. Anal. Chem., 67 (2012) 486-496.

[216] F. Pogacean, A.R. Biris, M. Coros, M.D. Lazar, F. Watanabe, G.K. Kannarpady, S.A. Al Said, A.S. Biris, S. Pruneanu, Direct electrochemical oxidation of S-captopril using gold

electrodes modified with graphene-AuAg nanocomposites, Int. J. Nanomed., 9 (2014) 1111-1125.

[217] I.C. Eleotério, M.A. Balbino, M.F. De Oliveira, Voltammetric Determination of Captopril Employing Platinum Electrode Modified with Iron (III) Hexacyanoferrate (II) Film, ECS Trans., 43 (2012) 345-351.

[218] P.T. Lee, D. Lowinsohn, R.G. Compton, Simultaneous Detection of Homocysteine and Cysteine in the Presence of Ascorbic Acid and Glutathione Using a Nanocarbon Modified Electrode, Electroanal., 26 (2014) 1488-1496.

[219] W.A. Gahl, J.G. Thoene, J.A. Schneider, Cystinosis, N. Engl. J. Med, 347 (2002) 111-121.

[220] J.B. van Meurs, R.A. Dhonukshe-Rutten, S.M. Pluijm, M. van der Klift, R. de Jonge, J. Lindemans, L.C. de Groot, A. Hofman, J.C. Witteman, J.P. van Leeuwen, M.M. Breteler, P. Lips, H.A. Pols, A.G. Uitterlinden, Homocysteine levels and the risk of osteoporotic fracture, N. Engl. J. Med, 350 (2004) 2033-2041.

[221] A. Merouani, J. Genest Jr., R. Rozen, M. Lambert, G.A. Mitchell, J. Dubois, P. Robitaille, Cerebral vascular complication and hyperhomocysteinemia in a cystinotic uremic child, Pediatr. Nephrol., 13 (1999) 73-76.

[222] D.E. Cole, D.C. Lehotay, J. Evrovski, Simplified simultaneous assay of total plasma homocysteine and methionine by HPLC and pulsed integrated amperometry, Clin. Chem., 44 (1998) 188-190.

[223] J.L. D'Erarno, A.E. Finkelstein, F.O. Boccazzi, O. Fridman, Total homocysteine levels in plasma: high-performance liquid chromatographic determination with electrochemical detection and glassy carbon electrode, J. Chromatogr. B, 720 (1998) 205-210.

[224] S.I.R. Malha, J. Mandli, A. Ourari, A. Amine, Carbon black-modified electrodes as sensitive tools for the electrochemical detection of nitrite and nitrate, Electroanal., 25 (2013) 2289-2297.

[225] J. Panchompoo, L. Aldous, R.G. Compton, Size-effects in the chemical modification of carbon black nanoparticals with 4-nitroaniline, New J. Chem., 34 (2010) 2643-2653.

[226] M. Levine, S.J. Padayatty, M.G. Espey, Vitamin C: A concentration-function approach yields pharmacology and therapeutic discoveries, Adv. Nutr., 2 (2011) 78-88.

[227] M.A. Ross, Determination of ascorbic acid and uric acid in plasma by high-performance liquid chromatography J. Chromatogr. B, 657 (1994) 197-200.

[228] D.J. VanderJagt, P.J. Garry, H.N. Bhaganvan, Ascorbic acid intake and plasma levels in healthy elderly people, Am. J. Clin. Nutr., 46 (1987) 290-294.

[229] D. Brubacher, U. Mosher, P. Jordan, Vitamin C concentration in plasma as a function of intake: a meta-analysis, Int. J. Vitam. Nutr. Res., 70 (2000) 225-237.

[230] C.A. Thorogood, G.G. Wildgoose, J.H. Jones, R.G. Compton, Identifying quinone-like species on the surface of graphitic carbon and multi-walled carbon nanotubes using reactions

with 2,4-dinitrophenylhydrazine to provide a voltammetric fingerprint, New J. Chem., 31 (2007) 958-965.

[231] A. Maleki, D. Nematollahi, J. Clausmeyer, J. Henig, N. Plumere, W. Schuhmann, Electrodeposition of catechol on glassy carbon electrode and its electrocatalytic activity towards NADH oxidation, Electroanal., 24 (2012) 1932-1936.

[232] J.B. Raoof, R. Ojani, D. Nematollahi, Digital simulation of the cyclic voltammetry study of the catechol electrooxidation in the presence of some nitrogen and carbon nucleophiles, Int. J. Electrochem. Sci., 4 (2009) 810-819.

[233] J. Wang, M. Musameh, Carbon nanotube screen-printed electrochemical sensors, Analyst, 129 (2004) 1-2.

[234] N. Thiyagarajan, J. Chang, K. Senthilkumar, J. Zen, Disposable electrochemical sensors: A mini review, Electrochem. Comm., 38 (2014) 86-90.

[235] F. Arduini, F.C. Nardo, A. Amine, L. Micheli, G. Palleschi, D. Moscone, Carbon black-modified screen printed electrodes as electroanalytical tools, Electroanal., 24 (2012) 743-751.

[236] R. Saetre, D.L. Rabenstein, Determination of Cysteine in Plasma and Urine and Homocysteine in Plasma by High-Pressure Liquid Chromatography, Anal. Biochem., 90 (1978) 684-692.

[237] K. Kusmierek, R. Glowacki, E. Bald, Analysis of urine for cysteine, cysteinylglycine, and homocysteine by high-performance liquid chromatography, Anal. Bioanal. Chem., 385 (2006) 855-860.

[238] P.T. Lee, R.G. Compton, Selective thiol detection in authentic biological samples with the use of screen printed electrodes, Anal. Sci., (accepted 2015).

[239] P.T. Lee, L.M. Goncalves, R.G. Compton, Electrochemical determination of free and total glutathione in human saliva samples, (submitted 2015).

[240] M.C. Dillon, D.C. Opris, R. Kopanczyk, J. Lickliter, H.N. Cornwell, E.G. Bridges, A.M. Nazar, K.G. Bridges, Detection of Homocysteine and C-Reactive Protein in the Saliva of Healthy Adults: Comparison with Blood Levels, Biomarker Insights, 5 (2010) 57-61.

[241] F.R. Smith, D.S. Goodman, The effects of diseases of the liver, thyroid, and kidneys on the transport of vitamin A in human plasma, J. Clin. Invest., 50 (1971) 2426-2436.

[242] W.H. Stein, S. Moore, The Free Amino Acids of Human Blood Plasma, J. Biol. Chem., 211 (1954) 915-926.

[243] M. Filella, N. Belzile, Y.-W. Chen, Human Exposure to Antimony. IV. Contents in Human Blood, Crit. Rev. Env. Sci. Tec., 43 (2013) 2071-2105.

[244] H.A. Krebs, Chemical composition of blood plasma and serum, Annu. Rev. Biochem., 19 (1950) 409-430.

[245] S. Melnyk, M. Pogribna, I. Pogribny, R.J. Hine, S.J. James, A new HPLC method for the simultaneous determination of oxidized and reduced plasma aminothiols usng coulometric electrochemical detection, J. Nutr. Biochem., 10 (1999) 490-497.

[246] P.M. Ueland, H. Refrum, S.P. Stabler, M.R. Malinow, A. Andersson, R.H. Allen, Total homocysteine in plasma or serum: methods and clinical applications, Clin. Chem., 39 (1993) 1764-1779.

[247] Clinical Biochemistry Reference Ranges Handbook. http://www.esht.nhs.uk/EasysiteWeb/getresource.axd?AssetID=375157&type=full&servicetype=Attachment. Accessed on September 2014.

[248] P.J. Taylor, D.P. Cooper, R.D. Gordon, M. Stowasser, Measurement of aldosterone in human plasma by semiautomated HPLC-tandem mass spectrometry, Clin. Chem., 55 (2009) 1155-1162.

[249] J.A. Jacquez, J.W. Poppell, R. Jeltsch, Solubility of ammonia in human plasma, J. Appl. Physiol., 14 (1959) 255-258.

[250] F.K. Trefz, D.J. Byrd, W. Kochen, Quantitative determination of cortisol in human plasma by high-pressure liquid chromatography, J. Chromatogr. A, 107 (1975) 181-189.

[251] J.H.M. Van den berg, C.R. Mol, R.S. Deelder, J.H.H. Thijssen, A quantitative assay of cortisol in human plasma by high performance liquid chromatography using a selective chemically bonded stationary phase, Clin. Chim. Acta, 78 (1977) 165-172.

[252] D. Weatherby, S. Ferguson, Blood Chemistry and CBC Analysis, 1st ed., USA: Bear Mountain; 2002.

[253] R. Achari, M. Mayersohn, K.A. Conrad, HPLC Analysis of Creatinine in Human Plasma and Urine, J. Chromatogr. Sci., 21 (1983) 278-281.

[254] B.N. Ames, R. Cathcart, E. Schwiers, P. Hochstein, Uric acid provides an antioxidant defence in humans against oxidant- and radical-caused aging and cancer: a hypothesis, Proc. Natl. Acad. Sci. U. S. A., 78 (1981) 6858-6862.

[255] S. Tan, R. Radi, F. Gaudier, R.A. Evans, A. Rivera, K.A. Kirk, D.A. Parks, Physiologic levels of uric acid inhibit xanthine oxidase in human plasma, Pediatr. Res., 34 (1993) 303-307.

[256] M. Kanai, A. Raz, D.S. Goodman, Retinol-binding protein: the transport protein for vitamin A in human plasma, J. Clin. Invest., 47 (1968) 2025-2044.

[257] R.W. Gray, D.R. Wilz, A.E. Caldas, J. Lemann, Jr., The importance of phosphate in regulating plasma 1,25-$(OH)_2$-vitamin D levels in humans: studies in healthy subjects in calcium-stone formers and in patients with primary hyperparathyroidism, J. Cllin. Endocr. Metab., 45 (1977) 299-306.

[258] P.W. Lambert, B.J. Syverson, C.D. Arnaud, T.C. Spelsberg, Isolation and quantitation of endogenous vitamin D and its physiologically important metabolites in human plasma by high pressure liquid chromatography, J. Steroid Biochem., 8 (1977) 929-937.

[259] T.C.B. Stamp, J.M. Round, Seasonal Changes in Human Plasma Levels of 25-Hydroxyvitamin D, Nature, 247 (1974) 563-565.

[260] E. Kaufman, I.B. Lamster, Analysis of saliva for periodontal diagnosis, J. Clin. Periodontol., 27 (2000) 453-465.

[261] S. Moore, K. A. C. Calder, N. J Miller, C.A. Rice-Evans, Antioxidant activity of saliva and periodontal disease, Free Radical Res., 21 (1994) 417-425.

[262] R. Nagler, S. Lischinsky, E. Diamond, N. Drigues, I. Klein, A.Z. Reznick, Effect of cigarette smoke on salivary proteins and enzyme activities, Arch. Biochem. Biophys., 379 (2000) 229-236.

[263] K. Inoue, T. Namiki, Y. Iwasaki, Y. Yoshimura, H. Nakazawa, Determination of uric acid in human saliva by high-performance liquid chromatography with amperometric electrochemical detection, J. Chromatogr. B, 785 (2003) 57-63.

[264] B. Zappacosta, S. Persichilli, P. De Sole, A. Mordente, B. Giardina, Effect of smoking one cigarette on antioxidant metabolites in the saliva of healthy smokers, Arch. Oral Biol., 44 (1999) 485-488.

[265] S. Sentellas, O. Morales-Ibanez, M. Zanuy, J.J. Alberti, GSSG/GSH ratios in cryopreserved rat and human hepatocytes as a biomarker for drug induced oxidative stress, Toxicol. In Vitro, 28 (2014) 1006-1015.

[266] G.L. Ellman, Tissue sulfhydryl groups, Arch. Biochem. Biophys., 82 (1959) 70-77.

[267] M. Soukup, I. Biesiada, A. Henderson, B. Idowu, D. Rodeback, L. Ridpath, E.G. Bridges, A.M. Nazar, K.G. Bridges, Salivary uric acid as a noninvasive biomarker of metabolic syndrome, Diabetol Metab Syndr, 4 (2012) 14.

[268] J.L. Morris, V. Jersey, Chemical constituents of saliva as indices of glandular activity, J. Biol. Chem., 56 (1923) 31-42.

[269] K. Shibasaki, M. Kimura, R. Ikarashi, A. Yamaguchi, T. Watanabe, Uric acid concentration in saliva and its changes with the patients receiving treatment for hyperuricemia, Metabolomics, 8 (2011) 484-491.

[270] D. Pietraforte, M. Castelli, A. Metere, G. Scorza, P. Samoggia, A. Menditto, M. Minetti, Salivary uric acid at the acidic pH of the stomach is the principal defense against nitrite-derived reactive species: sparing effects of chlorogenic acid and serum albumin, Free Radical Bio. Med., 41 (2006) 1753-1763.